Pharmacy
PH
R637

AWPP
R637e
1984.

EFFECT OF CRYSTALLIZATION KINETIC PARAMETERS ON THE PARTICLE SIZE DISTRIBUTION OF OXALIC ACID DIHYDRATE

By

NAIR RODRIGUEZ HORNEDO

A thesis submitted in partial fulfillment of the

requirements for the degree of

Doctor of Philosophy

(Pharmacy)

at the

UNIVERSITY OF WISCONSIN-MADISON

1984

Pharmacy
AW
R637

EFFECT OF CRYSTALLIZATION KINETIC PARAMETERS ON THE PARTICLE SIZE DISTRIBUTION OF OXALIC ACID DIHYDRATE

A thesis submitted to the Graduate School of the University of Wisconsin-Madison in partial fulfillment of the requirements for the degree of Doctor of Philosophy

by

NAIR RODRIGUEZ HORNEDO

Degree to be awarded: December 19____ May 19 84 August 19____

Approved by Thesis Reading Committee:

J. T. Carstensen — **Major Professor**

3/15 - 84 — **Date of Examination**

George Zografi

Vincent A. Conner

Ronald A. Barnitt

Robert M. Bock — **Dean, Graduate School**

EFFECT OF CRYSTALLIZATION KINETIC PARAMETERS ON THE PARTICLE SIZE DISTRIBUTION OF OXALIC ACID DIHYDRATE

by

Nair Rodriguez Hornedo

(Under the supervision of Professor Jens T. Carstensen)

The external properties of solid drug substances are exceedingly important in the processes by which they are converted into solid dosage forms (e.g., tablets). Such properties as flow, blending efficiency and dissolution rate are but three examples of properties that are affected by the crystal size and shape of the drug substance. It is therefore important to understand the factors during crystallization, which affect the magnitude of the mean particle size and shape of the distribution.

In the present study oxalic acid dihydrate has been crystallized non-isothermally from different binary mixtures of: glycerine/water, acetone/water and ethanol/water. The particle size distributions as a function of a characteristic dimension (z) are log-normally distributed in glycerine/water and acetone/water solvent systems. In glycerine/water they were log normally distributed with respect to the breadth/length ratio (b/a) and the mean geometric value of (b/a) decreased as the glycerine concentration increased. They were normally distributed for the acetone/water system. The ethanol/water solvent system was not pursued due to the formation of diethyl ester oxalate.

A second goal of this study was to explain the crystal size distributions obtained on the basis of the fundamental processes of crystallization, viz., nucleation and growth. A physically plausible model based on numerical evaluation of the nucleation and growth rates is proposed for the crystallization of oxalic acid dihydrate from its saturated solutions during linear programmed cooling. This model is in good agreement with the concentration and supersaturation-time profiles measured. It allows for calculation of the nucleation and growth rate constants when used with established values of the nucleation and growth orders. It also explains the log-normal crystal size distributions obtained when the supersaturation-time profile follows an exponential decay.

APPROVED: Jens T. Carstensen

Jens T. Carstensen, Professor

DATE: 3/15-84

To

my parents

ACKNOWLEDGEMENTS

I wish to thank Prof. Jens T. Carstensen for his guidance and suggestions during the course of this investigation.

Appreciation is extended to Prof. Dan McCammon for the time and advice given to me during the design and construction of a temperature programmer used in this study.

A special thanks to Cristina Reyes for her assistance with particle size measurements and sample assays and Angie Burgos for her enthusiastic help in the preparation of this thesis.

I also thank Faraneh Attarchi and Xin Pu Hou for their cooperation at all times. They made the days spent in the lab more enjoyable.

Deep gratitude is expressed to my family whose love, understanding and moral encouragement made this work possible.

Finally I gratefully acknowledge the generous financial support given to me by the Government of Puerto Rico.

TABLE OF CONTENTS

	Page
DEDICATION	ii
ACKNOWLEDGEMENTS	iii
TABLE OF CONTENTS	iv
LIST OF TABLES	xv
LIST OF FIGURES	viii
I INTRODUCTION	1
I-1 General Overview	1
I-2 Previous Work	6
I-2-1 Nucleation	6
I-2-2 Crystal Growth	14
I-2-3 Factors Influencing Crystal Shape and Size Distribution	19
I-2-3 a. Effect of Thermal History of a Solution	20
I-2-3 b. Effect of Solvent	23
I-2-3 c. Effect of Additives	26
I-2-3 d. Effect of Crystallization Conditions	29
I-2-4 Crystal Size Distributions	30
I-3 Statement of the Problem	35
II EXPERIMENTAL	36
II-1 Materials	36
II-2 Equipment	36

		Page
II-2-1	Differential Thermal Analysis	37
II-2-2	Crystal Sizing Equipment	37
II-2-3	Temperature Programmer	37
	II-2-3 a. Design Rationale	38
	II-2-3 b. Description of Equipment	39
	II-2-3 c. Temperature Measurement	41
	II-2-3 d. Specifications	41
	II-2-3 e. Operation Controls and Program Modes	42
	II-2-3 f. Temperature Sensor Calibration Procedure	46
	II-2-3 g. Operating Procedure	47
II-2-4	Crystallizing Unit	49
II-3	Methods	51
II-3-1	Purity Determination by means of Differential Thermal Analysis	51
II-3-2	Refractive Index Measurement	52
II-3-3	Density Determinations	54
II-3-4	Viscosity Determinations	55
II-3-5	Solubility Determinations	57
II-4	Crystallization Runs	58
II-4-1	Seeding	60
II-4-2	Non-linear Temperature Control	60
II-4-3	Linear Temperature Control	61
II-4-4	Desupersaturation of Oxalic Acid Dihydrate Solutions.	61

		Page
	II-4-5 Temperature-Time Profiles	63
	II-4-6 Handling and Drying of Samples	63
	II-4-7 Sampling and Sieve Analysis	65
	II-5 Measurement of Particle Shape Factors	66
	II-5-1 Particle Weight Determination	66
	II-5-2 Microscopy	68
	II-6 Identification of Reaction Product in Ethanol Solution	69
III	RESULTS	72
	III-1 Density	72
	III-2 Viscosity	76
	III-3 Solubility	87
	III-4 Thermal Histories of Solutions	103
	III-5 Desupersaturation Profiles	106
	III-6 Crystal Size Distributions	131
	III-6-1 Number Distribution of Oxalic Acid Dihydrate as a Function of z	131
	III-6-2 (b/a)-Frequencies Presented as Number Distributions	137
IV	DISCUSSION	155
	IV-1 Thermal History of Solutions	155
	IV-2 Evaluation of Growth and Nucleation Rate Parameters	155
	IV-2-1 Simulation of the Crystallization Process During Desupersaturation of Solutions	156

Page

IV-2-2 Crystal Size Distributions Predicted from the Kinetics of Nucleation and Growth 181

IV-2-3 Growth During Constant Supersaturation 203

IV-3 Effect of Temperature on Rate Constants 209

IV-4 Effect of Temperature on Standard Deviation 217

IV-5 Effect of Solvent Properties on Crystallization Kinetic Parameters 218

IV-6 Effect of Solvent Properties on Crystal Size and Shape Distributions 219

V CONCLUSIONS 235

REFERENCES 237

APPENDIX A 244

APPENDIX B 258

APPENDIX C 267

APPENDIX D 277

APPENDIX E 280

LIST OF FIGURES

Figure		Page
I-1-1	Diagram relating the nucleation rate, growth rate, mean size of crystals and super-saturation of solutions.	4
I-2-1	Solubility-supersolubility diagram.	12
I-2-2	The effect of overheating by 50°C on the width of metastability regions of solutions of KH_2PO_4 saturated at 20°C.	22
II-2-1	Schematic diagram of temperature programmer.	40
II-2-2	Front panel view of temperature programmer.	43
II-2-3	Principle of proportional control.	45
II-2-4	Crystallization Unit.	50
II-3-1	Typical Melting Curve from DTA.	53
II-4-1	Temperature-time course of a crystallization.	59
II-4-2	Typical temperature error recording during a crystallization experiment.	64
II-6-1	Proton NMR spectrum for diethyl ester oxalate. TMS was used as an internal standard and deuterochloroform as the solvent.	71
III-2-1	Plot of viscosity data at various temperatures as a function of acetone concentration in acetone/water solutions.	80
III-2-2	Plot of viscosity data for various concentrations of oxalic acid dihydrate as a function of acetone concentration in acetone/water solutions at a temperature of 44.9°C.	81
III-2-3	Arrhenius plot of viscosity for oxalic acid dihydrate-glycerine-water solutions for various concentrations of glycerine in the glycerine/water solvent system. Oxalic acid dihydrate concentration of 17.14%.	82

Figure		Page
III-2-4	Viscosity as a function of oxalic acid dihydrate concentrations of various temperatures and glycerine concentrations in the solvent.	83
III-2-5	Viscosity as a function of glycerine concentration in glycerine/water solutions for various concentrations of oxalic acid dihydrate at a temperature of 60.6°C.	84
III-3-1	Van't Hoff plots of oxalic acid dihydrate in ethanol/water solutions.	94
III-3-2	Van't Hoff plots in acetone/water solutions.	95
III-3-3	Van't Hoff plots of oxalic acid dihydrate in glycerine/water solutions.	96
III-3-4	Experimental and predicted values of the solubility of oxalic acid dihydrate as a function of 1/E.	102
III-5-1	Concentration and solubility profiles during cooling and crystallization of oxalic acid dihydrate from 15% glycerine/water saturated at 30°C.	118
III-5-2	Supersaturation profile during cooling and crystallization of oxalic acid dihydrate from 15% glycerine/water saturated at 30°C.	119
III-5-3	Concentration and solubility profiles during cooling and crystallization of oxalic acid dihydrate from 15% glycerine/water saturated at 40°C.	120
III-5-4	Supersaturation profile during cooling and crystallization of oxalic acid dihydrate from 15% glycerine/water saturated at 40°C.	121
III-5-5	Concentration and solubility profiles during cooling and crystallization of oxalic acid dihydrate from 50% acetone/water saturated at 30°C.	122

Figure		Page
III-5-6	Supersaturation profile during cooling and crystallization of oxalic acid dihydrate from 50% acetone/water saturated at 30°C.	123
III-5-7	Concentration and solubility profiles during cooling and crystallization of oxalic acid dihydrate from 50% acetone/water saturated at 40°C.	124
III-5-8	Supersaturation profile during cooling and crystallization of oxalic acid dihydrate from 50% acetone/water saturated at 40°C.	125
III-5-9	Concentration and solubility profiles during cooling and crystallization of oxalic acid dihydrate from water saturated at 30°C.	126
III-5-10	Supersaturation profile during cooling and crystallization of oxalic acid dihydrate from water saturated ato 30°C.	127
III-5-11	Concentration and solubility profiles during cooling and crystallization of oxalic acid dihydrate from water saturated at 40°C.	128
III-5-12	Supersaturation profile during cooling and crystallization of oxalic acid dihydrate from water saturated at 40°C.	129
III-6-1	Normal standard deviate as a function of: (i) z and (ii) ln z.	143
III-6-2	Normal standard deviate as a function of: (i) (b/a) and (ii) ln (b/a).	154
IV-2-1	Characteristic concentration and solubility profile during cooling and crystallization of oxalic and dihydrate.	157
IV-2-2	Schematic presentation of the crystallization process.	162
IV-2-3	Concentration profile predicted by simulation of the crystallization process as a function of J*, for G*=0.050, j=4.0, g=2.0, S_F*=90 and C_O*=108.	165

Figure		Page
IV-2-4	Supersaturation profile predicted by simulation of the crystallization process as a function of J*, for G*=0.050, j=4.0, g=2.0, S_F*=90 and C_0*=108.	166
IV-2-5	Concentration profile predicted by simulation of the crystallization process as a function of G*, for J*=8.0, j=4.0, g=2.0, S_F*=90 and C_0*=108.	167
IV-2-6	Supersaturation profile predicted by simulation of the crystallization process as a function of G*, for J*=8.0, j=4.0, g=2.0, S_F*=90 and C_0*=108.	168
IV-2-7	Concentration profile predicted by simulation of the crystallization process as a function of j, for g=1.0, G*=0.050, J*=8.0, S_F*=90 and C_0*=108.	169
IV-2-8	Supersaturation profile predicted by simulation of the crystallization process as a function of j, for g=1.0, G*=0.050, J*=8.0, S_F*=90 and C_0*=108.	170
IV-2-9	Concentration profile predicted by simulation of the crystallization process as a function of j, for g=2.0, G*=0.050, J*=8.0, S_F*=90 and C_0*=108.	171
IV-2-10	Supersaturation profile predicted by simulation of the crystallization process as a function of j, for g=2.0, G*=0.050.	172
IV-2-11	Concentration profile predicted by simulation of the crystallization process as a function of j, for g=3.0, G*-0.050, J*=8.0, S_F*=90 and C_0*=108.	173
IV-2-12	Supersaturation profile predicted by simulation of the crystallization process as a function of j, for g=3.0, G*=0.050, J*=8.0.	174
IV-2-13	Linear regression plot for the supersaturation dependence on time during crystallization of oxalic acid dihydrate from 15% glycerine/water solution saturated at 30°C.	176

Figure		Page
IV-2-14	Dependency of slope (g) on G* for simulated supersaturation profiles.	178
IV-2-15	Dependency of slope (g) on C_O* for simulated supersaturation profiles.	179
IV-2-16	Dependency of N on J*, G*, C_O* and S_F* for simulation of nucleation and growth.	182
IV-2-17	Experimental and predicted concentration profiles during crystallization of oxalic dihydrate generated by simulation of nucleation and growth rates. 15% glycerine/water saturated at 30°C.	184
IV-2-18	Experimental and predicted supersaturation profiles during crystallization of oxalic acid dihydrate generated by simulation of nucleation and growth rates. 15% glycerine/ water saturated at 30°C.	185
IV-2-19	Experimental and predicted concentration profiles during crystallization of oxalic acid dihydrate generated by simulation of nucleation and growth rates. 15% glycerine/water saturated at 40°C.	186
IV-2-20	Experimental and predicted supersaturation profiles during crystallization of oxalic acid dihydrate generated by simulation of nucleation and growth rates. 15% glycerine water, saturated at 40°C.	187
IV-2-21	Experimental and predicted concentration profiles during crystallization of oxalic acid dihydrate generated by simulation of nucleation and growth rates. 50% acetone/water saturated at 30°C.	188
IV-2-22	Experimental and predicted supersaturation profiles during crystallization of oxalic acid dihydrate generated by simulation of nucleation and growth rates. 50% acetone water, saturated at 30°C.	189
IV-2-23	Experimental and predicted concentration profiles during crystallization of oxalic acid dihydrate generated by simulation of nucleation and growth rates. 50% acetone/water saturated at 40°C.	190

Figure		Page
IV-2-24	Experimental and predicted supersaturation profiles during crystallization of oxalic acid dihydrate generated by simulation of nucleation and growth rates. 50% acetone water, saturated at 40°C.	191
IV-2-25	Experimental and predicted concentration profiles during crystallization of oxalic acid dihydrate generated by simulation of nucleation and growth rates. Water saturated at 30°C.	192
IV-2-26	Experimental and predicted supersaturation profiles during crystallization of oxalic acid dihydrate generated by simulation of nucleation and growth rates. Water saturated at 30°C.	193
IV-2-27	Experimental and predicted concentration profiles during crystallization of oxalic acid dihydrate generated by simulation of nucleation and growth rates. Water saturated at 40°C.	194
IV-2-28	Experimental and predicted supersaturation profiles during crystallization of oxalic acid dihydrate generated by simulation of nucleation and growth rates. Water saturated at 40°C.	195
IV-2-29	Cumulative distribution plot for oxalic acid dihydrate crystallized from 15% glycerine/water, saturated at 30°C. Generated curve according to Eq. (IV-2-38).	205
IV-2-30	Cumulative distribution plot for oxalic acid dihydrate crystallized from aqueous solution saturated at 30°C. Generated curve according to Eq. (IV-2-38).	206
IV-2-31	Cumulative distribution plot for oxalic acid dihydrate crystallized from aqueous solution saturated at 40°C. Generated curve according to Eq. (IV-2-38).	207
IV-2-32	Cube root of the mass crystallized as a function of time according to Eq. (IV-2-45). 50% acetone/ water solvent, saturated at 40°C.	212

Figure		Page
IV-2-33	Cube root of the mass crystallized as a function of time according to Eq. (IV-2-45). 15% glycerine/water solvent, saturated at 40°C.	213
IV-6-1	Plots of predicted vs observed t-values according to: (i) normal crystal size distributions and (ii) log-normal crystal size distributions. Glycerine/water solvent system.	221
IV-6-2	Plots of predicted vs observed t-values according to: (i) normal crystal size distributions and (ii) log-normal crystal size distributions. Acetone/water solvent system.	222
IV-6-3	Plots of predicted vs observed t-values according to (i) normal crystal shape distributions and (ii) log-normal crystal shape distributions. Glycerine/water solvent system.	227
IV-6-4	Plots of predicted vs observed t-values according to: (i) normal crystal shape distributions and (ii) log-normal crystal shape distributions. Acetone/water solvent system.	228
IV-6-5	Photomicrographs of oxalic acid dihydrate, 30/40 mesh fraction, recrystallized from (a) water, (b) 7% glycerine/water, (c) 25% glycerine/water and (d) 10% ethanol/water. T_S=40°C.	234

LIST OF TABLES

Table		Page
III-1-1	Density of Oxalic Acid Dihydrate-Water Solutions.	73
III-1-2	Density of Oxalic Acid Dihydrate-Acetone-Water Solutions.	74
III-1-3	Density of Oxalic Acid Dihydrate-Glycerine-Water Solutions.	75
III-2-1	Viscosity of Oxalic Acid Dihydrate-Water Solutions.	77
III-2-2	Viscosity of Oxalic Acid Dihydrate-Acetone-Water Solutions.	78
III-2-3	Viscosity of Oxalic Acid Dihydrate-Glycerine-Water Solutions.	79
III-2-4	Multiple Regression Analysis of the Influence of Absolute Temperature, Solvent Composition and Oxalic Acid Dihydrate Concentration on the Viscosity of the Solution.	85
III-3-1	Oxalic Acid Dihydrate Solubility in Ethanol/Water.	88
III-3-2	Oxalic Acid Dihydrate Solubility in Acetone/Water.	89
III-3-3	Oxalic Acid Dihydrate Solubility in Glycerine/Water.	91
III-3-4	Solubility of Oxalic Acid Dihydrate in Water, at Different Temperatures.	93
III-3-5	Linear Regression Analysis of the Influence of the Absolute Temperature on the Mole Fraction Solubility of Oxalic Acid Dihydrate in Ethanol-Water.	97
III-3-6	Van't Hoff Plot for Oxalic Acid Dihydrate in Acetone Water.	98

Table		Page
III-3-7	Linear Regression Analysis of the Influence of the Absolute Temperature on the Mole Fraction Solubility of Oxalic Acid Dihydrate in Glycerine/Water.	99
III-3-8	Multiple Regression Analysis of the Influence of the Absolute Temperature and the Dielectric Constant on the Mole Fraction Solubility of Oxalic Acid Dihydrate in Glycerine/Water.	101
III-4-1	Effect of Overheating Temperature and Time on the Nucleation Temperature and Mass Particle Size of Oxalic Acid Dihydrate Crystallized from Aqueous Solution. (Non-Linear Cooling).	104
III-4-2	Effect of Overheating Temperature on the Nucleation Temperature and Mean Particle Size of Oxalic Acid Dihydrate Crystallized from Aqueous Solution.	105
III-5-1	Desupersaturation of a Solution of Oxalic Acid Dihydrate in 15% Glycerine/Water, Saturated at 30°C.	107
III-5-2	Desupersaturation of a Solution of Oxalic Acid Dihydrate in 15% Glycerine/Water, Saturated at 40°C.	109
III-5-3	Desupersaturation of a Solution of Oxalic Acid Dihydrate in 50% Acetone/Water, Saturated at 30°C.	111
III-5-4	Desupersaturation of a Solution of Oxalic Acid Dihydrate in 50% Acetone/Water, Saturated at 40°C.	113
III-5-5	Desupersaturation of Aqueous Solution of Oxalic Acid Dihydrate, Saturated at 30°C.	115
III-5-6	Desupersaturation of Aqueous Solution of Oxalic Acid Dihydrate, Saturated at 40°C.	116
III-5-7	Solution Temperature at the Onset of Crystallization.	130

Table		Page
III-6-1	Individual Crystal Weights (System: Glycerine/Water, T_S = 30°C).	132
III-6-2	Individual Crystal Weights (System: Glycerine/Water, T_S = 40°C).	133
III-6-3	Individual Crystal Weights (System: Acetone/Water, T_S = 30°C).	134
III-6-4	Individual Crystal Weights (System: Acetone/Water, T_S = 40°C).	135
III-6-5	Number of Crystals of Oxalic Acid Dihydrate at the End of a Crystallization Run.	136
III-6-6	Distribution of Shape Factor (Glycerine/Water, T_S = 30°C).	138
III-6-7	Distribution of Shape Factor (Glycerine/Water, T_S = 40°C).	140
III-6-8	Distribution of Shape Factor (Acetone/Water, T_S = 30°C).	141
III-6-9	Distribution of Shape Factor (Acetone/Water, T_S = 40°C).	142
III-6-10	Crystal Size and Shape Distribution (Example Calculation). A. Crystal Size Distribution (Number).	145
III-6-11	Crystal Size and Shape Distribution (Example Calculation). B. Crystal Shape Distribution.	146
III-6-12	Crystal Size and Shape Distribution (Example Calculation). B. Crystal Shape Distribution.	147
III-6-13	Crystal Size and Shape Distribution (Example Calculation). B. Crystal Shape Distribution.	148
III-6-14	Distribution of Shape Factors (Glycerine/Water, T_S = 30°C).	149
III-6-15	Distribution of Shape Factor (Glycerine/Water, T_S = 40°C).	151

Table		Page
III-6-16	Distribution of Shape Factor (Acetone/Water T_S = 30°C).	152
III-6-17	Distribution of Shape Factor (Acetone/Water, T_S = 40°C).	153
IV-2-1	Linear Regression Analysis for the Supersaturation Dependence on Time.	177
IV-2-2	Multiple Regression Analysis Results for the Equation: $q = a' + b'G^* + d'C_O^*$.	180
IV-2-3	Multiple Regression Analysis Results for the Equation: $\ln (N) = a'' + b''C_O^* + d''S_F^* + e'' \ln J^* + h'' \ln G^*$.	183
IV-2-4	Parameter Values Used in the Simulation of the Supersaturation-Time Profiles.	196
IV-2-5	Comparison between the Experimental and Predicted Crystal Yield.	197
IV-2-6	Experimental Values of r and R and Fitted Parameter F for Oxalic Acid Dihydrate Crystal Size Distributions, According to Equation (VI-2-38).	204
IV-2-7	Results from Crystallization of Oxalic Acid Dihydrate in Two Different Solvent Systems, in the Case where the Supersaturation Is Constant.	210
IV-2-8	Linear Regression Analysis of the Cube Root of the Mass Crystallized As a Function of Time.	214
IV-2-9	Values of the Growth Rate Constants Obtained by Three Different Approaches.	215
IV-6-1	Properties of Regression Model for Predicted Versus Observed t-values as a Function of z and ln (z).	223
IV-6-2	Properties of Regression Model for Predicted Versus Observed t-values as a Function of (b/a) and ln (b/a).	229

Table		Page
IV-6-3	Values of the Geometric Mean Diameter and Standard Deviations of Oxalic Acid Dihydrate Crystal Size Distributions as a Function of Solvent and Saturation Temperature.	225
IV-6-4	Values of the Geometric Mean Elongation Ratios and Standard Deviations of Oxalic Acid Dihydrate Crystal Size Distrubutions in Glycerine/Water Solvent Systems.	230
IV-6-5	Values of the Mean Elongation Ratios and Standard Deviations of Oxalic Acid Dihydrate Crystal Size Distributions in Acetone/Water Systems.	231

I INTRODUCTION

Crystallization from solution is important in many stages of the development of a drug dosage form because crystal habit, shape and size may alter the performance of a drug substance by affecting its physical, chemical and biological properties. Prior to describing a general review of the literature, it is worthwhile to examine the effect that the micromeritics of a drug substance have on the resulting dosage form.

I-1 General Overview

Crystal habit and particle and shape size distributions affect (a) mechanical properties such as powder flow (Danish and Parrott, 1971),mixing (Carstensen and Patel, 1975), interparticle cohesion and (Van Der Zwan and Siskens, 1982), (b) interfacial properties particularly wettability (El-Gindy et al., 1982). There is also an effect on such processes as comminution (Ridgway and Rupp, 1969), compression and drying (Fowler and Glastonbury, 1959, Pilpel, 1965). Changes in dissolution rates (Florence et al., 1974, Chiou et al., 1976, Naggar et al., 1980) and changes in compaction and tablet properties (York, 1983, Shell, 1963) may result as crystal properties change. It is therefore advantageous to have a knowledge of what factors during crystallization affect particle size distribution and particle shape.

In the scale-up and development of a new drug substance, changes

in crystallization equipment type and size often occur. The last step in a synthesis is usually some crystallization step, and this is usually from solution (although sublimation is at times used). Recrystallization (and also reprecipitation) is based on the principle that when the concentration, C e.g. in moles/mole, of a solute in solution exceeds the equilibrium solubility concentration, S e.g. in moles/mole, then a driving force for a phase change exists. C-S is called the supersaturation. Supersaturation is accomplished in a number of ways, but primarily by (a) cooling, (b) evaporation of solvent, (c) the addition of a third component to reduce the solubility of the solute (precipitation) or (d) chemical reaction in a solvent in which the resulting product has a low solubility.

Nucleation and crystal growth were described by Gibbs as discontinuous changes of phase which are large in degree, but, at least initially, small in extent in space. When one phase transforms to a more stable phase, then the atoms or molecules in some region of the first phase must become arranged in the characteristic configuration of the second, if indeed such a characteristic configuration exists. A phase change resulting in crystal formation does result in such a characteristic formation. The formation of a crystal in a homogeneous fluid requires that an energy barrier be scaled. The total energy required is the sum of the work to form the particle surface and the work to form the bulk of the particle. The overall excess free energy between the small solid particle of the solute and the solute in solution is equal to the sum of the surface

excess free energy ΔG_s (i.e. the excess free energy between the surface of the crystal and the bulk of the crystal) and the volume excess free energy ΔG_v (i.e. the excess free energy between the very large crystal and the solute in solution). ΔG_s is positive, its magnitude being proportional to r^2, where r is the radius or the side length of the crystal. In a supersaturated solution ΔG_v is a negative quantity proportional to r^3. Thus, the supersaturation is the measurable quantity giving rise to phase change, namely nucleation and crystal growth.

The two phenomena compete for solute in terms of their respective dependence on supersaturation. The resulting size distribution of product crystals is determined by the amount of formed solid phase and the relationship between the competing kinetic rates. These are growth rates of individual particles and number of particles where the latter depends on the birth rate of crystal nuclei. This is schematically demonstrated in Fig. I-1-1.

A large number of factors can combine to yield the resulting crystal size distribution. Presence of impurities, nature of solvent, degree of agitation, supersaturation and mode of cooling are the factors considered most important.

While it is true that the interrelation of the above factors is quite complex, it is essential for control of the crystal population characteristics that studies be made concerning their effect on the crystallization kinetics and the product distribution. Considerable amounts of data have been published concerning crystal growth and

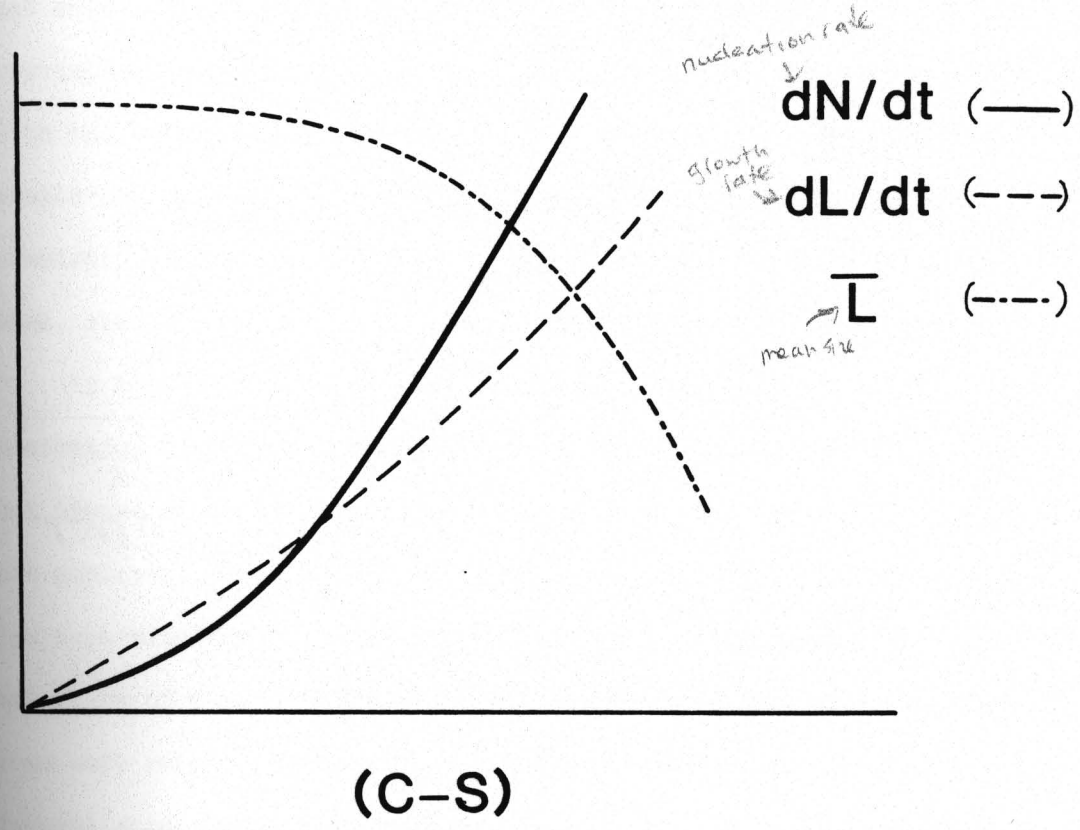

Figure I-1-1. Diagram relating the nucleation rate, growth rate, mean size of crystals and supersaturation of solutions. (After Nyvlt, 1971).

nucleation rates. Yet, few have been reported where both nucleation and crystal growth were occurring simultaneously and at realistic crystallization conditions. Most work in this area has been concerned with the effect of temperature and impurities on the growth rate of single crystals when the crystallization equipment was operating at a constant temperature and degree of supersaturation. In most early work, either nucleation or growth rate was followed, rarely both.

In addition to this, the classical equations describing growth or nucleation are based primarily on, and supported by conditions that do not always occur in a cooling crystallizer. The growth kinetics which are employed, describe the growth of single crystals in a solution of low supersaturation, while the nucleation kinetics apply to clear solutions of high supersaturation. In recent years there has been some work published in the area of mixed suspension, mixed product removal crystallization, usually referred to simply as MSMPR (Nyvlt, 1978, Randolph and Larson, 1971). In these systems growth and nucleation rates were studied by analyzing the crystal size distribution utilizing the population balance theory. Some of the limitations for the general validity of the obtained relations are due to the constraints and assumptions used in MSMPR. These assumptions and constraints are, among others: (a) steady state operation, (b) a full and uniform particle size continuum exists; and (c) constant suspension density exists. There is a lack of data relating the effect of crystallization conditions and system properties (e.g. solvent nature) on the competition between crystal nucleation and

growth and their effect on the product shape and size distributon.

In the writing and work to follow, an attempt is made to obtain clear ideas on the time dependence of supersaturation during cooling of a batch crystallizer and on how this dependence will affect crystal shape and size distributions. It is the purpose of this work to (a) study the crystal distributions of oxalic acid dihydrate crystallized from a variety of solvents; (b) to propose a model that explains this type of distribution and (c) to attempt to establish knowledge of growth and nucleation rate constants by means of the data.

I-2 Previous work

The material to follow is a survey of crystallization literature such as it applies to the thesis.

I-2-1 Nucleation

It has been shown that new crystal formation can result from homogeneous nucleation, heterogeneous nucleation and secondary nucleation. Homogeneous nucleation occurs from a solution that is pure, while in the presence of a foreign solid phase, nucleation is referred to as heterogeneous. Secondary nucleation refers to nucleation induced by the presence of suspended crystals of the solute. It may follow various mechanisms which have been divided into two groups: (a) nucleation due to abrasion and (b) nucleation due to boundary layer (Strickland-Constable, 1972; Garside et al., 1979, Mullin and Leci, 1972). Both mechanisms are still poorly understood.

If one considers the free energy changes associated with the process of homogeneous nucleation, it can be concluded that the behavior of a newly created crystalline lattice structure in a supersaturated solution depends on its size; it can either grow or redissolve depending on which process results in a decrease of the free energy of the particle. The critical size for a nucleus represents the minimum size of a stable nucleus (Nyvlt, 1971).

According to the Volmer-Becker-Doering theory, the rate of nucleation can be expressed in the form of an Arrhenius velocity equation:

$$dN/dt = A_1 \exp(-\Delta G^*/kT) \qquad \text{Eq. I-2-1}$$

where N = number of nuclei

ΔG^* = free energy of formation of a nucleus

k = Boltzmann's constant

T = absolute temperature and

t = time.

A_1 is the collision factor and is estimated for instance for the precipitation of $BaSO_4$ to be of the order of 10^{30} cm^{-3} sec^{-1} (Nielsen, 1964). The free energy ΔG^* is the sum of a bulk and a surface contribution. Taking into account the relationships connecting geometry, surface tension and the supersaturation ratio it can be expressed as

$$\Delta G^* = 16 \pi \sigma^3 v^2 / (3(kT \ln S^*)^2) \qquad \text{Eq. I-2-2}$$

where

v = molecular volume

σ = surface energy per unit area and

S^* = C/S, where

C = concentration of solute in the bulk of solution and

S = equilibrium saturation concentration of the solute.

The difficulty with the above expression is that it predicts nucleation only at extremely high supersaturations, a phenomenon not observed in most crystallization systems. Since homogeneous nucleation is not ordinarily an important phenomenon occurring, it is heterogeneous or secondary nucleation which is largely prevailing. In addition to the fact that the equation does not predict nucleation rates in a practical sense, the surface tension is usually unknown (Nielsen, 1964).

Tamman (1925) first demonstrated the abnormal nucleation characteristics of organic melts. He found that initially the number of nuclei increase with the degree of supercooling, but reached a maximum and subsequently decreased. At very high supercoolings a glassy state was frequently formed without nucleation occurring. He suggested that it was due to the sharp increase in viscosity with supercooling which restricted molecular movement and inhibited the formation of ordered crystal structures. Ubbelohde (1965) has referred to this same phenomenon and explained it on the basis of the

formation of crystalline and anticrystalline clusters. Mullin and Leci (1969) have observed a similar behavior in aqueous solutions of citric acid and their results support Tamman's view of the importance of viscosity; it is also suggested that the tendency for hydrogen bonding in this system is an added factor.

Turnbull and Fischer (1949) quantified this behavior by a modification of equation I-2-1:

$$dN/dt = A \exp\ (-16 \pi \sigma^3 v^2/(3(kT\ln S^*)^2) - \Delta G'/kT) \qquad \text{Eq. I-2-3}$$

where $\Delta G'$, the activation energy for molecular motion across the embryo-matrix interface is very large for highly viscous systems, and the other exponential term is small (e.g. at high supersaturations). $\Delta G'$ is the dominant factor in this rate equation and a decrease in nucleation rate is predicted.

Other nucleation models have been proposed which account for heterogeneous effects (Turnbull and Fisher, 1949) and for secondary nucleation (Cise and Randolph, 1972, Randolph and Larson, 1971). Correlations of these effects are rare and little success has been achieved in predicting experimental behavior.

Nielsen (1964) and Nyvlt (1968) have approximated the classical nucleation relationship (Eq. I-2-2) by a power law function of supersaturation at a given temperature:

$$dN/dt = J\,(C-S)^{j} \qquad \text{Eq. I-2-4}$$

This relation has been applied successfully to many real system (Misra and White, 1971, Carstensen, 1980). (C-S) is the supersaturation and J is the nucleation rate constant, and they can be functions of fluid properties and operating conditions such as temperature and degree of agitation (Bransom et al., 1949, Mullin, 1972).

The temperature dependence of the nucleation rate constant has been described for many systems by the Arrhenius equation (Misra and White, 1971, Genck and Larson, 1972, Nyvlt, 1971, and Wey and Terwilliger, 1980)

$$d\ln J/dT = -E_{nucl}/RT^{2} \qquad \text{Eq. I-2-5}$$

where E_{nucl} is the activation energy of nucleation. Values of 24.0 and 10.8 kcal/mole for potassium alum and potassium sulfate respectively have been reported (Cise and Randolph, 1972, Wey and Terwilliger, 1980). Negative values have been reported by Sikdar and Randolph (1976) for magnesium sulfate and citric acid and by Helt and Larson (1977) for potassium nitrate. The latter explained this phenomenon on the basis of secondary nucleation; at higher temperatures the increased surface diffusion rate and increased reaction rate deplete the fluidized layer faster than it is regenerated by fresh solute from the solution, decreasing the

secondary nucleation. They also suggest that E_{nucl} represents an overall activation energy for nucleation and that in the temperature range studied the viscosity term in Eq. I-2-3 would have the controlling influence.

Recently, Wey and Terwilliger (1980) developed an analysis that consolidates the variety of possible temperature behaviors that can occur in a continuous MSMPR crystallizer; it relates the nucleation and growth rates observed with the supersaturation, activation energies and the kinetic order. However, no temperature dependence has been observed on the kinetic order, for many systems.

Eq. I-2-4 is based on the concept of a metastable region. This was developed by Miers and Isaac (1906) in experiments with solutions of sodium nitrate. Fig. I-2-1 illustrates the results of these experiments. The solid curve represents a section of the solubility curve for a solute/solvent system. The upper dashed curve is referred to as the supersolubility curve and denotes the temperature and concentration where spontaneous crystallization occurs. This boundary is not well defined as its position depends on a number of parameters: agitation, presence of additives, rate of cooling (Ting and McCabe, 1934) and thermal history of a solution (Nyvlt, 1962, Myl, 1968 and Nakai, 1972, 1973, a,b).

The diagram can be evaluated on the basis of three zones:

-the <u>stable zone</u> which is unsaturated and where crystal growth is not possible;

-the <u>metastable zone</u> where spontaneous nucleation is

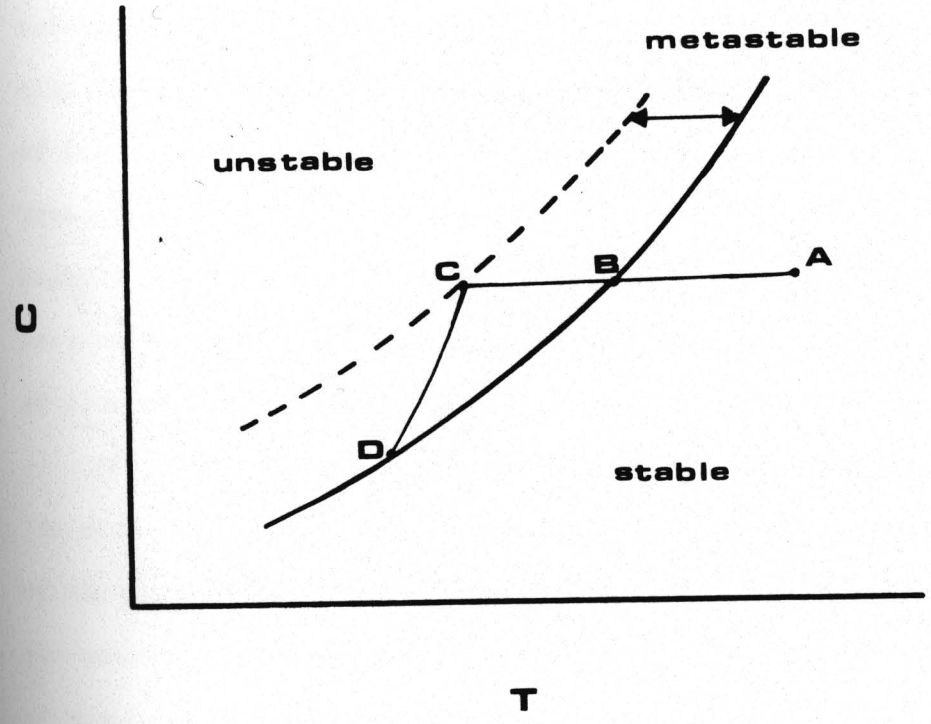

Figure I-2-1. Solubility-supersolubility diagram.

improbable, but crystal growth on a seed would occur

-the labile zone where spontaneous nucleation occurs.

When a solution represented by point A is cooled without the loss of solvent (line ABC),spontaneous crystallization will occur, when conditions corresponding to point C are attained. The concentration of the solution decreases as crystals are born and grow until the final temperature at D is reached. "Controlled crystallization" is usually achieved within the metastable zone by slow cooling and seeding of the system (Mullin (1972)); there is no sudden deposition of fine crystals because the system does not enter the labile zone.

Efforts have been made to correlate, more or less empirically, the adjustable parameters of nucleation with some physical properties of the crystallizing substance (Nyvlt, 1968, Sohnel, 1976). Methods for measuring nucleation kinetics consist essentially in an evaluation of model crystallization experiments based on the population density balance (Randolph and Larson, 1971) or in an evaluation of experimental data on the metastable zone width (Nyvlt, 1968). The latter has proved extremely useful for assessing the nucleation behavior of agitated supersaturated solutions, and data measured in this manner are now available for a large number of compounds (Nyvlt et al., 1970, Mullin and Jancic, 1979). Briefly, the method consists of measuring the maximum undercooling allowed by an agitated solution before it nucleates: the solution is cooled at a constant rate and the onset of nucleaton is detected visually or by electron particle counter. The slope of the line obtained by plotting the maximum

undercooling of the solution and the cooling rate, on logarithmic coordinates, represents the order of the nucleation process. This then makes possible the calculation of the nucleation rate constant. For aqueous solutions the order of nucleation ranges from 1 to 9 (Nyvlt, 1978).

I-2-2 Crystal Growth

Once nuclei are formed in a supersaturated solution, they begin to grow into crystals of visible size. The mechanism of crystal growth from solution requires that solute be transported to the crystal surface and then oriented into the crystal lattice. Early theories of crystal growth, reviewed by Mullin (1972) considered only the diffusional part of the process, probably because of observations made on systems where diffusion was rate determining. By assuming that solute molecules diffuse through a thin laminar film of liquid adjacent to the crystal face, the mass growth rate may be expressed by:

$$dm/dt = (D/x)\ A\ (C-S) \qquad \text{Eq. I-2-6}$$

where D is a diffusion coefficient, x is a film thickness and A is the surface area of the crystal; (C-S) is the degree of supersaturation and is thought of as the driving force for growth.

The theory that crystal growth is simply a diffusional process has obvious weaknesses. Since the thickness of the laminar film

depends on the relative solid-liquid velocity, Eq. I-2-6 implies that no limiting value of growth rate would be achieved as the film thickness is reduced. Also a substance generally dissolves at a faster rate than it grows, which disagrees with the mechanism of pure diffusion.

The diffusion theory was modified by Berthoud (1912) to include a first order surface reaction, giving the following equation:

$$dm/dt = (DA/(x + (D/G))) (C-S) \qquad \text{Eq. I-2-7}$$

where G is the reaction rate constant. For a rapid surface reaction, G is large and Eq. 1-2-7 reduces to Eq. I-2-6. If the diffusional resistance is low, x is small and the surface reaction is controlling. Although Eq. I-2-7 provides a qualitative description of the two step growth process, the assumption of a first order surface reaction cannot be generalized to all materials (Mullin, 1972).

Frank (1949) in his classic work, showed that if a crystal contains a dislocation which is self-perpetuating, then the often occurring large discrepancy between theoretically estimated and experimentally observed growth rates of a number of materials can be explained. Nielsen (1964) points out that the dislocation growth spiral may be rate determining for very small crystals at measurable supersaturations, but not for large crystals except at very low supersaturations. Some authors (Nyvlt, 1971, Mullin, 1972, Strickland – Constable, 1968) have treated the previously mentioned cases of

diffusion, surface reaction and dislocation controlled growth in detail. Since the exact growth mechanism of a substance is frequently in doubt, growth rate is often expressed as a function of supersaturation in the following fashion:

$$dm/dt = G\ A\ (C-S)^g \qquad \text{Eq. I-2-8}$$

where G here is an overall crystal growth coefficient. The exponent, g, is usually referred to as the order of growth and some authors claim that no fundamental significance should be attached to it whereas others claim that the growth mechanism can be inferred from the value of g and from the dependence of G on growth conditions (i.e. temperature, solution velocity). For example the growth process can be considered to be diffusion controlled if g is equal to one and G is influenced by the solution velocity. When g is greater than one and G is not influenced by the solution velocity, then the growth process is most likely controlled by a surface integration mechanism (Nielsen, 1964, Misra and White, 1971). For many substances, mainly inorganic, crystallizing from aqueous solution results in growth rate orders in the range of 1 to 3 (Nyvlt, 1978; Randolph and Larson, 1971).

Temperature increases generally lead to an increase in crystallization rate (Nyvlt, 1971). The magnitude of the activation energy for the growth process lies in the range from 3 to 24 kcal/mole (Helt and Larson, 1977; Wey and Terwilliger, 1980).

Nielsen (1964) developed the technique of chronomal analysis and applied it to the precipitation of a range of materials. (The term "chronomal" implies the integrated form corresponding to the assumed growth law, with time as the dependent variable). The method, then, consists of determining the chronomal and plotting it for given supersaturations as a function of time. A straight line graph would confirm the growth law assumed. However, several major assumptions have limited the applicability of the method. For instance it assumes that the number of nuclei is fixed and that the crystals have identical size and shape. Cardew (1982) has developed this technique further to include size distributions and seedings. Some of the assumptions of the earlier model were dropped, but the fixed number of nuclei and no growth dispersion were retained.

Alexandru (1969) developed a macroscopic model for the habit of crystals grown from solution. By defining a normal habit as a time approximation of a real one and assuming a power growth law as in Eq. I-2-8, the surface area and mass of a crystal of an arbitrary shape can be determined at every moment.

Crystal growth rates may be expressed in various ways. Linear face growth rates for example, are best determined from direct observation of the individual crystal faces (Nyvlt and Matuchova, 1976, Mullin and Garside, 1967a). On the other hand, when a large number of crystals are grown in an agitated vessel, the growth rate is more conveniently expressed as an overall mass deposition rate (Mullin and Garside, 1967b, Garside et al., 1973) calculated from the increase

in crystal mass over the growth period. These quantities can be interrelated by the use of volume and surface shape factors.

McCabe and Stevens (1951) observed that each crystal in a suspension grows at the same rate irrespective of its size if it is subjected to the same conditions. Exceptions to this principle, known as McCabe's L law, have been found in industrial crystallizers (Randolph and Larson, 1971). Factors causing this size dependence of growth rate are poorly understood. The effect in some cases has been explained on the basis of the higher settling velocities of larger crystals, which reduce their resistance to diffusion and consequently they grow faster than smaller crystals. Various empirical models intended to account for this phenomenon have been proposed (Bransom, 1960, Nyvlt, 1979). However, if agitation is effective and the velocities of crystals of different size relative to the solution are the same, the law generally holds (McCabe and Stevens, 1951).

Many different experimental techniques have been employed to facilitate growth rate measurements. These include following growth rates by direct microscopic observation (Mullin et al., 1970); overall growth rates of single crystals fixed in an agitated vessel (Botsaris and Denk, 1970); overall growth rates in multiparticle systems (Randolph and Larson, 1971, Nyvlt, 1978) by analysis of the crystal size distribution during continuous crystallization. Calorimetric methods have also been used successfully to measure growth rates and supersaturation (Pekarek et al., 1975, Shrivanek et al, 1975).

The changes in solution concentration that occur during

crystallization are of considerable interest if models relating the kinetic rates to supersaturation are to be developed. A number of methods have been used to measure the solution concentration during crystallization. Among them are: viscosity, density, chemical analysis, conductance and refractive index determinations. The last two methods have been the most used. The former is based on the dependence of conductivity on concentration of many aqueous solutions of salts. (The conductivity usually passes through a maximum). The method has been used in systems involving sparingly soluble salts (Nyvlt, 1978; Dugua and Simon, 1978). Accurate refractive index measurement has been obtained by Mullin and Leci (1972) with an immersion refractometer modified so that it could be applied to liquids with suspended particles.

I-2-3 Factors Influencing Crystal Shape and Size Distribution

Although crystals can be classified according to the elements of symmetry into systems (e.g. regular, orthorhombic), faces of a particular crystal may be developed to different extents. Habit is the description of the appearance of a crystal. The shape of a growing crystal depends on the rate of growth of the individual faces, which is influenced by both the equilibrium surface energy anisotropy (Gibbs, 1928) and the non-equilibrium kinetic process of atomic attachment (Burton, 1949). Theoretical work based on thermodynamic and kinetic considerations have been performed (Cline, 1981, Julg and Debrick, 1983, Aquilano et al., 1983). Nevertheless the phenomenon is

complicated, owing to the fact that one must distinguish the equilibrium form from the growth habit. The approach to the problem was first based on obtaining the equilibrium shape of the crystal by minimizing the surface free energy and finally including an interfacial resistance. In this manner equations are obtained for the shape change during crystal growth. Another approach by Julg and Debrick (1983) considered a direct study on a molecular scale using quantum chemical methods.

If the environment of a growing crystal affects its external shape without changing its internal structure, a different habit results. Nearly all manufactured and natural crystals are distorted to some degree: an elongated growth of a prismatic habit gives a needle-shaped crystal (acicular habit) and a stunted growth gives a flat plate-like crystal (tabular or flaky habit). Some factors that modify crystal habits will be described. These include: the conditions of growth, the nature of the solvent and the presence of a cosolute or a cosolvent.

I-2-3 a. Effect of Thermal History of a Solution

It has been observed, for many years, that solutions being kept several hours at temperatures sufficiently elevated above the equilibrium temperature, show lower nucleation ability than solutions kept close above the equilibrium temperature (Frenkel, 1955; Myl, 1968, Nyvlt, 1962). It has been recognized that the metastable zone of a solution is influenced appreciably by its thermal history (time

and temperature of overheating). The effect of overheating by 50°C on the width of the metastability region of solutions of KH_2PO_4 saturated at 20°C is presented in Fig. I-2-2 (Myl, 1968). Smid et al.(1962) determined a relationship between the degree of temperature undersaturation and supersolubility with four kinds of aqueous salt solutions. Birchall and Davey (1981) compared the effect of overheating a saturated solution of sodium chloride on the maximum undercooling with the undercooling in the presence of polysaccharides as additives. Nyvlt (1962) studied the same type of effect for the case of urea.

Various possible explanations have been offered for the effect of thermal history on nucleation: (a) the heating inactivates heterogeneous nucleation centers, which dissolve as a result of inactivation (Birchall and Davey, 1981) or (b) there is a decrease in the degree of association of subcritical nuclei. The explanation of the effect has usually been based on the latter (Nyvlt, 1962, Nakai, 1972). Nyvlt (1962) has tried to explain the effect of thermal history on the structure of solutions by the assumption that molecules of the solute form subcritical clusters even in undersaturated solutions. If a solution is kept at a temperature higher than saturation for a very long time, the cluster size distribution corresponds to equilibrium conditions. On subsequent cooling the structure of the solution slowly changes, i.e. the mean cluster size increases. This delay results in the observed widened metastable region. An analysis of experiments on the metastable zone width has

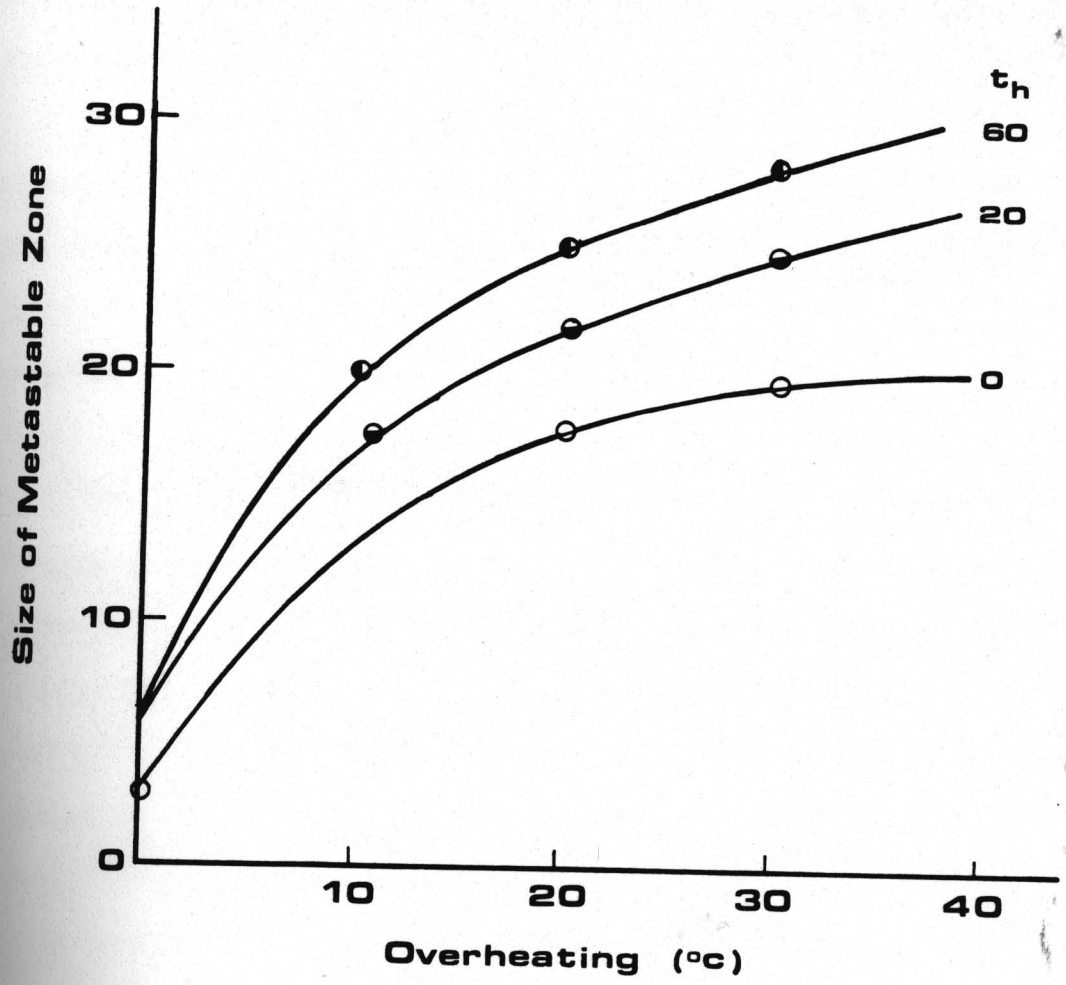

Figure I-2-2. The effect of overheating by 50°C on the width of metastability regions of solutions of KH_2PO_4 saturated at 20°C. (After Myl, 1968).

shown that kinetics of change of the distribution of aggregates of a characteristic size can be approximated by an equation of first order.

Nakai (1972) in his study based on considerations of the kinetic theory of liquids, derived simple equations describing the effect of the overheating temperature on the induction periods of nucleation and verified this theoretical result by experiments with aqueous sodium chlorate solutions. Making use of thermal history in the case of copper in industrial crystallization has been very effective (i.e. resulted in widening the metastable zone and depressing nucleation). Consequently the mean particle size of the product was increased (Nakai et al., 1973a, b). Recently Nyvlt and Pekarek (1980) have studied the thermal history effect on the dynamics of the crystallization process. The spontaneous crystallization of a closed sample of supersaturated solution of $KClO_3$ with defined thermal histories was measured calorimetrically, and the results were compared with simulation of the crystallization process, where the kinetics of nucleation are described by means of the induction period.

At the present time, no predictions are possible for the behavior of sytems in general; a greater number of systems than those available would have to be studied. So far, only preliminary experiments have been done concerning the effect of thermal histories on the crystal size distribution parameters.

I-2-3 b. Effect of Solvent

The shape of a crystal is a function not only of the internal structure of the crystal itself, but also of the interaction between

the atoms (molecules) in the various faces of the crystal with the solvent. For instance, naphthalene crystallizes in the form of needles from cyclohexane and as thin plates from methanol. Pentaerythritol crystallizes in the form of tetragonal bipyramids from water and tetragonal plates from acetone (Pamplin, 1975, Wells, 1946). This difference is explained on the basis of affinity of the solvent to be adsorbed on certain faces of the crystal resulting in the development of large faces of that type on the final crystal, since the most prominent faces are those with the lower growth rates.

Garti and Tibika (1980) achieved crystal habit modifications of nitrofurantoin, an antibacterial drug (used in urinary infections), crystallized from formic acid mixtures. The length to width ratio varied by a factor of 2 when crystallization was carried out from pure formic acid as opposed to a mixture of formic acid with water or with ethanol.

The subject of polymorphism is not within the scope of this work, but could be the result of the crystallization phenomena of an extensive number of compounds (Haleblian, 1975). Polymorphism is associated with different internal packing arrangements of atomic components or molecules, or differences in the orientation of atoms or molecules at lattice sites. Several studies have examined the relationship between polymorphism with solvent and crystallization conditions. The crystal structure modification of stearic acid was found to depend on solvent, polarity and cooling rate (Garti et al., 1980, Sato and Okada, 1977).

Using Eq. I-2-4 to correlate the nucleation rate to the width of the metastable zone, corresponding to the maximum allowable undercooling, the nucleation rate can be expressed in terms of the rate of creation of undercooling:

$$dN/dt = k\,(dS/dt)(dT/dt) \qquad \text{Eq. I-2-9}$$

where dS/dT is the slope of the solubility curve and

dT/dt is the cooling rate.

Sohnel and Nyvlt (1976) have shown that

$$\Delta C_{max} = (dS/dT)\ \Delta T_{max} \qquad \text{Eq. I-2-10}$$

These equations imply that for a given rate of cooling, the rate of nucleation of a solute in various solvents may increase with increasing solubility power of the solvent.

Leci et al. (1981) studied the correlation between the maximum attainable undercooling and solubility in solutions of 1,4-di-t-butylbenzene in a series of solvents with a wide range of polarity. They found that as the solubility power of the solvents increased, so did the value of ΔC_{max} for any cooling rate. Garti et al. (1981) observed that the length to width ratio of the crystals varied from 1.2 to 20, and that it was correlated with the maximum attainable supersaturation. Similar findings were reported for nitrofurantoin in formic acid mixtures (Garti and Tibika, 1980). In

addition the crystal dimensions decreased considerably with an increase in supersaturation.

I-2-3 c. Effect of Additives

Traces of chemical additives are often used to suppress or promote nucleation and/or promote better crystal growth and habit. Very few quantitative data have been published on the effect of additives on nucleation kinetics. One published example is the effect of various soluble additives on the size distribution of potassium nitrate crystals (Shor and Larson, 1971). They showed that by using $Cr(NO_3)_3$ as an ionic additive, the nucleation rate was decreased, and the growth rate was increased. This resulted in a crystal product of larger size. This is consistent with the view that large, highly charged anions block nucleation sites on the surface of the crystal. Three surface active agents, methylamine hydrochloride, dodecylamine hydrochloride and a fluorocarbon were also used, and found to increase nucleation rates and decrease growth rates. The order of nucleation was increased in presence of surfactants and unaffected by the additive concentration.

No generality should be attached to these results, however. Other quantitative studies include the effect of traces of foreign ions, Pb^{+2} for instance, on sodium and potassium chloride crystallizations (Botsaris et al., 1972) of the surfactants sodium-dodecylbenzene sulfonate and cetyldimethylbenzene ammonium chloride on sodium triphosphate (Troost, 1968). Additives are usually

found to be quite specific in their effect on nucleation and surface active agents are known to inhibit, rather than accelerate nucleation.

A general explanation of the phenomenon of nucleation suppression by added impurities is not available, but certain patterns of behavior have emerged. For example the higher the charge of the cation, the more powerful the inhibiting effect. There also often appears to be a threshold concentration of impurity, above which the inhibiting effect may be weakened, and this may be associated with critical micellar concentrations. In the case of high molecular weight substances the mode of action is quite different from that of ionic (e.g. cationic) additives. The former may have their main action on the heteronuclei, rendering them inactive by adsorbing on their surface. This has been demonstrated for sodium chloride crystallized from aqueous solutions in the presence of polysaccharides (Birchall and Davey, 1981), whereas the cations may act as structure breakers in solution. Botsaris, Denk and Chua (1972) report an interesting effect of the action of Pb^{+2} on the nucleation of potassium chloride. If the dissolved impurity suppresses spontaneous nucleation, secondary nucleation can occur if the uptake of the impurity by the growing crystals is significant. In this case a seed crystal creates an impurity concentration gradient about itself, and the impurity concentration near the crystal surface becomes lower than the concentration in the bulk solution. If it is reduced low enough then spontaneous nucleation can occur.

Surfactants in the crystallization medium can similarly modify

crystal habit. The work of Michaels and Colville (1960) demonstrated that crystallization of adipic acid in aqueous solutions containing high concentrations of anionic surfactants produced long, thin needles, and in the presence of cationic surfactants thin, flaky plates. Fairbrother and Grant (1978) reported similar findings with the use of n-alkanoic acids as impurities. These effects were attributed to selective adsorption of the additives on the various faces, altering their relative growth rates. These were correlated with the hydroxyl densities on the faces. Anionic agents appeared to be physically adsorbed, whereas cationic agents appeared to be chemisorbed. It was also observed that surfactants in general exhibited a greater retarding influence on the growth of very small crystals than on large ones, and it was suggested that growth from dislocations is less sensitive to the influence of adsorbed contaminants than is the growth by two dimensional nucleation.

In these studies, nucleation rates have been inferred by examination of the precipitated phase by application of the population balance, and growth rates by time dependence of growth on a given face. It is clear that it is dangerous to generalize on the effect of foreign, soluble material on nucleation and growth kinetics, since only the relative values of these affect the crystal size distribution. In order to clearly determine the kinetic factors that are altered, it is necessary to measure supersaturation precisely during the crystallization experiment.

I-2-3 d. Effect of Crystallization Conditions

The rate of cooling of a solution has been well documented to affect not only the width of the metastable zone, but also the crystal growth, in this way modifying the shape of the product (Mullin, 1972, Randolph and Larson, 1971). Rapid cooling, for example, will cause preferential growth of a crystal in one particular direction, leading to the formation of needles, a habit which permits rapid heat dissipation.

Mullin and Leci (1972) studied the desupersaturation characteristics of seeded, metastable solutions of citric acid, and the effect of seed size, surface area and supersaturation. By increasing seed size for a given surface area, the induction period was increased and the desupersaturation rate was decreased. The desupersaturation rate increased as the initial seed surface decreased. An increase in the initial level of supersaturation decreased the induction period and increased the desupersaturation rate.

The influence of agitation on nucleation and crystallization is very complex. Although it is generally agreed that mechanical disturbances can enhance nucleation, it has been shown by Mullin and Raven (1962) that an increase in the intensity of agitation may reduce the tendency of the system to nucleate. This was explained by assuming that agitation can lead to the disruption of subcritical size nuclei in the solution. Agitation can have an impact on the overall crystal growth mechanism, e.g. from diffusion to integration control

(Hixson, 1944, Mullin and Amatavivadhana, 1967).

The effect of viscosity on nucleation rates has already been introduced. Its effect on crystal growth has been reported by some workers (Jenkins, 1925, Mullin, 1972, Tamman,1925). These studies have been on single crystal growth from solution or growth from melts and most often the viscosity used is that of the saturated solution.

I-2-4 Crystal Size Distributions

Phase changes in solution crystallization result in a collection of discrete particles of various sizes, shapes and ages. This is determined by the particle birth rate, growth rate and when applicable death rate. It has been most frequently characterized as some function of crystal size (Randolph and Larson, 1971, Carstensen and Sheridan, 1979). It is a difficult matter to characterize a population from a sample of particulates of irregular shapes, and in general particle sizes are taken as the linear dimension which best characterizes the material within the context of their typical shape (Riley, 1976).

Alexandru and Motoc (1972) studied the size distributions of Rochelle salt crystals as a function of growth conditions (temperature, saturation, impurities). They point out the importance of distribution representation with reference to mass, linear parameter characteristics of the crystal shape, ratios of these parameters and habit factor, in order to explain the nucleation and growth process. Analytical functions were fitted to mass and linear parameters, the former one giving limited success. The distributions

were asymmetrical and in some cases had a secondary maximum. They explain this by assuming both primary and secondary nucleation.

Blickle and Halasz (1973) have studied the relation between the crystal growth kinetics and particle size distribution of crystals produced from solution. Their conclusions are that (a) an increase in primary nucleation rate constants decreases both particle size and scatter of the distributions, (b) an increase in secondary nucleation rate constants increases the scattering while the particle size decreases, (c) an increase in diffusion and surface reaction rate constants decreases the scattering and the particle size increases, and (d) an increase in lattice defect growth rate constants increases both mentioned characteristics.

Takeuchi et al. (1979) found good agreement between the overall growth rates in a fluidized bed crystallizer and linear growth rates of a single crystal. Using an empirical size dependent growth rate model and the seed size distribution with a sine function, the particle size distribution was determined as a function of time and it was found to correlate with experimental data.

Larson and Randolph (1969) have developed an analysis for use of the population balance in relating crystallization kinetics with size distributions in a continuous mixed suspension, mixed product removal crystallizer (MSMPR). This is achieved by representing the distribution of sizes in terms of population density, which is the slope of a cumulative number versus size curve. It may also be obtained in terms of a limit

$$n = \lim_{L \to 0} (\Delta N / \Delta L) = dN/dL \qquad \text{Eq. I-2-11}$$

where n is population density (number of particles/ length) and ΔN is the number of particles in the size increment ΔL. Certain restrictions are imposed: perfect mixing, no classification at withdrawal, breakage assumed negligible and uniform shape factor. The following steady state distribution results:

$$n = n^{o} \exp(-\Delta L/Gt) \qquad \text{Eq. I-2-12}$$

where n^{o} is the nucleus population density, L is the particle diameter and G and t are steady state growth rate and residence time.

A method for determining growth and nucleation rates from steady state data has been developed by Branson et al. (1949) and Larson and Randolph (1969). From the plots of log n versus L, it is possible to calculate the growth rate from the slope. A relationship between nucleation rate and supersaturation of the form of Eq. I-2-4 is used. Nucleation rate can be related through a common dependency on supersaturation to growth rate, which permits the determination of the kinetic order of nucleation. This method has been very successful in relating crystal growth and nucleation processes to the product size distribution.

Misra and White (1971) applied the population balance method to batch crystallization of aluminum trihydroxide by seeding a supersaturated solution at constant temperature. By following the

size distribution during a run by Coulter counter, and measuring the supersaturation of the solution, they were able to calculate growth rates and nucleation rates and relate these to the models of crystal growth and nucleation that would describe the desupersaturation rates and the variation in the number of particles with time.

Carstensen and Sheridan (1979) correlated growth and nucleation kinetics under isothermal conditions with the product size distribution. They assumed a power law growth rate of second order with respect to the supersaturation and that the supersaturation as a function of time follows an exponential decay. With these assumptions and using shape factors to correlate the linear dimension growth rate with the mass deposition rate they were able to explain a log-normal distribution of particles.

Nyvlt (1974) proposed a model that relates the effect of the mode of the cooling on the time dependence of supersaturation and on how this dependence affects size distribution of crystals produced in a batch crystallizer. Their results of the model calculations based on data for the system ammonium sulfate-water, demonstrated that the mean crystal size is increasing from the non-controlled to the linear programmed cooling and for higher cooling rates smaller crystals were obtained. They also found that as the initial supersaturation increased, the maximum of the differential size distribution curve was shifted to smaller values and a more uniform product was obtained. This was explained by nucleation taking place mainly at the beginning of the process while during the process crystal growth (mostly) took

place.

The log-normal distribution law has been applied by several authors (Carstensen, 1981, Herdan, 1960) to the distribution of sizes of particles obtained by crystallization and milled particles. A log-normal distribution follows the relation:

$$f(\ln d) = 1/(\ln(s_g)\ (2\pi)^{0.5})\ \exp(-(\ln d - \ln(d_g))^2/(2(\ln s_g)^2)) \qquad \text{Eq. 1-2-13}$$

where d_g is the geometric mean diameter, s_g is the geometric standard deviation and f(ln d) is the number of particles having diameters, d, between ln d and lnd + d(lnd).

Materials showing a normal size distribution are rare. They are found mainly as particulate substances produced by processes such as condensation and precipitation (Irani and Callis, 1963). The normal distribution of particles is given by

$$f(d) = 1/(s(2\pi)^{0.5})\ \exp(-(d-d_{avg})^2/(2\ s^2)) \qquad \text{Eq. I-2-14}$$

where d_{avg} is the arithmetic mean diameter and s the number standard deviation. Several empirical equations have also been proposed to represent the distribution data when the above mentioned relationships failed. One of the most frequently used ones is the Rosin-Rambler distribution law:

$$R = 100\, e^{-b x^n} \qquad \text{Eq. I-2-15}$$

or in linearized form:

$$\ln(\ln(100/R)) = \ln b + n \ln x \qquad \text{Eq. I-2-16}$$

where R is the oversize cumulative distribution percentage, x is the particle size, b is a measure of the spread and n a constant, characteristic of the substance.

In the literature reviewed, no reported effort has been made to correlate the product crystal size distributions with the kinetics of nucleation and growth from solutions in a cooling crystallizer.

I-3 Statement of the Problem

It is the purpose of this study to:

1. Study the effects of thermal history and solvent nature on the crystal size distributions of oxalic acid dihydrate,

2. develop a model that explains the type of distribution obtained and

3. establish knowledge of the growth and nucleation rate constant from the data.

II EXPERIMENTAL

To accomplish the aims of this work the following experiments were necessary: (a) melting point determination by differential thermal analysis (DTA), (b) refractive index measurements, (c) density determinations of solutions, (d) viscosity determinations, (e) solubility determinations, (f) crystallization studies via measurement of the temperature and concentration change during the process and (g) particle size distribution measurements.

II-1 Materials

Oxalic acid dihydrate (Analytical Reagent grade) was obtained from Mallinckrodt Inc. (Paris, Kentucky). Glycerine was obtained from Aldrich Chemicals (Milwaukee, Wisconsin) and was redistilled at low pressure at 134-135°C. Acetone was obtained from M.C.B. (E.M.Industries, Gibbstown, N.J.), and was doubly redistilled. Ethanol (U.S.P.) dehydrated was obtained from U.S. Industrial Chemicals Co. (Division of National Distillers and Chemical Corporation, New York, N.Y.), and was used as received. Water was doubly redistilled with potassium permanganate and sodium hydroxide.

II-2 Equipment

In order to elucidate the crystallization process in solution, it is necessary to consider several factors that affect the environment in which the crystals grow and to quantitate the product

characteristics. The creation, control and measurement of some of these will be described.

II-2-1 Differential Thermal Analysis

A Thermal Analyzer, TA 2000 (Mettler Instruments, Princeton, N.J.) was used for the purpose of determining sample purity, and to ascertain identity of morphology. The system determines the heat flow to a sample as it is heated, cooled or kept at constant temperature. The heat flow (mcal/sec) to the sample is converted into an electrical signal by means of a differential temperature thermopile. The signal is transmitted to a recorder to be evaluated.

II-2-2 Crystal Sizing Equipment

To determine particle size distribution, a set of 5 inch, U.S. Standard Sieves was used in conjunction with a Nikon Polarizing Microscope, Model POH-II (Nikon Inc., Garden City, N.Y.). All samples were sieved in the same manner and for the same length of time with a Cenco-Meinzer Sieve Shaker (Central Scientific Co., Division of Cenco Inc., 2600 S. Kostner Ave., Chicago, ILL). This type of shaker uses an electromagnetically induced high speed, short stroke vibration with a rheostat to vary the intensity of the sieving action.

II-2-3 Temperature Programmer

The section to follow is divided up into the following sections: design rationale, description of equipment, specifications,

operation controls, operating procedure and temperature sensor calibration.

II-2-3 a. Design Rationale

In the majority of crystal growth processes it is necessary to effectuate and control temperatures above and below room temperature. In fact, temperature is unquestionably a universal parameter which is manipulated by crystal growth process operators to achieve their experimental objectives. It is, therefore, useful to have a means of controlling and recording thermal histories.

An instrument that would allow for the above mentioned considerations was designed and constructed on this location. We have developed such a system and have used it with considerable success over a period of years. We do not claim it to be novel, however, it does contain a number of features which together contribute to an accurate, reliable and simple way of controlling the crystallization experiment.

In developing the design for the temperature programmer, we were basically concerned with the following criteria related to experimental factors:

- the magnitude of the operating temperature
- the available heating and cooling methods
- the required power for heating and cooling
- the heating and cooling rates

- the requirement of programming temperatures
- the crystallization environment (e.g. volume of solutions, water bath)
- the efficiency of energy transfer
- the availability and suitability of components
- the cost and convenience of utilization of the equipment.

Consideration of these factors led to the development of the apparatus shown diagrammatically in Fig. II-2-1. A detailed description of the electrical circuits is given in Appendix A.

II-2-3 b. Description of Equipment

The temperature programmer consists of a digital set point generator with high and low limit circuits. Temperature can be programmed upscale or downscale in a linear fashion and may be changed or stopped and restarted at any time. Transistor switches are used to drive 24 volts, 250 psi, solenoid valves (Skinner Electric Valve, New Britain, Connecticut) connected to the water and steam lines. A solid state relay is also included in the circuitry, that would allow for the use of a resistance type electric breaker of up to 2300 watts (115 V, 10 A). An integrated circuit temperature sensor is used, that can monitor the temperature inside the crystallization vessel. Proportioning controls and rate-of-change feedback allow for stable temperature control of the process while heating and cooling are applied to a water bath the contents of which are circulated through

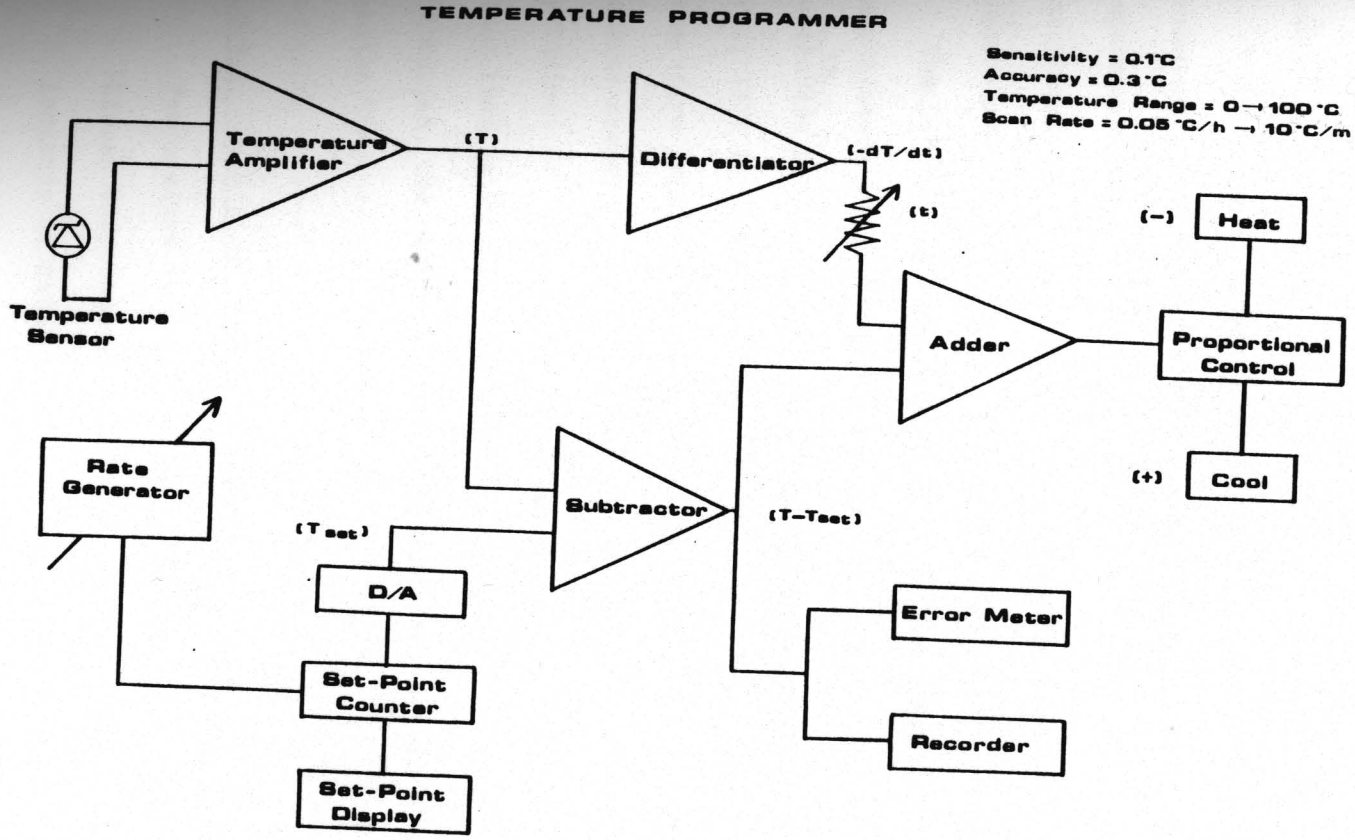

Figure II-2-1. Schematic diagram of temperature programmer.

the jacket of the crystallization vessel.

II-2-3 c. Temperature Measurement

The choice of a measuring device requires consideration of parameters such as accuracy of the measured magnitude, operating temperature range, simplicity, ease of calibration, fragility and cost. Based on these criteria an integrated circuit temperature sensor that behaves like a zener diode was the one of choice.

The bandgap voltage reference variation with temperature of a zener diode makes it possible to use it as a transducer for temperature measurement. The LM335 (made by National Semicondutor Corp., 1177 Kern Ave., Sunnyvale, CA) is a convenient two-terminal temperature sensor that generates an output voltage proportional to absolute temperature. It provides a "temp" output with a linear coefficient of +10 mV/^{o}K. It comes with an initial accuracy better than $\pm$1^{o}C, and it is externally trimmed. After calibration, the device will have higher accuracy (0.3^{o}C). It operates from -10 to + 100^{o}C.

II-2-3 d. Specifications

Temperature range	0 to 100^{o}C
Linear temperature rates	0.05^{o}C/hour to 10^{o}C/min
Accuracy of rates	stable to 1%
Proportional band	adjustable from 0 to 20^{o}C
Rate-of-change feedback	adjustable from 0 to 20 min

Temperature sensor	Integrated circuit based on zener diode
Accuracy	$0.3^{\circ}C$
Sensitivity	$0.1^{\circ}C$

II-2-3 e. Operation Controls and Program Modes

Details of the front panel controls are illustrated in Fig. II-2-2

Program Modes:

Scan-set: This allows for resetting of the program or adjustment of the control point. A fast and slow switch provides quick and correct setting of the desired display temperature. Temperature can be programmed up scale or down scale with the up-down switch.

Rate Selector: Program rates are continuously adjustable via a 10 turn dial, over a variety of spans calibrated directly in $^{\circ}C$/min or $^{\circ}C$/hour ($0.05^{\circ}C$/hour up to $10^{\circ}C$/min).

Temperature Limits: This program mode stops the temperature scan at the desired limit during up scale movement (high limit) or down scale movement (low limit).

Temperature Display: The set temperature is displayed with seven segment light emitting diodes. It affords continuous indication of the current set-point-temperature to the nearest tenth of a degree.

System Constants: For precise temperature control, proportional power switching is employed. The duty cycle of the power supplied to the load is varied with the magnitude of the temperature

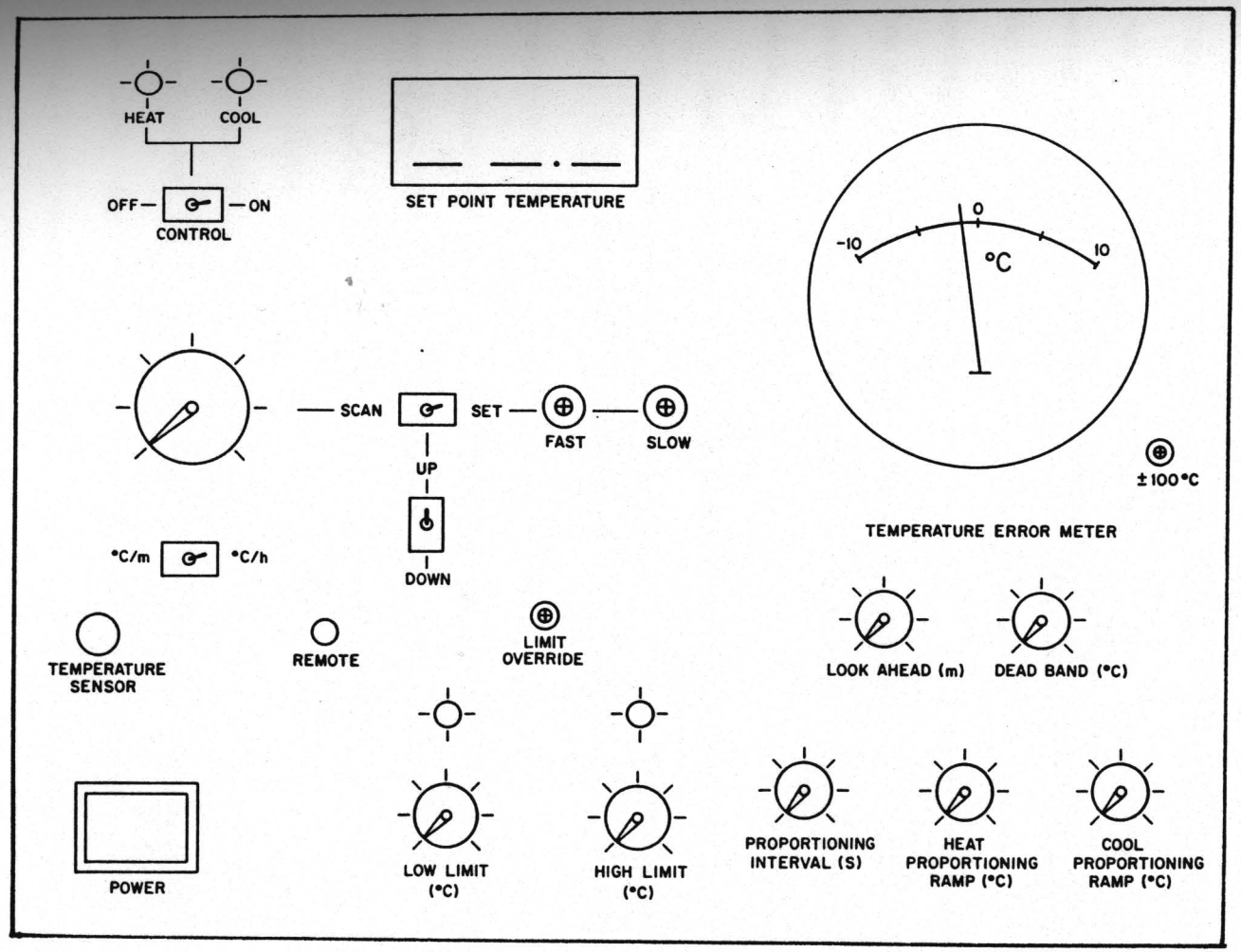

Figure II-2-2. Front panel view of temperature programmer.

error and its rate of change. For example, when the temperature setting is increased in an "on-off" type of controller, full power (100-per-cent duty cycle) is supplied to the system. This effect results in significant temperature excursions because there is no anticipatory circuit to reduce the power gradually before the actual set temperature is achieved. However, with the proportional control technique, less power is supplied to the load (reduced duty cycle) as the error signal is reduced (sensed temperature approaches the set temperature). Fig. II-2-3 illustrates the principle of proportional control.

Dead Band: This defines a temperature range over which the heating or cooling source will not be activated. A small dead band is useful to avoid having the heating and cooling turned on simultaneously.

Proportioning Ramp: This defines the temperature deviation over which proportional cooling and heating is performed.

Proportioning Interval: This sets the period for the proportioning cycle.

Look Ahead: To control temperature overshoot in systems with large thermal lag times, the rate of heating or cooling is reduced if the system temperature is approaching the set point at a high rate. During a programmed temperature scan, this will produce a constant temperature lag behind the set point of

$$T = (dT/dt)(t_{LA}) + (T_{DB}) \qquad \text{Eq. II-2-1}$$

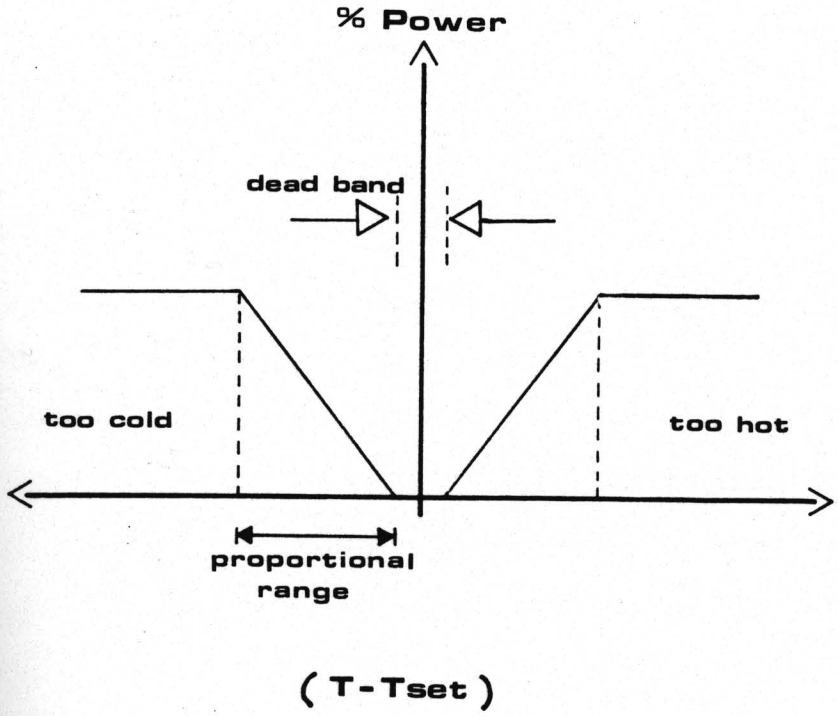

Figure II-2-3. Principle of proportional control.

where

(dT/dt) = scanning rate (^{o}C/min)

t_{LA} = look ahead time (min)

T_{DB} = dead band interval (^{o}C)

Valve Switch: This allows for setting the desired temperature program without activating the solenoid valves.

Error Meter: The temperature deviation, the difference between the set-point-temperature and the measured temperature, is indicated on the scale of $\pm$ 10^{o}C or $\pm$ 100^{o}C.

Chart Recorder: A recorder (Linear, 17282, Eastman Ave, Irvine, CA 92714) is connected to the error meter and provides a way of keeping a file of the temperature histories of the solutions over the entire crystallization run.

II-2-3 f. Temperature Sensor Calibration Procedure

The procedure to follow is required if the sensor, operational amplifier or 10 volt reference is changed:

1. The sensor is placed in an ice-bath. (The temperature sensor should be inside a thin glass tube filled with a liquid with a low dielectric constant, such as mineral oil). Mineral oil was used in this work.

2. The "zero" trim is adjusted for 0.00 volts at TP(1).

3. The sensor is placed in a bath at an accurately known temperature between 50 and 100 ^{o}C.

4. The "scale" trim is adjusted for -0.0625 (T) volts, at TP(1), where T is the bath temperature in ^{o}C.

If the set point generator has already been calibrated, then the above procedure may be done without a voltmeter by setting the set-point to 0.0^{o}C for step two and adjusting the "zero" trimmer for zero temperature error, indicated on the error meter. At step four, the set-point is set to the same temperature as the bath, and the "scale" trimmer is adjusted for zero error.

II-2-3 g. Operating Procedure

Referring to the points enumerated above, the operation of the system is as follows:

(i) The solenoid valves for the steam and cold water or electric heater should be connected in the back panel of the instrument.

(ii) With the valve switch in the OFF position and the temperature sensor plugged into the jacket connector in the front panel, the power of the instrument is turned ON. The set-point-temperature display should read 25.0^{o}C.

(iii) With the program on the SET mode, the temperature is dialed with the FAST and SLOW button and the UP/DOWN switch, until the desired set-point-temperature is read on the display.

(iv) If the temperature is to be lowered or raised in a linear fashion the rate should be set on the dial with the switch set to (^{o}C/min) or (^{o}C/hr) as appropriate. The temperature limit

dials can be set at this time. Initial temperature can be set beyond the limits by holding down the override button. Once a limit is reached, the scan will be stopped and the light above the limit dial will go on.

(v) The temperature sensor is placed in position, where the process of interest needs to be monitored (e.g. vessel with saturated solution).

(vi) The look ahead dial is set at the expected thermal time constant of the system.

(vii) Proportional controls are set to the desired interval over which proportional heating or cooling will take place.

(viii) The valve switch is turned to the ON position. When heat is supplied to the system the red light is ON, and a green light lights up when the cold valve is open.

(ix) If only constant temperature control is desired the program mode switch is left at the SET position. When linear temperature rates are to be generated, the system is left at the SET mode until the temperature error is constant and then the mode switch is put in the SCAN position.

Note: The set-point-temperature display will show the temperature generated during scanning. Once the system catches up with the cooling or heating, a constant temperature deviation should be observed.

(x) Adjustments of proportioning controls and look ahead is performed. If the temperature overshoots the desired temperature, the

system requires a longer look ahead time; if the temperature oscillates about the set temperature it requires a larger proportioning range.

II-2-4 Crystallizing Unit

The solution is contained in a 3000 ml, 3 neck jacketed flask (ACE Glass, Inc., 1430 Northwest Boulevard, Vineland, N.J. 08360). A precision ground button type stirring shaft, 10 mm in diameter, with a ground joint bearing prevented the loss of solvent. Agitation was provided by a teflon blade (19 x 60 mm) and it was driven by a 150 rpm dissolution test stirrer, model 163 (Hanson Research Corporation, Northridge, CA). With this stirring rate, temperature gradients do not develop within the solution, and it is below the point where nuclei start to be destroyed. An integrated circuit temperature sensor (LM 335) connected to the temperature programmer, was used with a thermometer adaptor with a ground joint at the bottom and a threaded nylon bushing at the top to tighten the seal. A condenser was used, to prevent solvent loss by evaporation.

The solution temperature is controlled via the external 30 liter water bath. The bath temperature is maintained by electric heater or steam, and cold water valves that allow flow through copper coils immersed in the water. The water from the bath was continuously circulated through the crystallization vessel with a centrifugal pump (Micro Pump, 1035 Shary Court, Concord, CA). The crystallization unit is shown in Fig. II-2-4.

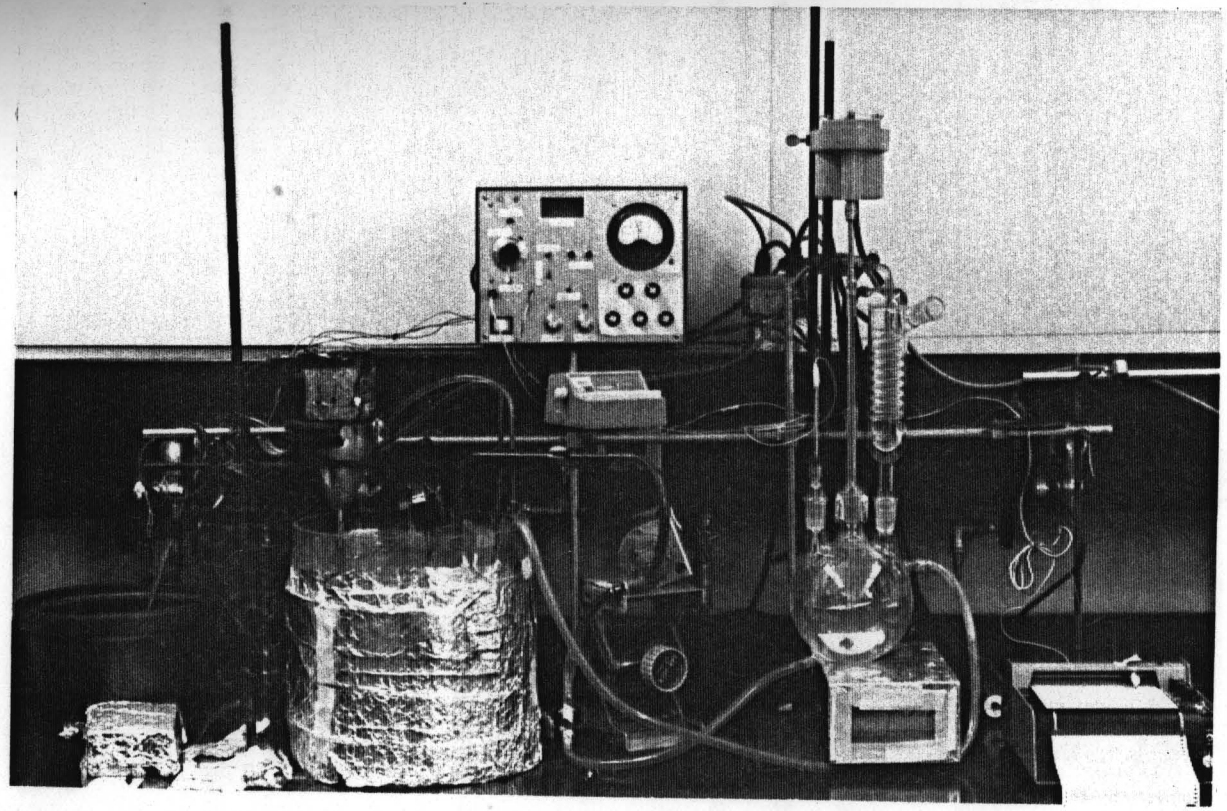

Figure II-2-4. Crystallization Unit.

II-3 Methods

The experimental procedures and methods used in this study are described in the sections to follow:

II-3-1 Purity Determination by Means of Differential Thermal Analysis

The instrument was calibrated with indium (99.99% purity and a melting point of 156.6°C). The sample temperature was obtained by correcting the furnace temperature for thermal lag. This lag was determined from the slope of the leading edge of the indium endotherm, which was found to be 0.4 min. Then

$$T_p = T_f + (\Delta U/S) - 0.4(dT/dt) \qquad \text{Eq. II-3-1}$$

where T_p and T_f are the sample and furnace temperatures respectively; S (100 μV/°C) is the thermoelement slope; dT/dt (°C/min) is the heating rate and ΔU (μV) is the DTA signal which is sometimes negligible. In this latter case

$$T_p = T_f - 0.4\ (dT/dt) \qquad \text{Eq. II-3-2}$$

According to Van't Hoff's law the melting point depression is directly proportional to the mole fraction of impurity (at low impurity concentration), i.e.

$$X_2 = (\Delta H/R\ T_o^2)/(\Delta T) \qquad \text{Eq. II-3-3}$$

where X_2 is the mole fraction of the impurity in the liquid phase

ΔT is the melting point depression (^oK)

T_o is the melting point of the pure substance (^oK)

R is the gas constant (1.987 cal/ K-mole)

ΔH is the heat of fusion.

The value for ΔH is obtained by determining the area under the melting curve. This area is proportional to the heat absorbed by the sample during fusion. The procedure used was as follows: The sample was weighed directly into a DTA sample crucible and then sealed. The closed crucible was inserted in the DTA cell of the Mettler TA 2000 system and heated at a rate of 5^oC/min. Fig. II-3-1 shows a typical melting curve.

Samples of oxalic acid dihydrate recrystallized from different solvent systems were tested and melting points compared with literature values.

II-3-2 Refractive Index Measurement

The Abbe refractometer (Bausch and Lomb Optical Co., Rochester, N.Y.) measures the critical angle of refraction relative to a glass prism, and was used to determine concentrations of binary solvent mixtures, to ascertain correctness of composition. Both prisms were

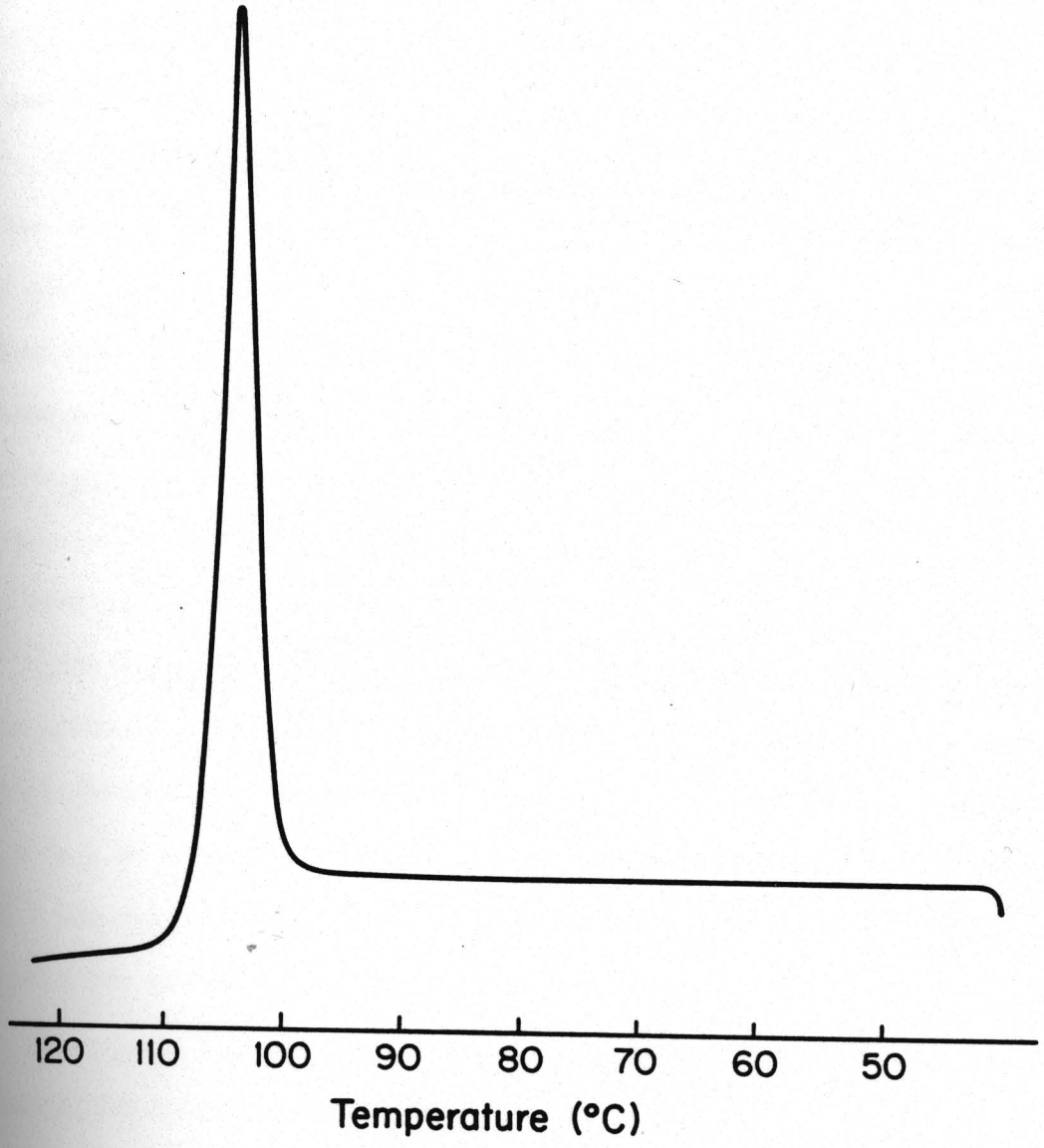

Figure II-3-1. Typical Melting Curve from DTA.

mounted in a jacket through which thermostated water was circulated. The temperature was controlled to $\pm 0.2^{\circ}C$ to realize maximum accuracy of the instrument (n_D to $\pm$ 0.0002). The scale reads directly in n_D. The instrument was used with daylight.

After cleaning the prism surfaces with distilled water and soft lens paper, it was rinsed with the liquid under investigation. A drop of the liquid was then placed on the ground surface and the two prisms were locked together. Time was allowed for establishment of temperature equilibrium; with slow motion of the alidade the sharp critical boundary crossed exactly through the intersection of the cross hairs, and the reading was then recorded. The reproducibility of individual readings is $\pm$ 0.0001.

The instrument was calibrated with distilled water by measuring the difference δn between the known n-value of the standard and the scale reading n'. Numerical corrections are applied to all readings, i.e. $n = n' + \delta n$. All readings were done at a temperature of $20^{\circ}C$ and the values obtained compared with literature values to obtain the concentration of the solvent mixture.

II-3-3 Density Determinations

Densities of the various concentrations of oxalic acid dihydrate in the three solvent systems were measured in 25 ml Weld type pycnometers. The pycnometer was initially filled to bring the liquid level about half way up the throat of the reservoir; in this manner the pycnometer will be "full" after thermostating at the higher

temperatures used for density determination. A parafilm cover was put in position to prevent evaporation from the exposed liquid surface. The pycnometers with wire loops were hung in a constant temperature bath with the main body below the surface of the water. When temperature equilibrium had been reached (2 hours) the cover was removed and the capillary plug was inserted. Any excess liquid on the tip of the plug was wiped off with a piece of filter paper, care being taken to avoid removing liquid from the capillary in the process. The pycnometer was then removed from the constant temperature bath, wiped dry with a lintless cloth and weighed on an analytical balance. In this fashion, duplicate determinations were made of the liquid required to fill the pycnometers at various temperatures of the constant temperature bath, both for water and for each of the solutions used. The volume of the pycnometer was obtained by use of density figures published in literature (Int.Crit.Tables).

II-3-4 Viscosity Determinations

Viscosities of binary mixtures of the solvents with oxalic acid dihydrate were measured using Ostwald capillary viscometers #50 obtained from Sargent-Welch (P.O.Box 1076, Skokie, Ill.).

Solutions of oxalic acid dihydrate in the various solvent systems were prepared by weight. Ten ml of the solution were poured into clean viscometers and allowed to equilibrate to the desired temperature in a water bath for 2 hours. Flow times were measured in duplicate and they were all greater than 100 sec.

Flow times were measured at a number of temperatures and viscosities determined by the following equation

$$\eta_1 = (\rho_1 \, t_1 \, \eta_2)/(\rho_2 \, t_2) \qquad \text{Eq. II-3-4}$$

where

ρ = density (g/ml)

t = flow time (sec)

η = viscosity (mp).

The subscript 2 stands for the calibration solvent (water).

To avoid measurement of densities at all combinations of solvents and temperature, in order to calculate the viscosity, densities were measured for some solutions and temperatures, as described in section II-3-3 and compared to ρ-values calculated by the following relation:

$$\rho = \frac{(\rho_1 \, \rho_o)}{(f_1(\rho_o - \rho_1) + \rho_1)} \qquad \text{Eq.II-3-5}$$

where f_1 = fraction of oxalic acid (g dihydrate/g solution

ρ_o = density of solvent (g/ml)

ρ_1 = density of oxalic acid dihydrate (g/ml)

ρ = density of the solution (g/ml)

This equation is based on the assumption that the specific volume of the mixture (v) is additively composed of the specific volumes of

the solvent (v_o) and of the solute (v_1), i.e. on the assumption that

$$v = f_1 v_1 + (1-f_1)(v_o) \qquad \text{Eq. II-3-6}$$

Viscometers were calibrated with water. The viscosity of the solutions was determined at a number of temperatures over the range 25 to 60°C, in order to obtain viscosities of supersaturated solutions by extrapolation.

II-3-5 Solubility Determinations

It is evident that to characterize a crystallization, knowledge of solubility of the solid in the solvent in the given temperature range is required. Solubility determinations were therefore carried out.

The solubility of oxalic acid dihydrate was determined in the particular solvents used in the study by using a shaker bath (Aquatherm Water Bath Shaker, Model G86, New Brunswick Scientific Co., Inc., 1130 Somerset St., New Brunswick, N.J. 08903). An excess of solid and 10 ml of the appropriate solvent were placed in an ampule which was then sealed. The ampule was placed in the shaker bath thermostated to the desired temperature ($\pm$ 0.2°C), and shaken for 96 hours. Samples were then withdrawn and aliquots were removed with pre-weighed syringes (B.D. Luer-lok tip, 5 cc syringe, Becton, Dickinson and Co., Rutherford, N.J. 07070). They were then weighed,

and the sample weight of oxalic acid dihydrate determined by difference. The total contents were diluted with water and assayed titrimetrically with sodium hydroxide, using phenolphthalein as indicator. Runs were carried out in quadruplicate and results were averaged.

The solvent systems used are glycerin/water, acetone/water, and ethanol/water. The mixed solvents were prepared by weight and refractive index measurements were done to ascertain the composition of the binary mixtures.

II-4 Crystallization Runs

The binary solvents were prepared by weight and filtered through a 0.45 μm Millipore filter (Millipore Corporation, Bedford, MA 01730). Once the desired initial temperature had been achieved within the crystallization flask, a weighed amount of oxalic acid dihydrate was added, followed by 350 g of solvent.

The general temperature-time course of a recrystallization run is shown in Fig. II-4-1. The suspension of oxalic acid dihydrate in the respective solvent was heated from room temperature to T_H. At time t_1 the saturation temperature, T_S, was reached, and theoretically the oxalic acid dihydrate should go into solution at this point. It would do so if it were kept for a sufficiently long time (dissolution rate controlled), but in crystallization practice, the system is heated to the higher temperature T_H to assure dissolution within a reasonable length of time. This practice was

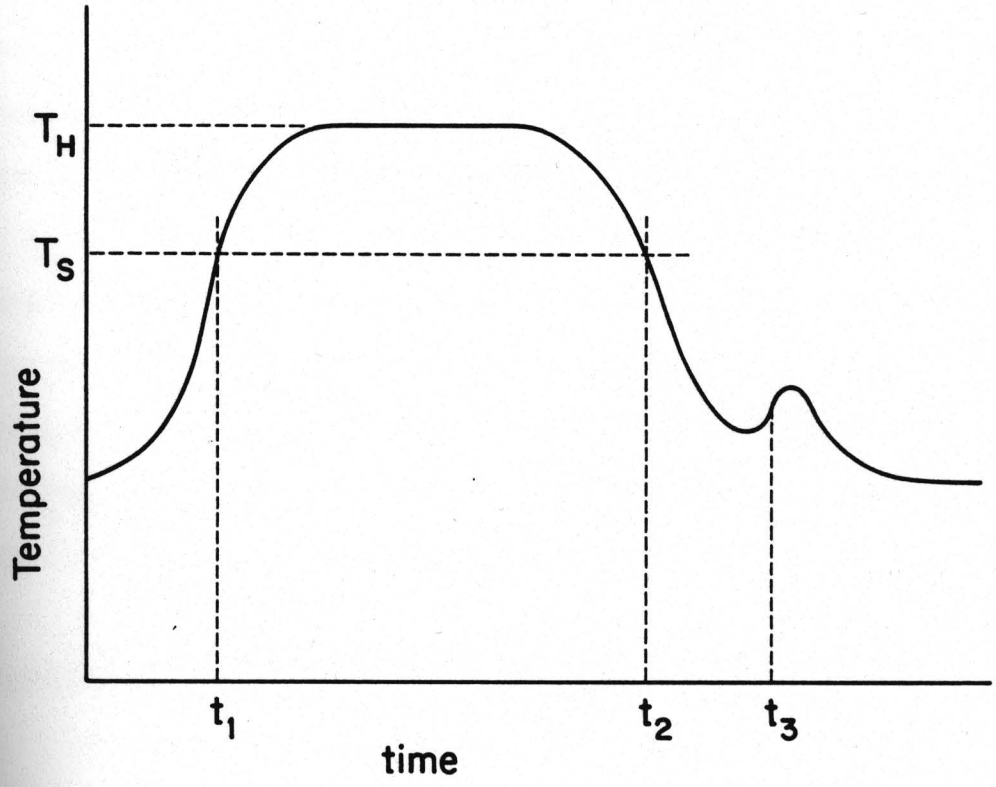

Figure II-4-1. Temperature-time course of a crystallization.

followed in this study as well, and the system was kept at the higher temperture T_H for a period of time, the curing time, and then cooled. Making reference to the figure, precipitation theoretically should start at time t_2 ($T = T_S$), but supercooling always occurs, and precipitation will start at a later time, t_3.

Two kinds of experiments (based on the shape of the cooling and heating rates) were done, in order to elucidate the influence that the overheating temperature and the curing time of the solutions might have on the crystal size distribution. In one case the temperature was changed in a linear mode, in the second case it was changed in a non-linear mode.

II-4-1 Seeding

Seeding was employed in some of the experiments where the effect of the solvent was being studied. Seeds were well defined oxalic acid dihydrate crystals chosen from a 10/20 mesh cut. The solutions were seeded with three crystals at a point during the temperature scanning where the temperature was $2^{\circ}C$ below saturation.

II-4-2 Non-Linear Temperature Control

Solutions were made of oxalic acid dihydrate in water at different concentrations to represent various degrees of undersaturation at different elevated temperatures. Hot water from a thermostated bath was pumped into the jacket of the crystallization flask. As soon as the solution had reached the desired temperature,

time was taken to allow for various curing times. Cold water was next pumped into the jacket to bring the solutions into the domain of supersaturation. Once the final temperature was reached it was kept there for one hour.

II-4-3 Linear Temperature Control

Another set of experiments was carried out by heating and cooling in a linear fashion. The rate of temperature changes was controlled by the temperature programmer described previously (Section II-2-3). To keep the cooling time short, because changes in the structure of the solution could occur, the solution (saturated at temperature T) was held at $0.5^{o}C$ above the saturation temperature for one hour. The temperature was then raised to $T + \Delta T_H$ for a duration of t_H minutes. Afterwards it was cooled with a cooling rate of $40^{o}C$/hour. Heating and cooling rates were the same throughout this type of experiment.

In a third series of experiments where the solvent effect was being studied, the temperature of the solution was raised $5^{o}C$ above saturation for one hour. The solutions were then cooled at a rate of $10V^{o}C$/hour to a final temperature of $24^{o}C$, where they were kept for one hour. These crystallization runs were done by seeding the solutions as described in Section II-4-1.

II-4-4 Desupersaturation of Oxalic Acid Dihydrate Solutions

A crystallization is completely described when we know the

particle size distribution, and perhaps the individual shapes. However, it is difficult to obtain information from the final distribution concerning the finer details of what happens during the crystallization process. The advancement of this reaction can be followed as a function of time by measuring the changes in solution concentration.

Desupersaturation studies may be approached from two different angles: by considering either the mass deposition or the fall in solution concentration as the crystals are born and grow. The difficulty with the former method is that periodic size analysis of the growing crystals would have to be made, and this was not possible with the present system, due to the inconvenience of separating the crystals at different times and temperatures. The other possible method in this case was to measure the concentration changes occurring during crystallization.

Solution samples were removed from the crystallization vessel, through glass wool placed in a piece of tygon tubing attached to the tip of a pre-weighed syringe. The sample weight was obtained by difference. The total content was diluted with water and assayed titrimetically with sodium hydroxide, using phenolphthalein as indicator. Runs were carried out in duplicate for some solvents with very good reproducibility.

Samples were taken at close time intervals in order to profile the desupersaturation curves. The time and temperature profiles allow calculation of the solubility at each point.

The solvent systems used for this study are water, 15% glycerine/water and 50% acetone/water at two saturation temperatures each, viz. 30 and 40°C.

II-4-5 Temperature-Time Profiles

The signal recorded from the temperature programmer is $(T-T_{set})$, which is the temperature error as a function of time. Fig. II-4-2 depicts a typical example (i.e. T_{error} as a function of time). To calculate the actual temperature, (T), as a function of time the following equations were employed:

$$T = T_{set} + T_{error} \qquad \text{Eq. II-4-1}$$

$$T = T_o + ((dT/dt)/(dx/dt))\ x + (dT/dy)\ y \qquad \text{Eq. II-4-2}$$

where T_o = initial temperature (°C)

dT/dt = scanning rate (°C/min)

dx/dt = chart speed (cm/min)

dT/dy = recorder sensitivity (°C/cm)

x = displacement on the horizontal axis

y = displacement on the vertical axis.

II-4-6 Handling and Drying of Samples

Once the crystallization experiments were finished, the crystals were separated from the mother liquor in the following fashion: The

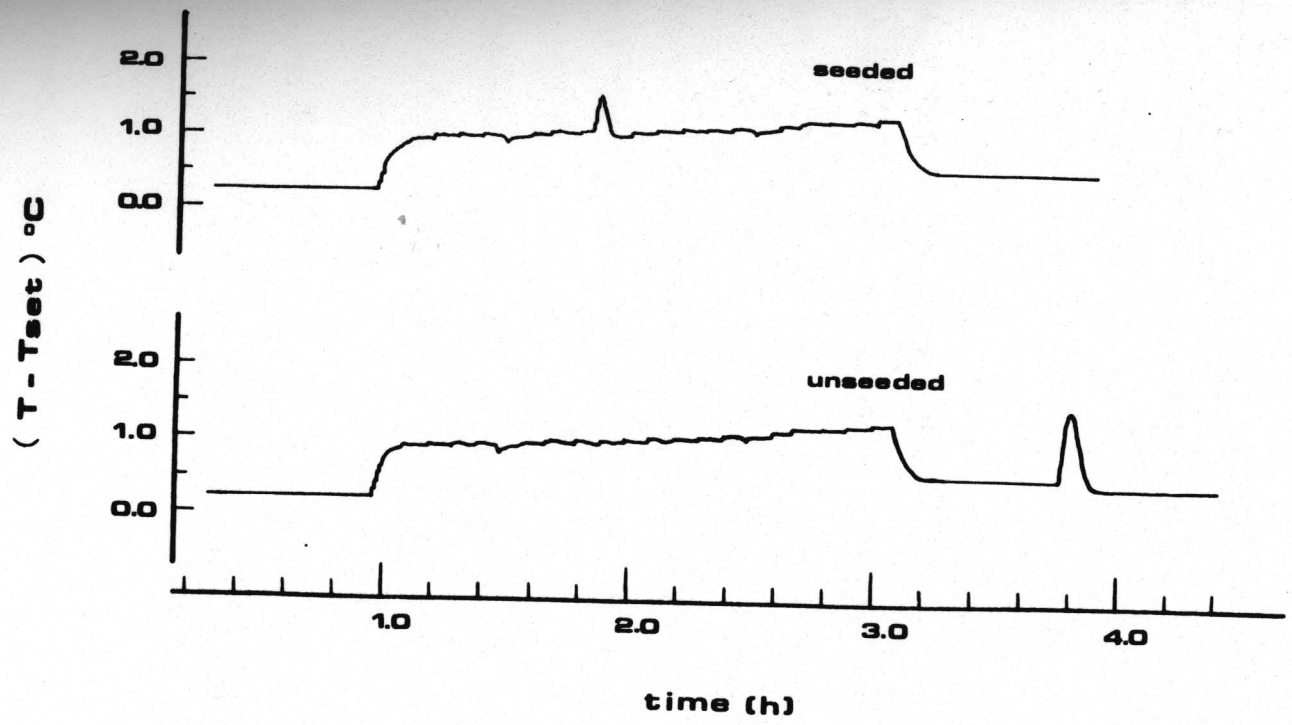

Figure II-4-2. Typical temperature error recording during a crystallization experiment.

suspension was poured into a Buchner funnel and the solvent was removed by vacuum into a suction flask. The crystals were dried under a flow of filtered air. The relative humidity of this air was measured with a sling psychrometer. If the relative humidity was below 13%, then the sample was stored in a desiccator over a saturated solution of magnesium chloride hexahydrate, which exhibits a relative humidity of 33% (based on ideality) at room temperature.

II-4-7 Sampling and Sieve Analysis

Great care was taken to obtain samples of the dry oxalic acid dihydrate crystals that were truly representative of the lot being tested. The sampling procedure that was followed was to cone and quarter a pile of crystals. This was particularly applicable to crystals obtained at high saturation temperatures, since these give a greater yield.

The test sample size was determined based on a table for suggested bulk volume of test sample for sieve analysis (ASTM-STP 447). To determine the sieving time, a sample of the appropriate weight was sieved for 5, 10, 15 and 20 minutes. The end-point was set up on the basis of shaking the nest of sieves until not more than 0.5% of the material on the finer sieves passed that sieve in a 5 minute period.

The following procedure was then adopted as a standard: 15 g of dry crystals were sieved in a nest of 5 inch sieves and compared to the same sieving in standard sieves. Shaking was provided by a

Cenco-Meinzer sieve shaker. Each sample was shaken for 10 minutes. Sieves of the following mesh and aperture sizes were used, where the apertures are expressed in micrometers, in parenthesis: 20 (840), 30 (590), 40 (420), 50 (300), 60 (250), 80 (177), 100 (149) and the pan. Each size fraction was removed from the sieve by inverting the sieve and tapping the side of the frame. The contents were placed on weighing paper and weighed to the nearest 0.1 mg.

II-5 Measurement of Particle Shape Factors

Particle size distribution cannot alone describe a particle population, and for some purposes it becomes necessary to measure the particle shape within closely sized ranges. Some instances of the use of shape factors are in estimating approximate surface areas, calculating the number of particles in a size range and investigating the variation of particle shape with size. Their experimental determination is laborious: since it may be necessary to sample, count and weigh several thousand closely sized particles.

The procedures used in this study are based on microscopy and particle weight determination.

II-5-1 Particle Weight Determination

If the average weight of a fairly monodisperse powder is to be determined, it is possible, for larger particles, to simply select crystals and weigh them. For finer particles, however, this is not possible, and with a population (sample) of particles, the question

then becomes, how does one separate out and count a certain number of particles? Once this is accomplished, it is of course possible to obtain the total weight of the particles, and get the weight per particle by averaging. The method of selecting the particles randomly, and being able to count them is then the problem. The procedure used here is based on a method reported for coal particles (Harris, 1960). It involves the use of a sieve which is the limiting screen for the closely sized particles under investigation. The sieve has attached to its underside a weighed strip of masking tape of known area. Consequently, the number of covered apertures can be calculated.

The particles within a sieve fraction were dusted over this "working surface" and generally one particle per aperture was retained by the adhesive film. However, a few exceptions were noted. If a wide range of shapes occurred within a size fraction, it was found that the number of particles per aperture would vary from none to two or three. While these frequently averaged one per aperture, a few sample rows were counted under a magnifying glass. In other instances where particles were elongated, a screen greater than the limiting screen for the fraction was used.

With the larger particle sizes a simple precaution was necessary; because the tape must cover an integral number of apertures, it was preferable to measure the effective area of the working surface after dusting with particles and re-weighing then made possible the determination of the average weight (and volume) of a single particle.

II-5-2 Microscopy

Since sieve analysis is based on the second largest dimension of a particle, microscopy was used to better define the shape of the crystals.

An eyepiece micrometer disc reticule (Bausch and Lomb Optical Co., Rochester, N.Y.) with a 5 mm scale ruled on the disc, divided into 50 parts of 0.1 mm each, was used. The apparent length of each scale division of the micrometer disc depends on the total magnification to be used. Consequently, the scale of the disc must be calibrated for each combination of eyepiece and objective used.

The procedure for calibrating the scale was as follows: A stage micrometer slide (Spencer Hemocytometer, American Optical Corp. Buffalo, N.Y.) was placed on the microscope stage. The accurately ruled squares on the slide were brought into sharp focus. Its image would appear superimposed on the scale of the eyepiece micrometer disc. The dimension of each division of the eyepiece micrometer scale was determined in terms of the scale of the stage micrometer for a specific magnification. It is necessary only to determine how many divisions or parts of a division of the eyepiece micrometer scale equal one division of the scale of the stage micrometer. The ratio of the two is, then, the calibration constant. Once determined for a specific combination of eyepiece and objective it was used subsequently without repeating the procedure. The true size of a crystal, length and breadth, were determined by multiplying the size

measure on the eyepiece micrometer scale, by the calibration constant.

Microscopic sizing of crystals was performed on all sieve fractions. A sample of closely sized crystals of oxalic acid dihydrate was placed on a microscope slide. In some cases two or three drops of mineral oil were added in order to take advantage of the increase in refractive index difference between the particles and fluid. The largest dimension and second largest dimension perpendicular to the former were measured, fourteen to twenty crystals within each sieve fraction.

Photomicrographs were taken to provide a more thorough study of the different crystals of oxalic acid dihydrate. A 35 mm SLR Minolta Camera was used. A microscope adapter was built for mounting the camera on the microscope body tube. This allowed for a light-tight connection between camera and microscope. The lens of the camera was removed and the camera body was held rigidly on the adapter. Image focusing was achieved through microscope adjustment. The film used was Kodak Plus-X Pan.

II-6 Identification of Reaction Product in Ethanol Solution

Part of the experimental strategy was to investigate the effect of solvents and of viscosity on recrystallization outcomes. To this end, binary solvent mixtures of water and various solvents were used. Ethanol was one of these solvents, and gave rise to peculiar results. An interaction was suspected, and the following identification procedure was used: A solution of oxalic acid dihydrate in 92%

ethanol/water was extracted exhaustively with hexane. The organic layer was then extracted with an aqueous saturated solution of sodium bicarbonate to remove the oxalic acid. It was then washed with water, dried with anhydrous sodium sulfate and concentrated with a Rota-evaporator. A pale yellow oil was obtained, and this was distilled at 176-177^{o}C. This is in agreement with the boiling point for the diethyl ester of oxalic acid (Merck Index, 1980). In addition an NMR spectrum was obtained with a VARIAN EM90 (90 MHz). The internal standard reference was tetramethylsilane (1% in deuterochloroform). The signals shown in Fig.II-6-1 correspond to that expected for the ester (Sadtler, 1973).

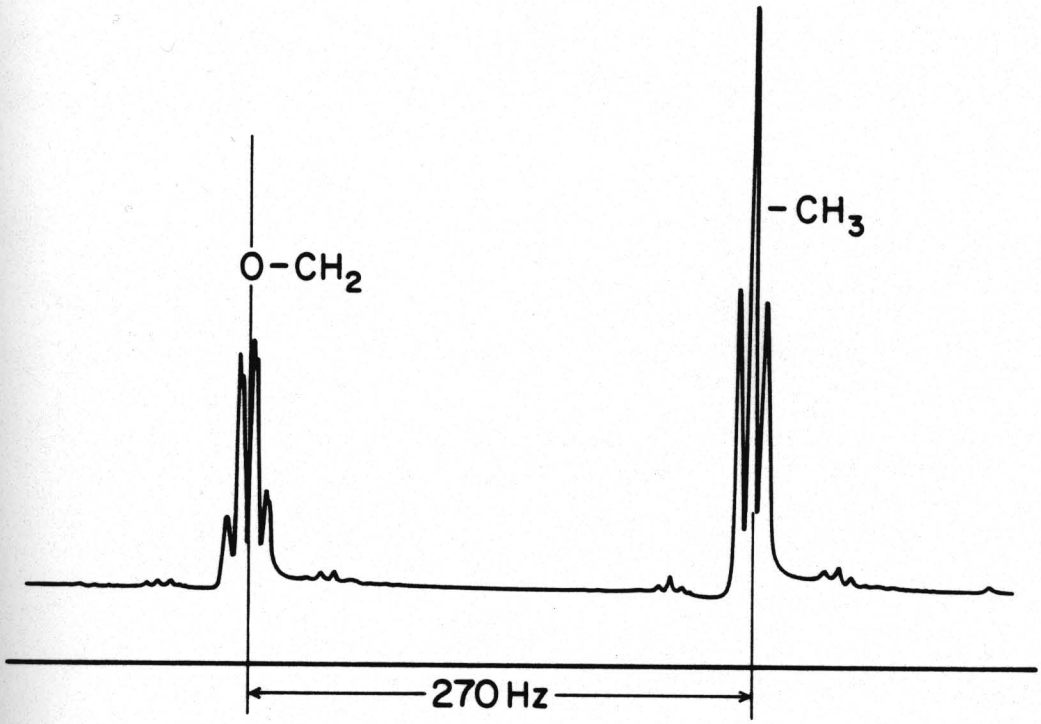

Figure II-6-1. Proton NMR spectrum (90mHz) for diethyl ester oxalate. TMS was used as an internal standard and deuterochloroform as the solvent.

III RESULTS

The results are treated in the same sequence as they are shown in the experimental section, i.e. density, viscosity, solubility, thermal history, desupersaturation profiles and particle size distributions.

III-1 Density

The density of oxalic acid dihydrate in water, water/acetone, and water/glycerine mixtures was determined as described in Section II-3-3.

The results are shown in Tables III-1-1, III-1-2 and III-1-3.

Table III-1-1

Density of Oxalic Acid Dihydrate-Water Solutions.

T (°C)	Oxalic Acid Dihydrate gm/100 gm solution	ρ (g/ml)
34.9	9.09	1.0252
	17.14	1.0528
44.9	9.09	1.0208
	24.50	1.0747
60.6	9.09	1.0116
	17.14	1.0390
	24.50	1.0624

Table III-1-2

Density of Oxalic Acid Dihydrate-Acetone-Water Solutions.

T (°C)	Oxalic Acid Dihydrate (gm/100 gm solution)	ρ (g/ml) % acetone[a] 10	50
34.9	13.04		0.9519
	20.00		0.9771
44.9	24.50	1.0568	
	25.93		0.9905

[a]Percent by weight composition of solvent acetone/water.

Table III-1-3

Density of Oxalic Acid Dihydrate-Glycerine-Water Solutions.

T (°C)	Oxalic Acid Dihydrate (gm/100 gm solution)	ρ (g/ml) % glycerine[a] 4	10	25
34.9	9.09	1.0329		1.0807
	17.14	1.0608	1.0737	1.1055
44.9	9.09	1.0287		1.0755
	17.14		1.0684	1.1222
	24.50		1.0924	
60.6	9.09	1.0204		1.0633
	24.50	1.0702	1.0830	1.1117

[a]Percent by weight composition of solvent glycerine/water.

III-2 Viscosity

The viscosities determined for oxalic acid dihydrate as described in Section II-3-4 are presented in Tables III-2-1, III-2-2 and III-2-3. Viscosities obtained from ideal density calculations differ from experimental values by 0.5% for an oxalic acid dihydrate concentration of 9.09%, by 1% for 17.14% oxalic acid dihydrate and by 2.5% for 24.5% oxalic acid dihydrate.

Fig. III-2-1 depicts data for the viscosity of acetone/water solutions reported in the literature (Timmermans, 1960). Systems of this kind, with a maximum in the viscosity-concentration curve, permit study of the effect of other variables (e.g. cosolute concentration) on the micromeritic characteristics of the population, under isoviscosity conditions. The effect of the concentration of oxalic acid dihydrate in solution with acetone/water as the solvent system is depicted in Fig. III-2-2.

To be able to characterize the viscosity environment during crystallization it is necessary to know the effect of oxalic acid dihydrate concentration and temperature on the viscosity of the solution. Figures III-2-3, III-2-4 and III-2-5 show the effect of temperature, oxalic acid dihydrate concentration and cosolute concentration (glycerine for the solvent glycerine/water) respectively on the viscosity. Since these variables have been expressed in linearized form, an equation that would allow for calculation of the viscosities of the supersaturated solutions was obtained by multiple regression of the data. The equation arrived at was

Table III-2-1

Viscosity of Oxalic Acid Dihydrate-Water Solutions.

T (°C)	Oxalic Acid Dihydrate (gm/100 gm solution)	η (m poise)
34.9	9.09	8.28[a]
	17.14	9.33[a]
44.9	9.09	6.81[a]
	17.14	7.81
	24.50	8.69[a]
60.6	9.09	5.28[a]
	17.14	5.94[a]
	24.50	6.59[a]

[a]Value for which density was measured.

Table III-2-2

Viscosity of Oxalic Acid Dihydrate-Acetone-Water Solutions.

T (°C)	Oxalic Acid Dihydrate (gm/100 gm solution)	η (m poise) % acetone[a] 10	25	50	75
25.3	13.04	12.52	15.30	15.46	10.66
34.9	13.04	10.03	12.06	12.22[b]	8.87
	20.00	11.36	13.25	13.76[b]	10.74
	25.93			15.36	12.65
44.9	13.04	8.16	9.67	9.83	7.37
	20.00	9.27	10.68	11.07	8.87
	25.93	10.14	11.63	12.28[b]	10.39
56.7	20.00	7.46	8.46	8.82	7.31
	25.93	8.17	9.23	9.73	8.43

[a]Percent by weight composition of solvent acetone/water.

[b]Value for which density was measured.

Table III-2-3

Viscosity of Oxalic Acid Dihydrate-Glycerine-Water Solutions.

T (°C)	Oxalic Acid Dihydrate (gm/100 gm solution)	η (m poise) % glycerine[a] 4	10	25
34.9	9.09	9.14[b]	10.52	15.75[b]
	13.04			16.79
	17.14	10.16[b]	11.66[b]	17.52[b]
44.9	9.09	7.36[b]	8.61	12.67[b]
	13.04			13.07
	17.14	8.38	9.49[b]	14.36[b]
	24.50	9.62	10.54[b]	15.24
60.6	9.09	5.71[b]	6.57	9.24[b]
	17.14	6.50	7.33	10.47
	24.50	7.15[b]	8.00[b]	11.21[b]

[a]Percent by weight composition of solvent, glycerine/water.

[b]Value for which density was measured.

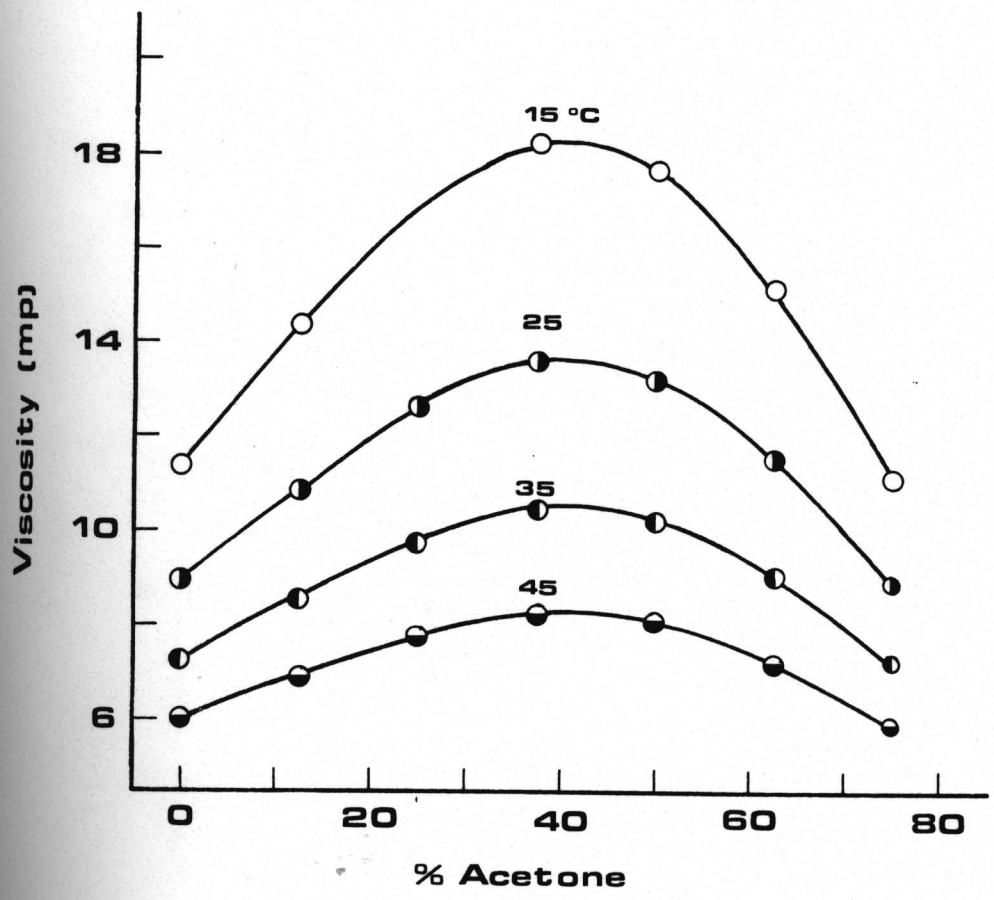

Figure III-2-1. Plot of viscosity data at various temperatures as a function of acetone concentration in acetone/water solutions. (After Timmermans, 1960).

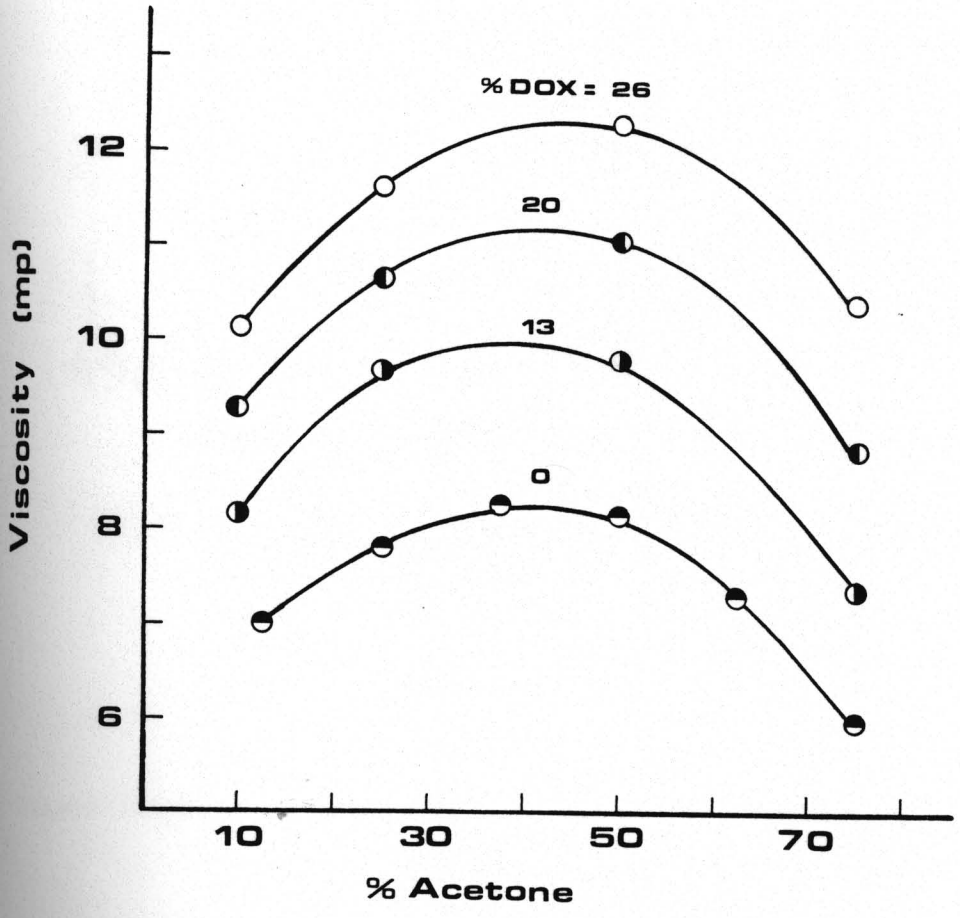

Figure III-2-2. Plot of viscosity data for various concentrations of oxalic acid dihydrate (DOX) as a function of acetone concentration in acetone/water solutions at a temperature of 44.9°C.

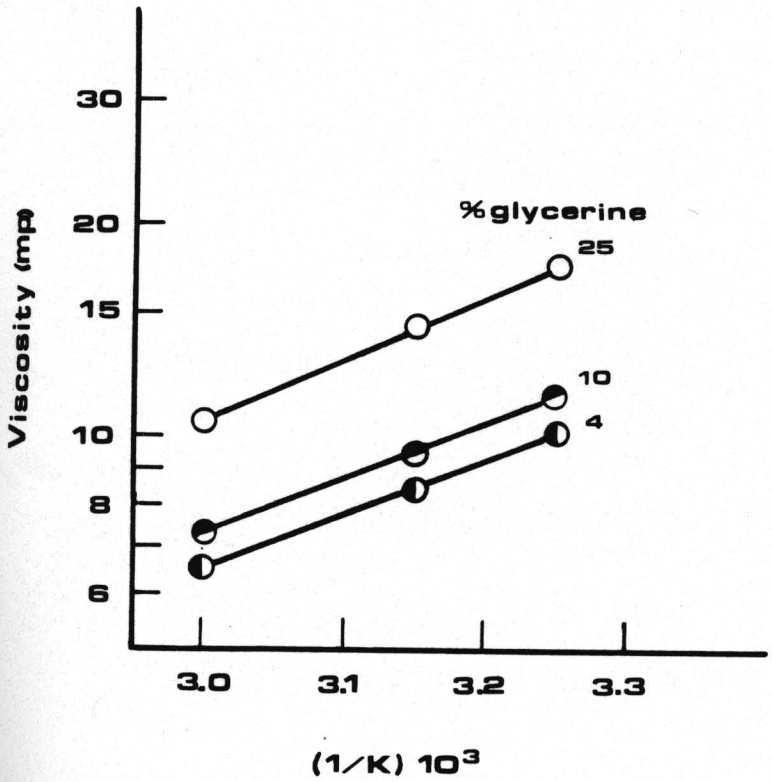

Figure III-2-3. Arrhenius plot of viscosity for oxalic acid dihydrate-glycerine-water solutions for various concentrations of glycerine in the glycerine/water solvent system. Oxalic acid dihydrate concentration of 17.14%.

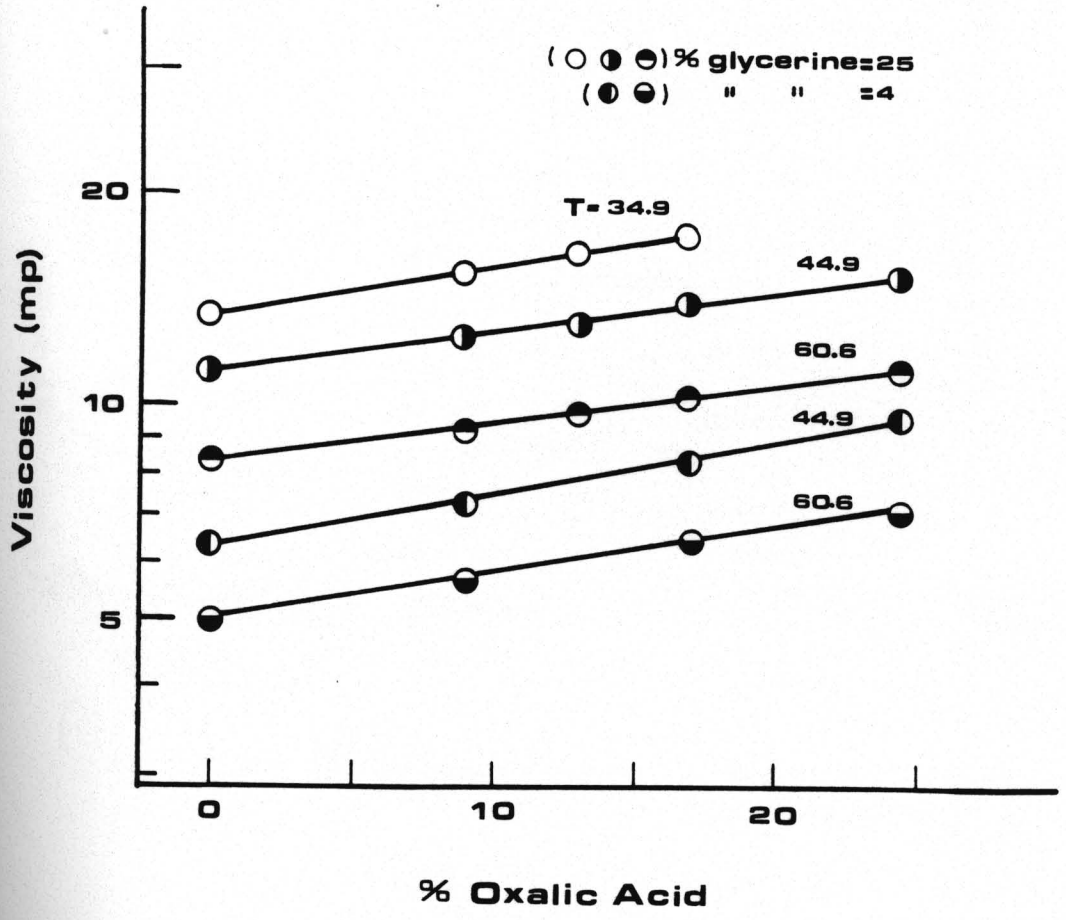

Figure III-2-4. Viscosity as a function of oxalic acid dihydrate concentrations of various temperatures and glycerine concentrations in the solvent.

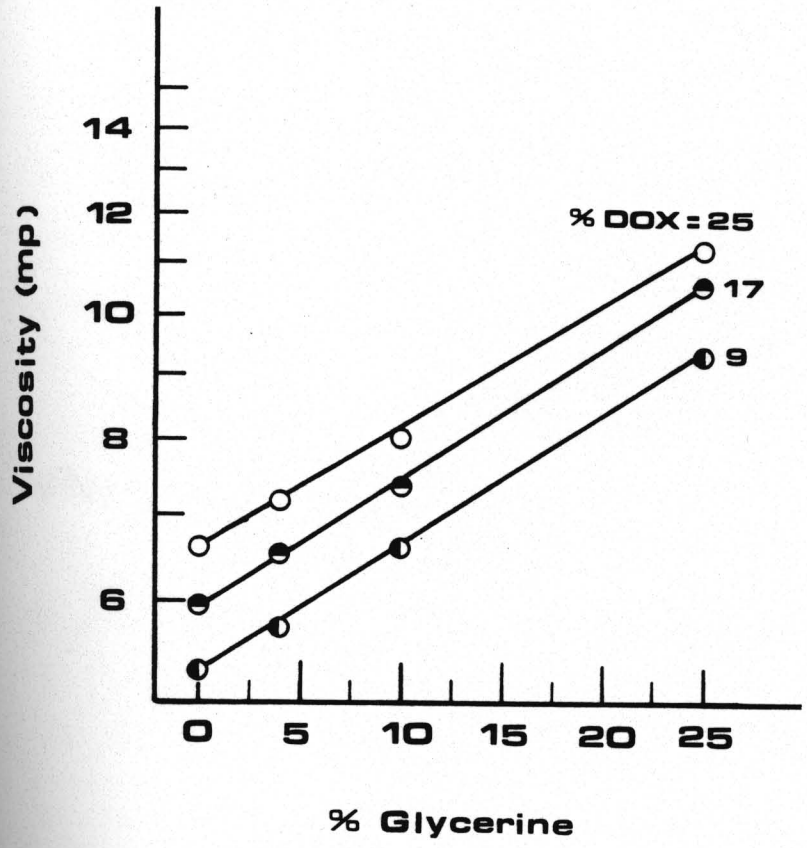

Figure III-2-5. Viscosity as a function of glycerine concentration in glycerine/water solutions for various concentrations of oxalic acid dihydrate at a temperature of 60.6°C.

Table III-2-4

Multiple Regression Analysis of the Influence of Absolute Temperature (T), Solvent Composition (x) and Oxalic Acid Dihydrate Concentration (c), on the Viscosity of the Solution (η) According to the Equation:

$$\ln(\eta) = \alpha' c + \beta' x + \frac{\gamma'}{T} + \delta'$$

Variable	Coefficient	R^2
	-4.258	
c	0.0140 (0.0006)	
x	0.0239 (0.0004)	
1/T	1927 (39)	0.996

$$\ln(\eta) = \alpha' c + \beta' x + (\gamma'/T) + \delta' \qquad \text{Eq. III-2-1}$$

where

c = oxalic acid dihydrate (% by weight)

x = glycerine concentration of the solvent glycerine/water (% weight)

T = absolute temperature (^{o}K)

Values for the coefficients obtained from multiple regression analysis are presented in Table III-2-4.

III-3 Solubility.

Solubility of oxalic acid dihydrate was measured as described in section II-3-5 in the solvents of interest at various temperatures. These are included in Tables III-3-1, III-3-2 and III-3-3. Solubilities of oxalic acid dihydrate in water at various temperatures were obtained from Seidell (1940) and are presented in table III-3-4.

Linear solubility-temperature plots are often desirable, because they can be interpolated accurately. They, of course, can be treated by the usual statistics of linear regression and they can provide thermodynamic data for the solution process.

The Van't Hoff plots of the natural logarithm of solubility versus 1/T are shown in Figures III-3-1, III-3-2 and III-3-3. Parameter values from least squares fitting of the data in the presentation form

$$\ln (X) = -(\Delta H_s/(RT)) + b \qquad \text{Eq. III-3-1}$$

are presented in Tables III-3-5, III-3-6 and III-3-7.

To permit interpolation of the solubility of oxalic acid dihydrate in glycerine/water solvents at supersaturated compositions (which, of course, defy direct measurement), the correlation of solubility was fitted to the pertinent parameters by the following equation

$$T \ln (X) = \alpha + \beta T + (\gamma / \varepsilon) \qquad \text{Eq. III-3-2}$$

Table III-3-1

Oxalic Acid Dihydrate Solubility in Ethanol/Water.

Ethanol (%)[a]	T (°C)	mg/g Solvent	X^b (10^2)
10	19.9	141.7[c] (0.2)[d]	21.08[c] (0.02)[d]
	30.6	241.1 (0.9)	35.36 (0.13)
	41.1	388.3 (0.7)	55.74 (0.09)
42	19.9	237.7 (1.7)	43.61 (0.3)
	30.6	356.6 (2.0)	60.04 (0.3)
	41.1	506.4 (3.3)	88.55 (0.5)
92	19.9	399.9 (5.0)	115.01 (1.27)
	30.6	479.4 (1.2)	134.79 (0.29)
	41.1	591.6 (4.3)	161.27 (0.99)
100	19.9	418.2 (8.7)	132.60 (2.38)
	30.6	501.2 (1.8)	154.85 (0.46)
	41.1	605.3 (2.5)	181.20 (0.61)

[a](Weight/weight)percent.

[b]Mole fraction of oxalic acid dihydrate.

[c]Mean of four measurements.

[d]Standard deviation.

Table III-3-2

Oxalic Acid Dihydrate Solubility in Acetone/Water.

Acetone (%)[a]	T (°C)	mg/g Solvent	X^b (10^2)
5	39.5	341.2[c] (0.5)[d]	48.02 (0.06)
	39.3	337.0 (2.5)	47.46 (0.33)
	25.0	176.0 (0.3)	25.35 (0.05)
	15.2	109.7 (0.9)	15.96 (0.12)
10	39.5	361.1 (0.6)	52.46 (0.08)
	39.3	350.4 (3.5)	50.99 (0.48)
	25.0	187.0 (0.4)	27.87 (0.05)
	15.2	117.3 (0.1)	17.68 (0.02)
25	39.5	395.1 (6.6)	63.80 (0.99)
	39.3	393.5 (1.3)	63.56 (0.19)
	25.0	225.7 (0.3)	37.48 (0.05)
	15.2	148.4 (0.4)	24.97 (0.06)
50	39.5	442.9 (1.9)	88.03 (0.35)
	39.3	432.8 (1.7)	86.20 (0.31)
	25.0	282.9 (0.9)	58.08 (0.17)
	15.2	209.0 (0.4)	43.57 (0.09)
75	39.3	433.1 (2.0)	113.60 (0.47)
	25.0	309.0 (0.9)	83.79 (0.22)
	15.2	246.1 (0.6)	67.88 (0.15)

Acetone (%)[a]	T (°C)	mg/g Solvent	X^b (10^2)
100	39.5	488.3 (0.4)	183.67 (0.13)
	39.3	473.7 (0.9)	179.14 (0.28)
	25.0	350.5 (0.1)	139.02 (0.00)
	15.2	282.7 (0.4)	115.22 (0.15)

[a](Weight/weight) percent.

[b]Mole fraction of oxalic acid dihydrate.

[c]Mean for three measurements.

[d]Standard deviation.

Table III-3-3

Oxalic Acid Dihydrate Solubility in Glycerine/Water.

Glycerine (%)[a]	T (°C)	mg/g Solvent	X^b (10^3)
1	19.9	130.3[c] (0.6)[d]	18.41[c] (0.08)[d]
	40.7	338.3 (3.6)	46.42 (0.47)
	54.8	613.7 (6.7)	81.14 (0.81)
4	19.9	129.5 (0.5)	18.74 (0.08)
	40.7		
	54.8	610.8 (4.1)	82.64 (0.50)
7	19.9	128.7 (0.4)	19.09 (0.05)
	40.7	334.5 (3.1)	48.16 (0.43)
	54.8	610.1 (4.3)	84.49 (0.55)
10	19.9	127.9 (0.3)	19.47 (0.04)
	40.7	331.1 (1.5)	48.88 (0.20)
	54.8	603.2 (8.2)	85.62 (1.06)
25	19.9	124.6 (0.3)	21.77 (0.05)
	40.6	323.3 (1.0)	54.62 (0.16)
	54.5	582.8 (1.3)	94.31 (0.19)
37	19.9	126.2 (0.2)	25.01 (0.04)
	40.6	324.5 (2.4)	61.87 (0.42)
	54.5	581.9 (1.5)	105.76 (0.24)

Glycerine (%)[a]	T (°C)	mg/g Solvent	X^b (10^3)
50	19.9	134.0 (1.6)	31.01 (0.37)
	40.7	338.1 (2.7)	74.72 (0.42)
	54.8	609.5 (7.9)	127.07 (1.44)

[a](Weight/weight) percent.

[b]Mole fraction of oxalic acid dihydrate.

[c]Mean for five measurements.

[d]Standard deviation.

Table III-3-4

Solubility of Oxalic Acid Dihydrate in Water,

at Different Temperatures.

Temperature (°C)	Oxalic Acid Dihydrate[a] (gm/100 gm water)
10	8.51
20	13.32
30	19.92
40	30.12
50	44.03
60	62.01
70	85.49
80	118.26
90.2	168.80

[a]Values obtained from Seidell (1940).

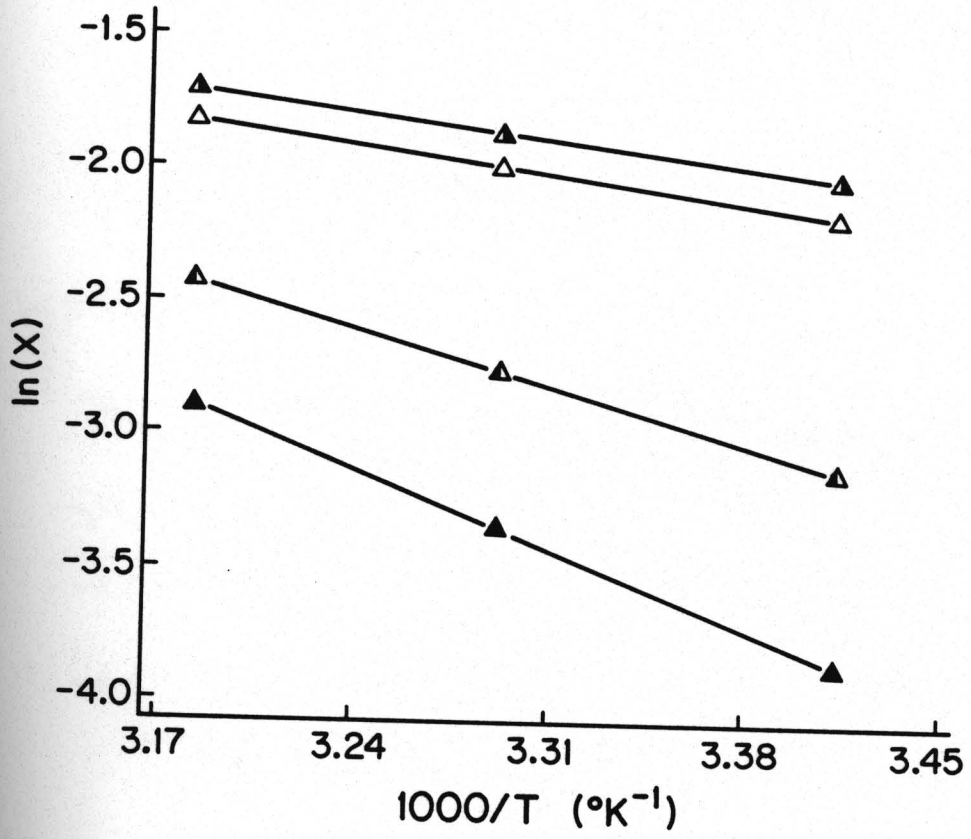

Figure III-3-1. Van't Hoff plots of oxalic acid dihydrate in ethanol/water solutions. (◭) 100% ethanol, (△) 92% ethanol, (◭) 42% ethanol, (▲) 10% ethanol.

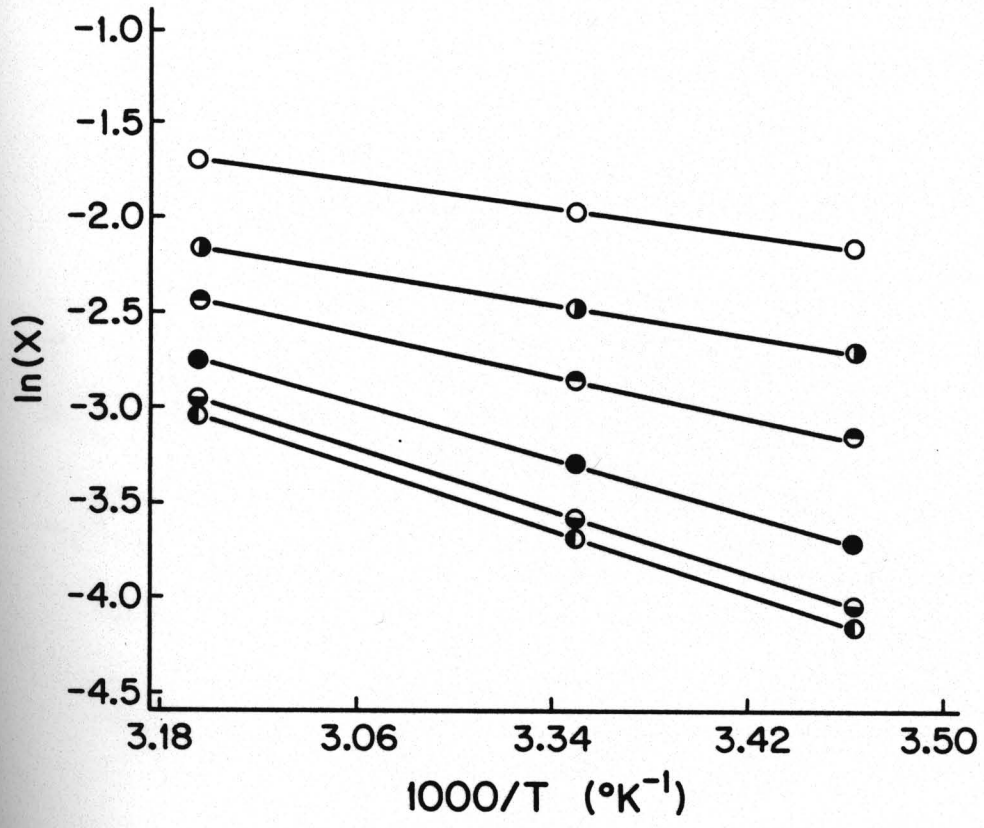

Figure III-3-2. Van't Hoff plots in acetone/water solutions. (○) 100% acetone, (◑) 75%, (◓) 50%, (●) 25%, (◒) 10% and (◐) 5%.

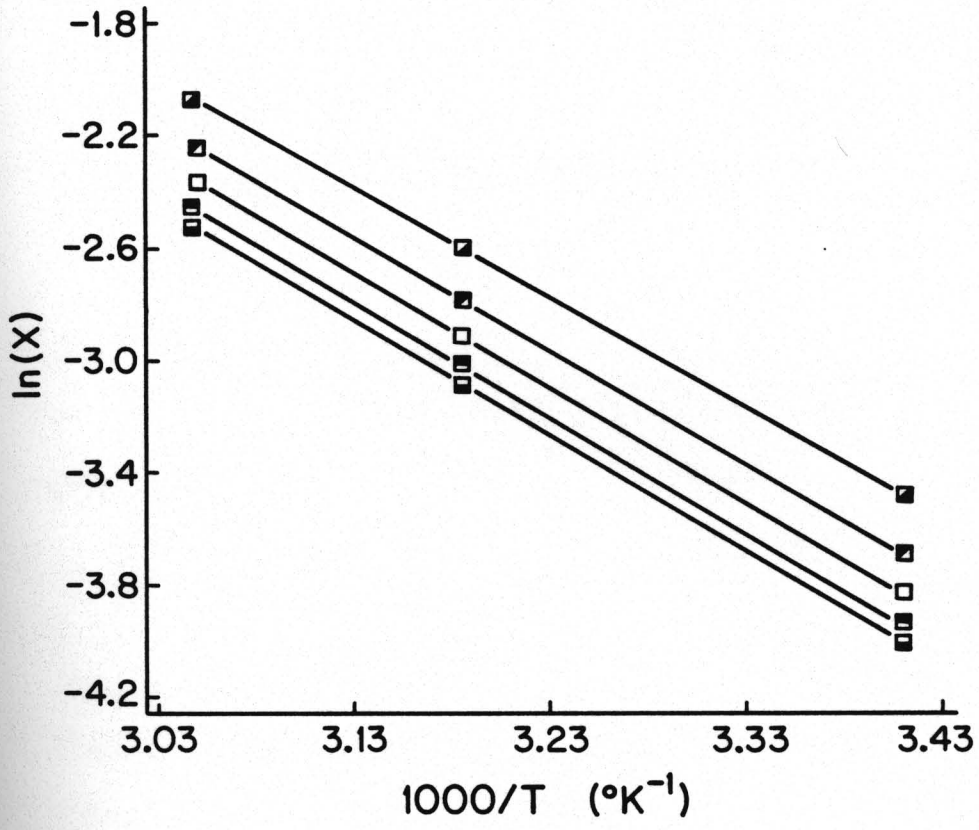

Figure III-3-3. Van't Hoff plots of oxalic acid dihydrate in glycerine/water solutions. (▬) 50% glycerine, (▬) 25%, (□) 10%, (◪) 7% and (◪) 1%.

Table III-3-5

Linear Regression Analysis of the Influence of the Absolute Temperature (T), on the Mole Fraction Solubility of Oxalic Acid Dihydrate (X) in Ethanol-Water, Analyzed According to the Van't Hoff Equation:

$$\ln (X) = \frac{-\Delta H_s}{R} \cdot \frac{1}{T} + b$$

% Ethanol[a]	Intercept	Slope	R^2[b]
10	10.54 (0.09)[c]	-4219 (26)[c]	1.00
42	7.37 (0.10)	-3077 (28)	1.00
92	2.84 (0.10)	-1467 (30)	1.00
100	2.61 (0.09)	-1358 (28)	1.00

[a](Weight/weight) percent.

[b]Variation explained by the regression.

[c]Standard error.

Table III-3-6

Linear Regression Analysis of the Influence of the Absolute Temperature (T), on the Mole Fraction Solubility of Oxalic Acid Dihydrate (X) in Acetone-Water, Analyzed According to the Van't Hoff Equation:

$$\ln (X) = \frac{-\Delta H_s}{R} \cdot \frac{1}{T} + b$$

% Acetone[a]	Intercept	Slope	R^2[b]
5	10.01 (0.04)[c]	-4080 (13)[c]	1.00
10	9.81 (0.10)	-3991 (29)	1.00
25	8.39 (0.05)	-3480 (14)	1.00
50	5.81 (0.08)	-2580 (23)	1.00
75	4.02 (0.05)	-1937 (16)	1.00
100	3.72 (0.09)	-1695 (27)	1.00

[a](Weight/weight) percent.

[b]Variation explained by the regression.

[c]Standard error.

Table III-3-7

Linear Regression Analysis of the Influence of the Absolute Temperature (T), on the Mole Fraction Solubility (X), of Oxalic Acid Dihydrate in Glycerine/Water, Analyzed According to the Van't Hoff Equation:

$$\ln X = -\frac{\Delta H_s}{R} \cdot \frac{1}{T} + b$$

% Glycerine[a]	Intercept	Slope	R^2[b]
1	9.94 (0.06)[c]	-4083 (19)[c]	1.00
7	10.01 (0.06)	-4094 (18)	1.00
10	9.97 (0.06)	-4076 (19)	1.00
25	10.06 (0.04)	-4069 (11)	1.00
37	9.98 (0.04)	-4003 (12)	1.00
50	9.78 (0.08)	-3883 (23)	1.00

[a](Weight/weight) percent.

[b]Variation explained by regression. $R^2 = \frac{\text{SS due to regression}}{\text{Total SS, corrected for mean}}$.

[c]Standard error.

where α , β and γ are constants. Values for dielectric constants, ε, were obtained from the literature (Glycerine Prod. Association, 1965). Analysis of the data gives the three coefficients α, β and γ.

Table III-3-8 represents the multiple regression parameters calculated from the solubility data for the glycerine/water system in the range 1 to 50%, and at temperatures from 19.9°C to 54.8°C. Experimental and predicted values of the solubility (expressed in mole fraction) have been obtained from Eq. III-3-2 as a function of $(1/\varepsilon)$ and are presented in Fig. III-3-4.

Table III-3-8

Multiple Regression Analysis of the Influence of the Absolute Temperature (T), and the Dielectric Constant (ε) on the Mole Fraction Solubility (X) of Oxalic Acid Dihydrate in Glycerine/Water, Analyzed According to the Following Equation:

$$T \ln(X) = \alpha + \beta(T) + \gamma/\varepsilon$$

% Glycerine Range	Temperature Range (°C)
1-50	19.9-54.8

Regression Coefficients		S. Error	R^2
α	-3695		
β	6.65	0.19	
γ	46438	1871	0.997

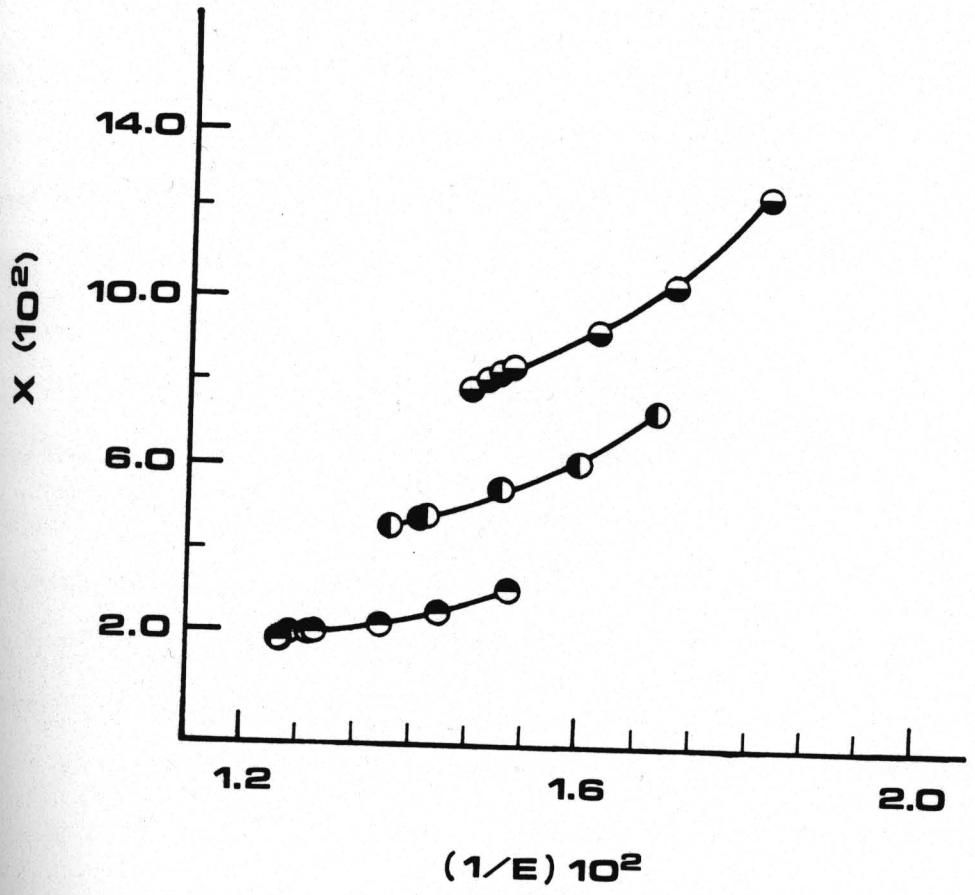

Figure III-3-4. Experimental and predicted values of the solubility of oxalic acid dihydrate as a function of 1/E. Temperatures (◒) 54.7°C, (◐) 40.7°C and (◓) 19.9°C.

III-4 Thermal Histories of Solutions

Experiments were performed with aqueous solutions of oxalic acid dihydrate as described in Section II-4. The purpose was to determine the influence of the overheating temperature (T_H) and the overheating time (t_H) on the crystal size distribution and the degree of supercooling of solutions which had been saturated at various temperatures.

The first series of experiments was done with non-controlled cooling to a final temperature of 24°C where the systems were kept for one hour. As explained in Section II-4-2, values of the temperature at which the first crystals are visible and the weight mean diameter of the populations were determined, and these are tabulated in Table III-4-1.

A second series of experiments was performed with programmed linear cooling, 40°C per hour, to a final temperature of 24°C and 18°C. The values of the mean diameters of the populations are presented in Table III-4-2.

Table III-4-1

Effect of Overheating Temperature and Time on the Nucleation Temperature and Mass Particle Size of Oxalic Acid Dihydrate Crystallized from Aqueous Solution. (Non-linear Cooling).

T_H (°C)	T_S (°C)	t_H (min)			
		0	15	30	120
65.0	41.0	358.4[a] (33.5)[b]	331.6 (33.5)		
65.0	50.0	354.5 (40.0)	333.8 (39.0)		340.7 (40.0)
65.0	55.0	365.1 (44.0)			312.0 (40.0)
85.0	41.0		335.6 (32.5)		
85.0	50.0	385.0 (40.5)	322.7 (42.0)	443.5±86.0[c] (38.5±1.0)	427.8 (42.0)
85.0	55.0	356.6 (44.0)	292.5 (43.0)		391.0 (44.0)
90	55			497.6±50.0[c] (43.3±0.6)	

(a) Weight mean diameter (μm)
(b) Temperature when first crystals appear (°C)
(c) Mean and standard deviation for duplicate runs.

Table III-4-2

Effect of Overheating Temperature on the Nucleation Temperature and Mean Particle Size of Oxalic Acid Dihydrate Crystallized from Aqueous Solution. (Programmed Linear Cooling, T_S=40°C, t_H=10 min).

T_H (°C)	Z (μm)	T_N (°C)
42	295	33.6
50	297	32.3
60	239	30.0
60	344	32.3

(a) Mean geometric diameter

III-5 Desupersaturation Profiles

Calculation of the supersaturation during crystallization was achieved using the analytical form of the temperature-time course (Eq. II-4-2) and the Van't Hoff equation to obtain the solubilty of oxalic acid dihydrate as a function of time in the different solvent systems.

Tables III-5-1 to III-5-6 include the calculated solubilities and the measured concentrations at different temperatures and times. Concentration, solubility and supersaturation profiles as a function of time are depicted in Figures III-5-1 to III-5-12.

The temperature-time profiles were recorded for all experiments in order to monitor the temperature changes during crystallization. Crystallization is an exothermal process and the heat released is responsible for the appearance of a peak in the profile (Fig. II-5-14). The temperature at the time the peaks starts appearing is presented for the crystallization of oxalic acid dihydrate in various solvents in table III-5-7. The cooling rate in these experiments is $10^{o}C$/hour.

Table III-5-1

Desupersaturation of a Solution of Oxalic Acid Dihydrate in 15% Glycerine/Water[a], Saturated at 30°C.

Time (min)	T (°C)	C[b] (gm/gm solvent)	S[c] (gm/gm solvent)	(C - S) (gm/gm solvent)
0.0	34.4	0.205	0.250	-0.050
6.8	34.0	0.204	0.245	-0.041
30.2	30.2	0.203	0.207	-0.004
42.9	28.2	0.202	0.189	0.013
48.6	27.2	0.203	0.181	0.022
52.4[d]	26.7	0.202	0.177[e]	0.025
54.4	26.4	0.201	0.174	0.027
55.2	26.2	0.199	0.173	0.026
58.1	26.0	0.192	0.171	0.021
59.4	25.9	0.187	0.170	0.017
60.7	25.7	0.182	0.169	0.013
62.8	25.2	0.173	0.165	0.008
65.3	24.5	0.166	0.160	0.006
67.9[f]	24.0	0.160	0.157	0.003
71.3	23.8	0.155	0.155	0.000
81.4	23.6	0.154	0.154	0.000

Time (min)	T (°C)	C[b] (gm/gm solvent)	S[c] (gm/gm solvent)	(C - S) (gm/gm solvent)
113.4	23.7	0.154	0.154	0.000
143.6	23.7	0.154	0.154	0.000

[a](Weight/weight) percent.

[b]Concentration of oxalic acid dihydrate measured titrimetrically.

[c]Solubility of oxalic acid dihydrate calculated from multiple regression equation (III-3-2).

[d]Value of time (t') used to calculate reduced variable.

[e]Value of Solubility (S_0) used to calculate reduced variable.

[f]Value of time (t") used to calculate reduced variable.

Table III-5-2

Desupersaturation of a Solution of Oxalic Acid Dihydrate in 15% Glycerine/Water[a], Saturated at 40°C.

Time (min)	T (°C)	C[b] (gm/gm solvent)	S[c] (gm/gm solvent)	(C - S) (gm/gm solvent)
0.0	44.6	0.314	0.401	-0.087
25.1	41.2	0.314	0.341	-0.027
45.5	38.0	0.312	0.294	0.018
53.4	36.7	0.312	0.278	0.034
57.2[d]	36.2	0.307	0.271[e]	0.036
58.9	36.0	0.297	0.269	0.028
60.7	35.7	0.288	0.266	0.022
63.1	35.1	0.273	0.259	0.014
65.7	34.6	0.260	0.252	0.008
68.5	34.1	0.252	0.247	0.005
74.9	33.1	0.240	0.236	0.004
82.3	31.9	0.228	0.224	0.004
87.5	31.1	0.219	0.215	0.004
95.4	29.8	0.207	0.203	0.004
105.4	28.3	0.194	0.190	0.006
120.4	25.8	0.174	0.170	0.004
126.3	24.9	0.168	0.163	0.005
142.1[f]	24.1	0.158	0.157	0.001
174.2	24.1	0.159	0.157	0.002

Time (min)	T (°C)	C[b] (gm/gm solvent)	S[c] (gm/gm solvent)	(C - S) (gm/gm solvent)
208.1	24.0	0.158	0.157	0.001
304.3	24.0	0.158	0.157	0.001

[a](Weight/weight) percent.

[b]Concentration of oxalic acid dihydrate measured titrimetrically.

[c]Solubility of oxalic acid dihydrate calculated from multiple regression equation (III-3-2).

[d]Value of time (t') used to calculate reduced variable.

[e]Value of solubility (S_0) used to calculate reduced variable.

[f]Value of time (t") used to calculate reduced variable.

Table III-5-3

Desupersaturation of a Solution of Oxalic Acid Dihydrate in 50% Acetone/Water[a], Saturated at 30°C.

Time (min)	T (°C)	C[b] (gm/gm solvent)	S[c] (gm/gm solvent)	(C - S) (gm/gm solvent)
0.0	35.4	0.335	0.388	-0.053
9.1	34.6	0.333	0.378	-0.045
43.1	29.1	0.334	0.320	0.014
46.5	28.5	0.336	0.315	0.021
47.8	28.3	0.335	0.313	0.022
49.3	28.1	0.334	0.310	0.024
50.3	27.9	0.334	0.309	0.025
51.2	27.8	0.333	0.308	0.025
51.9[d]	27.7	0.334	0.307[e]	0.027
52.8	27.6	0.330	0.306	0.024
53.9	27.5	0.325	0.305	0.020
55.1	27.4	0.322	0.304	0.018
56.1	27.3	0.316	0.304	0.012
57.0	27.2	0.310	0.303	0.007
58.0	27.0	0.307	0.301	0.006
60.0	26.5	0.300	0.296	0.004
61.1	26.2	0.297	0.294	0.003
63.8	25.8	0.291	0.289	0.002
64.5	25.6	0.289	0.288	0.001
71.7[f]	24.7	0.281	0.280	0.001

Time (min)	T (°C)	C[b] (gm/gm solvent)	S[c] (gm/gm solvent)	(C - S) (gm/gm solvent)
102.8	24.6	0.279	0.280	0.001
134.2	24.6	0.280	0.280	0.000

[a](Weight/weight) percent.

[b]Concentration of oxalic acid dihydrate measured titrimetrically.

[c]Solubility of oxalic acid dihydrate calculated from Van't Hoff's equation.

[d]Value of time (t') used to calculate reduced variable.

[e]Value of solubility (S_0) used to calculate reduced variable.

[f]Value of time (t") used to calculate reduced variable.

Table III-5-4

Desupersaturation of a Solution of Oxalic Acid Dihydrate in 50% Acetone/Water[a], Saturated at 40°C.

Time (min)	T (°C)	C[b] (gm/gm solvent)	S[c] (gm/gm solvent)	(C - S) (gm/gm solvent)
0.0	44.6	0.446	0.516	-0.070
9.1	43.8	0.443	0.503	-0.060
38.3	39.0	0.445	0.433	0.012
43.6	38.1	0.444	0.422	0.022
46.1	37.7	0.444	0.417	0.027
47.8	37.4	0.447	0.413	0.034
48.7	37.3	0.445	0.411	0.034
49.8	37.1	0.443	0.409	0.034
51.2[d]	37.0	0.442	0.407[e]	0.034
52.0	37.0	0.436	0.407	0.029
53.3	36.8	0.428	0.406	0.022
54.5	36.7	0.418	0.404	0.014
56.0	36.3	0.408	0.399	0.009
58.2	35.7	0.400	0.392	0.008
59.3	35.5	0.398	0.389	0.009
60.7	35.2	0.392	0.386	0.006
63.5	34.8	0.389	0.381	0.008
64.5	34.7	0.387	0.380	0.007
66.9	34.3	0.382	0.375	0.007
68.4	34.0	0.376	0.372	0.004

Time (min)	T (°C)	C[b] (gm/gm solvent)	S[c] (gm/gm solvent)	(C - S) (gm/gm solvent)
74.4	33.1	0.368	0.361	0.007
80.0	32.1	0.359	0.351	0.008
87.1	31.0	0.346	0.339	0.007
93.8	29.9	0.332	0.328	0.004
100.7	28.8	0.324	0.317	0.006
105.3	28.1	0.315	0.311	0.004
111.4	27.1	0.309	0.302	0.007
119.0	25.9	0.298	0.291	0.007
125.5	24.9	0.289	0.282	0.007
131.2	24.1	0.281	0.275	0.006
140.3[f]	23.9	0.280	0.274	0.006
161.6	23.0	0.277	0.273	0.004
193.5	23.9	0.278	0.273	0.005

[a](Weight/weight) percent.

[b]Concentration of oxalic acid dihydrate measured titrimetrically.

[c]Solubility of oxalic acid dihydrate calculated from Van't Hoff's equation.

[d]Value of time (t') used to calculate reduced variable.

[e]Value of solubility (S_0) used to calculate reduced variable.

[f]Value of time (t") used to calculate reduced variable.

Table III-5-5

Desupersaturation of Aqueous Solution of Oxalic Acid Dihydrate, Saturated at 30°C.

Time (min)	T (°C)	C[a] (gm/gm solvent)	S[b] (gm/gm solvent)	(C - S) (gm/gm solvent)
1.3	34.8	0.199	0.247	-0.048
29.7	30.5	0.199	0.207	-0.008
42.1	28.5	0.199	0.190	0.009
48.3	27.5	0.199	0.183	0.016
50.2	27.2	0.199	0.180	0.019
52.5[c]	26.9	0.197	0.178[d]	0.019
54.3	26.7	0.194	0.176	0.018
55.9	26.5	0.188	0.175	0.013
57.8	26.2	0.181	0.173	0.008
59.9	25.7	0.174	0.169	0.005
62.9	25.4	0.168	0.167	0.001
70.2[e]	24.0	0.158	0.158	0.000
83.7	23.9	0.157	0.157	0.000
107.5	23.9	0.157	0.157	0.000
139.6	23.9	0.157	0.157	0.000

[a] Concentration of oxalic acid dihydrate measured titrimetrically.

[b] Solubility of oxalic acid dihydrate calculated from Van't Hoff's equation.

[c] Value of time (t') used to calculate reduced variable.

[d] Value of solubility (S_0) used to calculate reduced variable.

[e] Value of time (t") used to calculate reduced variable.

Table III-5-6

Desupersaturation of Aqueous Solution of Oxalic Acid Dihydrate, Saturated at 40°C.

Time (min)	T (°C)	C[a] (gm/gm solvent)	S[b] (gm/gm solvent)	(C - S) (gm/gm solvent)
0.0	45.4	0.298	0.372	-0.074
27.6	41.6	0.301	0.321	-0.020
44.1	38.9	0.300	0.290	0.010
45.2	38.7	0.300	0.287	0.013
48.1	38.2	0.300	0.282	0.018
53.4	37.3	0.300	0.272	0.028
54.5	37.1	0.301	0.270	0.031
55.7	36.9	0.301	0.268	0.033
57.3	36.7	0.301	0.266	0.035
58.5	36.5	0.305	0.264	0.041
60.2	36.2	0.300	0.261	0.039
62.1[c]	36.0	0.300	0.258[d]	0.042
63.0	35.8	0.298	0.257	0.041
63.9	35.8	0.295	0.256	0.039
65.0	35.7	0.289	0.255	0.034
66.7	35.3	0.279	0.252	0.027
71.6	34.3	0.257	0.241	0.016
74.5	33.8	0.252	0.237	0.015
76.8	33.5	0.248	0.234	0.014
82.7	32.5	0.238	0.225	0.013

Time (m)	T (°C)	C[a] (gm/gm Solvent)	S[b] (gm/gm Solvent)	(C - S) (gm/gm Solvent)
87.5	31.8	0.230	0.218	0.012
95.6	30.9	0.217	0.210	0.007
106.3	28.7	0.200	0.192	0.008
113.0	27.5	0.189	0.183	0.006
120.2	26.4	0.180	0.174	0.005
126.5	25.4	0.171	0.167	0.004
143.3[e]	24.7	0.164	0.162	0.002
169.4	24.7	0.164	0.162	0.002
208.7	24.7	0.164	0.162	0.002

[a]Concentration of oxalic acid dihydrate.

[b]Solubility of oxalic acid dihydrate.

[c]Value of time (t') used to calculate reduced variable.

[d]Value os Solubility (S_0) used to calculate reduced variable.

[e]Value of time (t") used to calculate reduced variable.

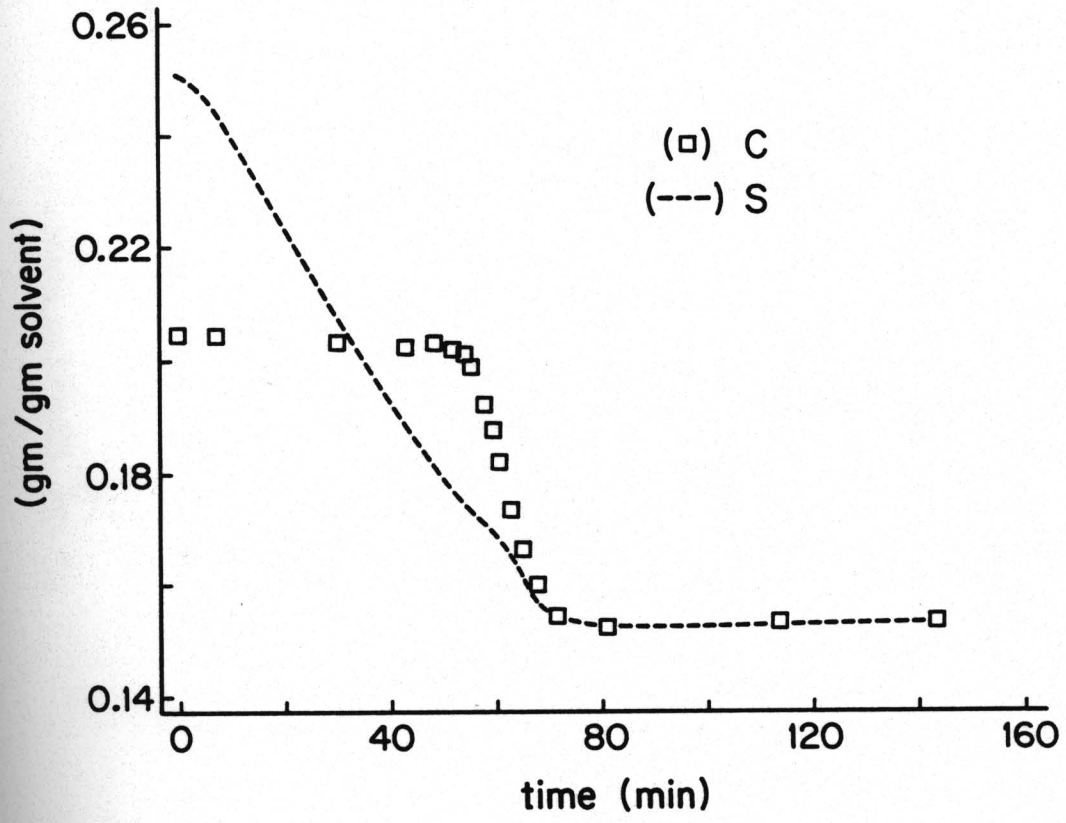

Figure III-5-1. Concentration (□) and solubility (←--→) profiles during cooling and crystallization of oxalic acid dihydrate from 15% glycerine/water saturated at 30°C.

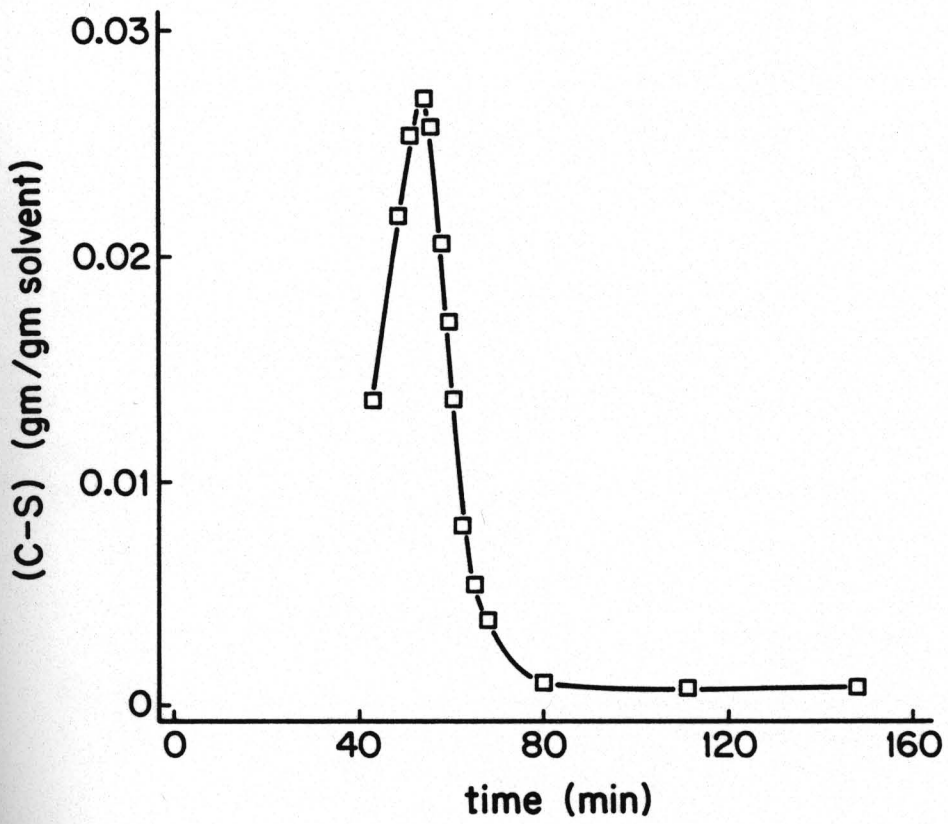

Figure III-5-2. Supersaturation profile during cooling and crystallization of oxalic acid dihydrate from 15% glycerine/water saturated at 30°C.

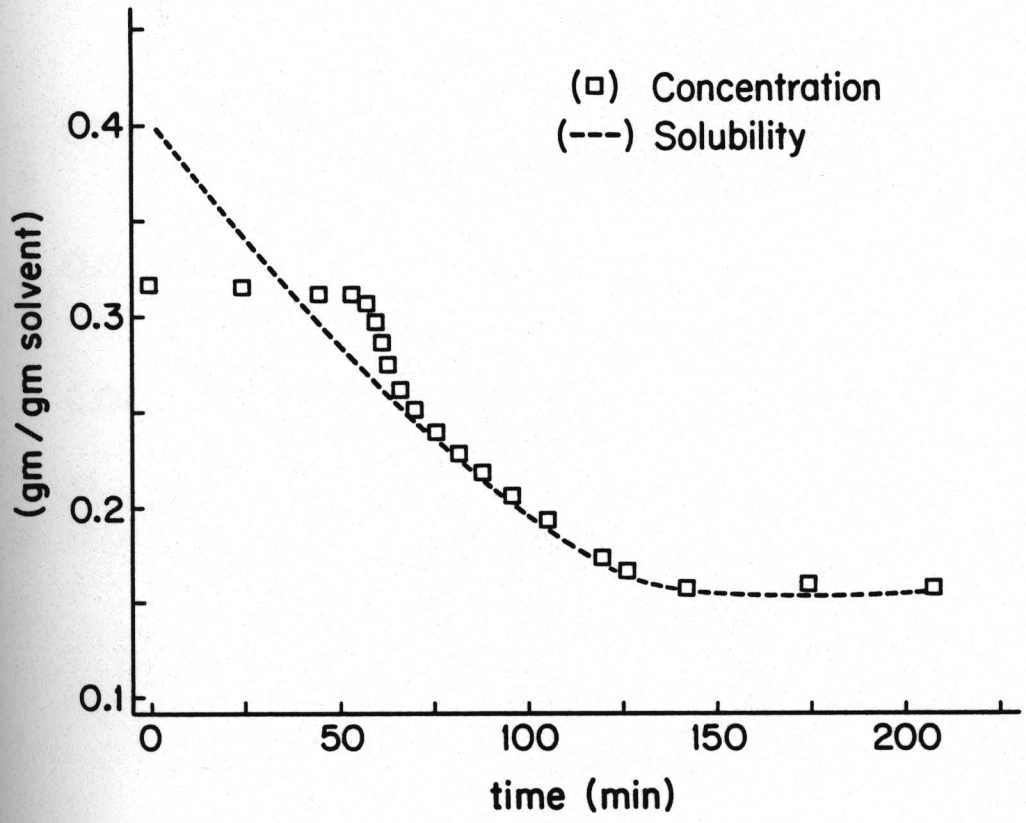

Figure III-5-3. Concentration (□) and solubility (---) profiles during cooling and crystallization of oxalic acid dihydrate from 15% glycerine/water saturated at 40°C.

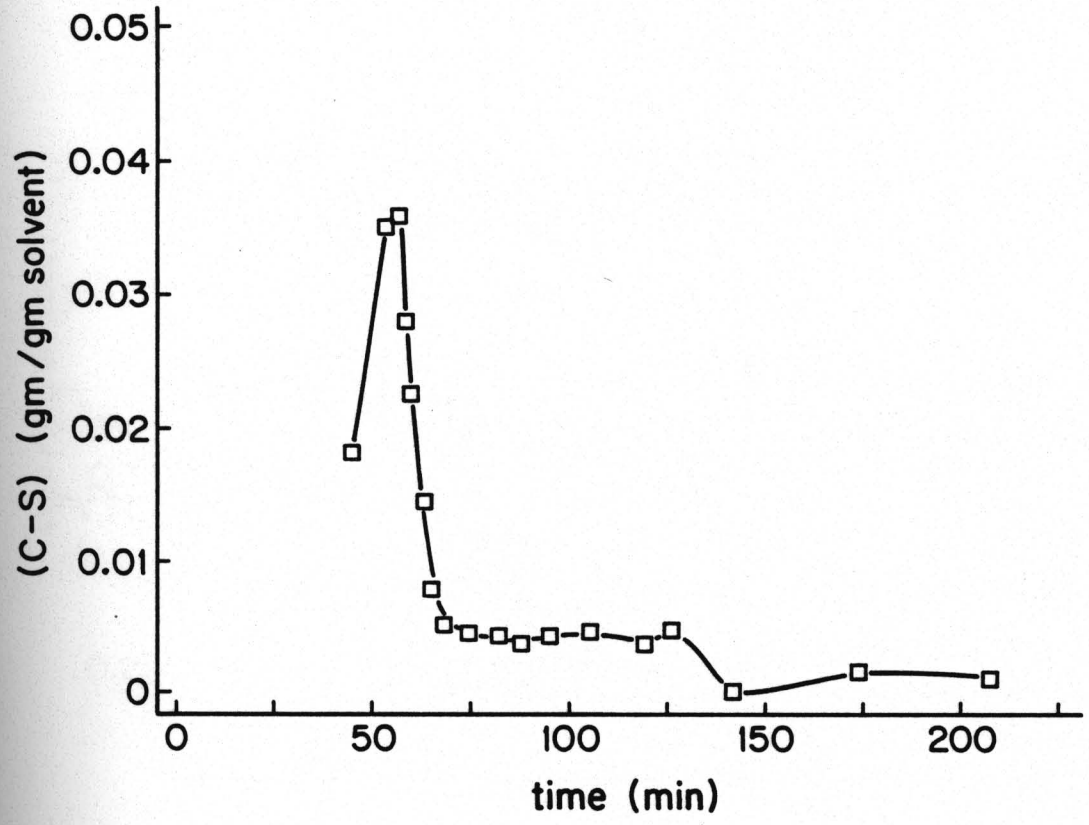

Figure III-5-4. Supersaturation profile during cooling and crystallization of oxalic acid dihydrate from 15% glycerine/water saturated at 40°C.

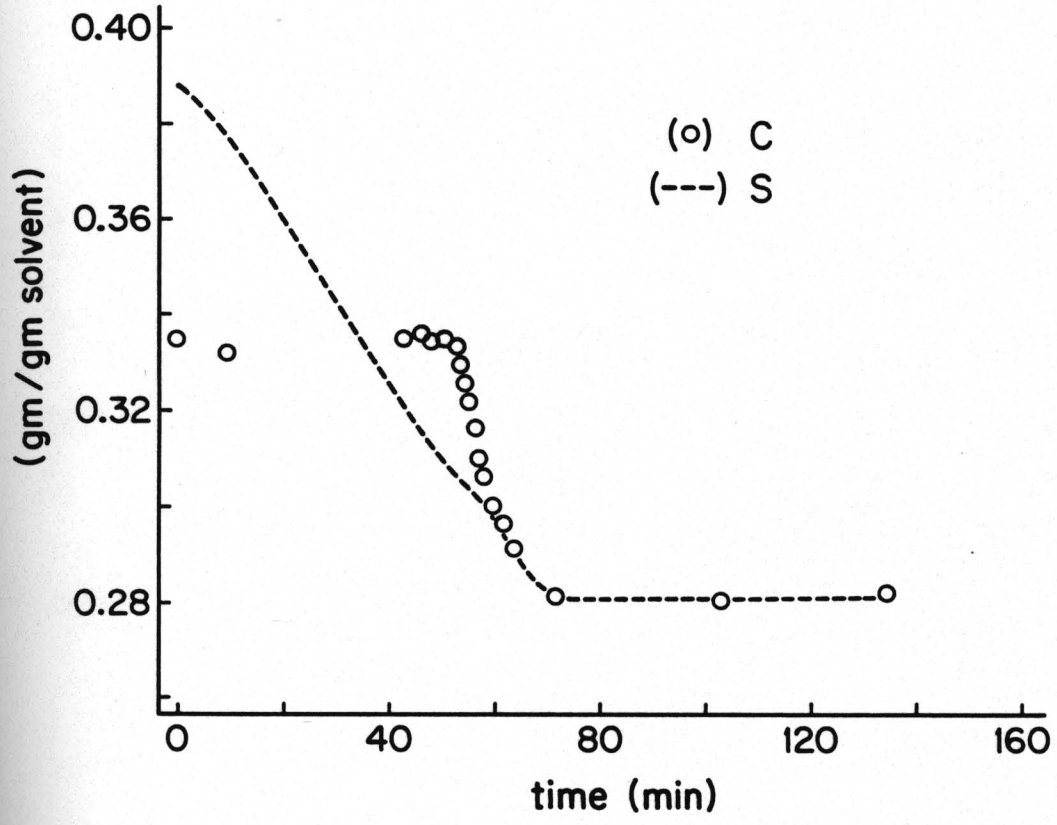

Figure III-5-5. Concentration (o) and solubility (---) profiles during cooling and crystallization of oxalic acid dihydrate from 50% acetone/water saturated at 30°C.

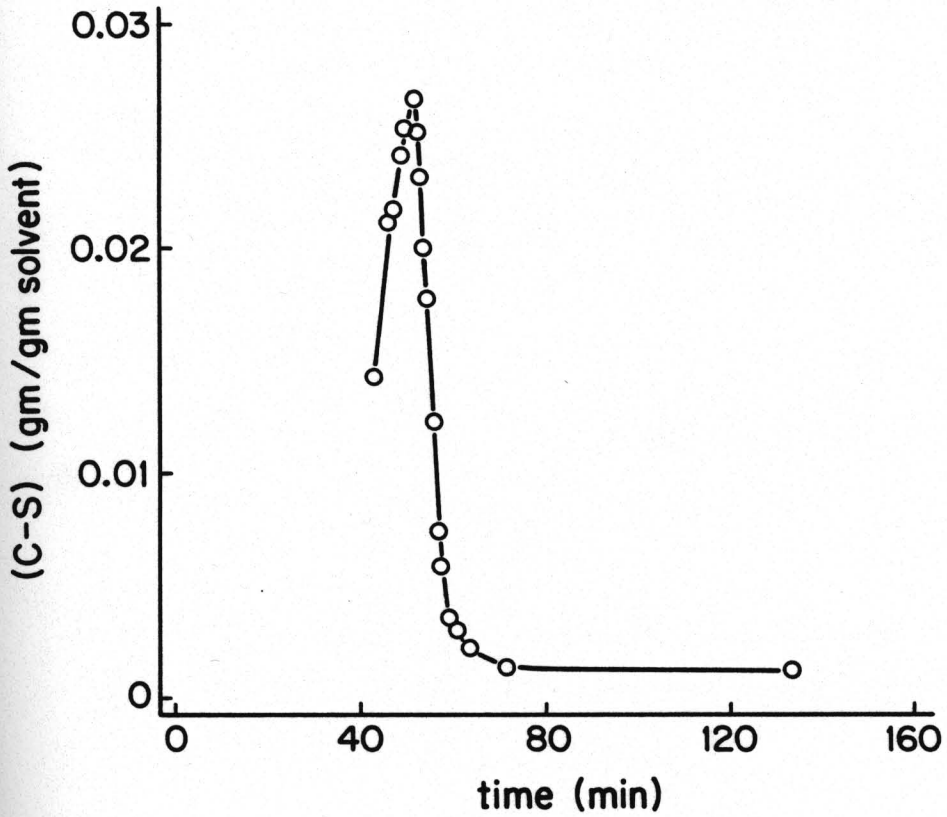

Figure III-5-6. Supersaturation profile during cooling and crystallization of oxalic acid dihydrate from 50% acetone/water saturated at 30°C.

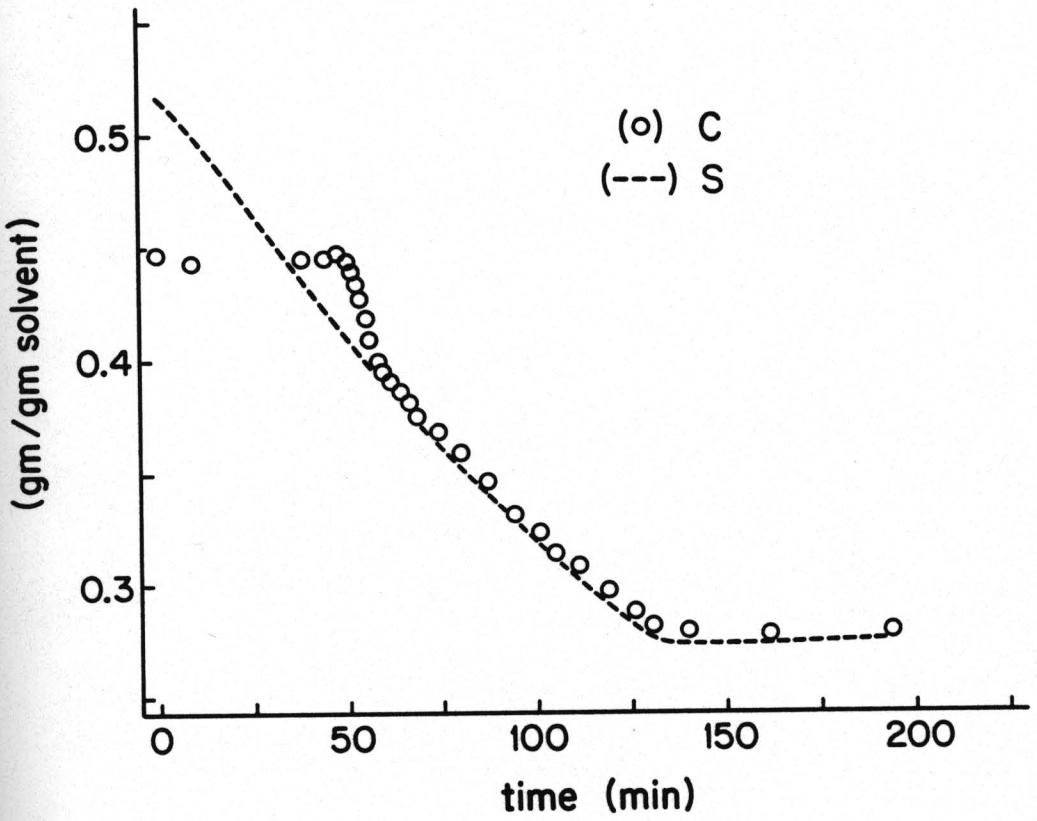

Figure III-5-7. Concentration (o) and solubility (---) profiles during cooling and crystallization of oxalic acid dihydrate from 50% acetone/water saturated at 40°C.

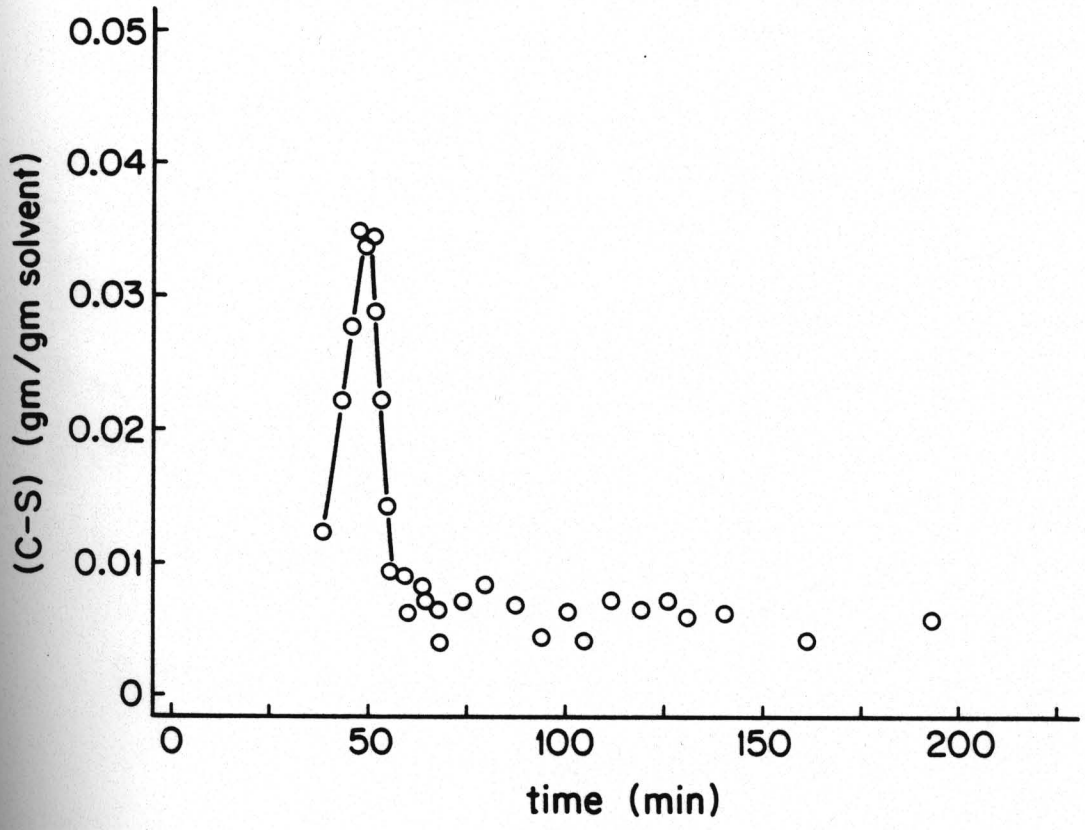

Figure III-5-8. Supersaturation profile during cooling and crystallization of oxalic acid dihydrate from 50% acetone/water saturated at 40°C.

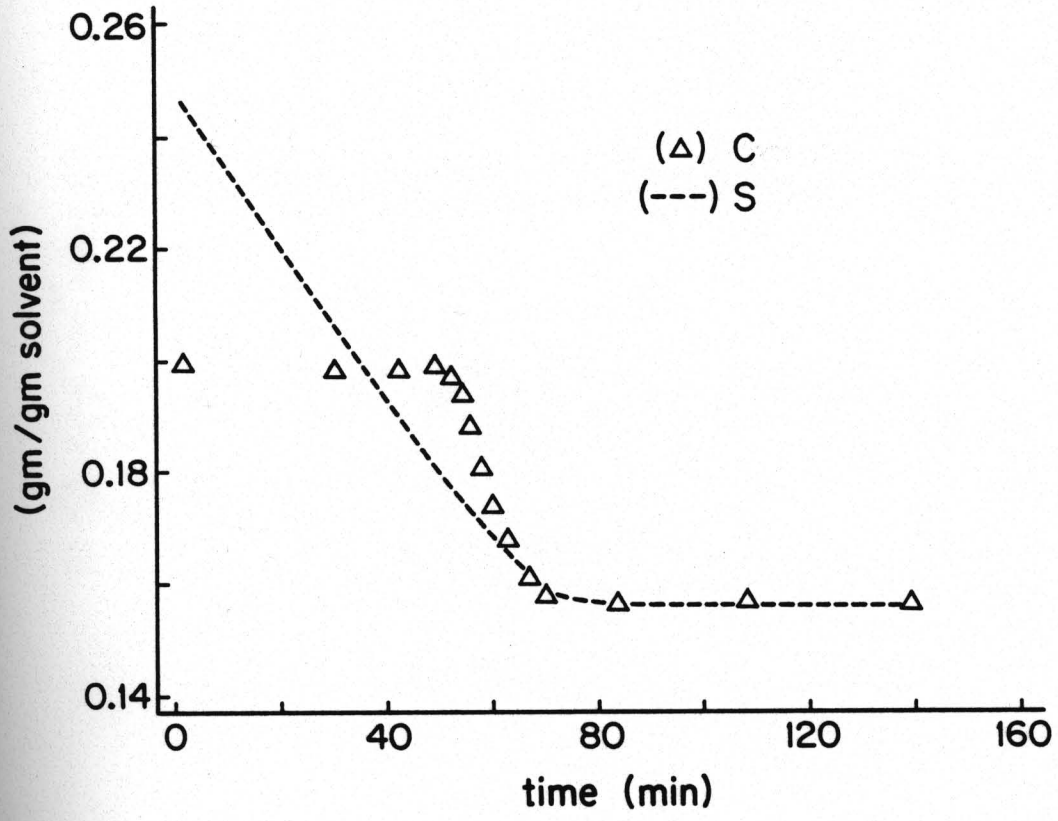

Figure III-5-9. Concentration (△) and solubility (---) profiles during cooling and crystallization of oxalic acid dihydrate from water saturated at 30°C.

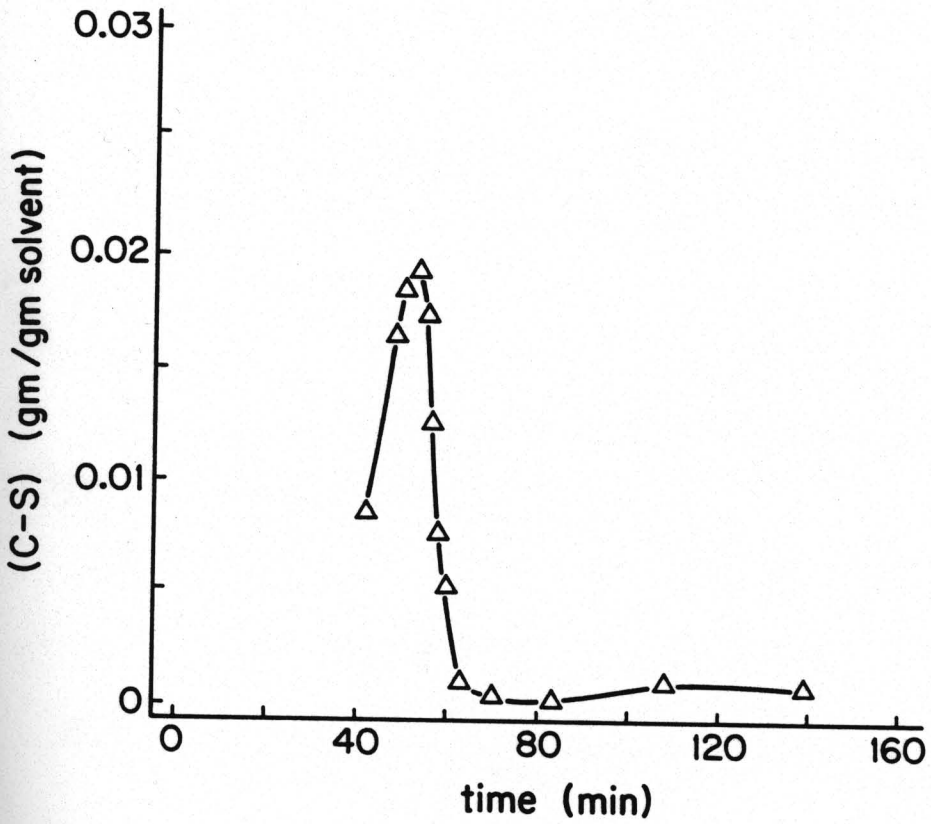

Figure III-5-10. Supersaturation profile during cooling and crystallization of oxalic acid dihydrate from water saturated at 30°C.

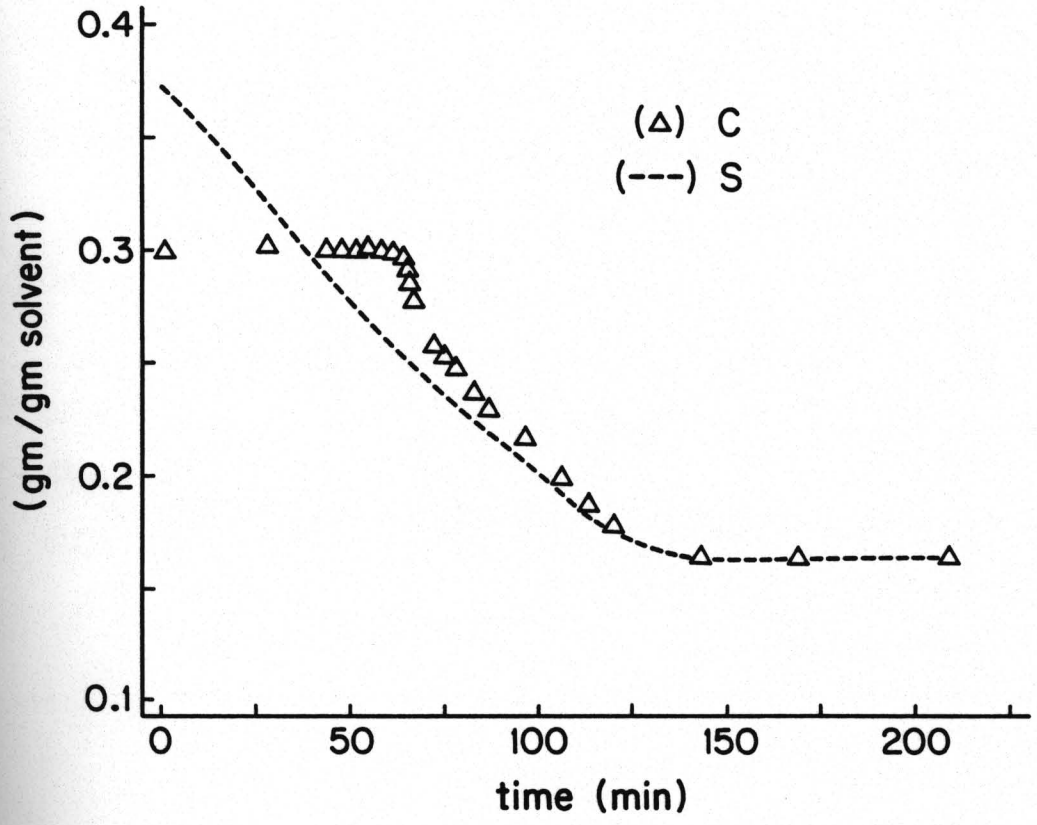

Figure III-5-11. Concentration (△) and solubility (---) profiles during cooling and crystallization of oxalic acid dihydrate from water saturated at 40°C.

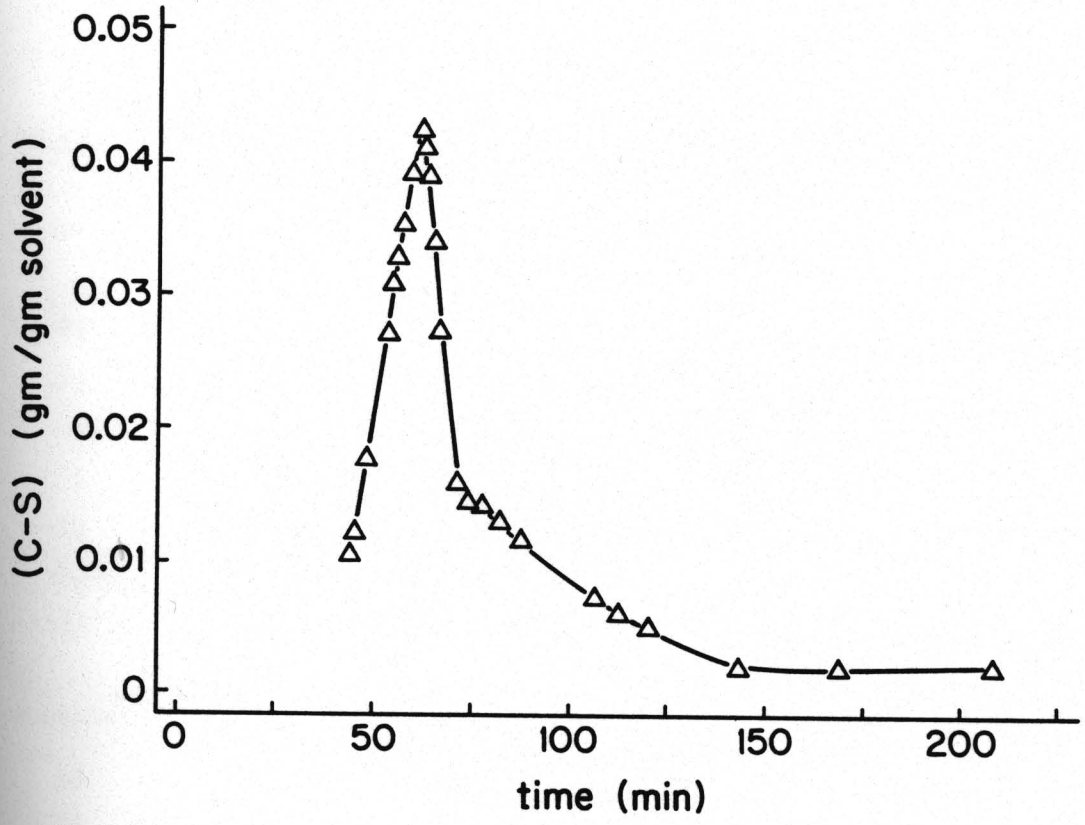

Figure III-5-12. Supersaturation profile during cooling and crystallization of oxalic acid dihydrate from water saturated at 40°C.

Table III-5-7

Solution Temperature at the Onset of Crystallization[a]

Solvent(% weight)	T_s=30°C	T_s=40°C
Water	26.8(0.4)[b]	35.9(0.1) 34.0[c]
Glycerine		
1	27.0	37.2
4	26.9	36.9
1	26.8	37.0
10	26.6	36.4
15	26.6(0.3)	36.3(0.1)
25	26.6	35.3
Acetone		
10	27.3	37.6
50	27.7(0.0)	37.3(0.3)
100	27.7	37.7

(a) Calculated from temperature-time profile.
(b) Standard deviation for duplicate crystallization runs.
(c) Unseeded solution.

III-6 Crystal Size Distributions

One of the goals of this study is, as has been mentioned, attempted explanations of the type of particle size distribution deriving from the fundamental processes of the crystallization. To this end experiments were carried out in several solvents to study (a) the type of distribution encountered and (b) what possible effects solvents and physical parameters (viscosity, saturation temperature) might have on the distribution.

From a fundamental point of view the distribution results from (a) the birth of a particle and (b) its growth thereafter. The former controls the number of particles, and growth controls their size, so that the distributions that result, in a primary sense, are number distributions, not weight distributions. The results to follow will deal with number distributions as a function of a characteristic linear dimension (z) and a shape factor, b/a, which is the breadth to length ratio of the crystal.

III-6-1 Number Distribution of Oxalic Acid Dihydrate as a Function of z

Data representing the particle weights from the mesh fractions for crystals obtained in the different solvent systems are shown in Tables III-6-1 to III-6-4. Particle size distributions from sieve analysis, by weight, have been converted into number distributions through knowledge of density and particle size. The total number of crystals calculated in this way are shown in Table III-6-5. The

Table III-6-1

Individual Crystal Weights (System: Glycerine/Water, T_S = 30°C).

Mesh fraction	Weight (gm/crystal) x 10^4						
	% glycerine[a]						
	0	1	4	7	10	15	25
20	6.63	8.27	7.11 (1.71)[b]	8.58	6.25	6.11	2.88
20/30	3.16	2.87 (0.17)	2.20 (0.90)	1.95	1.81 (0.39)	1.33 (0.23)	1.40
30/40	0.80	0.78 (0.18)	0.83 (0.38)	0.65	0.57 (0.23)	0.76	0.83 (0.10)
40/50	0.38	0.30	0.30 (0.02)	0.22	0.45 (0.05)	0.29	0.35 (0.06)
50/60	0.17	0.14	0.13	0.11	0.13	0.14	0.29 (0.05)
60/80	0.11	0.09					
80/100	0.05	0.42					
100/pan	0.0						

[a] Percent by weight.

[b] Standard deviation of triplicate measurements.

Table III-6-2

Individual Crystal Weights (System: Glycerine/Water, T_S = 40°C).

Mesh fraction	Weight (gm/crystal) x 10^4						
	% glycerine[a]						
	0	1	4	7	10	15	25
20	10.57 (0.07)	9.76	12.70	10.90	9.76	6.88	4.37
20/30	3.46 (0.04)	2.99	2.17 (0.28)[b]	3.28	4.26	4.70	1.48 (0.06)
30/40	1.12 (0.01)	0.95	0.88 (0.18)	0.82	0.79 (0.34)	0.70	0.67 (0.30)
40/50	0.47 (0.04)	0.38	0.348 (0.004)	0.48	0.32 (0.01)	0.34	0.42
50/60	0.22 (0.03)	0.20	0.19	0.20	0.17		0.21 (0.01)
60/80	0.121 (0.004)						0.09 (0.02)
80/100	0.06 (0.01)						0.04 (0.01)
100/pan							0.024 (0.003)

[a]Percent by weight.

[b]Standard deviation of triplicate measurements.

Table III-6-3

Individual Crystal Weights (System: Acetone/Water, T_S = 30°C).

Mesh fraction	Weight (gm/crystal) x 10^4			
	% acetone[a]			
	10	50	75	100
20	7.30	6.49		9.29
20/30	2.90	2.82	3.25	3.02
30/40	0.94	0.92	0.97	0.89
40/50	0.41	0.39	0.42	0.35
50/60	0.19	0.23	0.20	0.20
60/80	0.12	0.11	0.11	
80/100			0.06	

[a]Percent by weight.

Table III-6-4

Individual Crystal Weights (System: Acetone/Water, T_S = 40°C).

Mesh fraction	Weight (gm/crystal) x 10^4			
	% acetone[a]			
	10	25	50	100
20	15.0	14.7 (1.1)[b]	10.7	10.6
20/30	3.40	3.63 (0.13)	3.09	3.15
30/40	0.92	1.12 (0.03)	1.04	0.87
40/50	0.49	0.42 (0.04)	0.40	0.42
50/60		0.22 (0.01)	0.20	0.18
60/80			0.13	0.13
80/100			0.06	0.05

[a]Percent by weight.

[b]Standard deviation of duplicate measurements.

Table III-6-5

Number of Crystals of Oxalic Acid Dihydrate at the End of a Crystallization Run.

Solvent (% weight)	Number of crystals x 10^{-2}/gm of solvent	
	T_S = 30°C	T_S = 40°C
Acetone/Water		
10	8.8	11.8
25	8.9	12.8
50	8.9	13.6 (3.3)[a]
75	8.1	8.7
100	4.9	5.7
Glycerine/Water		
1	14.7	14.8
1	3.2[b]	11.9[c]
4	9.6	20.6
7	4.5	12.7
10	5.3	20.9
15	6.7	16.5
25	6.9	83.0
Water	10.3	10.9

[a]Standard deviation for duplicate runs.

[b]Cooling rate at 2°C/hour.

[c]Seed size 40/60 mesh (335 μm).

number distributions in general are represented as a function of a characteristic linear dimension of the particles in question. In literature this is frequently a sieve diameter aperture or some other dimension related to the crystal size (Carstensen, 1981, Irani and Callis, 1963). However, since sieve analysis measures the second largest dimension of a particle, a different dimension, z, has been used in this study. z is given by

$$z = (w/\rho)^{1/3} \qquad \text{Eq.III-6}$$

where w is the weight (in grams) per crystal and ρ is the density. Values of z, sieve diameters and cumulative percent by number of crystals and weight are included in Appendix B. Rather than using the cumulative percent as the dependent varible, the normalized standard deviate, t, has been chosen since this would represent the kind of distribution (normal or log normal) in linearized form. Tables III-6-6 through III-6-9 include linear regression analysis results for all the populations studied as a function of z and ln z. Some graphic forms of these are presented in Figure III-6-1.

III-6-2 (b/a) - Frequencies Presented as Number Distributions

Microscopy was performed as described in Section II-5-2 to better define the geometry of the crystals. The breadth/length ratio, b/a, is the parameter scrutinized.

Knowledge of the particle dimensions allow for the conversion of

Table III-6-6

Distribution of Shape Factor (z)

(Glycerine/Water, T_s = 30°C).

t-value plotted against	R^2	Intercept	Slope	Sum of squares[a]	% Glycerine
z	0.978	-1.09	0.0050	0.03	0
ln (z)	0.954	-9.84	1.84	0.07	
z	0.974	-1.21	0.0052	0.05	1
ln (z)	0.977	-10.65	1.98	0.05	
z	0.994	-3.64	0.0071	0.02	4
ln (z)	0.989	-20.82	3.38	0.04	
z	0.881	-2.51	0.0069	0.41	4
ln (z)	0.955	-16.68	2.89	0.15	
z	0.945	-2.06	0.0047	0.11	7
ln (z)	0.989	-12.43	2.10	0.02	
z	0.952	-3.48	0.0077	0.17	10
ln (z)	0.977	-19.62	3.26	0.08	
z	0.977	-2.64	0.0068	0.06	15
ln (z)	0.995	-16.78	2.86	0.01	

t-value plotted against	R^2	Intercept	Slope	Sum of squares[a]	% Glycerine
z	0.980	-4.68	0.0123	0.06	25
ln (z)	0.983	-28.30	4.80	0.05	
z	0.913	-2.12	0.0046	0.16	1[b]
ln (z)	0.965	-12.09	2.02	0.07	

[a]Residual sum of squares.

[b]Cooling rate of 2°C/hour.

Table III-6-7

Distribution of Shape Factor (z)

(Glycerine/Water, T_s = 40°C).

t-value plotted against	R^2	Intercept	Slope	Sum of squares	% Glycerine
z	0.995	-2.08	0.0049	0.01	0
ln (z)	0.948	-11.66	1.98	0.10	
z	0.980	-1.60	0.0039	0.02	1[a]
ln (z)	0.964	-10.04	1.71	0.04	
z	0.903	-1.62	0.0043	0.15	1
ln (z)	0.958	-10.11	1.75	0.06	
z	0.859	-2.15	0.0051	0.41	4
ln (z)	0.966	-14.97	2.55	0.10	
z	0.951	-2.56	0.0054	0.13	7
ln (z)	0.994	-14.88	2.47	0.02	
z	0.905	-2.98	0.0068	0.43	10
ln (z)	0.967	-18.3	3.08	0.15	
z	0.963	-3.75	0.0079	0.17	15
ln (z)	0.987	-20.31	3.37	0.06	
z	0.989	-1.39	0.0072	0.02	25
ln (z)	0.965	-11.22	2.16	0.07	

[a]Seed size of (40/60) mesh cut (335 μm).

Table III-6-8

Distribution of Shape Factor (z)

(Acetone/Water, T_s = 30°C).

t-value plotted against	R^2	Intercept	Slope	Sum of squares	% Acetone
z	0.974	-1.87	0.0057	0.05	10
ln (z)	0.982	-13.70	2.40	0.04	
z	0.926	-1.89	0.0056	0.16	25
ln (z)	0.975	-13.78	2.41	0.05	
z	0.944	-1.85	0.0059	0.11	50
ln (z)	0.981	-13.85	2.44	0.04	
z	0.956	-2.00	0.0059	0.11	75
ln (z)	0.988	-15.64	2.71	0.03	
z	0.987	-2.17	0.0054	0.03	100
ln (z)	0.987	-13.81	2.36	0.03	

Table III-6-9

Distribution of Shape Factor (z)

(Acetone/Water, T_s = 40°C).

t-value plotted against	R^2	Intercept	Slope	Sum of squares	% Acetone
z	0.998	-1.15	0.0033	0.002	10
ln (z)	0.947	-8.20	1.44	0.06	
z	0.968	-1.47	0.0037	0.04	25
ln (z)	0.982	-9.46	1.63	0.02	
z	0.979	-1.48	0.0042	0.03	50
ln (z)	0.974	-9.83	1.72	0.04	
z	0.989	-1.52	0.0038	0.01	50
ln (z)	0.941	-8.92	1.53	0.07	
z	0.962	-1.34	0.0035	0.04	75
ln (z)	0.952	-8.33	1.44	0.05	
z	0.956	-1.50	0.0031	0.04	100
ln (z)	0.878	-7.32	1.21	0.10	

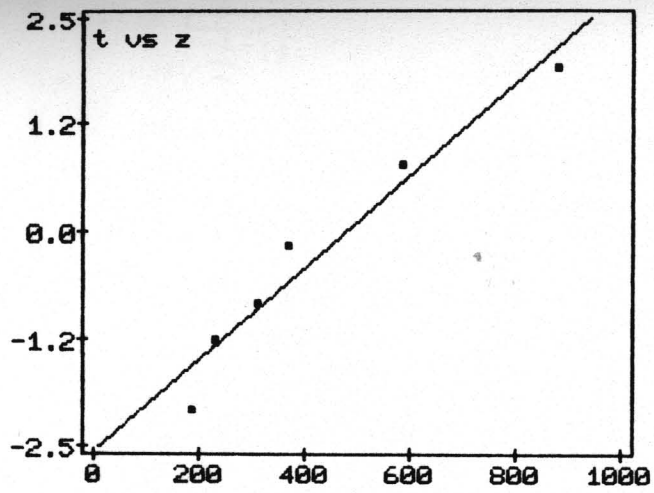

(i)

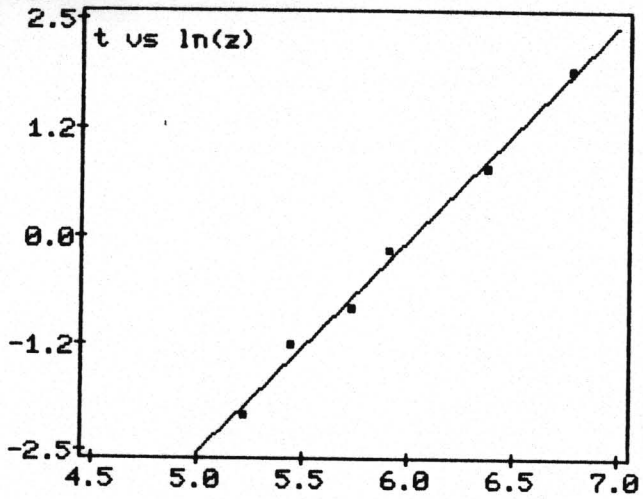

(ii)

Figure III-6-1. Normal standard deviate (t) as a function of: (i) z and (ii) ln z. (7% glycerine/water, T_S=40°C).

particle size distributions to particle shape distributions in the following manner: the number of particles measured, $N(i,\alpha)$ in the i^{th} mesh cut are categorized into a number, n of intervals (usually seven to ten) denoted $\alpha(1)$ to $\alpha(n)$. These cover the range of b/a-values for an experiment. Since the number of particles, N(i), in a mesh cut is known, then the fraction of these in an interval, e.g. $\alpha(1)$ to $\alpha(2)$ can be obtained, and is given by

$$\frac{N(i, \alpha(1), \alpha(2)) \quad N(i)}{N(i,\alpha)} \qquad \text{Eq. III-6-2}$$

The total number of particles within the interval is then

$$\sum_{i=1}^{j} \frac{N(i, \alpha(1), \alpha(2)) \quad N(i)}{N(i,\alpha)} \qquad \text{Eq.III-6-3}$$

where j is the total number of mesh cuts. This allows for calculation of the cumulative percents and t-values based on b/a-ratios. An example of this type of calculation is shown in Table III-6-10 through III-6-13. The data obtained in this fashion were treated by least squares fit and the results shown in Tables III-6-14 to III-6-17. Typical examples are presented in Figure III-6-2.

Table III-6-10

Crystal Size and Shape Distribution (Example Calculation).

A. Crystal Size Distribution (Number).

System: 25% glycerine, T_s = 40°C.

Mesh	g (retained)	(g/cryst)·10^4	crystal #	% crystals	cum % >
20	0.8771	4.37	2007	0.090	0.090
20/30	9.054	1.48	61176	2.74	2.83
30/40	11.9482	0.67	177273	7.93	10.76
40/50	9.0604	0.42	218323	9.77	20.52
50/60	5.537	0.21	250543	11.21	31.73
60/80	5.1313	0.09	583102	26.08	57.81
80/100	1.9838	0.04	476875	21.33	79.14
100/pan	0.914	0.02	466327	20.86	100

Table III-6-11

Crystal Size and Shape Distribution (Example Calculation).

B. Crystal Shape Distribution.

1. Number of Crystals Measured within an Interval (b/a).

b/a ↓ Interval	Mesh cut							
	20	20/30	30/40	40/50	50/60	60/80	80/100	100/pan
0.05-0.10[a]								3
0.10-0.20		3	8	4	8	7	4	4
0.20-0.30		10	12	7	14	8	8	5
0.30-0.40	1	8	2	8	6	4	12	4
0.40-0.50	1	3	2	4	-	5	4	2
0.50-0.60		3	3	4	-	2	1	-
0.60-0.70	2	1		1		2	1	
0.70-0.80	1		2	1		2	1	
0.80-0.90	3	1			1			
0.90-1.0	2	1						

[a] Low < x ≤ high.

Table III-6-12

Crystal Size and Shape Distribution (Example Calculation).

B. Crystal Shape Distribution.

2. Number of Crystals from the Population within an Interval.[a]

Interval	20	20/30	30/40	40/50	50/60	60/80	80/100	100/pan
0.05-0.10								77721
0.10-0.20	-	6118	48903[b]	30114	66812	136057	61532	103628
0.20-0.30	-	20392	73354	52699	116920	155494	123065	129535
0.30-0.40	201	16314	12226	60227	50109	77747	184596	103628
0.40-0.50	201	6118	12226	30114	-	97184	61532	51814
0.50-0.60	-	6118	18339	30114	-	38873	15383	-
0.60-0.70	401	2039	-	7528	-	38873	15383	-
0.70-0.80	201	-	12226	7528	-	38873	15383	-
0.80-0.90	602	2039	-	-	16703	-	-	-
0.90-1.0	401	2039	-	-	-	-	-	-

[a] $\frac{N(i,\alpha(1),\alpha(2))}{N(i,\alpha)} \cdot N(i)$

[b] $\frac{8}{29} \cdot 177273.$

Table III-6-13

Crystal Size and Shape Distribution (Example Calculation).

B. Crystal Shape Distribution.

3. Cumulative Number of Crystals.

Interval	Crystal #[a]	Cum. (% >)	Cum. (% <)	(t) (% <)
0.05-0.10	77721	100	3.48	1.82
0.10-0.20	453164[b]	90.64	23.75	0.71
0.20-0.30	671458	58.65	53.78	-0.10
0.30-0.40	505047	34.60	76.37	-0.72
0.40-0.50	259187	16.29	87.97	-1.17
0.50-0.60	108826	8.74	92.83	-1.46
0.60-0.70	64226	5.26	95.71	-1.72
0.70-0.80	74211	2.18	99.03	-2.34
0.80-0.90	19344	0.48	99.89	-3.0
0.90-1.0	2440	0.10	100	

[a] $\sum_{i=1}^{j} = \frac{N(i,\alpha(1),\alpha(2))}{N(i,\alpha)} \cdot N(i)$

[b] 6118 + 48903 + 30114 + 66812 + 136057 + 61532 + 103628.

Table III-6-14

Distribution of Shape Factors (b/a)

(Glycerine/Water, T_s = 30°C).

t-value plotted against	R^2	Intercept	Slope	Sum of squares[a]	% Glycerine
b/a	0.980	3.57	-5.63	0.04	0
ln (b/a)	0.998	-1.61	-3.13	0.001	
b/a	0.996	2.064	-3.811	0.02	1
ln (b/a)	0.992	-1.524	-2.302	0.01	
b/a	0.9645	2.98	-4.89	0.04	4
ln (b/a)	0.980	-1.62	-3.05	0.02	
b/a	0.958	3.70	-5.84	0.08	4
ln (b/a)	0.988	-1.68	-3.27	0.02	
b/a	0.981	2.41	-5.08	0.03	7
ln (b/a)	0.965	-2.24	-2.78	0.05	
b/a	0.968	3.97	-14.82	0.11	10
ln (b/a)	0.993	-5.51	-3.98	0.02	
b/a	0.939	1.42	-4.65	0.06	15
ln (b/a)	0.982	-2.56	-.218	0.02	

t-value plotted against	R^2	Intercept	Slope	Sum of[a] squares	% Glycerine
b/a	0.893	-1.16	-4.26	0.12	25
ln (b/a)	0.977	-2.52	-1.96	0.03	
b/a	0.971	3.82	-6.29	0.07	1[b]
ln (b/a)	0.995	-1.97	-3.51	0.01	

[a]Residual sum of squares.

[b]Cooling rate of 2°C/hour.

Table III-6-15

Distribution of Shape Factor (b/a)

(Glycerine/Water, T_s = 40°C).

t-value plotted against	R^2	Intercept	Slope	Sum of squares	% Glycerine
b/a	0.997	3.64	-5.31	0.01	0
ln (b/a)	0.980	-1.21	-2.90	0.03	
b/a	0.980	1.95	-3.85	0.02	1
ln (b/a)	0.991	-1.46	-1.84	0.01	
b/a	0.948	2.83	-5.48	0.09	1[a]
ln (b/a)	0.990	-1.85	-2.46	0.02	
b/a	0.930	1.75	-4.32	0.08	4
ln (b/a)	0.989	-2.11	-2.21	0.01	
b/a	0.940	2.04	-4.78	0.10	7
ln (b/a)	0.965	-2.35	-2.57	0.06	
b/a	0.904	2.19	-5.45	0.22	10
ln (b/a)	0.975	-2.69	-2.69	0.06	
b/a	0.936	1.65	-4.85	0.14	15
ln (b/a)	0.990	-2.68	-2.24	0.02	
b/a	0.958	1.61	-5.07	0.08	25
ln (b/a)	0.992	-2.70	-2.14	0.02	

[a]Seeds used are 40/60 mesh (335 μm).

Table III-6-16

Distribution of Shape Factor (b/a)

(Acetone/Water, T_s = 30°C).

t-value plotted against	R^2	Intercept	Slope	Sum of squares	% Acetone
b/a	0.962	3.68	-5.29	0.05	10
ln (b/a)	0.929	-1.26	-3.22	0.09	
b/a	0.979	3.95	-5.74	0.03	25
ln (b/a)	0.939	-1.41	-3.48	0.09	
b/a	0.985	4.52	-6.25	0.03	50
ln (b/a)	0.958	-1.32	-3.81	0.07	
b/a	0.999	3.43	-4.69	0.003	75
ln (b/a)	0.987	-0.96	-2.88	0.01	
b/a	0.991	3.79	-5.37	0.01	100
ln (b/a)	0.980	-1.11	-2.94	0.03	

Table III-6-17

Distribution of Shape Factor (b/a)

(Acetone/Water, T_s = 40°C).

t-value plotted against	R^2	Intercept	Slope	Sum of squares	% Acetone
b/a	0.990	3.66	-5.28	0.02	10
ln (b/a)	0.981	-1.30	-3.18	0.03	
b/a	0.991	3.79	-5.37	0.01	25
ln (b/a)	0.980	-1.12	-2.94	0.03	
b/a	0.988	3.58	-5.68	0.03	50
ln (b/a)	0.942	-1.58	-2.96	0.13	
b/a	0.982	3.19	-4.88	0.02	75
ln (b/a)	0.999	-1.43	-2.98	0.002	
b/a	0.996	3.37	-4.97	0.01	100
ln (b/a)	0.975	-1.17	-2.71	0.04	

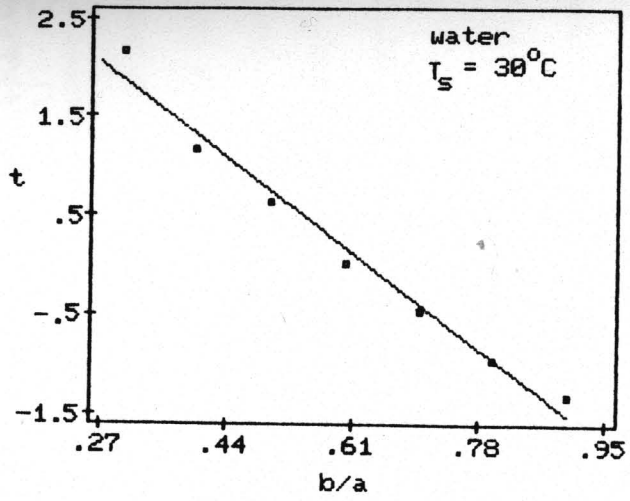

(i)

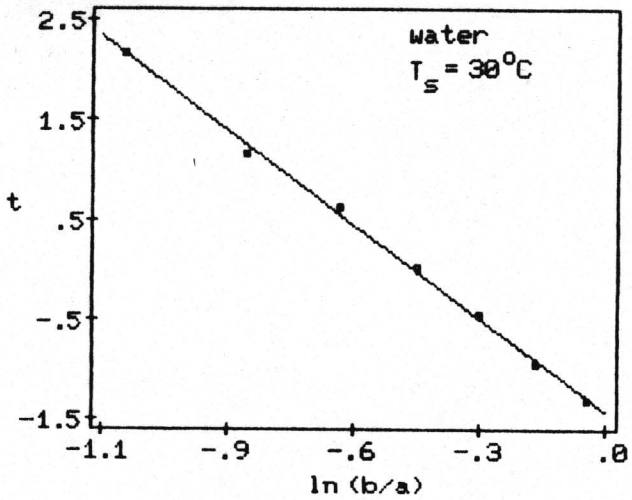

(ii)

Figure III-6-2. Normal standard deviate (t) as a function of: (i) (b/a) and (ii) ln (b/a). (Water, T_S=30°C).

IV DISCUSSION

IV-1 Thermal History of Solutions

Experiments done to study the effect of thermal history of a solution are summarized in Tables III-4-1 and III-4-2. It is apparent from these that there is no such significant effect in the oxalic acid dihydrate system. The statement, of course, is that the experiments failed to show such a difference, and it should be pointed out that Nyvlt et al. (1970) reported that the reproducibility of the metastable zone width measurements is better with anhydrous substances than with hydrates. It is assumed hereafter, that there is no thermal history effect. It should be noted, that experiments were carried out with careful attention to the time temperature profile, so that even if there may be an effect, comparisons in the following have always been performed between samples with as close to identical histories as possible.

IV-2 Evaluation of Growth and Nucleation Rate Parameters

Crystal size distributions are determined by the particle birth rate and by the growth rate. In order to evaluate the rate parameters that control the crystal size distribution during non-isothermal crystallization, the following will be described: (a) simulation of the concentration and saturation-time profiles during crystallization and (b) application of the model that explains the desupersaturation

to the crystal size distributions.

IV-2-1 Simulation of the Crystallization Process During Desupersaturation of Solutions

The curves of concentration of oxalic acid dihydrate and its saturation concentration as a function of time during linear cooling of a supersaturated solution have been presented in Section III-5. In general they correspond to the situation in Fig. IV-2-1.

During the period $t < t'$ the temperature drops, i.e. the solubility drops, but the concentration of material in solution (M/Q) stays constant. Once precipitation starts (at t') the concentration of material in solution (C) will decrease until the solution reaches the final temperature at time t". It is convenient to define reduced variables for comparison purposes. The crystallization processes (nucleation and growth) occur in an interval which in reduced times is from zero to one. Hence intermittent times, t*, are defined by

$$t^* = (t-t')/(t''-t') \qquad \text{Eq. IV-2-1}$$

where t is real time (i.e. in real time units). t*, of course, is dimensionless. The concentration of oxalic acid dihydrate is represented in reduced form by

$$C^* = (100\ C/S_0) \qquad \text{Eq. IV-2-2}$$

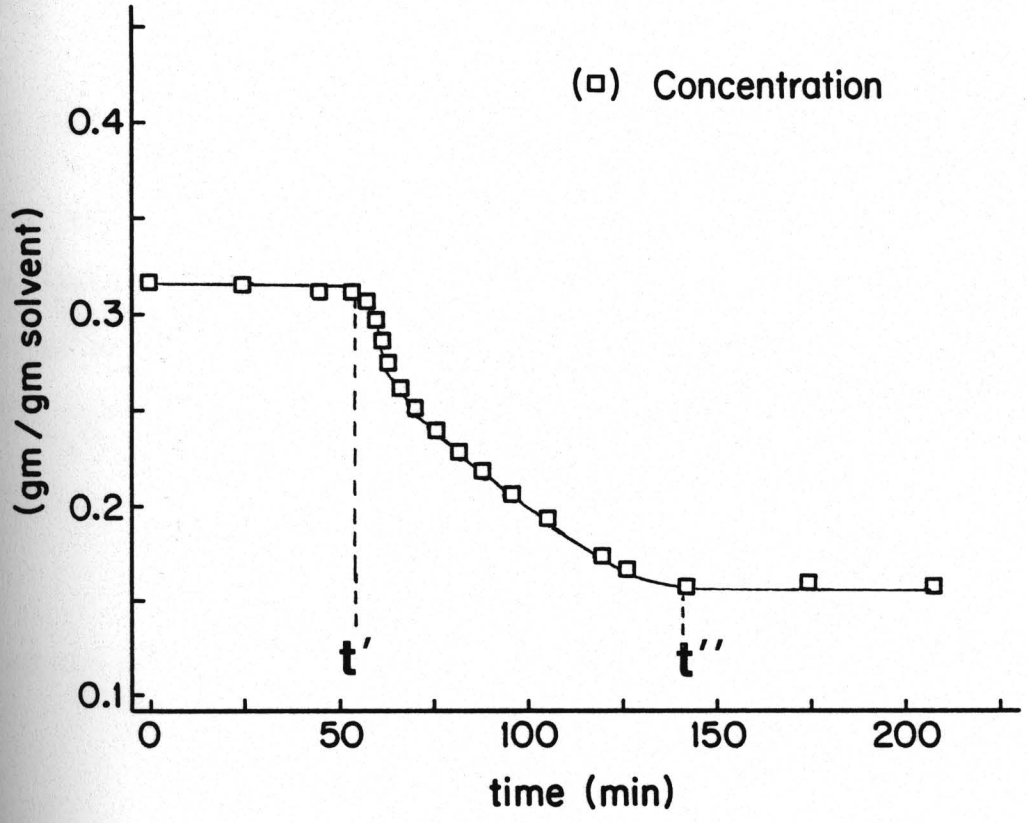

Figure IV-2-1. Characteristic concentration and solubility profile during cooling and crystallization of oxalic and dihydrate.

where S_0 is the solubility at the onset of the precipitation. Similarly, the solubility, in reduced form, is given by

$$S^* = (100\ S/S_0) \qquad \text{Eq. IV-2-3}$$

When the solution becomes supersaturated, the possibility for nucleation exists. The nucleation rate has, in many systems, been found to be proportional to the supersaturation, (C-S) to a power. The number of nuclei, dN, formed in a time interval, dt*, is given by

$$dN/dt^* = J^* (C^*-S^*)^j \qquad \text{Eq. IV-2-4}$$

and the number of crystals born from time t*=0 to t*=h* is

$$N = \int_0^{h^*} J^* (C^*-S^*)^j \, dt^* \qquad \text{Eq. IV-2-5}$$

where J* is the nucleation rate constant and j is the nucleation order. This latter for the case of oxalic acid dihydrate has been reported to be 3.8, from measurements of the metastable zone width (Nývlt, 1978). The size of the nucleus depends on the Gibbs energy and the surface energy of the substance (Mullin, 1972), but once the nucleus is formed, crystal growth is a voluntary process. Growth rates have been found to be proportional to the supersaturation to a

power and to the surface area of the crystal. Hence at time t*, the amount of material dM, precipitated in a time interval dt* is

$$dM/dt^* = A\ G^*\ (C^*-S^*)^g \qquad \text{Eq. IV-2-6}$$

where G* is the growth rate constant, g is the growth order and A is a function of the total surface area available for growth. The growth order has been reported in literature to have a value of 2.4 for oxalic acid dihydrate (Nyvlt, 1978).

The amount precipitated at time t* = h* is then

$$M = \int_0^{h^*} A\ G^*\ (C^*-S^*)^g\ dt^* \qquad \text{Eq. IV-2-7}$$

where A and both C* and S* are functions of time. The area of n(i) crystals with length r(i) for the required values of i to define the population is given by

$$A = f_a \sum_{i=1}^{j} n(i)\ (r(i)\ )^2 \qquad \text{Eq. IV-2-8}$$

where f_a is a surface shape factor. Due to the difficulty of measuring a dynamic particle size distribution, the dependency of the

area has been defined in terms of the concentration in the following way: the concentration in solution is expressed as amount of solute in solution by multiplying the concentration (expressed as g/g of solvent) by the mass of solvent (Q g). Then the amount precipitated is obtained by the difference between the initial amount, M_o, and the amount not precipitated at time t*. The latter is (C* Q). The area can then be expressed in a relationship similar to the area of an isometric particle:

$$A = f_{sv} (M/\rho)^{2/3} = f_{sv}(V)^{2/3} \qquad \text{Eq. IV-2-9}$$

Here ρ is the density and V is the volume. This is not strictly correct, but is so to a first approximation (Appendix C).

Since the crystallization is occurring in a non-isothermal fashion, S (the solubility) or S* (in reduced form) is also a function of time. It is for this reason that attempts to solve the integral in Eq. IV-2-7 in closed form have not been made.

Model experiments have been carried out to determine the concentration of oxalic acid dihydrate in solution during crystallization, as a function of temperature and time. The time dependency of the solubility was calculated from the Van't Hoff equations shown in Section III-3. It is noted from the desupersaturation profiles (Section III-5) that the solubility change with time between the onset of precipitation, t', and the end of precipitation, t", can be approximated by a straight line, and can be

expressed as

$$S = S_0 - i\,t \qquad \text{Eq. IV-2-10}$$

where $$i = (S_0 - S_F)/h \qquad \text{Eq. IV-2-11}$$

where h is the duration of the crystallization process, i.e.

$$h = t' - t'' \qquad \text{Eq. IV-2-12}$$

and where S_F is the solubility at time t".

Expressed in reduced variables Eq. IV-2-10 becomes

$$S^* = 100 - ((100 - S_F^*)\, t^*/h^*) \qquad \text{Eq. IV-2-13}$$

where according to the definition of t* (Eq. IV-2-1)

$$h^* = 1$$

Having, now, all the time dependent terms expressed as functions of t* and C*, the mode of approaching the solution to the growth and nucleation rate equations has been to evaluate them numerically in the way shown in diagram IV-2-2. Details of a Basic Program written for this purpose are included in Appendix D.

If one views the two processes, crystal birth and growth, as occurring simultaneously and being responsible for the depletion of solute from solution (i.e. reduction of concentration) one can generate, according to this scheme, a concentration and

Step Δt^*	Crystals Born	Area	Mass Created	Concentration in solution
0	———	———	———	C_0^*
1	$N_1 = J^*(C_0^* - S_0^*)^j \Delta t_1^*$	$A_1 = N_1 a^*$	$M_1 = A_1 G^*(C_0^* - S_0^*)^g \Delta t_1^*$	$C_0^* - (\frac{M1}{Q}) = C_1^*$
2	$N_2 = J^*(C_1^* - S_1^*)^j \Delta t_2^*$	$A_2 = (N_2 a^*) + f_{sv}\left[\frac{(C_0^* - C_1^*)Q}{\rho}\right]^{2/3}$	$M_2 = A_2 G^*(C_1^* - S_1^*)^g \Delta t_2^*$	$C_1^* - (\frac{M2}{Q}) = C_2^*$
3	$N_3 = J^*(C_2^* - S_2^*)^j \Delta t_3^*$	$A_3 = (N_3 a^*) + f_{sv}\left[\frac{(C_0^* - C_2^*)Q}{\rho}\right]^{2/3}$	$M_3 = A_3 G^*(C_2^* - S_2)^g \Delta t_3^*$	$C_2^* - (\frac{M3}{Q}) = C_3^*$

Figure IV-2-2. Schematic presentation of the crystallization model.

desupersaturation curve for given values of J* and G*. The process occurs from time t* = 0 to t* = 1 and it is divided into a certain number of intervals (1,000 in this case). One then calculates the number of nuclei born and mass precipitated during each interval. From this the concentration of solute remaining in solution C^*_n is calculated and used for the driving force term, $(C^*_n - S^*_n)$ of the next interval. These are the values shown in the last two columns of Fig. IV-2-2.

The initial area available for crystal growth (i.e. the area at the point in time when precipitation starts) comes from the nuclei that have been born in the first time interval. Their number is N_1 a*, where a* is the area of a nucleus. This cannot be evaluated, so for this first step it will be assumed that the growth rate is proportional to the number of nuclei. As growth and consecutive birth progresses, the area due to the crystals born (i.e. the nuclei formed) in an interval becomes negligible compared to the second term

$$f_{sv} \left((C_0^* - C_n^*)\, Q/\rho\right)^{2/3}$$

which includes the surface area available for growth due to the mass crystallized from t*=0 to t*. This is shown in Appendix C.

Having defined the model that describes the crystallizaton process one can compare the simulated concentration, supersaturation-time profiles and number of nuclei created through the whole process with experimentally found values. This, then, allows calculation of the rate constants J* and G*.

In order to understand the effect of the different parameters, growth and nucleation exponents, (g and j) and rate constants (J* and G*) on the desupersaturation of the solution and the final particle size distribution, several curves have been generated. These are presented in Figures IV-2-3 to IV-2-12. It is clear that by varying the four parameters one can obtain families of curves similar in shape to the experimentally determined profiles. However, the method of approach in this study has been to fix the exponents of growth and nucleation with the values reported in literature (Nyvlt, 1978). Although they are affected some by crystallization conditions (e.g. method of creating supersaturation, stirred or stagnant systems) they are the least sensitive parameters in the nucleation and growth rate equations. They are, for instance, not sensitive to temperature (Nielsen, 1964, Genck and Larson, 1972). These values have been determined in a crystallizaton environment similar to the one reported in this study. They were calculated from the dependence of the metastable zone width on the cooling rate of the soluton (Nyvlt et al., 1970, Nyvlt, 1978, Sohnel and Nyvlt, 1976).

In isothermal crystallization the shape of the supersaturation-time curve, (C-S), has been approximated in literature as following a relation of the form

$$\ln(C-S) = -q\ t + \ln(C_0-S) \qquad \text{Eq. IV-2-14}$$

The subscript zero denotes initial conditions, i.e. at the beginning

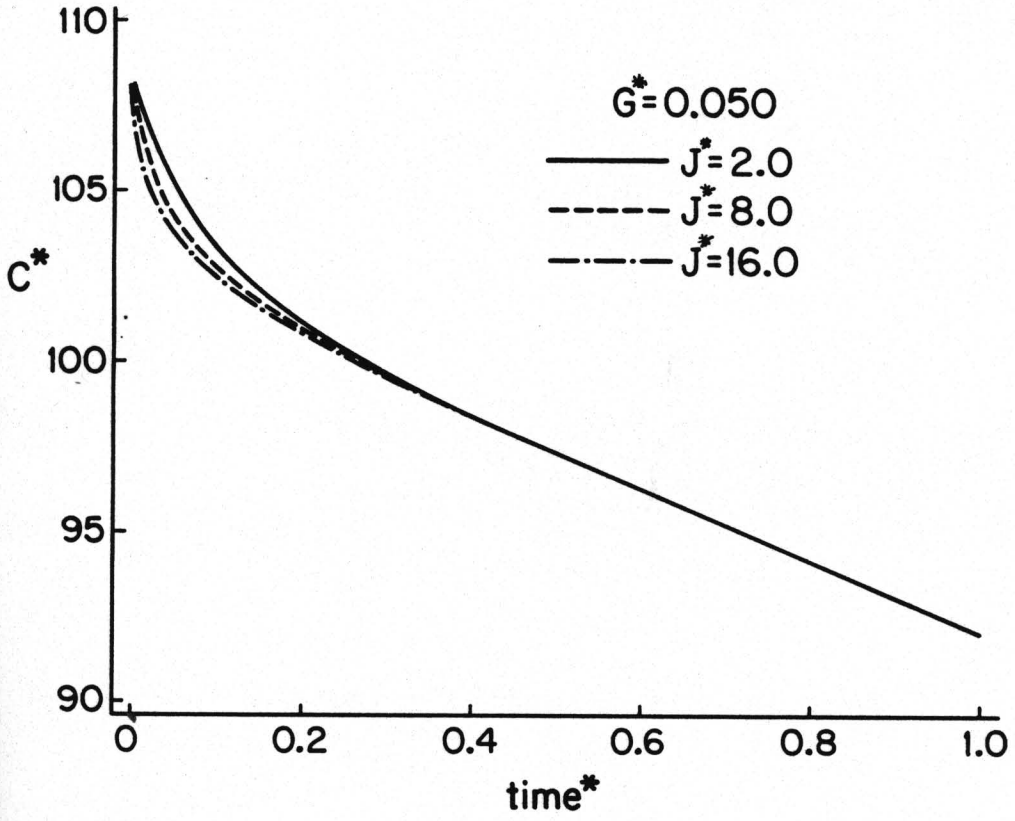

Figure IV-2-3. Concentration profile predicted by simulation of the crystallization process as a function of J*, for G*=0.050, j=4.0, g=2.0, S_F*=90 and C_O*=108.

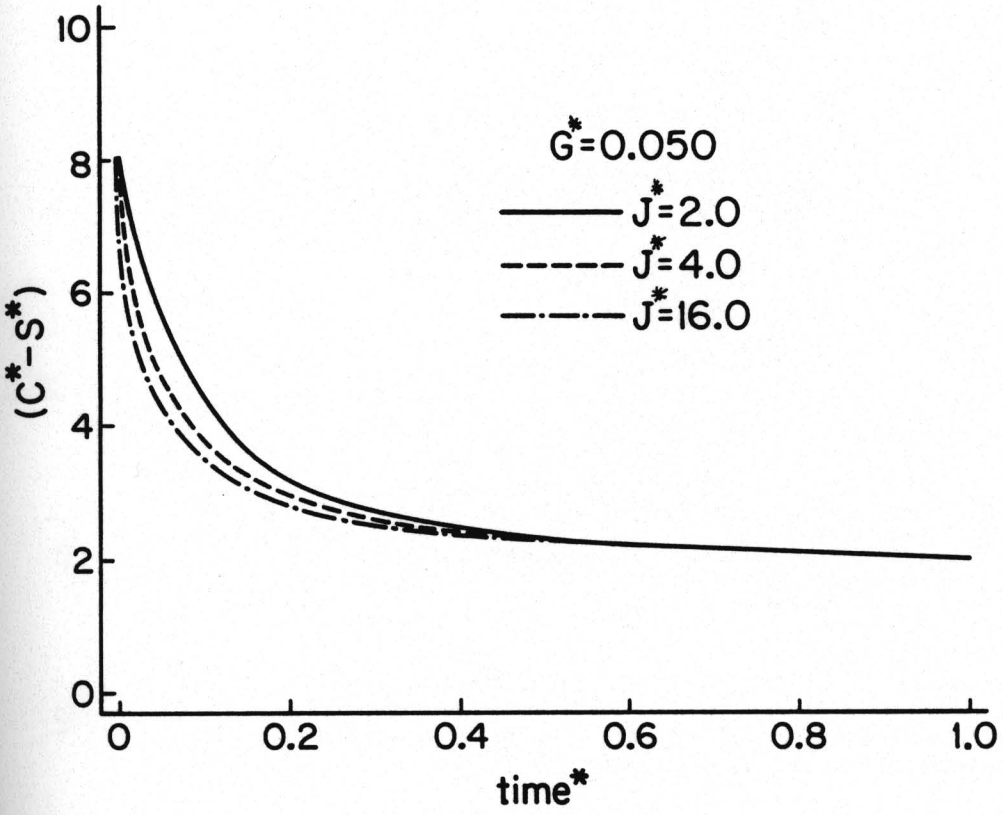

Figure IV-2-4. Supersaturation profile predicted by simulation of the crystallization process as a function of J*, for G*=0.050, j=4.0, g=2.0, S_F*=90 and C_O*=108.

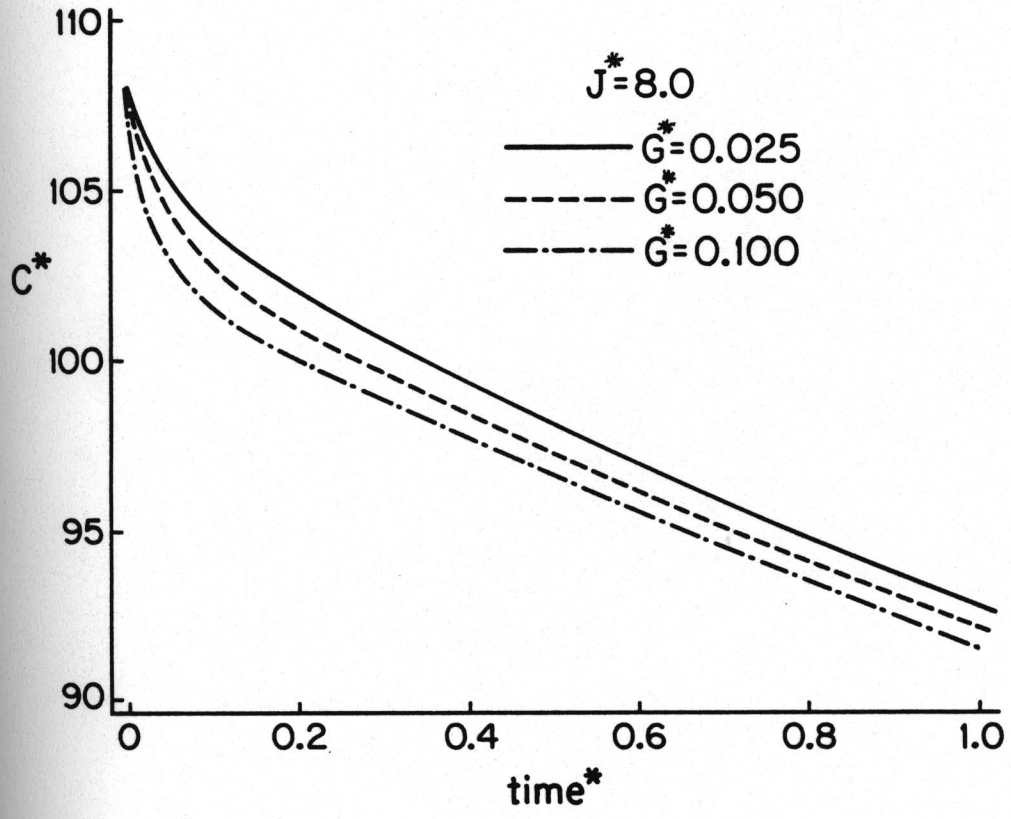

Figure IV-2-5. Concentration profile predicted by simulation of the crystallization process as a function of G*, for J*=8.0, j=4.0, g=2.0, S_F*=90 and C_0*=108.

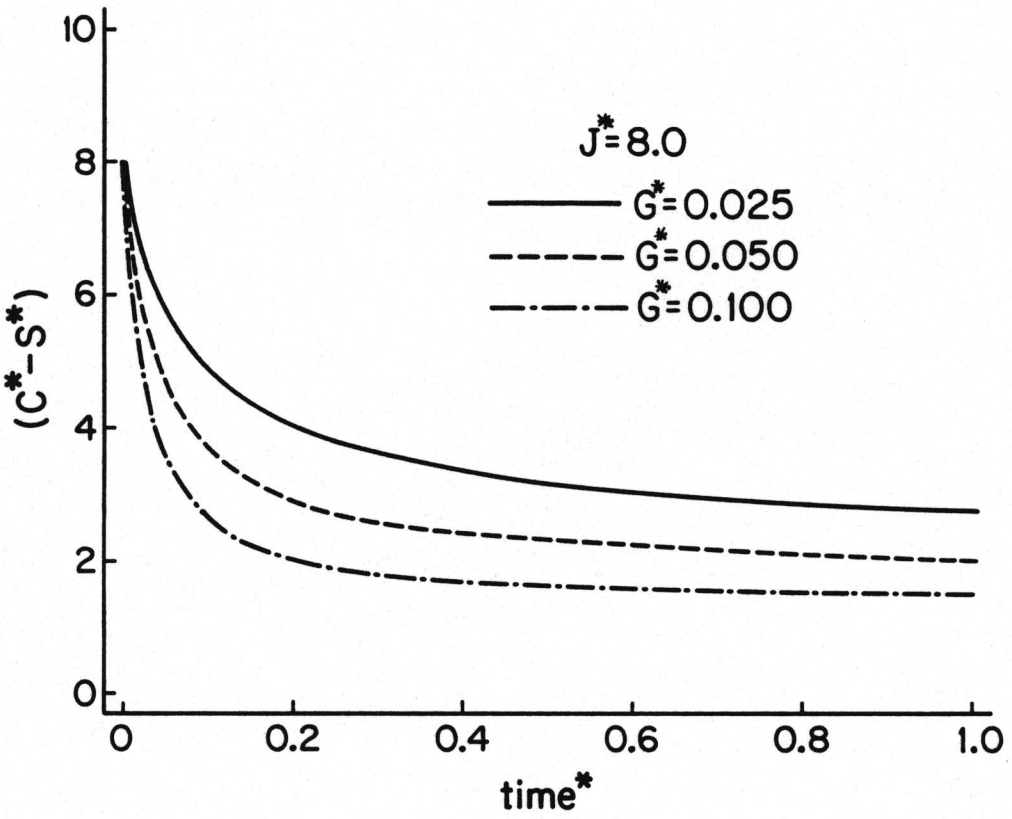

Figure IV-2-6. Supersaturation profile predicted by simulation of the crystallization process as a function of G*, for J*=8.0, j=4.0, g=2.0, S_F*=90 and C_O*=108.

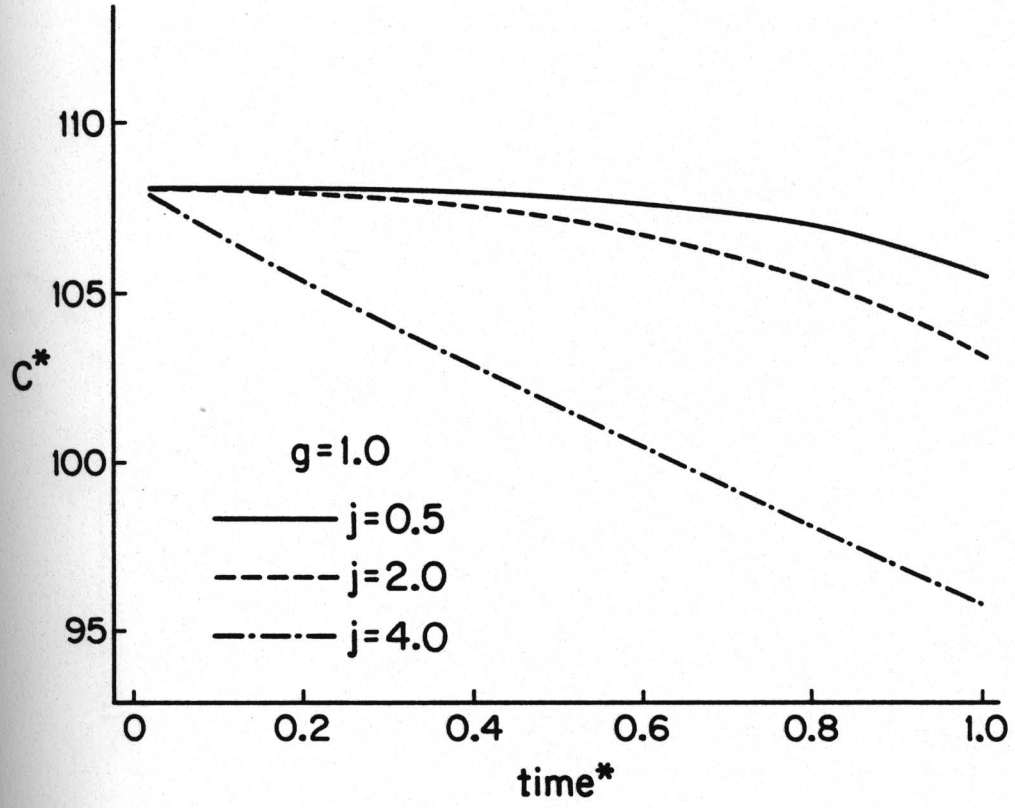

Figure IV-2-7. Concentration profile predicted by simulation of the crystallization process as a function of j, for g=1.0, G*=0.050, J*=8.0, S_F*=90 and C_0*=108.

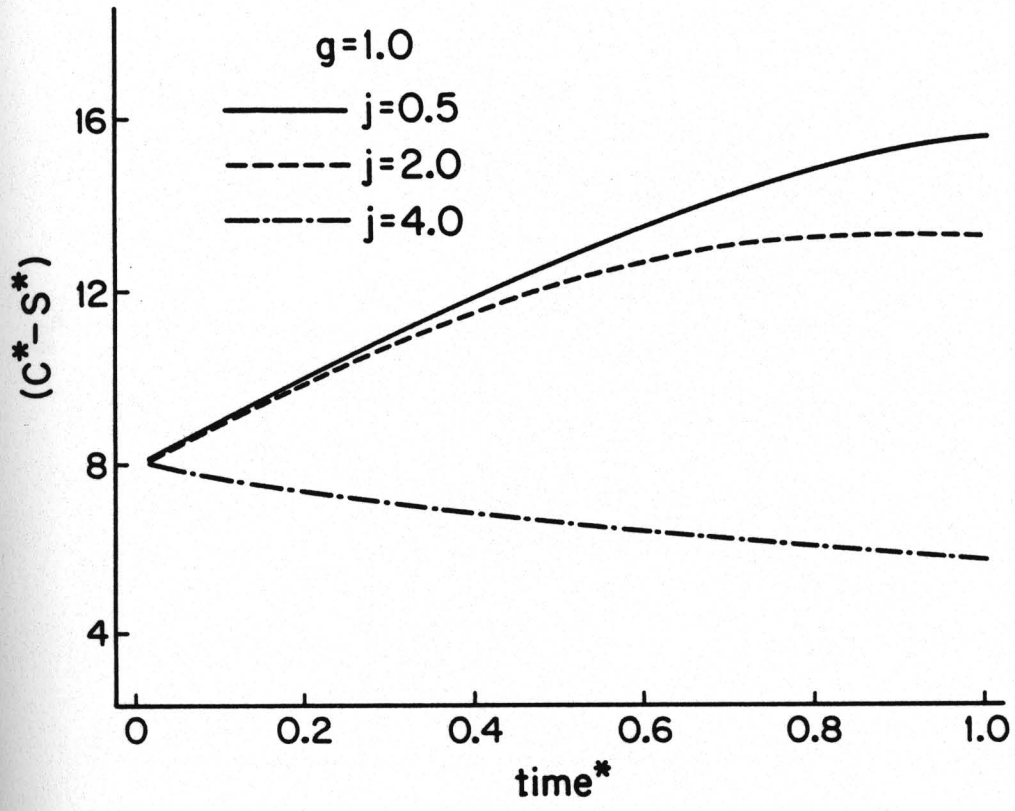

Figure IV-2-8. Supersaturation profile predicted by simulation of the crystallization process as a function of j, for g=1.0, G*=0.050, J*=8.0, S_F*=90 and C_0*=108.

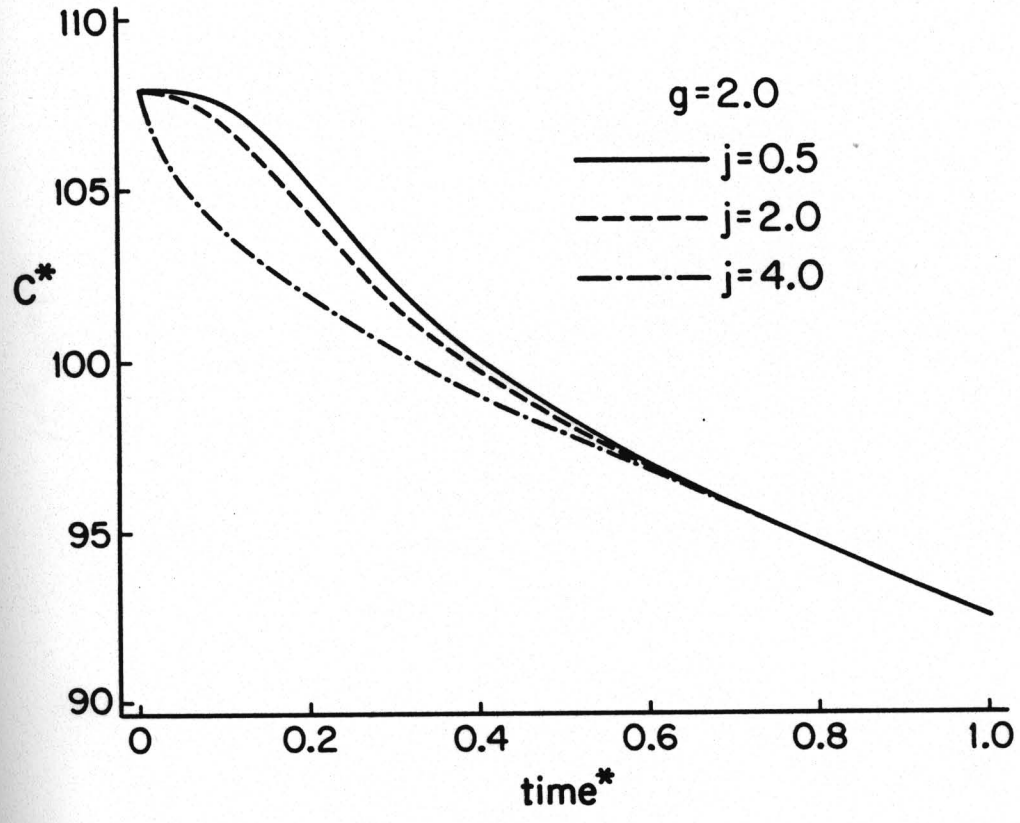

Figure IV-2-9. Concentration profile predicted by simulation of the crystallization process as a function of j, for g=2.0, G*=0.050, J*=8.0, S_F*=90 and C_O*=108.

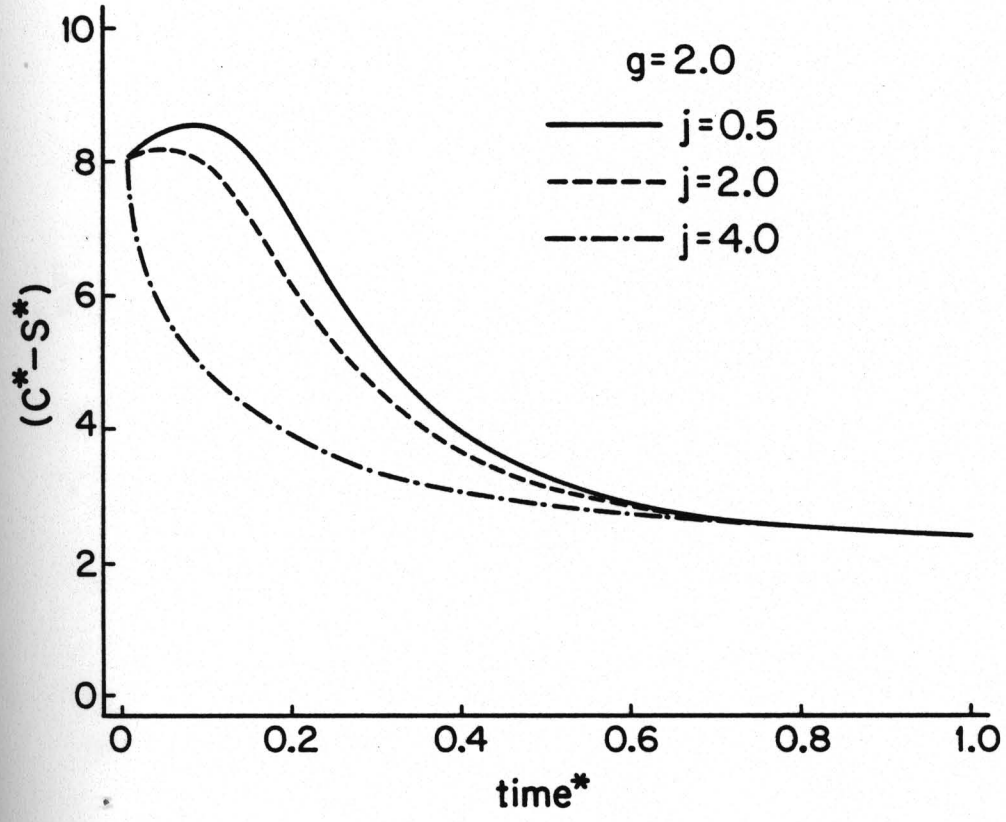

Figure IV-2-10. Supersaturation profile predicted by simulation of the crystallization process as a function of j, for g=2.0, G*=0.050.

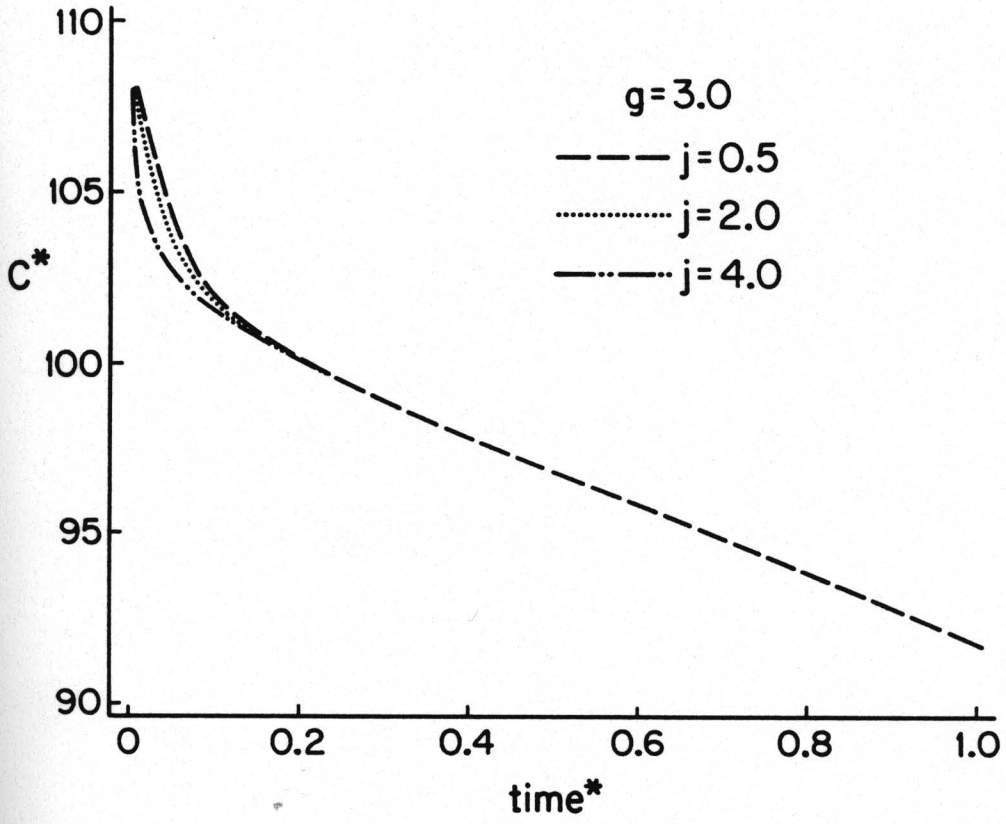

Figure IV-2-11. Concentration profile predicted by simulation of the crystallization process as a function of j, for g=3.0, G*-0.050, J*=8.0, S_F*=90 and C_O*=108.

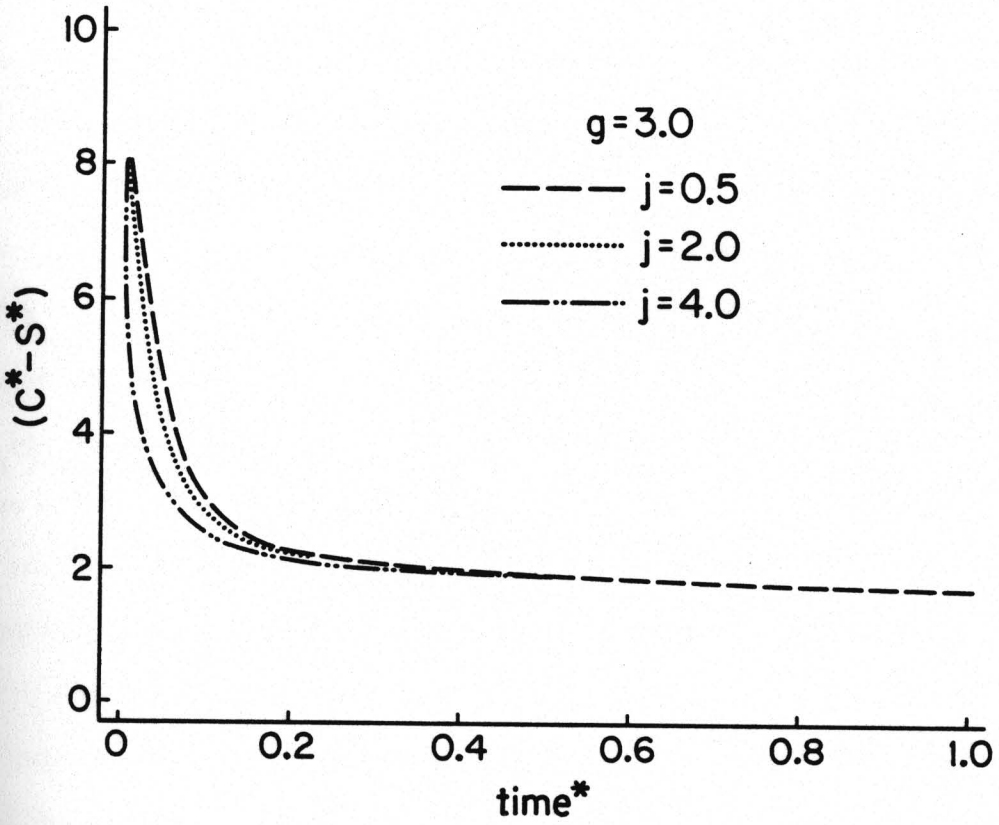

Figure IV-2-12. Supersaturation profile predicted by simulation of the crystallization process as a function of j, for g=3.0, G*=0.050, J*=8.0

of the crystallization.

A typical example of a plot of ln(C*-S*) versus t* corresponding to the experimental measurements is presented in Fig. IV-2-13. It is seen both graphically and by least squares fit (Table IV-2-1) that the fits are quite good (correlation coefficients being above 0.9). This approximation is quite reasonable and is used to estimate the values of G* to be used in the simulation to be compared with the experimental curves. The following procedure was adopted.

The value of the slope q was calculated for a large number of values of the rate constants J*, G*, the initial concentration, C_0*, and the final solubility, S_F* . Examples of the dependency of q on C_0* and G* are shown in Figures IV-2-14 and IV-2-15. There is slight curvature in the graphs, but linearity at this point has been deemed satisfactory, since the resulting relationships will be used for interpolation. Stepwise multiple regression was performed and the the following relation obtained:

$$q = a' + b'G^* + d'C_0^* \qquad \text{Eq. IV-2-15}$$

where a', b' and d' are constants. The values of these are listed in Table IV-2-2. The regression results did not change by adding the parameters S* and J*, so q does not appear to be a function of these two parameters. In a given experimental situation, C_0^* and q are known, so G* may be calculated.

A similar approach has been taken with regards to the total

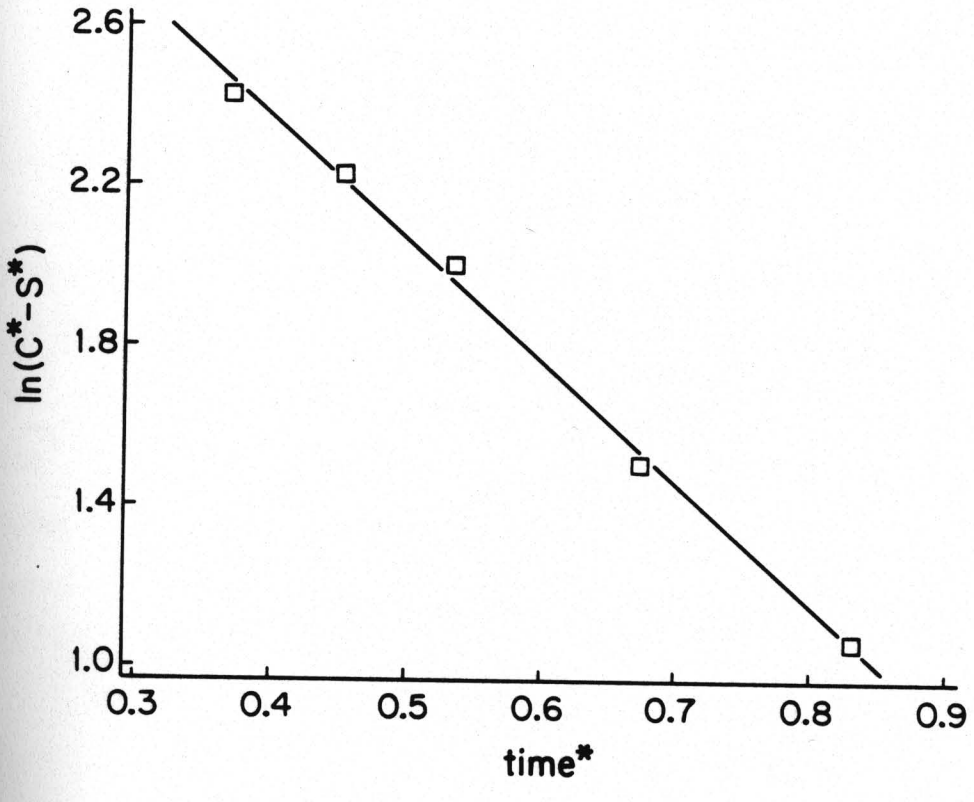

Figure IV-2-13. Linear regression plot for the supersaturation dependence on time during crystallization of oxalic acid dihydrate from 15% glycerine/water solution saturated at 30°C.

Table IV-2-1

Linear Regression Analysis for the Supersaturation Dependence on Time According to the Equation:

$$\ln (C^* - S^*) = -qt^* + E$$

Experiment				
Solvent	T_S (°C)	Slope (-q)	Intercept (E)	R^2
15% glycerine	30	-3.03	3.61	0.996
15% glycerine	40	-15.20	2.66	0.992
50% acetone	30	-5.26	2.34	0.958
50% acetone	40	-19.90	2.10	0.942
water	30	-3.81	2.67	0.992
water	40	-9.22	2.90	0.997

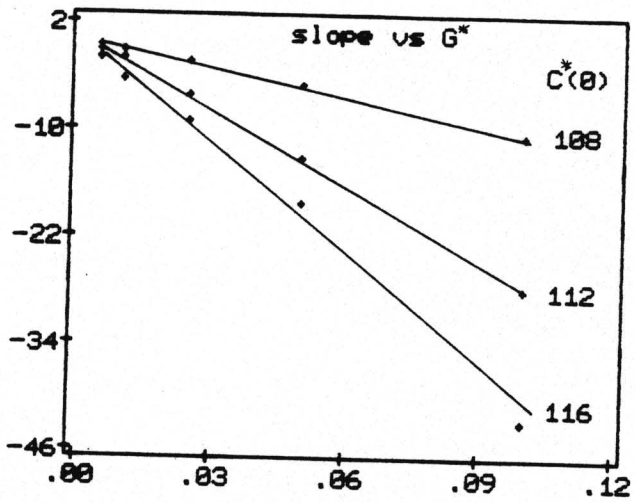

Figure IV-2-14. Dependency of slope (g) on G* for simulated supersaturation profiles.

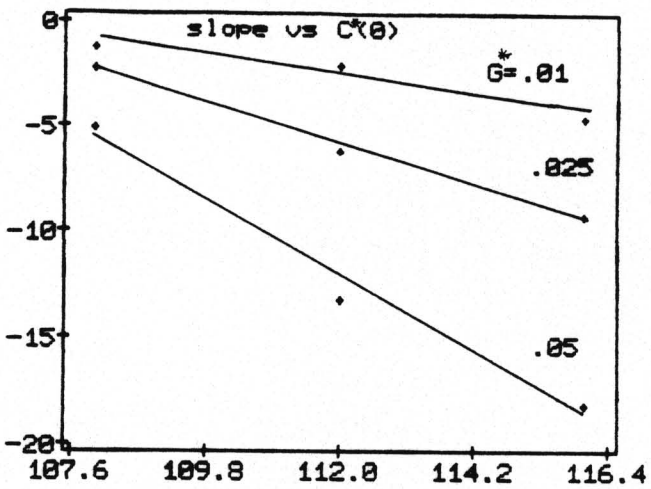

Figure IV-2-15. Dependency of slope (q) on C_0^* for simulated supersaturation profiles.

Table IV-2-2

Multiple Regression Analysis Results for the Equation:

$$q = a' + b'G^* + d'C_0^*$$

Variable	Coefficient	R^2
	138.6	
G*	-214.6 (37.0)[a]	
C_0*	-1.3 (0.3)	0.92

[a] Standard error.

number of crystals formed. The dependency of N on the parameters J*, G*, C_o* and S_F* is presented in Fig. IV-2-16. After stepwise multiple regression analysis the following relation was arrived at:

$$\ln N = a'' + b''C_o^* + d''S_F^* + e''\ln J^* + h''\ln G^* \qquad \text{Eq. IV-2-16}$$

where the superscripts " imply coefficients from the regression. These are listed in Table IV-2-3. The number of crystals formed is experimentally calculated, and the above equation can be solved for J*.

In this way initial values of the rate constants have been obtained for generating concentration and supersaturation-time profiles, and this have then been compared with experimental values. The results of these are presented in Figs. IV-2-17 to IV-2-28. Table IV-2-4 contains the G* and J*-values that fit the experimental curves best. Table IV-2-5 shows the experimental and predicted values of the number of crystals, N.

IV-2-2 Crystal Size Distributions Predicted From The Kinetics of Nucleation and Growth

As mentioned in the previous section, the nucleation and growth rates of oxalic acid dihydrate have been shown to follow Eqs. IV-2-4 to IV-2-6 with values of the exponents of j = 4.0 and g = 2.4 respectively. The fits of experimental data to the described model are good and lend credence to the values of these parameters. It is

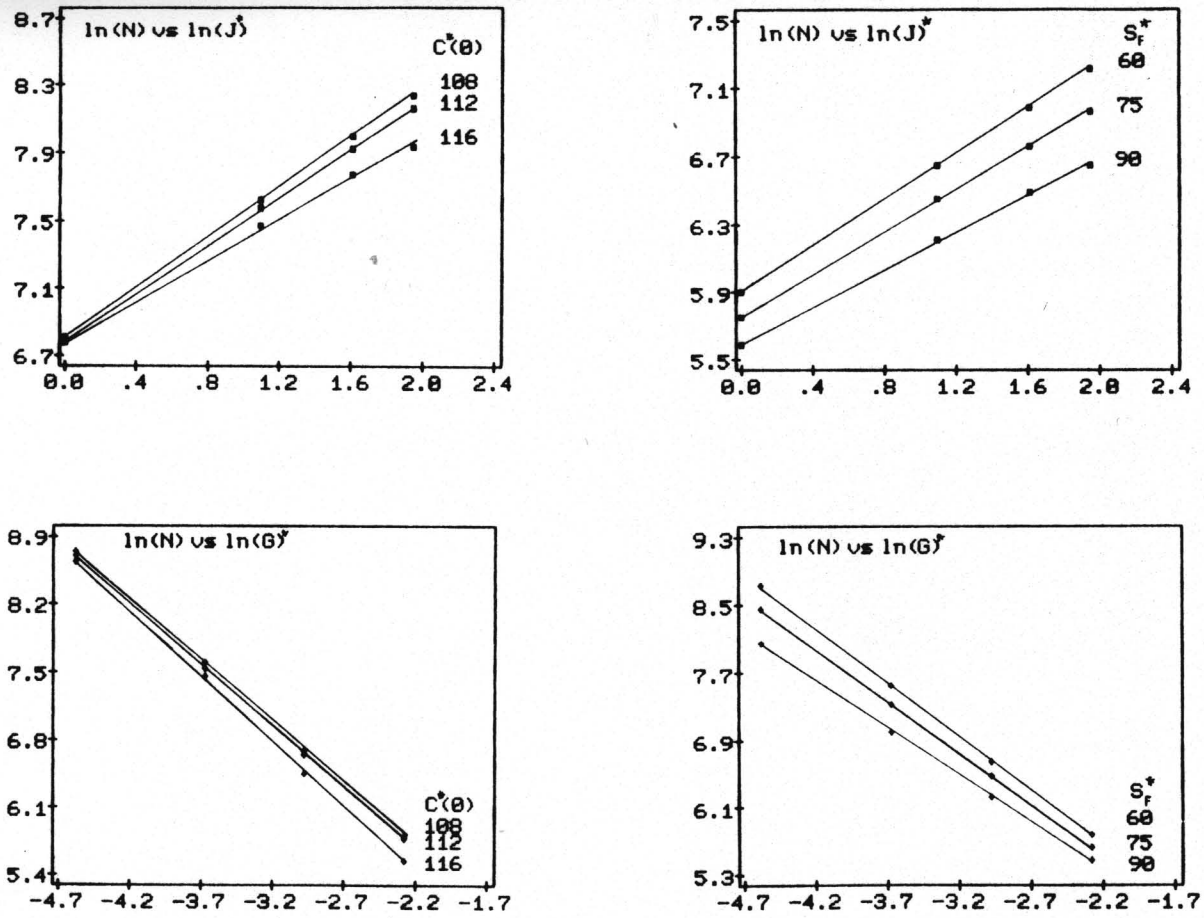

Figure IV-2-16. Dependency of N on J*, G*, C_O* and S_F* for simulation of nucleation and growth.

Table IV-2-3

Multiple Regression Analysis Results for the Equation:

$$\ln (N) = a'' + b''C_0^* + d''S_F^* + e'' \ln J^* + h'' \ln G^*$$

Variable	Coefficient	R^2
	5.09	
C_0^*	-0.015 (0.003)[a]	
S_F^*	-0.018 (0.001)	
ln J*	0.615 (0.013)	
ln G*	-1.230 (0.011)	0.992

[a] Standard error.

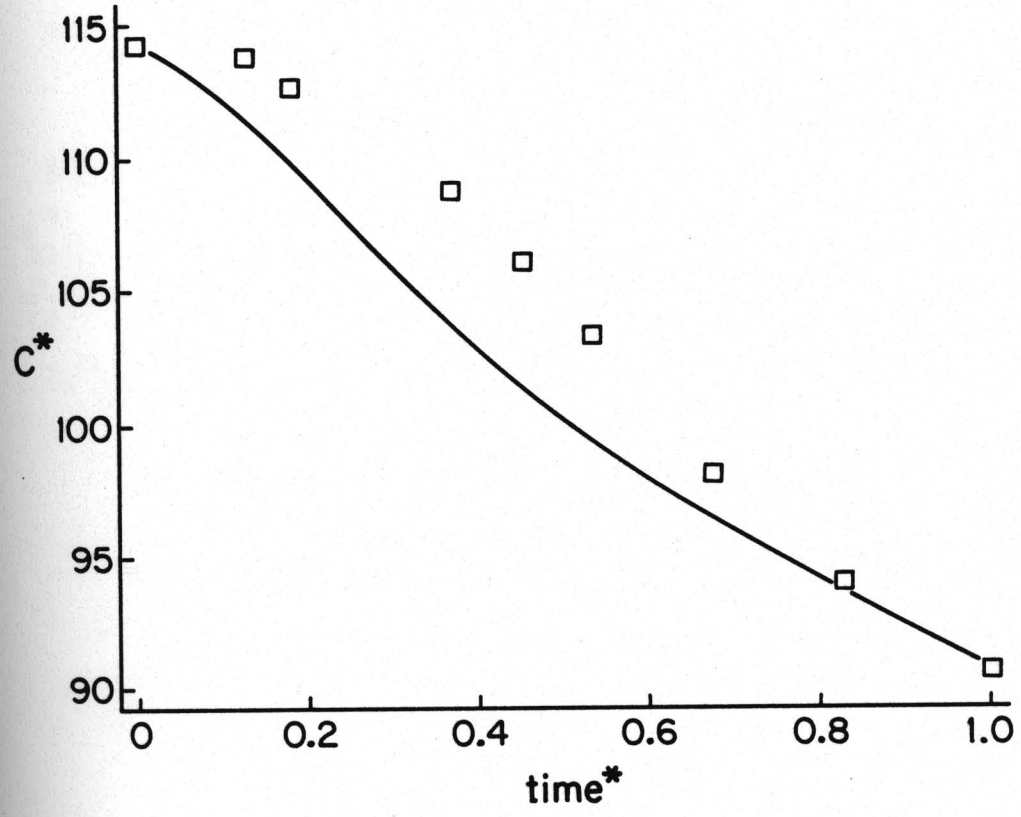

Figure IV-2-17. Experimental and predicted concentration profiles during crystallization of oxalic dihydrate generated by simulation of nucleation and growth rates. 15% glycerine/water saturated at 30°C.

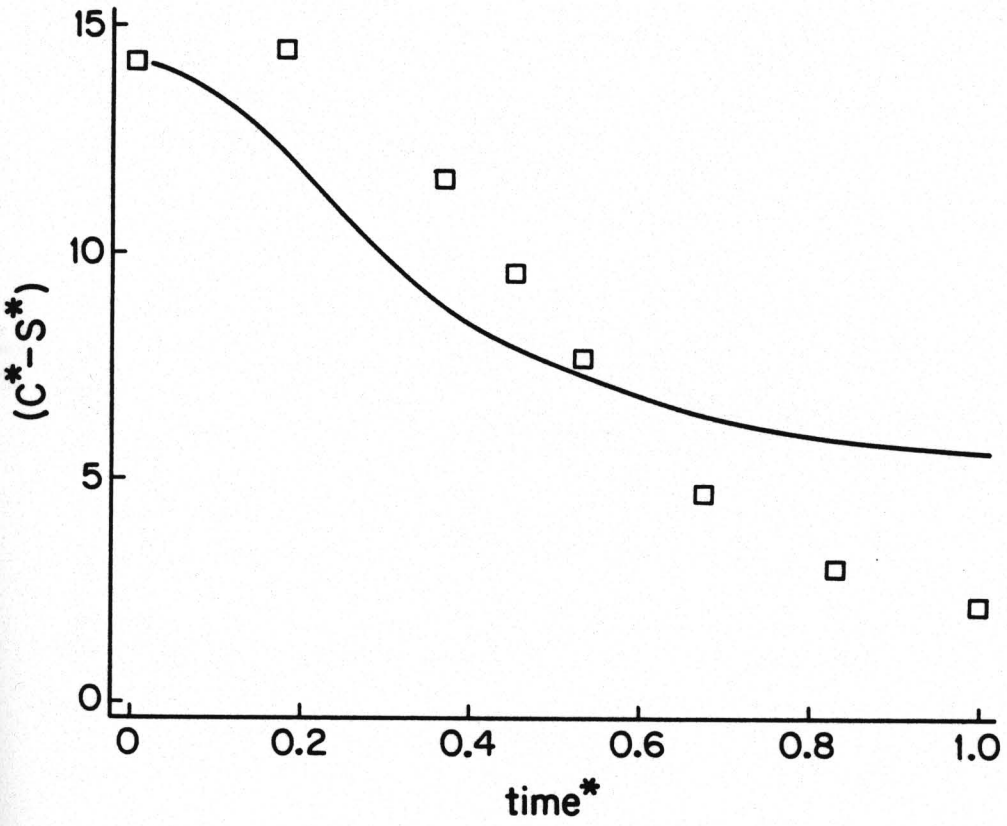

Figure IV-2-18. Experimental and predicted supersaturation profiles during crystallization of oxalic acid dihydrate generated by simulation of nucleation and growth rates. 15% glycerine/water saturated at 30°C.

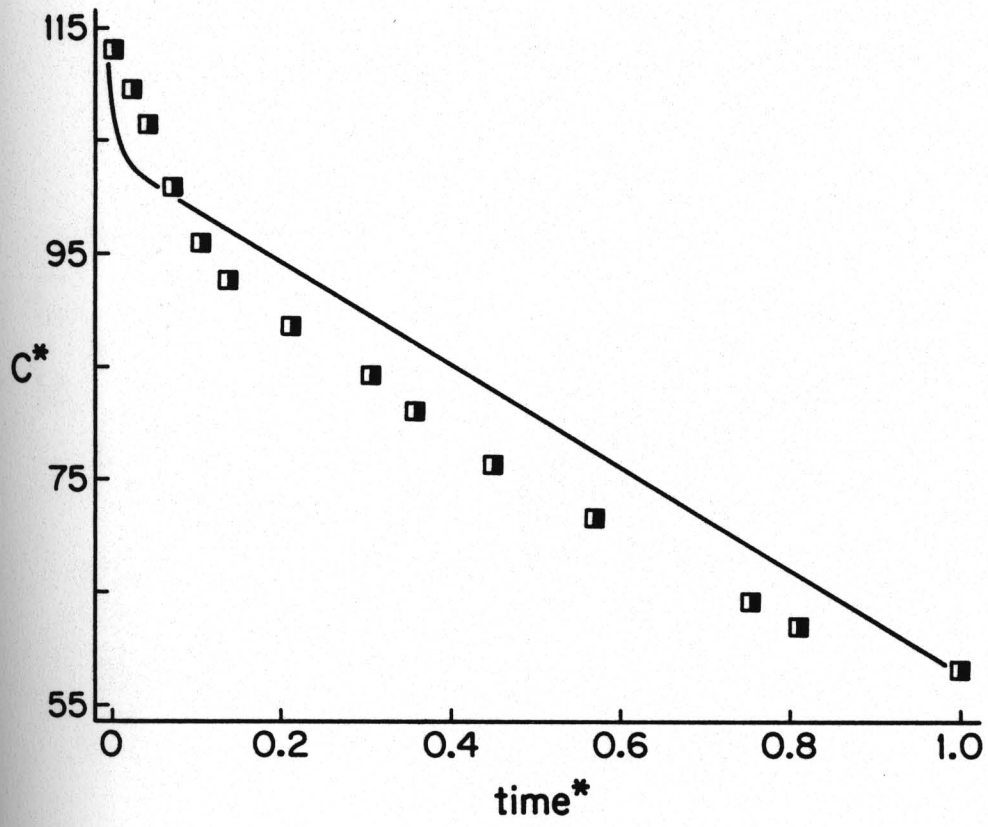

Figure IV-2-19. Experimental and predicted concentration profiles during crystallization of oxalic acid dihydrate generated by simulation of nucleation and growth rates. 15% glycerine/water saturated at 40°C.

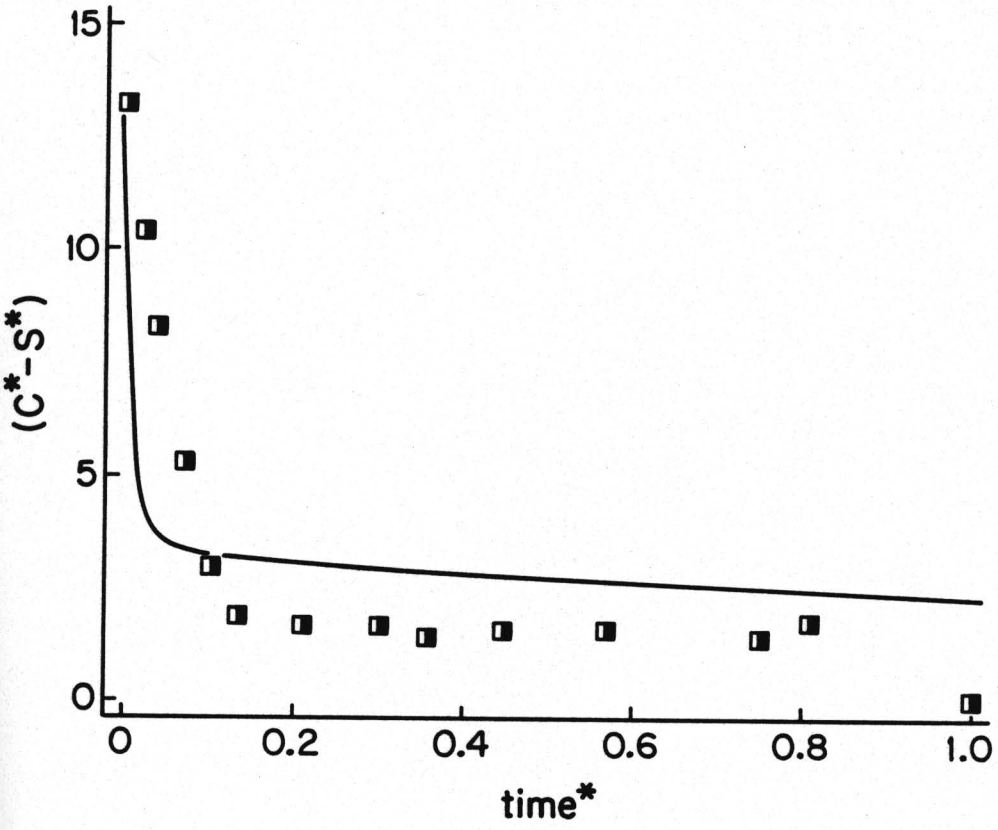

Figure IV-2-20. Experimental and predicted supersaturation profiles during crystallization of oxalic acid dihydrate generated by simulation of nucleation and growth rates. 15% glycerine water, saturated at 40°C.

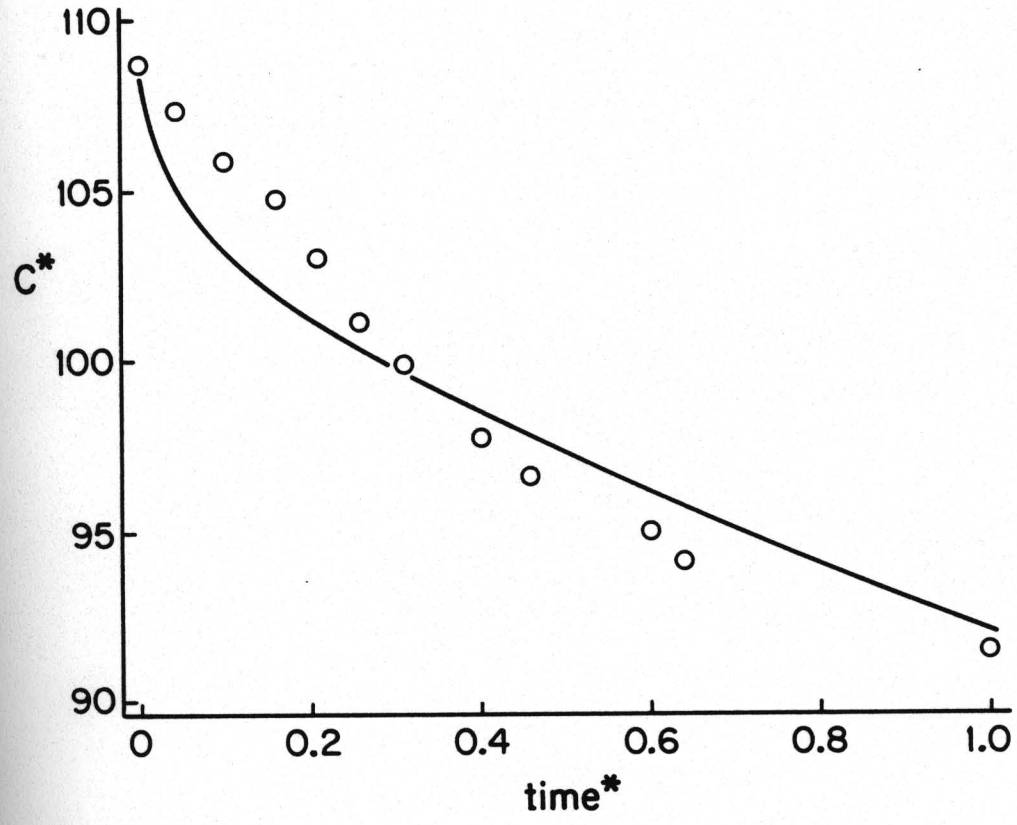

Figure IV-2-21. Experimental and predicted concentration profiles during crystallization of oxalic acid dihydrate generated by simulation of nucleation and growth rates. 50% acetone/water saturated at 30°.

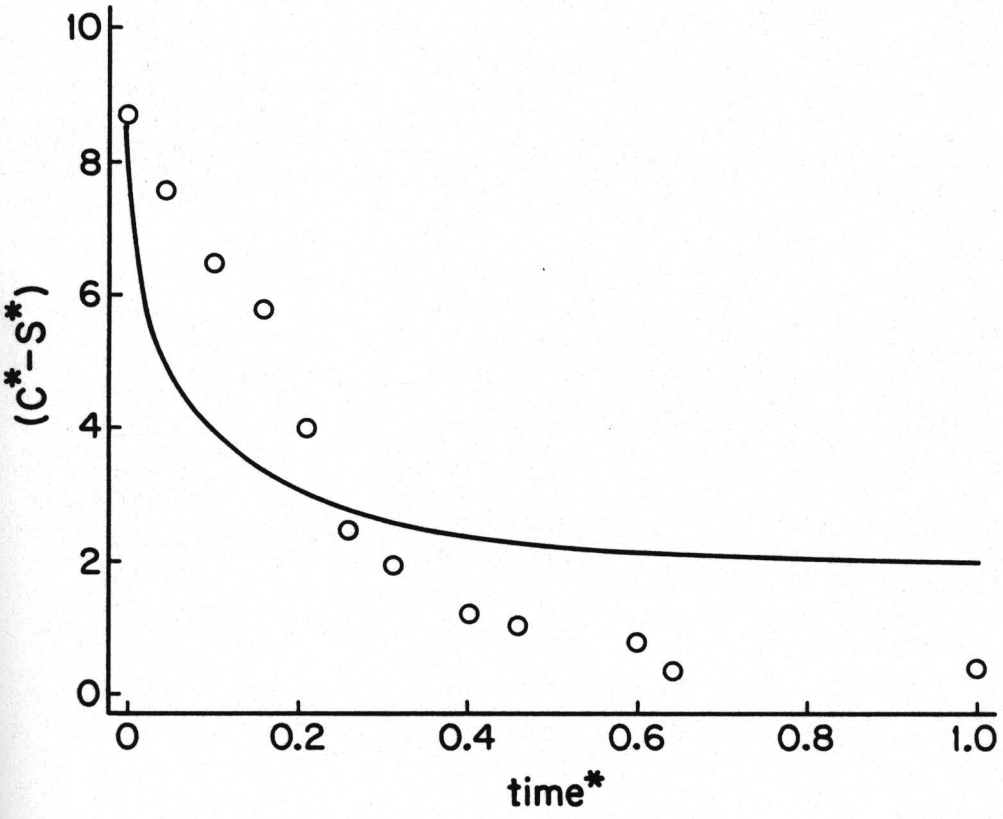

Figure IV-2-22. Experimental and predicted supersaturation profiles during crystallization of oxalic acid dihydrate generated by simulation of nucleation and growth rates. 50% acetone water, saturated at 30°C.

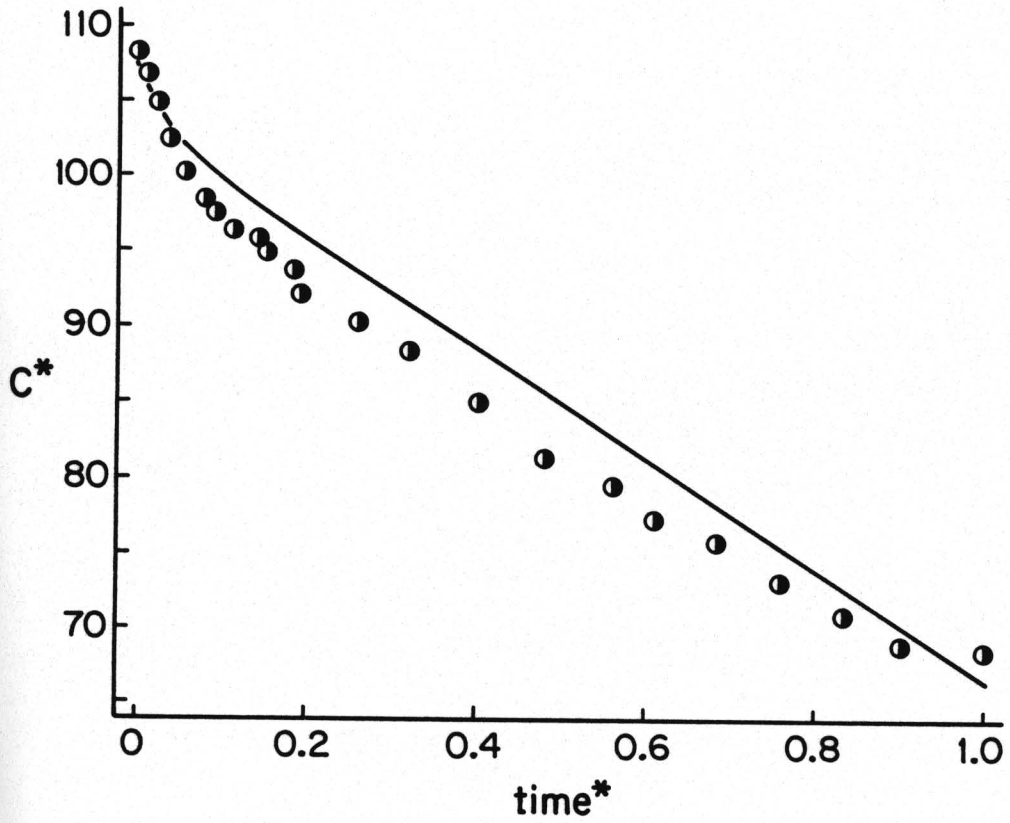

Figure IV-2-23. Experimental and predicted concentration profiles during crystallization of oxalic acid dihydrate generated by simulation of nucleation and growth rates. 50% acetone/water saturated at 40°C.

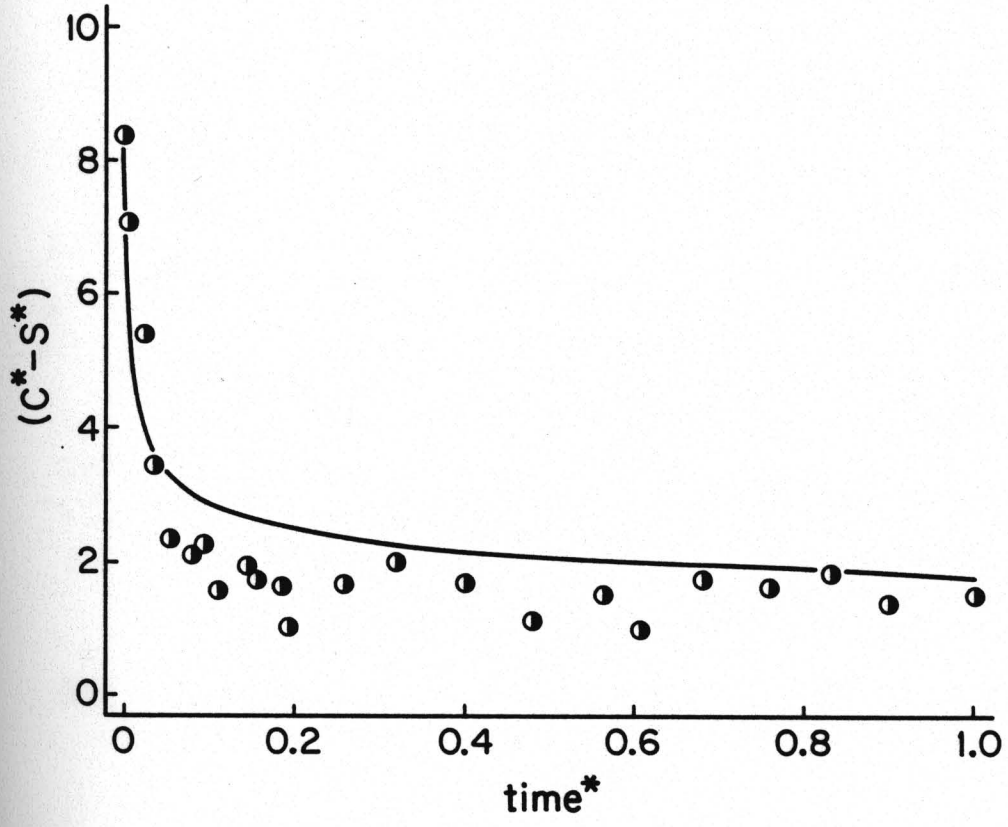

Figure IV-2-24. Experimental and predicted supersaturation profiles during crystallization of oxalic acid dihydrate generated by simulation of nucleation and growth rates. 50% acetone water, saturated at 40°C.

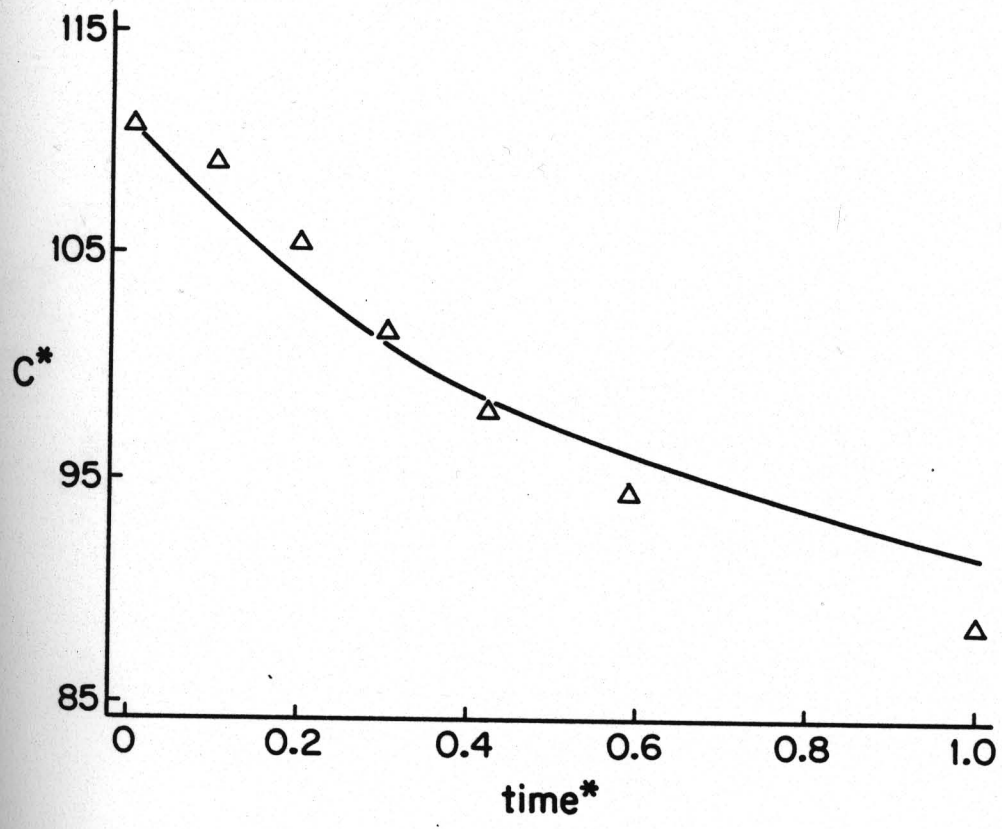

Figure IV-2-25. Experimental and predicted concentration profiles during crystallization of oxalic acid dihydrate generated by simulation of nucleation and growth rates. Water saturated at 30°C.

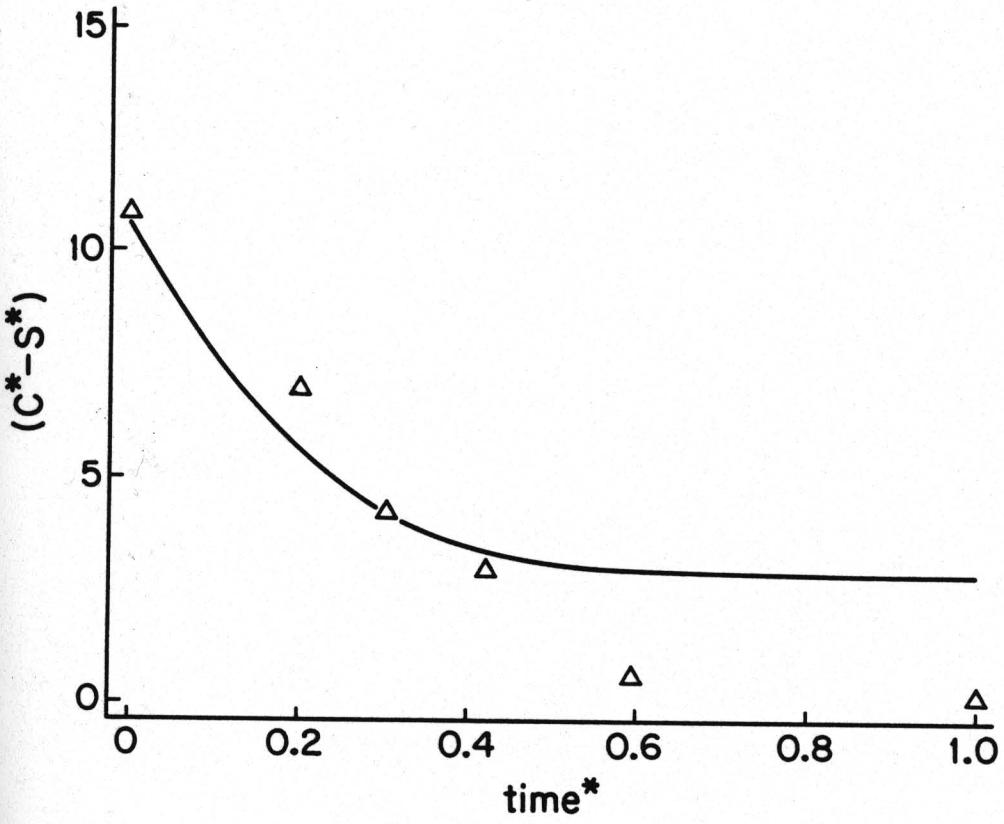

Figure IV-2-26. Experimental and predicted supersaturation profiles during crystallization of oxalic acid dihydrate generated by simulation of nucleation and growth rates. Water saturated at 30°C.

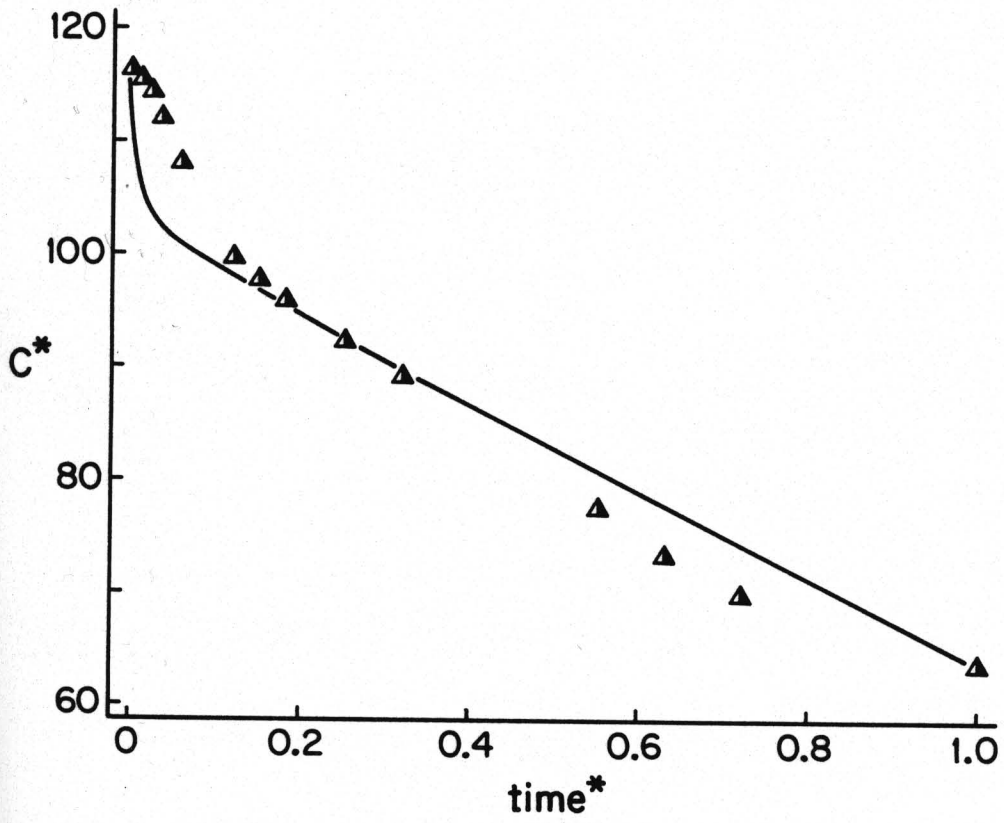

Figure IV-2-27. Experimental and predicted concentration profiles during crystallization of oxalic acid dihydrate generated by simulation of nucleation and growth rates. Water saturated at 40°C.

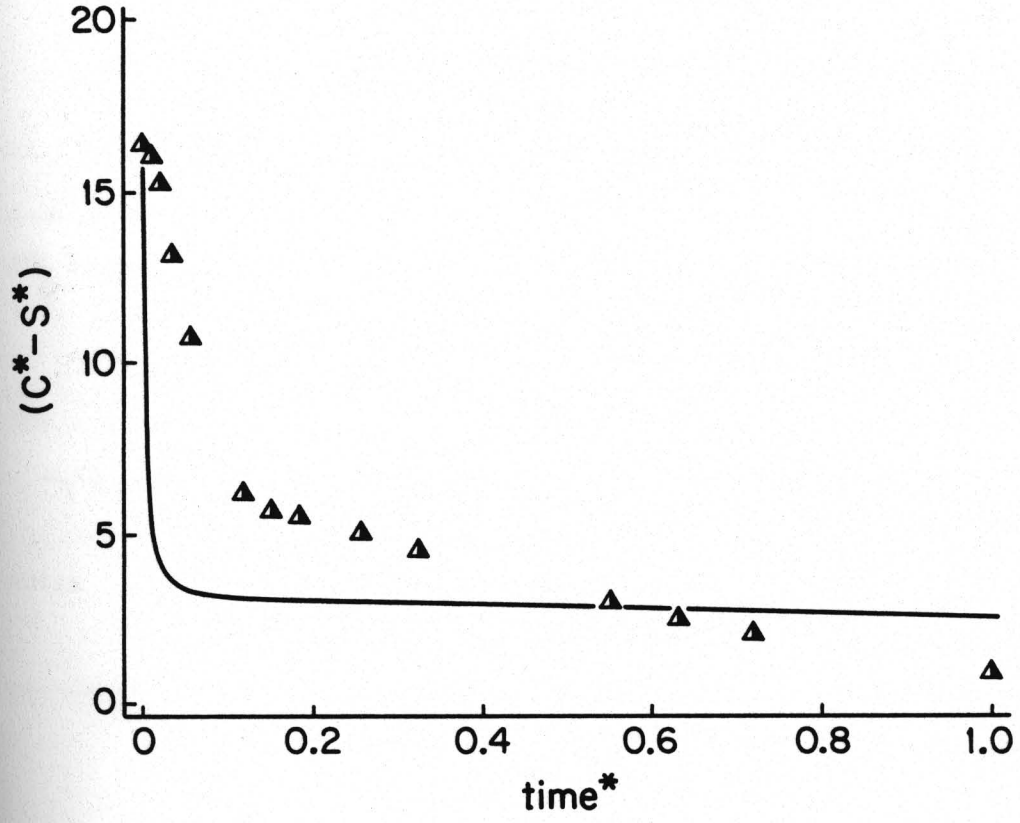

Figure IV-2-28. Experimental and predicted supersaturation profiles during crystallization of oxalic acid dihydrate generated by simulation of nucleation and growth rates. Water saturated at 40°C.

Table IV-2-4

Parameter Values Used in the Simulation of the Supersaturation-Time Profiles (nucleation order, j = 4.0 and growth order, g = 2.4).

Experiment					
Solvent	T (°C)	C_0*	S_F*	G*	J*
15% glycerine	30	114	88	0.005	0.07
	40	113	58	0.06	12.5
50% acetone	30	108	91	0.05	7.6
	40	108	67	0.12	28.0
water	30	110	89	0.02	1.3
	40	116	63	0.05	6.0

Table IV-2-5

Comparison between the Experimental

and Predicted Crystal Yield.

Experiment			
Solvent	T (°C)	$N^a \times 10^{-2}$ (experimental)	$N^a \times 10^{-2}$ (model)
15% glycerine	30	6.7	6.6
	40	16.7	13.3
50% acetone	30	8.9	8.8
	40	13.6 ± 3.3	11.4
water	30	10.3	8.9
	40	10.9	8.3

[a]Final number of crystals per gm of solvent.

the intent of the following to explain the particle size distribution resulting from crystallization based on the previously proposed model.

If the mass of a single crystal is denoted by m, then the growth rate of a particle will be governed by

$$dm/dt^* = G^* a (C^*-S^*)^g \qquad \text{Eq. IV-2-17}$$

The mass of the particle is related to the length of a characteristic dimension, r, by

$$m = f_v \rho r^3 \qquad \text{Eq. IV-2-18}$$

Therefore:

$$dm/dt^* = 3 f_v \rho r^2 dr/dt^* \qquad \text{Eq. IV-2-19}$$

The surface area of the particle is

$$a = f_a r^2 \qquad \text{Eq. IV-2-20}$$

Introducing Eqs. IV-2-19 and 20 into Eq. IV-2-17 gives

$$dm/dt^* = 3 f_v \rho r^2 dr/dt^* = G^* f_a r^2 (C^*-S^*)^g \qquad \text{Eq. IV-2-21}$$

or

$$dr/dt^* = G^* f_a (C^*-S^*)^g /(3 \rho f_v) \qquad \text{Eq.IV-2-22}$$

Equation IV-2-14 in exponential form becomes

$$(C^*-S^*) = E\, e^{-qt^*} \qquad \text{Eq. IV-2-23}$$

and introducing Eq. IV-2-23 into Eq.IV-2-22 then gives

$$dr/dt^* = g\, q\, F\, e^{-gqt^*} \qquad \text{Eq. IV-2-24}$$

where, for convenience, the term F has been introduced and is given by:

$$F = G^* f_a E^g/(3 f_v q g \rho) \qquad \text{Eq. IV-2-25}$$

A particle is born at a given time (L) and it grows until the end of the crystallization. If the time t' is taken as zero time, then the final time t" will occur at time H, and the radius of the particle born at time L will be given by

$$r_L = g\, q\, F \int_L^H e^{-gqt^*}\, dt^* =$$

$$r_L = F\ (\ e^{-gqL} - e^{-gqH})$$ Eq. IV-2-26

Similarly the largest particle, with length R, will have been born at time zero, so that its size is given by

$$R = F\ (1 - e^{-gqH})$$ Eq. IV-2-27

Subtraction of Eq. IV-2-26 from Eq. IV-2-27 then gives

$$R-r_L = F\ (1 - e^{-gqL})$$ Eq. IV-2-28

It is noted that when the time, L, is equal to zero then r_L is equal to R. When L = H then r_L is equal to zero, thus giving an expression equivalent to Eq. IV-2-27. This may be generalized by using time, t*, as a variable rather than L. The equation gives a relation between the size of the particle born at time t* on one hand and the time, t*, itself on the other. For later application it is convenient to present this relation in the following form

$$e^{-gqH} = 1 - (R/F)$$ Eq. IV-2-29

and

$$e^{-gqt^*} = 1 - ((R-r_t)/F)$$ Eq. IV-2-30

Nucleation occurs at a rate given by

$$dN/dt^* = J^* (C^*-S^*)^j \qquad \text{Eq. IV-2-31}$$

Inserting Eq. IV-2-23 into Eq. IV-2-31 then gives

$$dN/dt^* = J^* E^j e^{-jqt^*} \qquad \text{Eq. IV-2-32}$$

The total number of nuclei formed during the crystallization is therefore:

$$N = J^* E^j \int_0^H e^{-jqt^*} dt^* =$$

$$J^* E^j (1 - e^{-jqH})/(jq) \qquad \text{Eq. IV-2-33}$$

The fraction of particles having sizes between r_t and r_t + dr is obtained by dividing Eq. IV-2-32 by Eq. IV-2-33:

$$dN/N = jq\, e^{-jqt^*} (1-e^{-jqH})^{-1} dt^* \qquad \text{Eq. IV-2-34}$$

Integration of this from $\underline{t^*}$ to H gives the fraction of particles with particle size smaller than r_t

$$N(r_t)/N = (e^{-jqt^*} - e^{-jqH})/(1 - e^{-jqH}) \qquad \text{Eq.IV-2-35}$$

It is noted that this is in normalized form, since the frequency of the smallest particles (born at time H) should have a frequency of zero. Similarly the frequency of particles having a size smaller than the largest (born at time zero) should have a frequency of one, since all the particles are smaller than or equal to R. Eq. IV-2-35 is expressed in terms of time, as independent variable. To make it a function of size as independent variable, use is made of Eqs. IV-2-29 and 30. It is noted that

$$e^{-jqH} = (1-(R/F))^{j/g} \qquad \text{Eq. IV-2-36}$$

and

$$e^{-jqt^*} = (1 - (R-r_t/F))^{j/g} \qquad \text{Eq. IV-2-37}$$

When Eqs. IV-2-35 and 37 are inserted into Eq. IV-2-35, the following equation (in which subscripts have been dropped) results

$$N(r)/N = \frac{(1-((R-r)/F))^{j/g} - (1-(R/F))^{j/g}}{1 - (1-(R/F))^{j/g}} \qquad \text{Eq. IV-2-38}$$

This equation represents the fraction of particles smaller than r. It is noted that the nucleation rate constant J* does not appear in the expression. The contribution of nucleation rates to the

distribution lies in the exponential term, and in the total number of particles. Both growth rate constants play a part in the expression, G* being part of the factor F, and the order g being in the exponents. This distribution function has been generated for experimental values of R and r and the literature values of j and g (4.0 and 2.4 respectively). These generated values are shown in Table IV-2-6. Distributions with different values of F were generated. These values are tabulated in the table as well, and plots of the distribution are presented in Figs. IV-2-29 to IV-2-31.
There is a constancy of supersaturation over a significant fraction of the time during which crystallization occurs in the cases of 15% glycerine and 50% acetone, saturated at 40°C. In this case Eq. IV-2-23 does not hold and the following method was used.

IV-2-3 Growth During Constant Supersaturation

The growth rate is considered to be of the form of Eq. IV-2-6, where the amount of material precipitated in a time element dt* is

$$dM/dt^* = A\ G^*\ (C^*-S^*)^g \qquad \text{Eq. IV-2-39}$$

where A is a function of the total area available for growth. As described in Section IV-2-1 and Appendix C, A can be expressed by

$$A = f_{sv}\ (M/\rho)^{2/3} \qquad \text{Eq. IV-2-40}$$

Table IV-2-6

Experimental Values of r and R and Fitted Parameter F for Oxalic Acid Dihydrate Crystal Size Distributions, According to Equation (IV-2-38).

Solvent	T (°C)	r (μm)	R (μm)	F (μm)
15% glycerine	30	1	450	460
50% acetone	30	1	400	590
water	30	1	350	800
	40	1	500	600

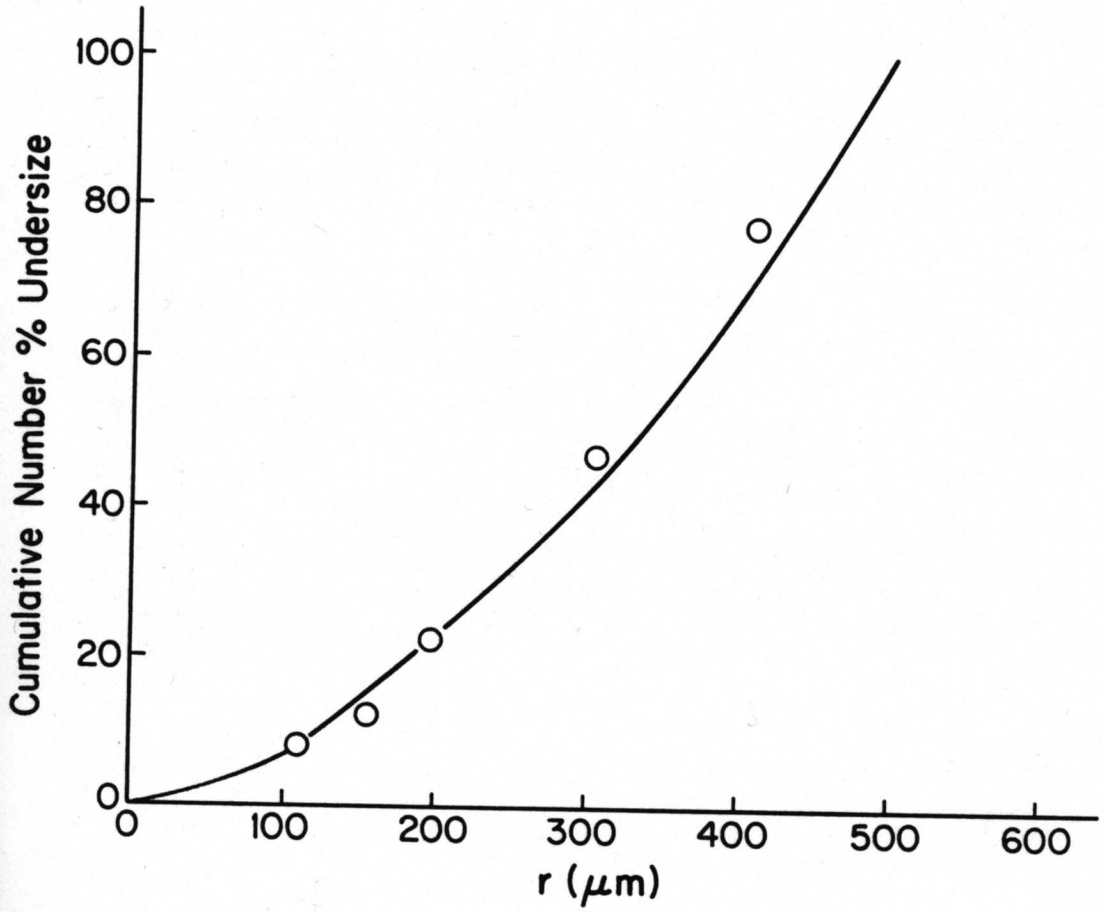

Figure IV-2-29. Cumulative distribution plot for oxalic acid dihydrate crystallized from 15% glycerine/water, saturated at 30°C. Generated curve according to Eq. (IV-2-38).

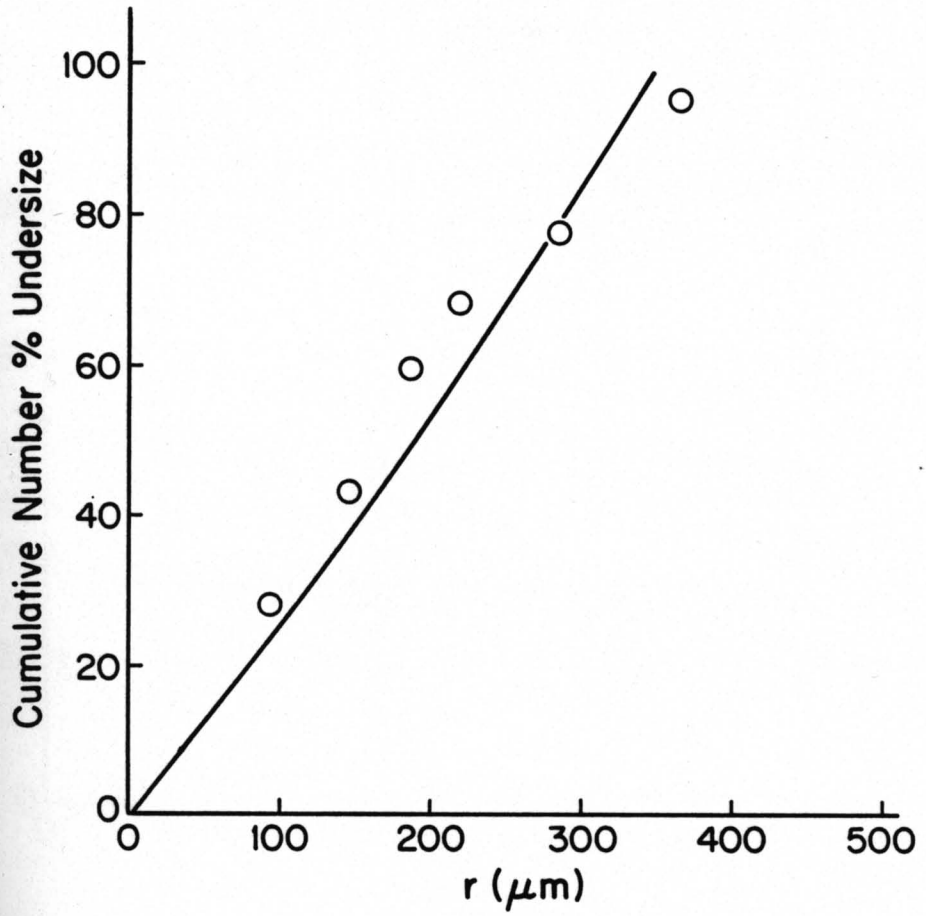

Figure IV-2-30. Cumulative distribution plot for oxalic acid dihydrate crystallized from aqueous solution saturated at 30°C. Generated curve according to Eq. (IV-2-38).

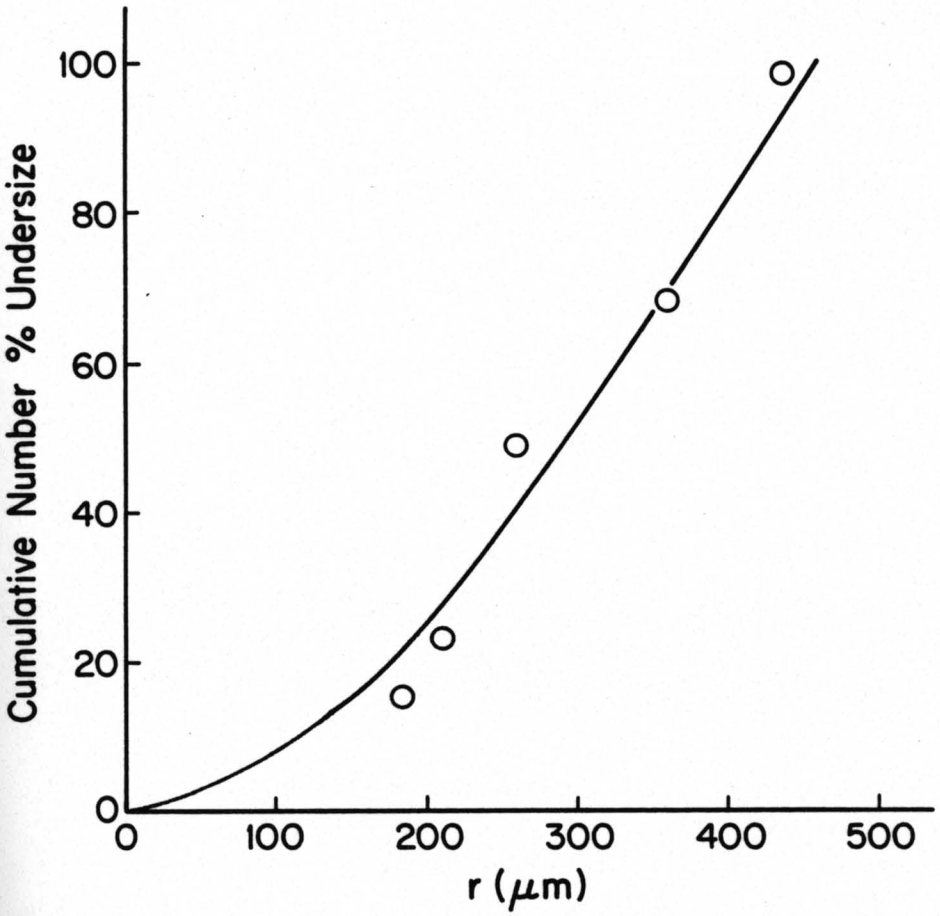

Figure IV-2-31. Cumulative distribution plot for oxalic acid dihydrate crystallized from aqueous solution saturated at 40°C. Generated curve according to Eq. (IV-2-38).

Inserting this into Eq. IV-2-39 gives

$$dM/dt^* = f_{sv} (M/\rho)^{2/3} G^* (C^*-S^*)^g \qquad \text{Eq. IV-2-41}$$

The time interval over which (C*-S*) remains constant is denoted $t^* > t_0^*$. Integration of Eq. IV-2-41 with these limits gives:

$$M^{1/3}-M_0^{1/3} = G^* f_{sv} (C^*-S^*)^g (t^*-t_0^*) \qquad \text{Eq. IV-2-42}$$

It is convenient to introduce the following reduced variable:

$$M^* = 100\ M/M_F \qquad \text{Eq. IV-2-43}$$

where M_F is the mass precipitated at the end of the interval. Eq. IV-2-42 in reduced form becomes

$$(M^*)^{1/3}-(M_0^*)^{1/3} = (G_1^* f_{sv}/\rho^{2/3})(C^* - S^*)^g (t^* - t_0^*) \qquad \text{Eq. IV-2-44}$$

Expressions including the relationship among various reduced forms of the growth rate constant are explained in Appendix E.

Equation IV-2-41 has been applied to the two systems: 15% glycerin and 50% acetone. The data were fitted to this equation in

the form:

$$\ln(M^{*1/3}-M_0^{*1/3}) = \ln(G_1^* f_{sv} (C^*-S^*)^g/\rho^{2/3}) + \ln(t^*-t_0^*) \qquad \text{Eq. IV-2-45}$$

where the intercept value allows calculation of G_1^*.

Results from these runs are included in Table IV-2-7 and plotted according to Eq. IV-2-45 in Figs IV-2-32 and IV-2-33.

The results of the regression analysis are shown in Table IV-2-8. They show that an equation of the same form as Eq. IV-2-45 is a proper fit to the data. The coefficient of the second term on the right hand side is not unity in this case, but rather a power function of the type $y = a(x^n)$.

The growth rate constants calculated from this analysis are in good agreement with the values obtained by the simulation method, and they are shown in Table IV-2-9.

IV-3 Effect of Temperature on Rate Constants

The Arrhenius equation has been applied to crystallization processes by many workers (Nyvlt, 1971, Wey and Terwilliger, 1980, Misra and White, 1971). Crystal growth processes are rarely purely surface - or diffusion- controlled. The surface reaction step may predominate at low temperatures and the diffusion step at high temperatures, but over a significant intermediate range, both processes may contribute. It is for this reason that Arrhenius plots

Table IV-2-7

Results from Crystallization of Oxalic Acid Dihydrate in Two Different Solvent Systems, in the Case where the Supersaturation Is Constant ($t^* > t_0^*$).

t^*	$t^* - t_0^*$	$C_0^* - C^*$	$M^{*1/3} - M_0^{*1/3}$	$(C^* - S^*)$
System (50% acetone, T_S = 40°C)				
0.1380	0.0000	12.8	0.00	1.66[a] (0.30)[b]
0.1492	0.0112	13.5	0.05	
0.1762	0.0382	14.7	0.15	
0.1927	0.0547	16.1	0.25	
0.2603	0.1223	18.1	0.39	
0.3226	0.1846	20.2	0.52	
0.4031	0.2651	23.4	0.71	
0.4782	0.3402	26.9	0.90	
0.5557	0.4177	29.0	1.00	
0.6065	0.4685	31.1	1.10	
0.6755	0.5375	32.6	1.17	
0.7608	0.6228	35.4	1.28	
0.8337	0.6957	37.5	1.37	
0.8971	0.7591	39.4	1.45	
System (15% glycerine, T_S = 40°C)				
0.2088	0.0000	24.4	0.00	1.59[a] (0.12)[b]
0.2955	0.0867	28.9	0.21	
0.3571	0.1483	32.2	0.35	

t^*	$t^* - t_0^*$	$C_0^* - C^*$	$M^{*1/3} - M_0^{*1/3}$	$(C^* - S^*)$
0.4501	0.2314	36.6	0.52	1.59[a] (0.12)[b]
0.5685	0.3597	41.4	0.70	
0.6511	0.4423	41.9	0.72	
0.7445	0.5357	49.0	0.95	
0.8142	0.6054	51.3	1.02	

[a] Average supersaturation $(C^* - S^*)$ over the time interval $t_0^* < t^* < t_F^*$.

[b] Standard deviation of supersaturation over the time interval $t_0^* < t^* < t_F^*$.

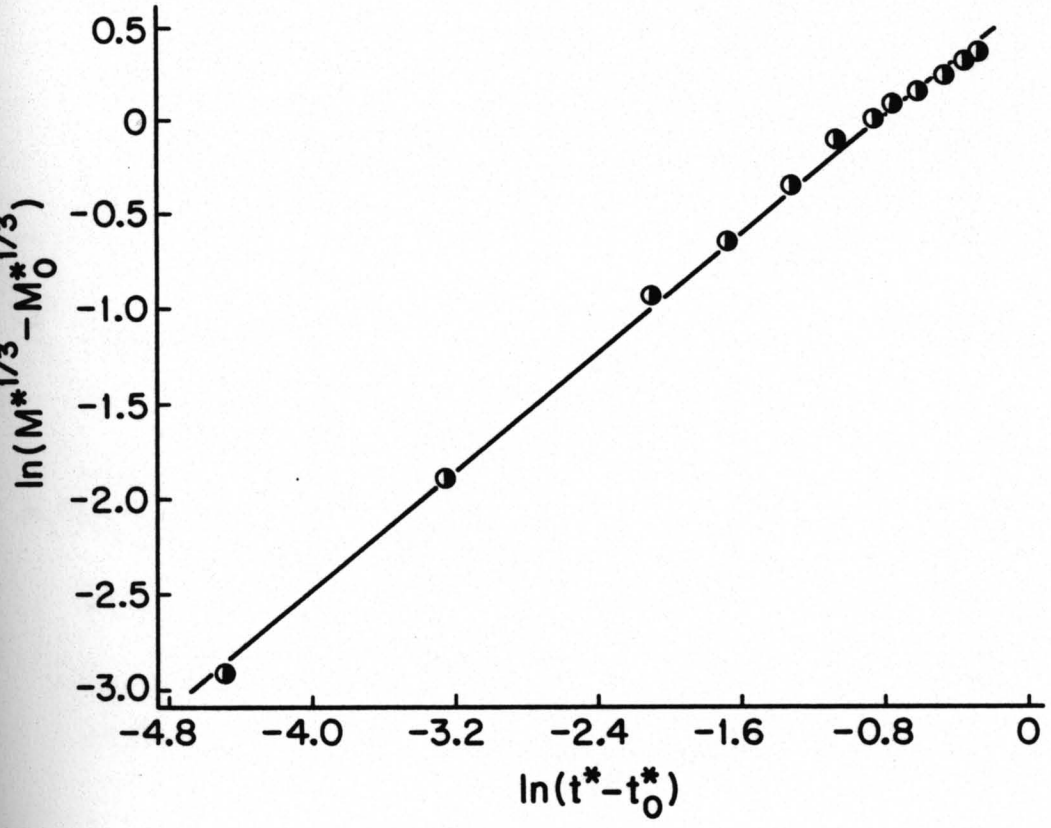

Figure IV-2-32. Cube root of the mass crystallized as a function of time according to Eq. (IV-2-45). 50% acetone /water solvent, saturated at 40°C.

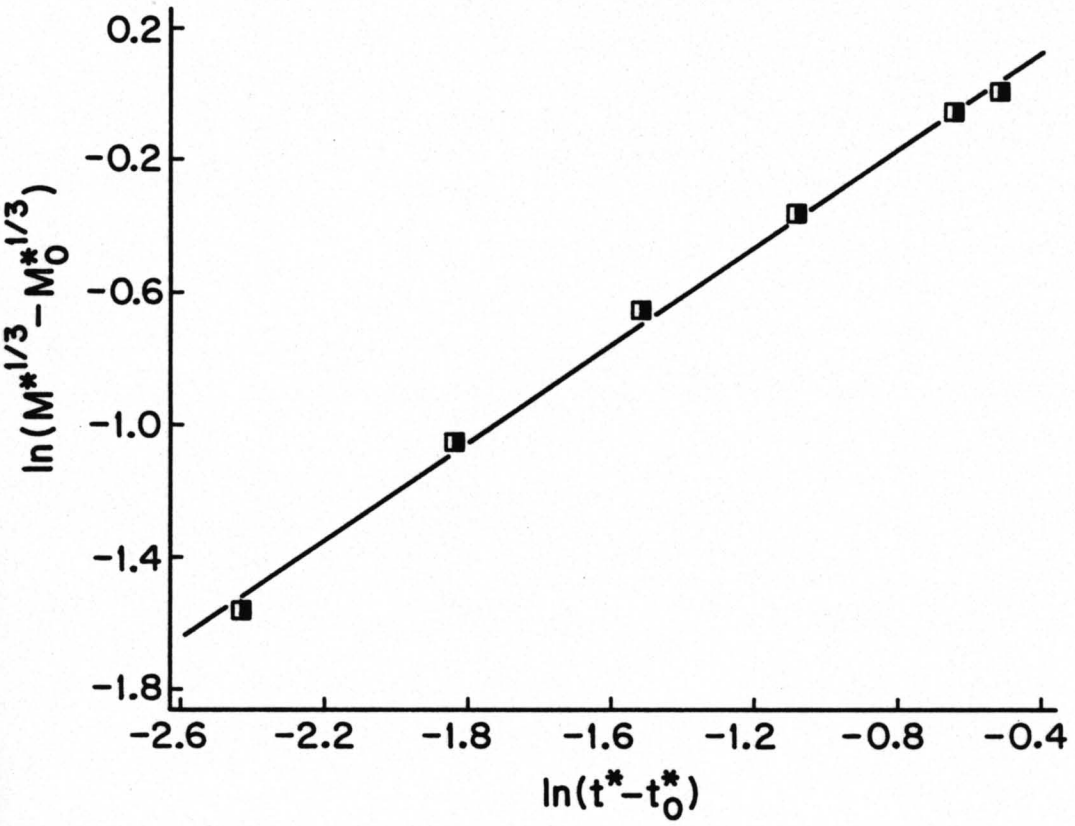

Figure IV-2-33. Cube root of the mass crystallized as a function of time according to Eq. (IV-2-45). 15% glycerine/water solvent, saturated at 40°C.

Table IV-2-8

Linear Regression Analysis of the Cube Root of the Mass Crystallized As a Function of Time According to the Equation:

$$\ln [M^{*1/3} - M_0^{*1/3}] = \ln G^* \frac{fsv}{\rho^{2/3}} (C^* - S^*)^g + \ln (t^* - t_0^*).$$

Experiment	Slope	Intercept	R^{2a}
50% acetone	0.78 (0.01)[b]	0.66 (0.02)	0.998
15% glycerine	0.81 (0.02)	0.46 (0.04)	0.996

[a]Variation explained by the regression equation.

[b]Standard error.

Table IV-2-9

Values of the Growth Rate Constants Obtained by

Three Different Approaches.

Experiment				
Solvent	T_S (°C)	G* (gm/cm^2) from simulation	G* (gm/cm^2) from particle size distribution	G* (gm/cm^2) from constant (C* - S*)
15% glycerine	30	0.005	0.007	
15% glycerine	40	0.06	--[a]	0.19
50% acetone	30	0.05	0.05	
50% acetone	40	0.12	--[a]	0.19
water	30	0.02	0.03	
water	40	0.05	0.05	

[a] Due to the constancy of the supersaturation over a significant fraction of the time during which crystallization occurs, these values have not been calculated.

for crystal growth data have been found to be curved rather than straight lines in many cases (Mullin, 1972). Such plots would seem to imply that the apparent activation energy for the over-all growth rate process is temperature dependent.

Nevertheless, Arrhenius plotting has been used successfully in many crystal growth systems. One of the criteria chosen to distinguish the predominant mechanism during growth has been to compare the activation energies of diffusion, viscosity and growth processes. Van Hook (1959) calculated activation energies for these processes in sucrose-water systems over a range of temperatures and found that at low temperatures, E_{growth} is larger than $E_{diffusion}$ which in turn is larger than $E_{viscosity}$ up to $60^{o}C$. At this temperature the values were comparable, so that diffusion becomes predominant. Similar findings for the system NaCl/water have been reported (Rumford and Bain, 1960).

In general, for the system under discussion, oxalic acid dihydrate, the growth rate constant increases by a factor 2.6 and greater over a temperature range of $10^{o}C$. This would imply an over-all activation energy for growth of greater than $E_{viscosity}$ and $E_{diffusion}$. The activation energy of the viscosity in the solvents studied was calculated by Arrhenius type plots and found to be in the range of 3.5-4.5 kcal/mole. The diffusion activation energy is of the same order of magnitude as the dissolution activation energy and was calculated from data reported on oxalic acid dihydrate dissolution (Carstensen and Patel, 1975) and found to be 1.2

kcal/mole.

The nucleation rate constants determined in this study increase with an increase in temperature. Work by other authors (Genck and Larson, 1972) has shown the same type of behavior with other systems, where, in the majority of cases, a positive activation energy for the process has been found. This also serves to explain the increase in the number of crystals produced at the higher saturation temperature, $40^{o}C$.

The fact that various processes are interacting and that the system under consideration is non-isothermal makes it difficult to give a logical and more detailed description of the effect of temperature.

IV-4 Effect of Temperature on Standard Deviation

The effect of a higher saturation temperature on the number of the crystals is greater than on the size of the crystals. This implies that nucleation rates are more sensitive than growth rates to (a) temperature (i.e. there is a substantial difference in activation energy between the two phenomena) and/or (b) the surface area created per g of solvent. The activation energy for nucleation has generally been reported to be higher than the activation energy for growth (Nyvlt, 1971 Wey and Terwilliger, 1980) in agreement with the observations reported in Table III-4-2.

IV-5 Effect of Solvent Properties on Crystallization Kinetic Parameters

The surface area of the crystals present during crystallization can in many instances and for many substances affect the nucleation rate (Mullin and Leci, 1972); this phenomenon is referred to as secondary nucleation. This has not been accounted for in the model presented here, and the justification for this omission is presented below.

Secondary nucleation is responsible for an additional breeding of nuclei due to the presence of solid phase of the solute in that nucleation is induced by clusters of critical size (i.e. nuclei) being swept away from the crystal surface (Strickland-Constable, 1972). The number of particles dislodged from the fluidized layer near the crystal surface will depend on the crystal size, the degree of supersaturation and the energy of contact. The supersaturation degree would affect the number of crystals produced by decreasing the critical size for nucleus survival; hence there would be more new viable crystals.

This would imply that if a mechanism of this kind were significant during crystallization, then increased suspension densities would increase nucleation rates, and that increased viscosity would decrease nucleation rates, under equal conditions of supersaturation.

The results from the study reported here show that as the saturation temperature is increased both the crystal numbers and

the rate constants for growth and nucleation, G* and J* respectively, increased. However, by increasing the viscosity of the solution an effect on the number of crystals produced is not observed. It can, therefore, be inferred that the process of secondary nucleation is not important in the study, and that, hence, omitting secondary nucleation terms in the proposed model is justified.

IV-6 Effect of Solvent Properties on Crystal Size and Shape Distributions

It is a general rule of thumb that "solids are log normally distributed". Several processes, indeed, lead theoretically to a log normal distribution e.g. milling (Carstensen and Patel, 1974) and fluid bed granulation (Carstensen and Zoglio, 1979), but in some cases (e.g. batch granulation) the choice between normal and log normal is difficult (Steiner et al., 1974). It would appear that if there indeed is merit to such a rule, then (a) either there is a natural reason for it, or (b) frequencies result from natural causes that are not log-normal (or normal) but are sufficiently close to be considered such. One of the goals of the study was elucidation of size distributions of both particle sizes and shapes to probe which of the two ((a) or (b)) is the case.

As a first step the crystal populations were examined by plotting cumulative frequency by probit (t) as ordinate and either size or log(size) as abscissa. The results from these analyses are shown in

Section III-6-1. In some cases the distributions are log-normal (e.g. 7% glycerine, T_S = 40°C) and in other cases the distributions are normal (e.g. water, T_S= 40°C). The linearization process of the cumulative frequencies takes the following form:

$$t = a' \ln(z) + b' \qquad \text{Eq IV-6-1}$$

in the case of a log normal distribution or

$$t = a''(z) + b'' \qquad \text{Eq. IV-6-2}$$

for a normal distribution. The coefficients a', a", b' and b" have been evaluated by least squares fit.

The best over-all presentation mode can be arrived at by comparing the correlation coefficients and the sum of squares, and these are included in Tables III-6-6 to III-6-9.

All the data are presented in Figures IV-6-1, IV-6-2 and Table IV-6-1 as the values predicted by Eq. IV-6-1 or IV-6-2 (denoted $\hat{t}$) versus observed values (t). It is noted that, over-all, the data are well presented by a log normal presentation mode. However, as mentioned above, this may be due to either (a) that natural causes result in a log normal distribution or (b) that the distribution arrived at from natural causes is (in many cases) sufficiently close to log normal, so that this latter is a good, practical presentation form. Here it serves, in a practical sense to allow a convenient set

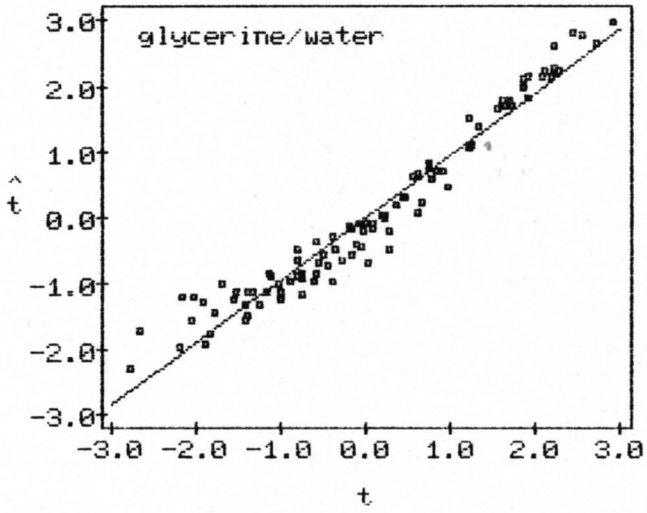

(i)

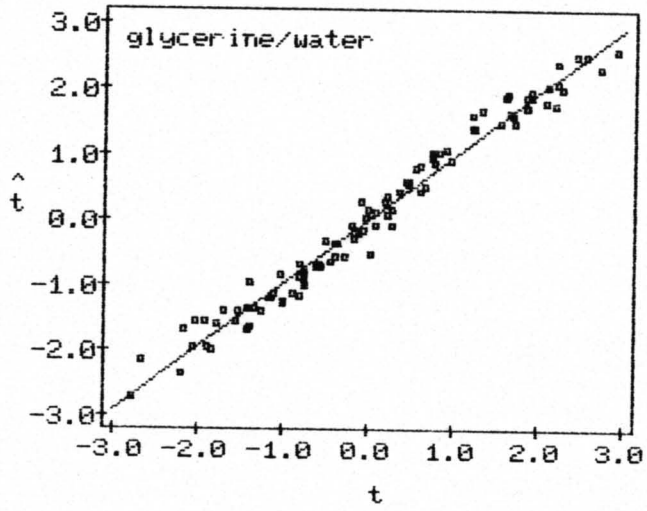

(ii)

Figure IV-6-1. Plots of predicted (t) vs observed (t) t-values according to: (i) normal crystal size (z) distributions and (ii) log-normal crystal size distributions. Glycerine/water solvent system.

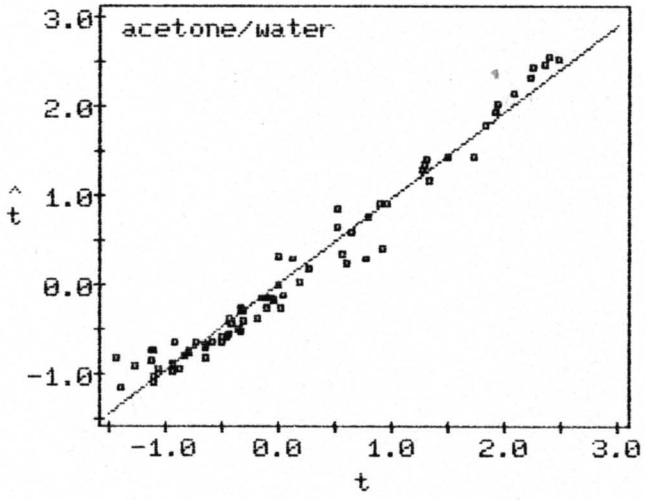

(i)

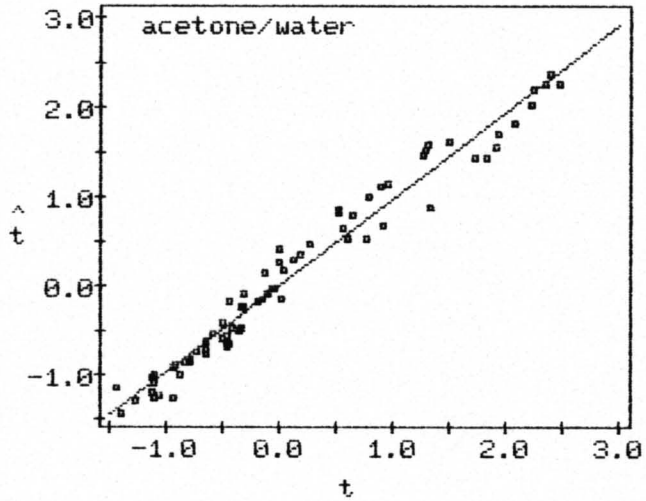

(ii)

Figure IV-6-2. Plots of predicted (t) vs observed (t) t-values according to: (i) normal crystal size (z) distributions and (ii) log-normal crystal size distributions. Acetone/water solvent system.

Table IV-6-1

Properties of Regression Model for Predicted Versus Observed t-values as a Function of z and ln (z).

System	t-value plotted against	R^2	Intercept	Slope	F^a	df_R [b]
glycerine/water	z	95.01	0.0074	0.9494	1921[c]	101
	ln (z)	97.51	-0.0010	0.9730	3450[c]	101
acetone/water	z	96.79	0.0083	0.9645	2108[c]	70
	ln (z)	96.96	0.0028	0.9707	2239[c]	70

[a] $F = \frac{\text{Regression mean SS}}{\text{Residual mean SS}}$.

[b] Residual degrees of freedom.

[c] Significant at $\alpha = 0.001$.

of parameters (mean and standard deviation) which can be used to gauge the effects of the experimental variables.

According to Eq. IV-6-1 the geometric mean diameter, ln z, is obtained by setting t = 0, i.e.

$$\ln z(0) = -b'/a' \qquad \text{Eq. IV-6-3}$$

The standard deviation, ln s, is obtained from the fact that when t = 1, ln z(1) = (1-b')/a', so that

$$\ln z(0) - \ln z(1) = \ln s = 1/a' \qquad \text{Eq. IV-6-4}$$

i.e. the standard deviation is the reciprocal of the slope. Values of ln z(0) and ln s are listed in Table IV-6-3. It is seen that ln z(0) seems to be neither a function of solvent nor solvent composition. In the case of glycerine the standard deviation decreases as a function of the glycerine concentration.

The same type analysis as described above has been applied to the crystal number distributions as a function of shape factor (b/a). In this case the equations simply become

$$t = a_1 \ln(b/a) + b_1 \qquad \text{Eq. IV-6-5}$$

for log normal distribution and

Table IV-6-3

Values of the Geometric Mean Diameter and Standard Deviations of Oxalic Acid Dihydrate Crystal Size Distributions as a Function of Solvent and Saturation Temperature.

	T_S = 30°C		T_S = 40°C	
Solvent	$\ln (z)_{geo}$	$\ln (S)_{geo}$	$\ln (z)_{geo}$	$\ln (S)_{geo}$
glycerine				
1%	5.38	0.51	5.78	0.57
1%	5.99[a]	0.50[a]	5.87[b]	0.59[b]
4%	5.77	0.35	5.87	0.39
7%	5.92	0.48	6.02	0.40
10%	6.02	0.31	5.94	0.33
15%	5.87	0.35	6.03	0.30
25%	5.90	0.21	5.19[c]	0.46[c]
acetone				
10%	5.71	0.42	5.69	0.69
25%	5.72	0.42	5.80	0.61
50%	5.68	0.41	5.78 $\pm$ 0.08[d]	0.62 $\pm$ 0.05[d]
75%	5.77	0.37	5.79	0.65
100%	5.85	0.42	6.05	0.83
water	5.35	0.54	5.89	0.51

[a] Cooling rate at 2°C/hour.

[b] (40/60) mesh cut seeds used (335 μm).

[c] Poor regression fit.

[d] Mean and standard deviations for duplicate crystallization runs.

$$t = a_2 (b/a) + b_2 \qquad \text{Eq. IV-6-6}$$

and results presented in these forms are shown in Section III-6-2 where the constants have been obtained by linear regression analysis (Tables III-6-14 to 17). Plots of predicted t ($\hat{t}$) versus observed t (t) according to Eqs. IV-6-5 and 6 are presented in Figures IV-6-3 and 4 and in Table IV-6-2. These show that the distributions are log normal for the glycerine/water system and normal for the acetone/water system. The values for geometric means (ln (b/a)) and ln s for the glycerine/water system and the arithmetic mean (b/a) and s for the acetone/water system are included in Tables IV-6-4 and 5 respectively. It is noted that the geometric mean breadth to length ratio (b/a) decreases as the glycerine percent increases. In the case of acetone there is no solvent dependency of either the mean b/a or its standard deviation.

The observed trend in b/a-ratios for the glycerine/water solvent system is demonstrated in the photographs in Fig. IV-6-5. The particles get more "flake-like" the higher the glycerine concentration. Ethanol/water shows the same shapes as glycerine but, as mentioned earlier, the study with ethanol was not pursued because of the fairly rapid ester formation (Section II-6). The effect on the b/a ratio is probably one of selective adsorption on particular crystal faces, inhibiting the growth of that particular face; the crystal faces with the higher growth rates will tend to disappear (Wells, 1946). It may be speculated that the OH-group tied to an

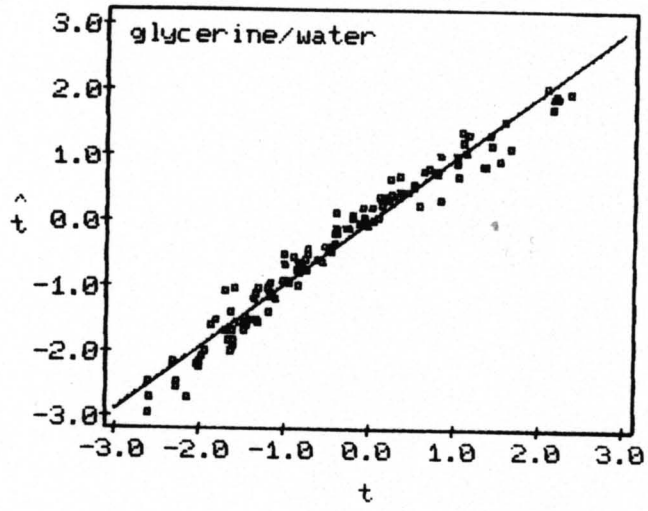

(i)

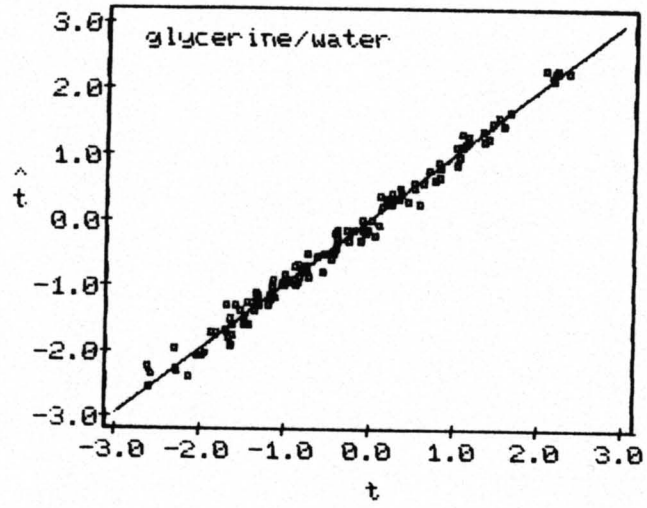

(ii)

Figure IV-6-3. Plots of predicted (t) vs observed (t) t-values according to (i) normal crystal shape (b/a) distributions and (ii) log-normal crystal shape distributions. Glycerine/water solvent system.

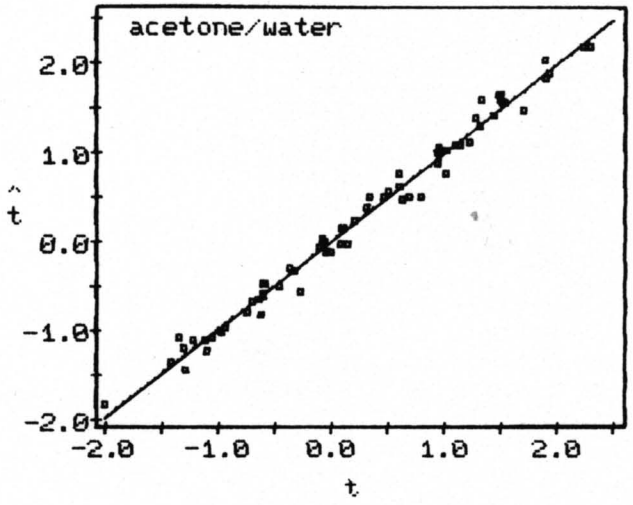

(i)

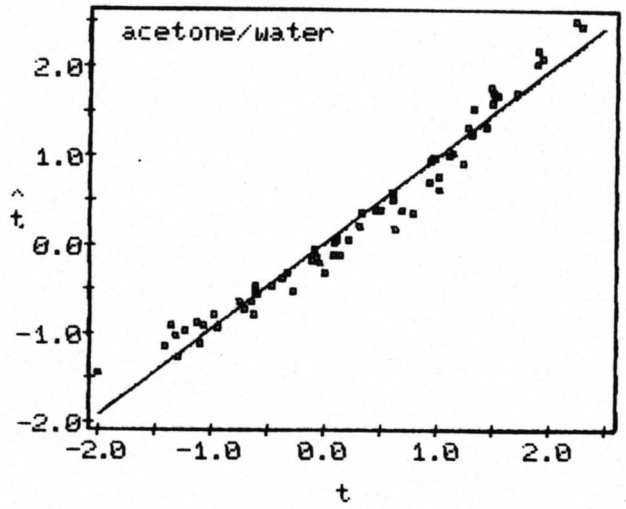

(ii)

Figure IV-6-4. Plots of predicted (t) vs observed (t) t-values according to: (i) normal crystal shape (b/a) distributions and (ii) log-normal crystal shape distributions. Acetone/water solvent system.

Table IV-6-2

Properties of Regression Model for Predicted Versus Observed t-values as a Function of (b/a) and ln (b/a).

System	t-value plotted against	R^2	Intercept	Slope	F	df_R [b]
glycerine/water	b/a	96.06	-0.0166	0.9605	2922[a]	120
	ln (b/a)	98.65	-0.0057	0.9870	8738[a]	120
acetone/water	b/a	98.67	0.0039	0.9870	4731[a]	64
	ln (b/a)	96.39	0.0104	0.9639	1701[a]	64

[a] Significant at $\alpha = 0.001$.

[b] Residual degrees of freedom.

Table IV-6-4

lues of the Geometric Mean Elongation Ratios and Standard Deviations of Oxalic Acid Dihydrate Crystal Size Distributions in Glycerine/Water Solvent Systems.

	T_S = 30°C		T_S = 40°C	
Solvent	$(b/a)_{geo}$	$\ln (S)_{geo}$	$(b/a)_{geo}$	$\ln (S)_{geo}$
ater	0.60	0.32	0.66	0.34
lycerine				
1%	0.52	0.43	0.45	0.54
1%	0.57[a]	0.28[a]	0.47[b]	0.41[b]
4%	0.60	0.31	0.38	0.45
7%	0.45	0.36	0.40	0.39
10%	0.25	0.25	0.37	0.37
15%	0.30	0.46	0.30	0.45
25%	0.28	0.51	0.28	0.47

Cooling rate at 2°C/hour.

40/60 mesh cut seeds (335 μm).

Table IV-6-5

Values of the Mean Elongation Ratios and Standard Deviations of Oxalic Acid Dihydrate Crystal Size Distributions in Acetone/Water Systems.

Acetone % (w/w)	T_S = 30°C		T_S = 40°C	
	(b/a)	(S)	(b/a)	(S)
10	0.70	0.19	0.69	0.19
25	0.69	0.17	0.71	0.19
50	0.72	0.16	0.63	0.18
75	0.73	0.21	0.65	0.21
100	0.69	0.19	0.68	0.20

organic radical is the common factor in ethanol and glycerine (and missing in water and acetone), and that this, somehow, is responsible for the selective adsorption.

Glycerine and other types of additives (Brice, 1973, Shor and Larson, 1971) have been used to control crystallization by virtue of adsorption on the crystal faces, for reasons of reducing the solubility of the solute or by its capability of changing the viscosity of the medium. The actual mechanism of these additives is a matter of controversy, with regards to isolating the factor responsible for the effect. Nevertheless, it has been reported by some workers (Mullin, 1972, Nyvlt, 1971, Jenkins, 1925) that an increase in the viscosity of the medium (a) inhibits nucleation, (b) decreases growth rate constants and (c) increases the uniformity of the product.

The effect of solution properties, i.e. viscosity and heats of solution, are reflected in the value of the nucleation rate constant, J*, and the number of crystals produced. The effect of the rate at which supersaturation is created and the solubility power of the solvent on nucleation have been studied earlier by Nyvlt (1971) and Leci et al. (1980), respectively. However, no attempt has been reported in literature to relate these variables to the micromeritic properties of the resulting particle population.

In a non-isothermal crystallization, the rate at which the solubility decreases with time is a function of (a) the temperature time profile during cooling and (b) the heat of solution of the

ystem. (i.e. for the same cooling rate the system with a higher heat f solution will have a faster change in solubility with time). This ffect has not specifically been investigated in this study but esupersaturation profiles have nevertheless been determined for a imited number of cases. There seems to be a slight dependence of the umber of crystals on the heat of solution, based on the results for he acetone/water system. The heat of solution of oxalic acid ihydrate calculated from Van't Hoff plots (section III-3) for 10% cetone/water is 8.1 kcal/mole. For 50% acetone/water it is 5.2 cal/mole and for 100% acetone it is 3.4 kcal/mole. Hence for onstant cooling rates during crystallization in these systems there s a 50% decrease in the rate at which the solubility changes with ime (from 10% acetone/water at one extreme and 100% acetone at the ther). This may be responsible for the decreased number of particles n the latter case.

Conversely the heats of solution of oxalic acid dihydrate in lycerine/water systems are not greatly affected by percent glycerine, iffering by no more than 5% in the concentration range 1 to 25% lycerine.

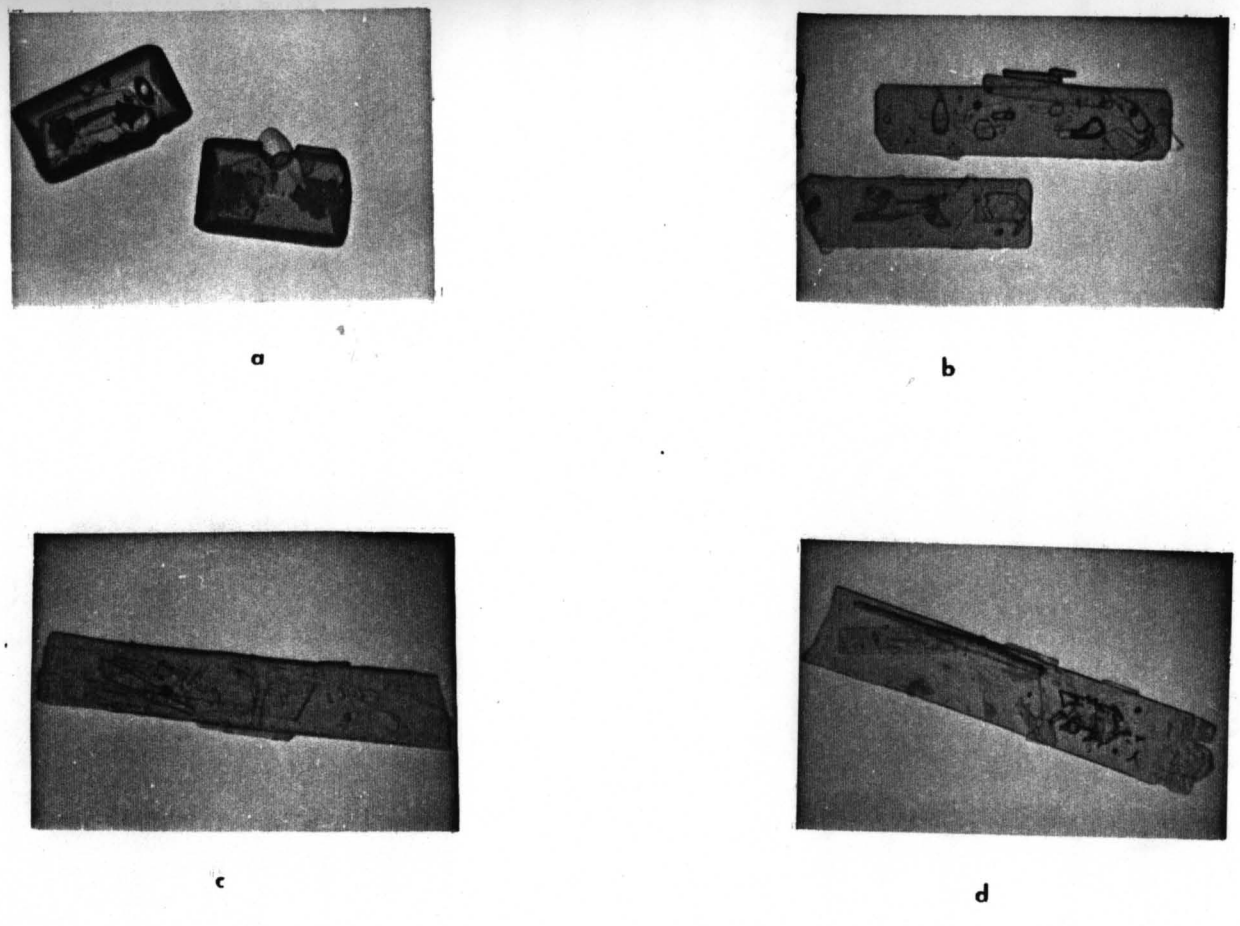

Figure IV-6-5. Photomicrographs of oxalic acid dihydrate, 30/40 mesh fraction, recrystallized from (a) water, (b) 7% glycerine/water, (c) 25% glycerine/water and (d) 10% ethanol/water. T_S=40°C.

V CONCLUSIONS

The work presented here has shown the following:

1. There is no apparent effect of the thermal histories of solutions on the degree of supercooling of supersaturated oxalic acid dihydrate solutions and on the mean particle size.

2. Number based crystal size distributions of oxalic acid dihydrate recrystallized from binary mixtures of solvents (glycerine/water and acetone/water) from seeded supersaturated solutions with programmed linear cooling are log-normal with respect to the characteristic length z. The geometric mean value of z is not affected by solvent or saturation temperature, however, the geometric standard deviation decreases with an increase in glycerine concentration.

3. When distributions are represented by the shape factor (b/a) they are log-normally distributed when recrystallized from glycerine/water solvent systems and the mean (b/a) decreases with increasing glycerine concentration. In contrast to this there is no appreciable solvent effect in water/acetone systems.

4. A model has been developed which describes the amount of mass precipitated with respect to time during non-isothermal crystallization. The model accounts for both nucleation and crystal growth. Reported values of the nucleation and growth orders (4.0 and 2.4 respectively) are reasonable and once this is established it is possible to account for the desupersaturation of solution as a

function of time by iteration. In this manner both nucleation and growth rate constants are obtained. Good agreement was found between the model and experimental concentration profiles.

5. A model that explains the crystal size distributions has been derived for the case where the decrease in supersaturation with time during crystallization follows an exponential decay. This approximation holds fairly well with linear temperature profiles in non-isothermal crystallization and the model describes the crystal size distributions well. The accuracy of the rate constants is adequate for application to the design of crystallization methods to control the micromeritic properties of the population.

6. Experiments where the supersaturation is constant during a significant time of the process allow for an independent determination of the growth rate constant. The assumption here is that the degree of supersaturation is small, so that only growth is occurring. A power function fit the data very well, and the growth rate constants obtained are in fair agreement with the other models here developed.

REFERENCES

H.V.Alexandru,, J.Crystal Growth, 5, 115 (1969)

H.V.Alexandru and C.Motoc, Rev. Roum. Phys., 17, 449 (1972)

D.Aquilano, M. Franchini-Angela, M. Rubbo, G. Mantovani and G.Vaccari, J.Crystal Growth, 61, 396 (1983)

ASTM Special Technical Publication 447, Manual on Test Sieving Methods, American Soc. for Testing and Materials, Philadelphia, Pa., (1969)

A.Berthoud, J.Chim.Phys., 10, 624 (1912)

J.D.Birchall and R.J.Davey, J.Crystal Growth, 54, 323 (1981)

T.Blickle and S.Halasz, Kristall u. Technik ,8, 679 (1973).

G.D.Botsaris and E.G.Denk, Ind. Eng.Chem.Fundam., 9, 276 (1970)

G.D.Botsaris, E.G.Denk and J.O.Chua, A.I.Ch.E.Symp. Series, 68 (121), 21 (1972)

S.H.Bransom, Brit.Chem.Eng., 5, 838 (1960)

S.H.Bransom, W.J.Dunning and B.Millard, Faraday Soc. Disc., 5, 83 (1949)

J.C.Brice, The Growth of Crystals From Liquids, American Elsevier Publishing Co., Inc., New York, N.Y., 1973, p.286.

W.K.Burton and N.Cabrera, Disc. Faraday Soc. 33(5), 40 (1949)

P.T.Cardew, J.Crystal Growth, 57, 391 (1982)

J.T.Carstensen, Solid Pharmaceutics, Mechanical Properties and Rate Phenomena, Academic Press, New York, N.Y., 1980, p 29

J.T.Carstensen and M.Patel, J.Pharm.Sci., 63, 1494 (1974)

J.T.Carstensen and M.Patel, J.Pharm.Sci., 64, 1770 (1975)

J.T.Carstensen and J.Sheridan, Acta Pharm.Techn.,25, 127 (1979)

J.T.Carstensen and M.A.Zoglio, Acta Pharm.Techn.,25, S17 (1979)

M.C.Cise and A.D.Randolph, A.I.Ch.E.Symp.Ser., 68(121), 42 (1972)

W.L.Chiou, S.J.Chen and N. Athanikar, J.Pharm.Sci., 65, 1702 (1976)

H.E.Cline, J.Crystal Growth, 51, 97 (1981)

E.G.Cooke, Kristall u. Technik , 1, 119 (1966)

F.Q.Danish and E.L.Parrott, J.Pharm.Sci., 60, 550 (1971)

J.Dugua and B. Simon, J.Crystal Growth, 44, 265 (1978)

J.E.Fairbrother and D.J.W.Grant, J.Pharm.Pharmacol., 30 19P (1978)

A.T.Florence, E.G.Salole, J.Pharm.Pharmacol., 28, 637 (1976)

A.T.Florence, E.G.Salole and J.B.Stenlake, J.Pharm.Pharmacol., 26, 479 (1974)

R.T.Fowler and J.R.Glastonbury, Chem. Eng. Sci., 10, 150 (1959)

F.C.Frank, Faraday Soc. Disc., 5, 48 (1949)

J.Frenkel, Kinetic Theory of Liquids, Dover (1955)

J.Garside, J.W.Mullin and S.N.Das, Ind. Eng.Chem.Process Des.Dev., 12, 369 (1973)

J.Garside, I.T.Rusli and M.A.Larson, A.I.Ch.E. J., 25, 57 (1979)

N.Garti and F.Tibika, Drug Dev.Ind.Pharm., 6, 379 (1980)

N.Garti, E.Wellner and S.Sarig, Krist.Tech,15, 1303 (1980)

N.Garti, C.L.Leci and S.Sarig, J.Crystal Growth,54, 227 (1981)

W.J.Genck and M.A.Larson, A.I.Ch.E.Symp.Ser., 68(121), 57 (1972)

N.A.El Gindy, A.A.Shalaby and M.M.Abd El Khalek, Drug Dev. and Ind.

Pharm., 8, 683 (1982)

J.W.Gibbs, Collected Works,Longmans, Green and Co., New York, N.Y.,1928, vol.1, p.55

Glycerine Producers Association, New York,N.Y., Physical Properties of Glycerine and its solutions (1963)

J.K.Haleblian, J.Pharm.Sci., 64, 1269 (1975)

C.C.Harris, Nature, 187, 401 (1960)

J.E.Helt and M.A.Larson, A.I.Ch.E.Symp.Ser., 23,822 (1977)

G.Herdan, Small Particle Statistics, Academic Press, New York, 1960, p.90-105

A.W.Hixson, Ind. Eng. Chem., 36, 488 (1944)

International Critical Tables of Numerical Data, Physics, Chemistry and Technology, Vol.III, (Ed. E.W.Washburn), McGraw-Hill Book Co.,Inc., N.Y., 1928, p. 25,26

R.R.Irani and C.F.Callis, Particle Size Measurement, Interpretation and Application, John Wiley and Sons, Inc., New York, N.Y., 1963, p. 34-57

J.D.Jenkins, J.Am.Chem.Soc., 47, 903 (1925)

A.Julg and B.Debrick, J.Crystal Growth, 62, 587 (1983)

M.A.Larson and A.D.Randolph, Chem. Eng. Progress, 65(95), 1 (1969)

C.L.Leci, N. Garti and S. Sarig, J.Crystal Growth, 51, 85 (1981)

C.Y.Lin, H.S.Tsuei and G.R.Yongquist, A.I.Ch.E.Symp.Ser., 67(110), 43 (1971)

W.L.McCabe and R.P.Stevens, Chem. Eng. Progress, 47(4), 168 (1951)

Merck Index, (M. Wirdholz, ed.), Merck & Co., Inc., N.J., 9th edition,

1976, p. 413

A.S.Michaels and A.R.Colville, J.Phys.Chem., 64, 13 (1960)

H.A.Miers and F.J.Isaac, Chem. Soc. Journal, 89, 413 (1906)

C.Misra and E.T.White, A.I.Ch.E.Symp.Ser., 67(110), 53 (1971)

J.Mullin, Crystallisation, C.R.C. Press, Cleveland, Ohio, 1972, p.137-213

J.W.Mullin and A.Amatavivadhana, J.Applied Chem., 17, 151 (1967)

J.W.Mullin and J.Garside, Trans.Inst.Chem.Eng., 45, 291 (1967)

J.W.Mullin and J.Garside, Trans.Inst.Chem.Eng., 45, 285 (1967)

J.W.Mullin and S.J.Jancic, Trans.Inst.Chem.Eng., 57, 188 (1979)

J.W.Mullin and C.L.Leci, J.Crystal Growth, 5, 75 (1969)

J.W.Mullin and C.L.Leci, A.I.Ch.E.Symp.Ser., 68(121), 8 (1972)

J.W.Mullin and K.D.Raven, Nature, 195, 35 (1962)

J.W.Mullin, A.Amatavivadhana and M.Chakraborty, J.Appl.Chem., 29, 153 (1970)

J.W.Mullin, M.Chbakraborty and K.Mehta, J.Applied Chem., 20,367 (1970)

J.Myl, Growth of Crystals, 5B, 49 (1968)

V.F.B.Naggar, S.El Gamal and M.A.Shams Eldeen, Sci.Pharm., 48, 335 (1980)

T.Nakai, J.Chinese Inst. Chem.Eng., 3(2), 83 (1972)

T.Nakai, Y.Aoyama and k.Miyake, Krist. Tech., 8, 1313 (1973a)

T.Nakai, Y.Aoyama and K.Miyake, Krist. Tech., 8, 1325 (1973b)

A.E.Nielsen, Kinetics of Precipitation, The Macmillan Co., New York, N.Y., 1964, p. 11-50

J.Nyvlt, Chem. Prumysl., 12, 606 (1962)

J.Nyvlt, J.Crystal Growth, 3,4 377 (1968)

J.Nyvlt, Industrial Crysallisation From Solutions, Chem. Rubber Publ. Co, Cleveland, OH, 1971

J.Nyvlt, Coll.Czechoslov.Chem.Commun., 39, 3463 (1974)

J.Nyvlt, ibid, 44(7), 2173 (1979)

J.Nyvlt, Industrial Crystallization - The Present State of the Art, Verlag Chemie, Weinheim, 1978, p. 75 - 100

J.Nyvlt and M.Matuchova, Kris.Tech., 11 245 (1976)

J.Nyvlt and V.Pekarek, Z.Phys.Chem.,122(2), 199 (1980)

J.Nyvlt, R.Rychly, J.Gottfried and J.Wurzelova, J.Crystal Growth, 6, 151 (1970)

J.D.O'Rourke and R.A.Johnson, Analytical Chemistry, 27, 1699 (1955)

B.Pamplin (ed.), Crystal Growth, International Series on the Science of the Solid State, Vol.16, 1980, p.397

V.Pekarek, T.Hostomsky and J.Skrivaneck, Krist.Tech., 10(1), K13 (1975)

N.Pilpel, Chem.Proc.Engn., 21, 167 (1965)

A.D.Randolph and M.A.Larson, Theory of Particulate Processes, Analysis and Techniques of Continuous Crystallization, Academic Press, New York, N.Y., 1971, p. 102-110

K.Ridgway and R.Rupp, J.Pharm.Pharmacol., 21, 305 (1969)

G.S.Riley, Powtech., Proceedings of the 3rd Intl. Powder Technology and Bulk Solids Conf., Powder Technology Publicaton Series No.

6., Heyden and Son, Ltd., New York, N.Y., 1976

F.Rumford and J.Bain, Trans.Inst.Chem.Engrs., 38, 10 (1960)

Sadtler Research Lab. Inc., NMR Spectra, Vol. 25, Philadelphia, 1973

K.Sato and M.Okada, J.Crystal Growth,42, 259 (1977)

A.Seidell, Solubility of Inorganic and Organic Compounds, D.Van Nostrand Co., Inc., New York, N.Y., 1940

J.Shell, J.Pharm.Sci., 52, 100 (1963)

S.M.Shor and M.A.Larson, A.I.Ch.E.Symp.Ser., 67 (110), 32 (1971)

S.K.Sikdar and A.D.Randolph, A.I.Ch.E.J., 22, 110 (1976)

I.Smid, J.Kvapil, J.Myl and S.Solz, Consultant Bureau (1962) by way of C.A.

S.Shrivanek, J.V.Pekarek and J.Hostomsky, Kris.Tech., 10(6), 617 (1975)

O.Sohnel, Kris.Tech., 11, 141 (1976)

O.Sohnel and J.Nyvlt, Chem.Prumysl. 25, 61 (1975)

O.Sohnel and J.Nyvlt, ibid., 25, 281 (1975)

O.Sohnel and J.Nyvlt, Coll. Czech.Chem.Comm., 40, 511 (1975)

O.Sohnel and J.Nyvlt, Chem. Prumysl., 26, 113 (1976)

O.Sohnel and J.Nyvlt, Kris.Tech., 11, 239 (1976)

G.Steiner, M.Patel and J.T.Carstensen, J.Pharm.Sci., 63, 1395 (1974)

R.F.Strickland-Constable, Kinetics and Mechanism of Crystallization from the Fluid Phase and of the Condensation and Evaporation of Liquids, Academic Press, London and New York, 1968

R.F.Strickland-Constable, A.I.Ch.E.Symp.Ser.,68 (121), 1 (1972)

Y.Tai, W.L.McCabe and R.W.Rousseau, A.I.Ch.E.J., 21, 351 (1975)

Takeuchi, K.Takahashi, K.Tomita and M.Imanaka, J.Chem.Eng.,Japan, 12(9), 209 (1979)

Tamman, States of Aggregation, Van Nostrand, New York, 1925

Timmermans, The Physicochemical Constants of Binary Systems in Concentrated Solutions, Interscience, New York, N.Y., 1960, p. 40-45

H.Ting and W.C.McCabe, Ind. and Eng. Chem., 26, 1201 (1934)

Troost, J.Crystal Growth, 3/4, 340 (1968)

Turnbull and J.C.Fisher, J.Chem.Phys., 17, 71 (1949)

R.Ubbelohde, Melting and Crystal Structure, Clarendon Press, Oxford, England , 1965, p. 289-290

Van Der Zwan and C.A.M.Siskens, Powder Tech.,33, 43 (1982)

Van Hook, Nucleation in Supersaturated Sucrose Solutions, Principles of Sugar Technology, Ed. P.Honig, Vol. 2, Elsevier, Amsterdam, 1959

S.Wey and J.P.Terwilliger, Chem.Eng.Commun, 4, 297 (1980)

F.Wells, Phil. Mag. 37, 184 (1946)

York, Int. J.Pharm., 14, 1 (1983)

APPENDIX A

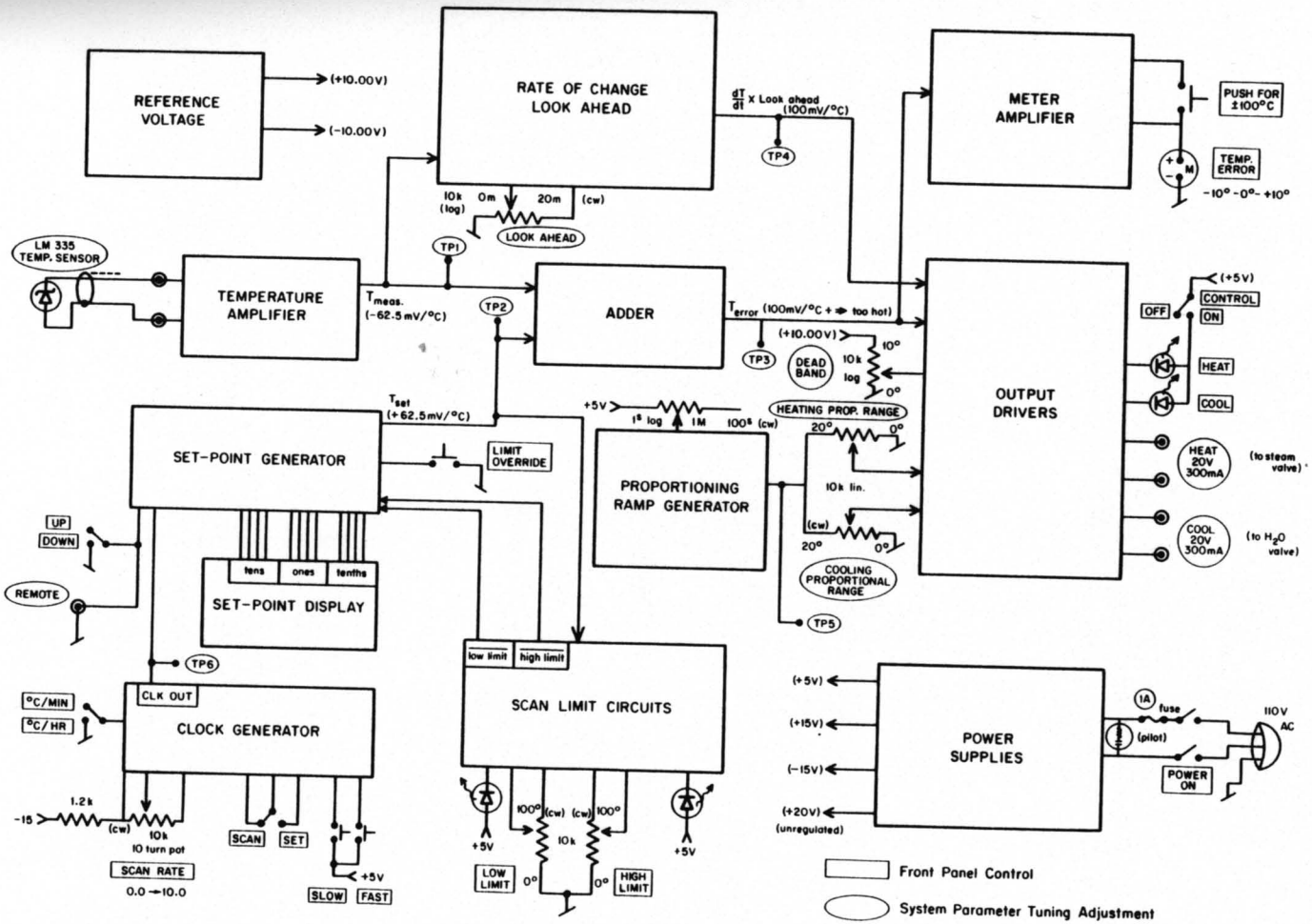

Temperature Programmer

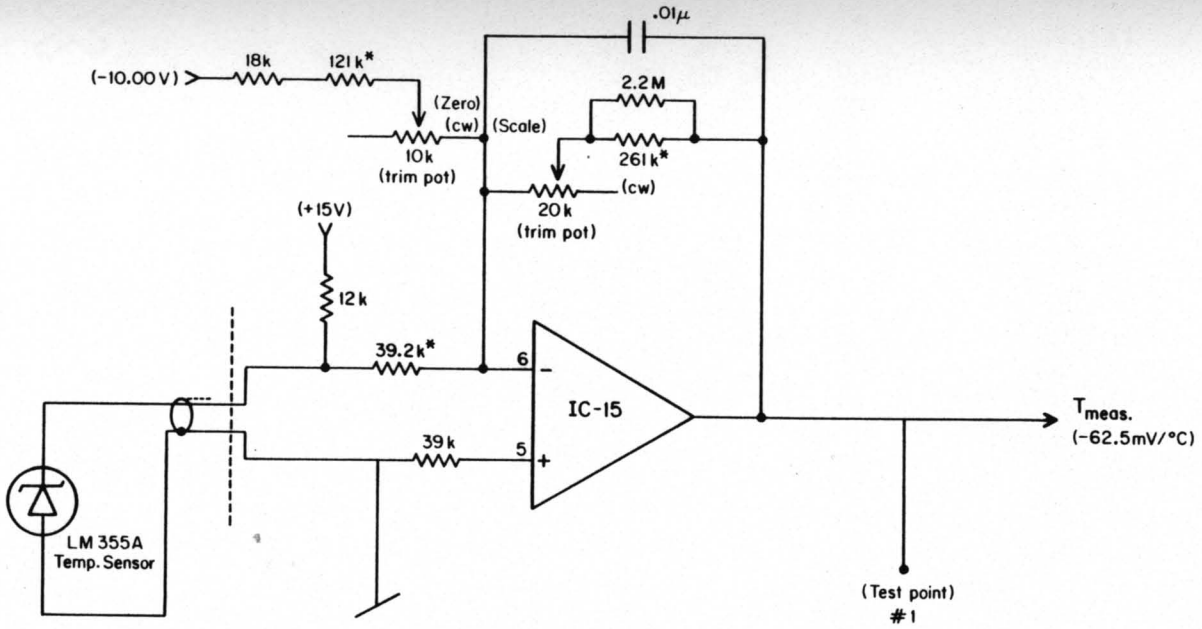

Temperature Amplifier

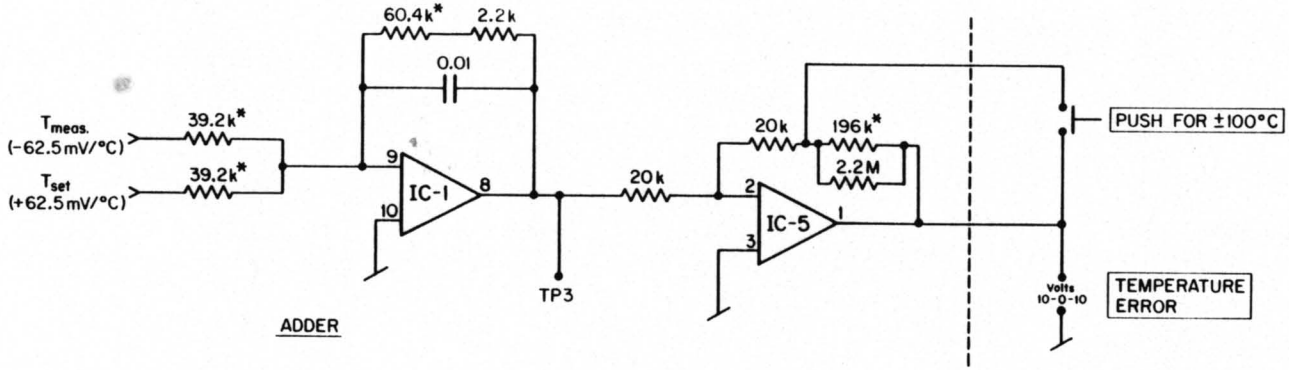

Meter Amplifier

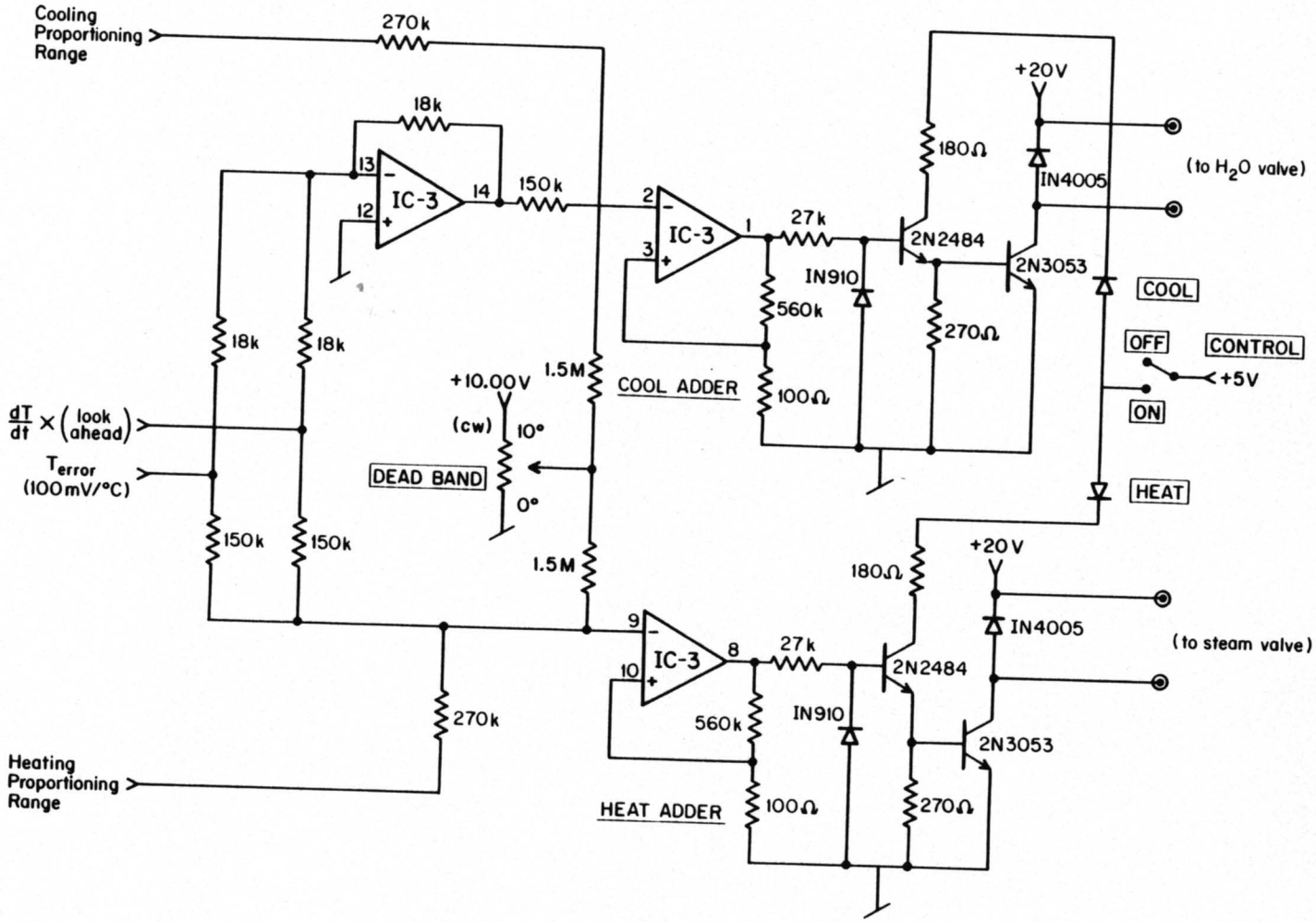

Output Drivers

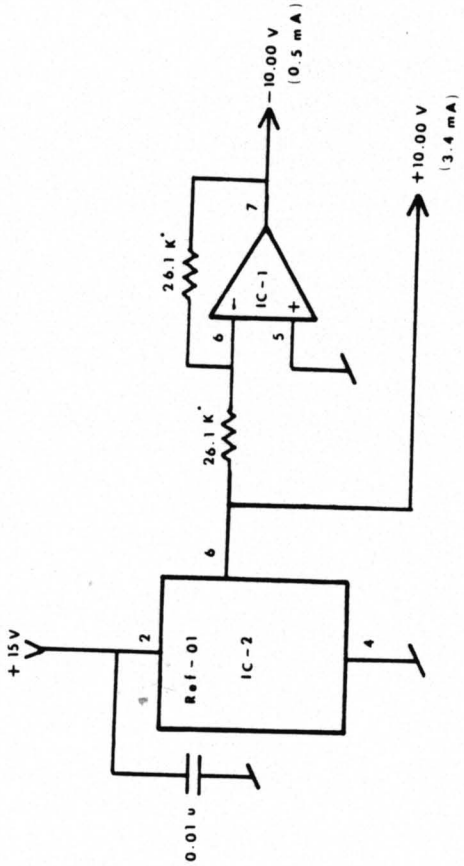

Reference Voltages

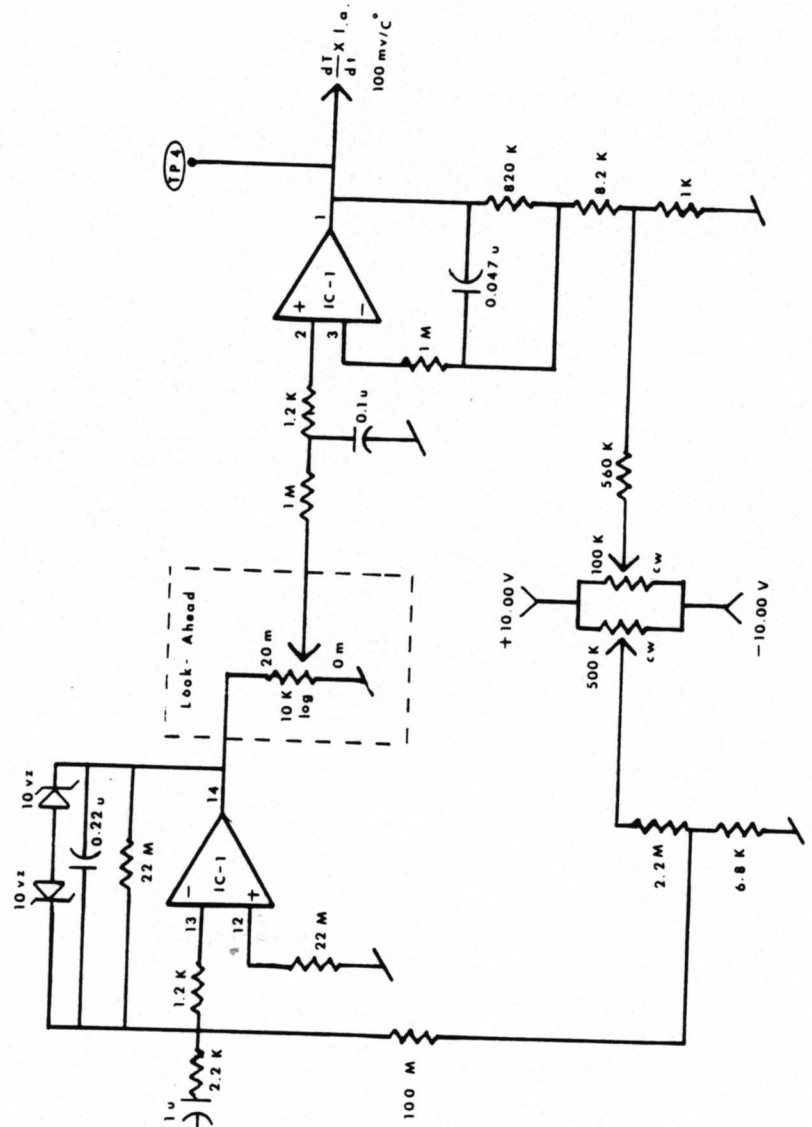

Rate of Change Look Ahead

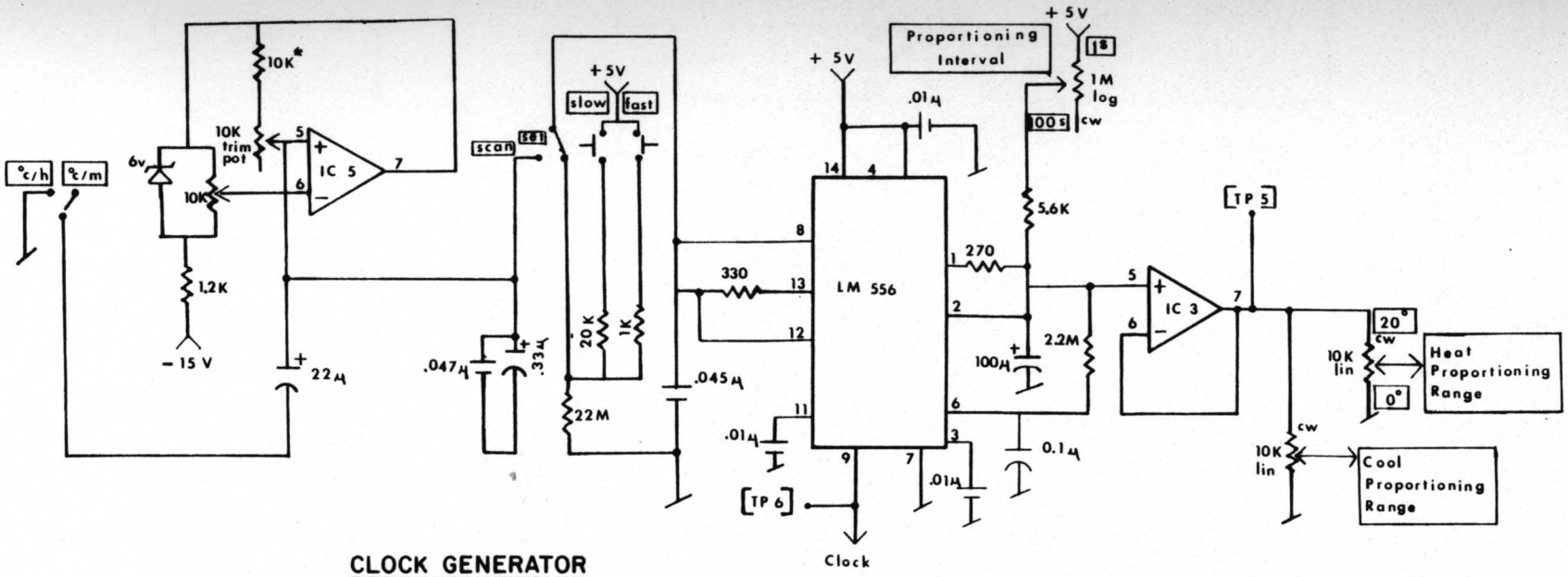

CLOCK GENERATOR

PROPORTIONING RAMP GENERATOR

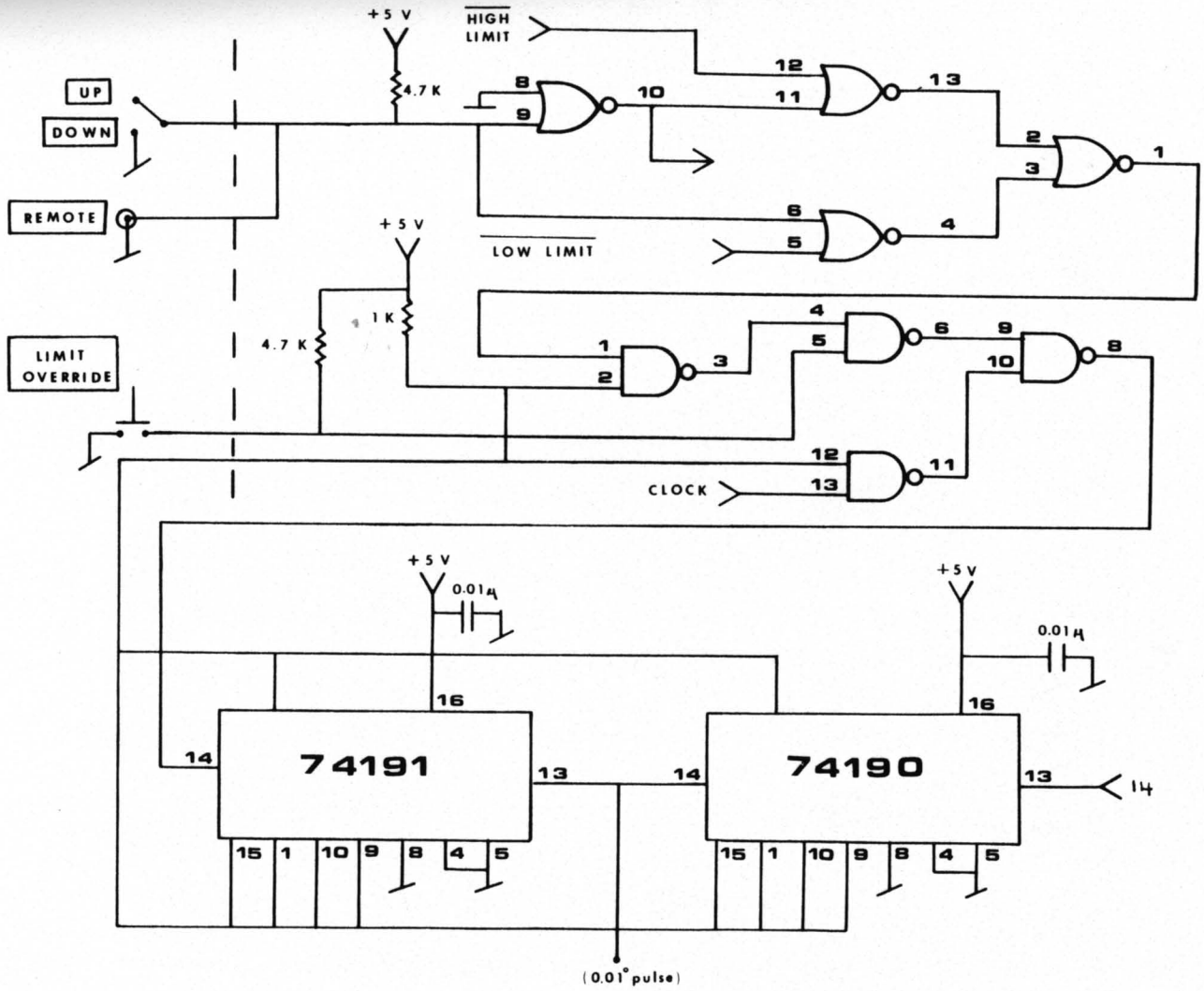

SET POINT GENERATOR

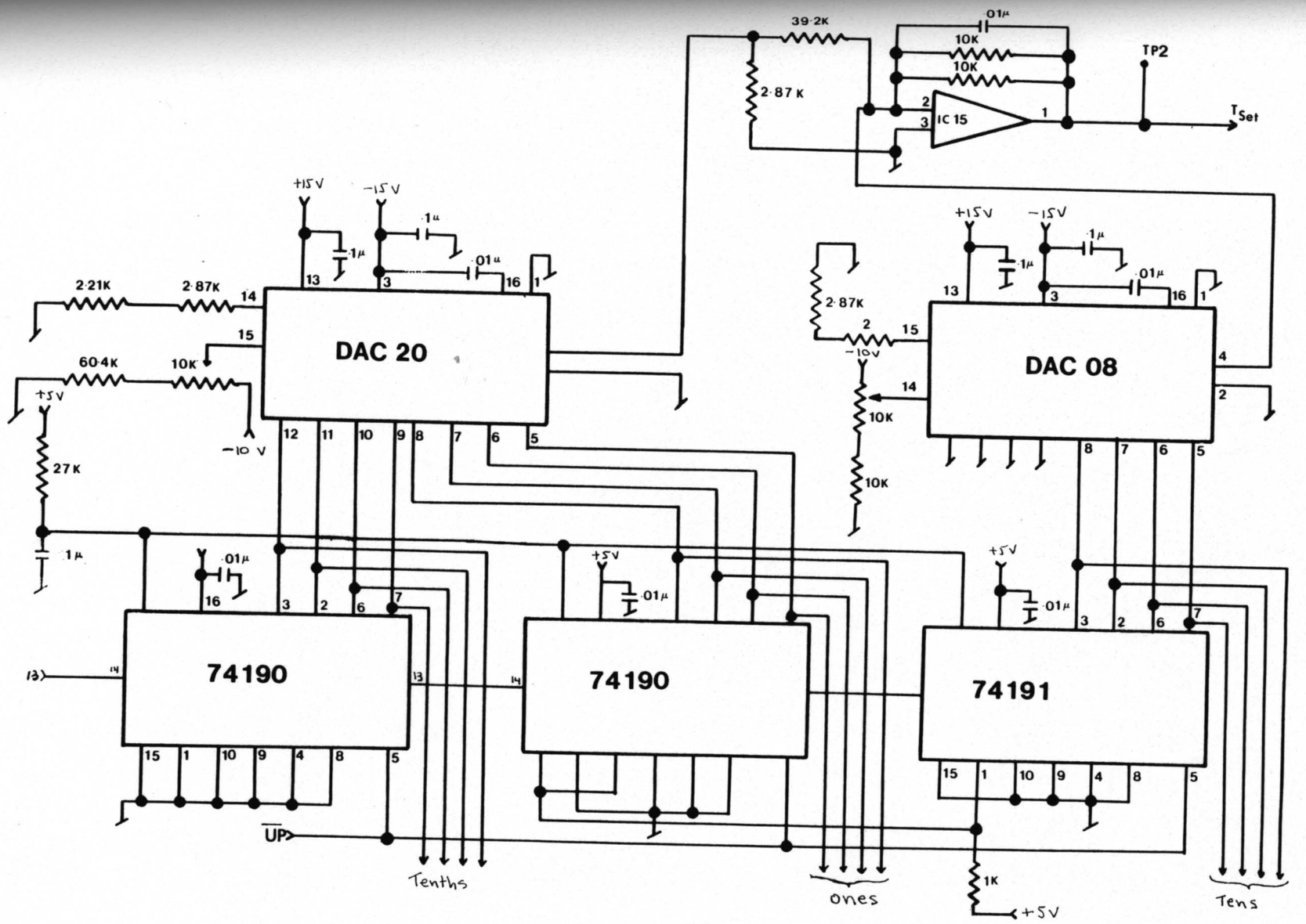

SET POINT GENERATOR

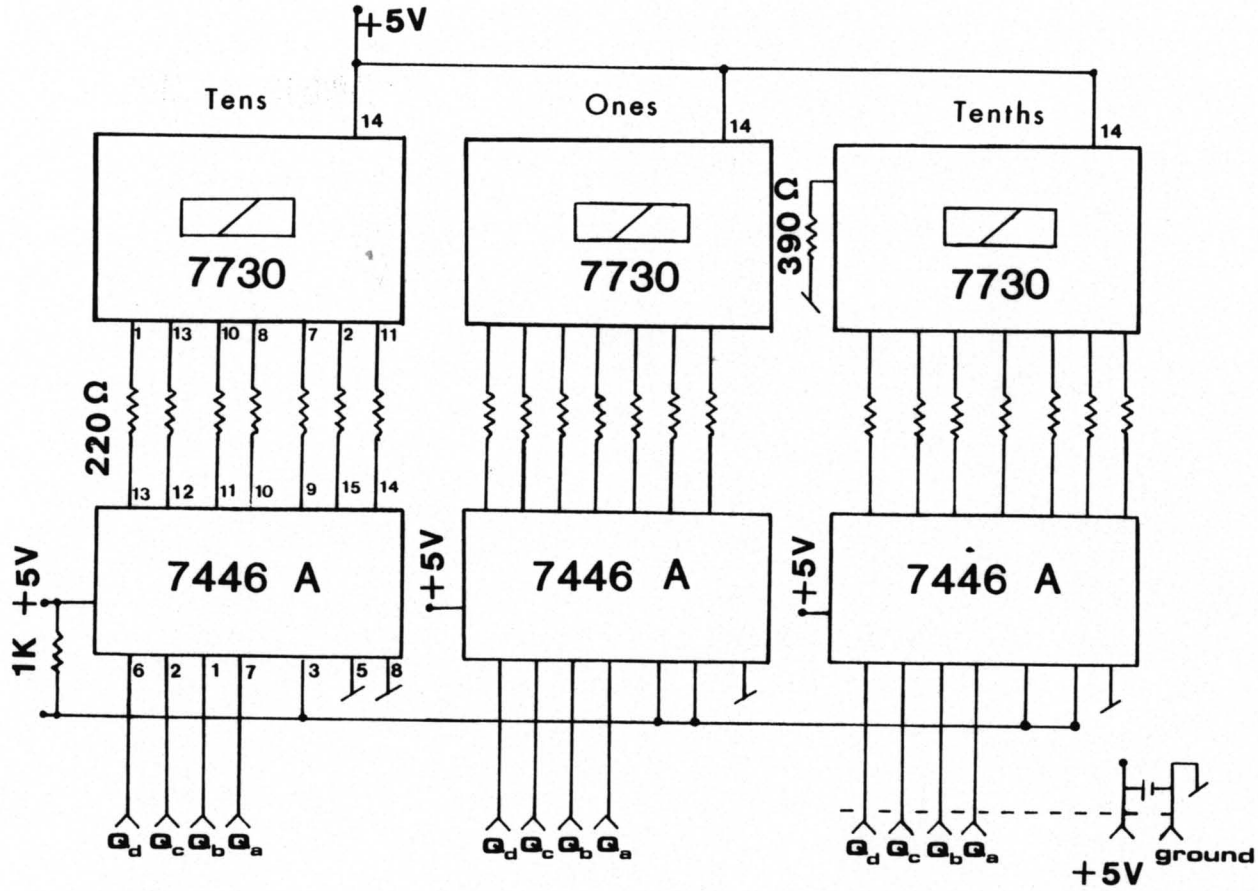

SET POINT DISPLAY

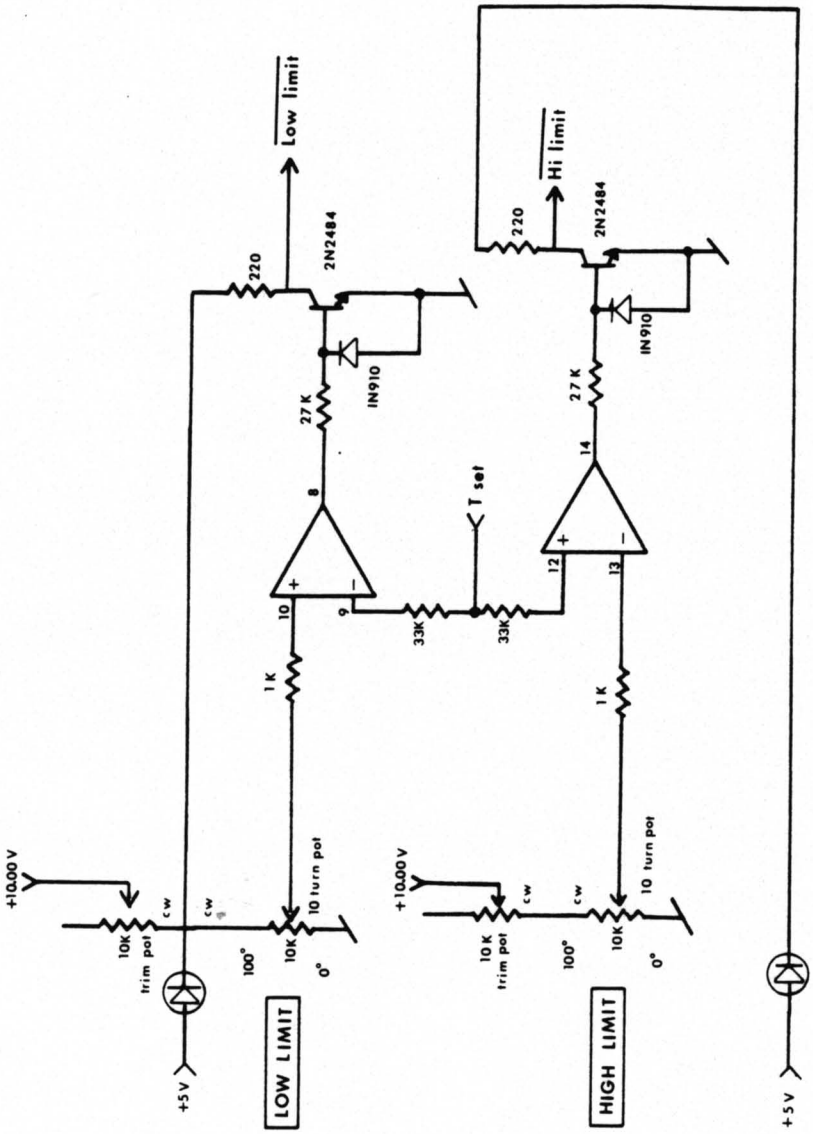

SCAN LIMIT CIRCUITS

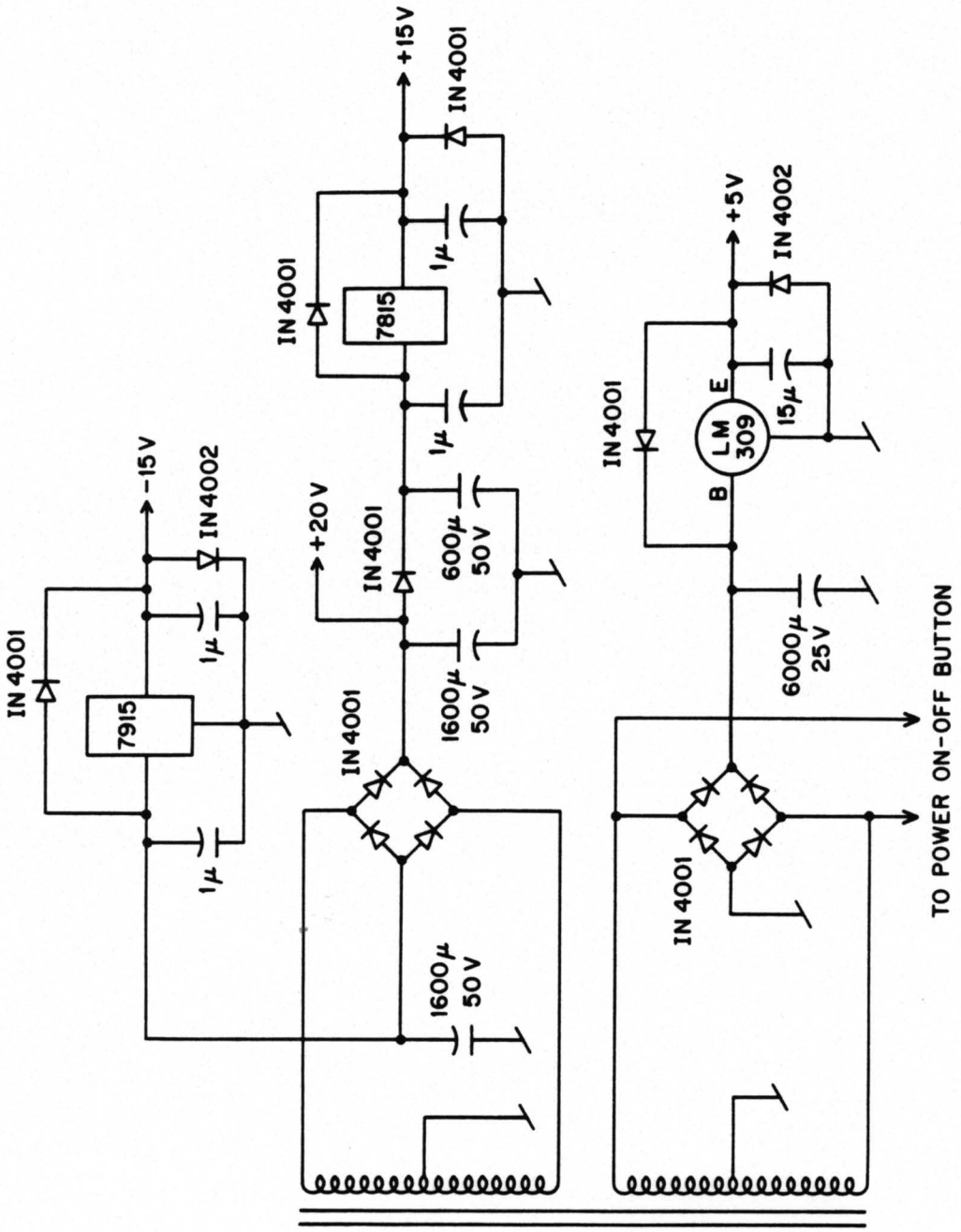

POWER SUPPLY

IC-#[a]	Component
1	TL-074
5	TL-074
3	TL-074
2	Ref-01
4	LM-556
6	74191
7-9	74190
10	74191
11	DAC-08
12	DAC-20
13	NAND
14	NOR
15	TL-074

[a] Number on the label of the integrated circuit chip.

APPENDIX B

Table B-1

Oxalic Acid Dihydrate Crystal Size Distributions

(Glycerine/Water System, T_S=30°C)

Glycerine Concentration (% weight)	Mesh Fraction	Z μ(m)	Cumulative Weight Percent Oversize	Cumulative Number Percent Oversize
1	20	801	4.1	0.2
	20/30	563	44.3	5.1
	30/40	366	72.8	18.0
	40/50	266	88.2	36.1
	50/60	204	92.5	47.0
	60/80	178	97.2	65.6
	80/100	138	98.9	79.1
4	20	762	9.6	0.7
	20/30	515	51.9	11.1
	30/40	372	76.8	27.4
	40/50	264	88.6	48.9
	50/60	199	98.5	90.9
	60/80	185	99.8	97.9
7	20	811	35.7	4.8
	20/30	495	80.5	31.4
	30/40	343	93.6	54.9
	40/50	240	97.9	77.3
	50/60	191	99.5	93.8
10	20	730	19.9	3.1
	20/30	483	61.8	25.4
	30/40	329	90.0	72.8
	40/50	304	99.0	91.8
	50/60	199	99.9	98.6
15	20	724	13.8	1.7
	20/30	436	67.6	32.5
	30/40	361	85.9	50.9
	40/50	263	96.2	77.5
	50/60	206	99.2	94.1

Glycerine Concentration (% weight)	Mesh Fraction	Z μ(m)	Cumulative Weight Percent Oversize	Cumulative Number Percent Oversize
25	20	564	5.4	1.3
	20/30	443	48.0	22.8
	30/40	372	76.0	46.6
	40/50	280	94.5	83.9
	50/60	261	99.5	96.2
1[a]	20	836	34.5	6.0
	20/30	611	81.1	26.6
	30/40	365	93.7	52.6
	40/50	279	97.8	71.8
	50/60	216	99.0	84.1
	60/80	183	99.8	97.2

(a) Cooling Rate 2°C/hour

Table B-2

Oxalic Acid Dihydrate Crystal Size Distributions

(Glycerine/Water System, T_S=40°C)

Glycerine Concentration (% weight)	Mesh Fraction	Z μ(m)	Cumulative Weight Percent Oversize	Cumulative Number Percent Oversize
1[a]	20	847	25.5	4.2
	20/30	571	75.7	29.2
	30/40	389	91.4	49.8
	40/50	288	96.3	63.6
	50/60	233	97.7	71.1
	60/80	185	99.4	86.5
1	20	847	26.9	3.2
	20/30	571	76.8	22.6
	30/40	389	92.4	41.7
	40/50	288	96.7	54.7
	50/60	233	97.8	61.0
	60/80	185	99.2	77.5
	90/100	144	99.9	95.5
4	20	924	19.9	1.3
	20/30	513	59.3	16.5
	30/40	380	82.8	38.6
	40/50	279	94.5	66.8
	50/60	229	97.8	81.0
	60/80	185	99.9	98.5
7	20	878	22.2	2.7
	20/30	589	68.6	68.6
	30/40	370	90.0	89.7
	40/50	311	97.7	97.7
	50/60	233	99.3	99.3
	60/80	185	99.9	99.9
10	20	847	6.4	0.5
	20/30	642	51.5	9.1
	30/40	366	81.1	39.4
	40/50	269	95.9	77.6
	50/60	221	99.0	92.0
	60/80	185	99.9	99.6

Glycerine Concentration (% weight)	Mesh Fraction	Z μ(m)	Cumulative Weight Percent Oversize	Cumulative Number Percent Oversize
15	20	753	6.7	1.0
	20/30	664	52.2	10.7
	30/40	351	89.7	64.8
	40/50	277	98.5	90.7
	50/60	233	99.6	96.2
	60/80	185	99.9	99.6
25	20	647	2.0	0.1
	20/30	452	22.3	2.8
	30/40	347	49.2	10.8
	40/50	296	69.5	20.5
	50/60	240	82.0	20.5
	60/80	176	93.5	31.7
	80/100	107	98.0	57.8

(a) Seed size 40/60 mesh (335 μm)

Table B-3

Oxalic Acid Dihydrate Crystal Size Distributions

(Acetone/Water System, T_S=30°C)

Acetone Concentration (% weight)	Mesh Fraction	Z μ(m)	Cumulative Weight Percent Oversize	Cumulative Number Percent Oversize
10	20	768	7.7	0.7
	20/30	565	48.5	9.8
	30/40	388	76.4	28.9
	40/50	294	90.8	51.7
	50/60	288	95.3	67.0
	60/80	196	99.0	86.4
25	20	773	13.3	1.2
	20/30	570	53.0	10.0
	30/40	383	76.8	27.5
	40/50	290	90.0	49.1
	50/60	233	95.1	67.0
	60/80	192	99.4	92.3
50	20	739	9.7	0.9
	20/30	560	48.2	9.5
	30/40	385	74.6	27.4
	40/50	289	90.4	52.7
	50/60	242	95.2	66.1
	60/80	191	99.0	86.9
75	20	773	10.6	0.8
	20 30	587	44.7	6.8
	30/40	392	70.4	22.0
	40/50	296	87.0	44.6
	50/60	231	93.3	63.0
	60/80	210	98.2	81.8
100	20	833	12.3	1.3
	20/30	573	59.8	16.9
	30/40	381	88.1	48.4
	40/50	280	96.6	72.0
	50/60	230	98.3	80.9
	60/80	192	99.6	91.8

Table B-4

Oxalic Acid Dihydrate Crystal Size Distributions

(Acetone/Water System, T_S=40°C)

Acetone Concentration (% weight)	Mesh Fraction	Z μ(m)	Cumulative Weight Percent Oversize	Cumulative Number Percent Oversize
10	20	977	26.7	2.8
	20/30	596	76.9	25.6
	30/40	385	94.6	55.3
	40/50	312	98.3	67.1
	50/60	233	99.2	74.1
	60/80	198	99.7	79.7
	80/100	152	99.8	82.6
25	20	955	26.8	2.7
	20/30	609	75.3	21.4
	30/40	411	92.5	43.0
	40/50	297	96.9	57.7
	50/60	237	98.4	67.2
	60/80	198	99.4	78.8
	80/100	152	99.9	89.7
50	20	873	19.4	1.9
	20/30	577	69.5	18.8
	30/40	401	90.2	39.5
	40/50	291	95.9	54.4
	50/60	233	97.6	63.5
	60/80	198	99.2	76.3
	80/100	152	99.8	87.1
50	20	873	24.6	3.4
	20/30	577	80.3	30.0
	30/40	401	94.5	50.1
	40/50	291	97.8	62.3
	50/60	233	98.8	69.6
	60/80	198	99.6	78.9
	80/100	152	99.8	85.6

Acetone Concentration (% weight)	Mesh Fraction	Z μ(m)	Cumulative Weight Percent Oversize	Cumulative Number Percent Oversize
75	20	872	30.2	4.2
	20/30	579	84.4	30.1
	30/40	396	94.6	45.4
	40/50	293	97.4	55.6
	50/60	228	98.5	63.8
	60/80	198	99.4	74.2
	80/100	152	99.8	86.7
100	20	870	38.8	9.1
	20/30	589	93.3	50.3
	30/40	389	97.9	62.4
	40/50	296	99.0	68.9
	50/60	222	99.4	73.8
	60/80	199	99.8	82.2
	80/100	148	99.9	86.5

Table B-5

Oxalic Acid Dihydrate Crystal Size Distributions

(Solvent:water)

T_S=30°C

Mesh Fraction	Z (μm)	Cumulative Weight Percent Oversize	Cumulative Number Percent Oversize
20	744	5.4	0.3
20/30	581	46.1	5.5
30/40	368	80.4	22.8
40/50	287	88.8	31.7
50/60	221	92.8	41.1
60/80	189	97.1	56.9
80/100	146	98.9	72.0

T_S=40°C

20	869	11.0	1.4
20/30	599	65.6	22.2
30/40	411	91.4	52.7
40/50	309	97.4	69.4
50/60	239	98.8	77.7
60/80	196	99.7	87.8
80/100	154	99.9	92.2

APPENDIX C

Surface Area

The equation describing the growth of crystals is of the form

$$dM/dt = N\ a\ G\ (C-s)^g \qquad \text{Eq. C-1}$$

where a is the area of a particular crystal. The time dependence of the concentration (C) and the solubility (S) are known from measurements. The only time dependent term remaining to be defined is the area (a) as a function of either time or concentration.

If there are n(i) particles with length r(i) for the required values of i to define the population, then at time t the total area, A, is given by

$$A = f_a \sum_{i=1}^{j} n(i)\ (r(i))^2 \qquad \text{Eq. C-2}$$

where f_a is a surface shape factor; it has the value six in the case of a cubical particle.

The total volume, V , is

$$V = f_v \sum_{i=1}^{j} n(i)(r(i))^3 \qquad \text{Eq. C-3}$$

where f_v is the volume shape factor. The area of the particle population can be expressed in terms of mass by

$$A = \frac{M f_a \Sigma n(i) (r(i))^2}{f_v \rho \Sigma n(i) (r(i))^3}$$

$$= M f_{sv} / (\rho r_{sv}) \qquad \text{Eq. C-4}$$

where f_{sv} is the over-all surface-volume shape factor and r_{sv} is the surface-volume mean diameter.

In the case of one particle:

$$a = f_a r^2 \qquad \text{Eq. C-5}$$

$$v = f_v r^3 = m/\rho \qquad \text{Eq. C-6}$$

$$\text{i.e. } r = (m/(\rho f_v))^{1/3}$$

Combining these then gives

$$a = f_a (m/(f_v \rho))^{2/3} =$$

$$f_a v^{2/3} f_v^{-2/3} \qquad \text{Eq. C-7}$$

Then for a group of crystals (homogeneous population):

$$A = N\,a = N\,f_a\,v^{2/3}\,f_v^{-2/3} \qquad \text{Eq. C-8}$$

Hypothetically it is possible to use this approach and define the area as a function of time but it is not practical due to the difficulty of measuring a dynamic particle size distribution (i.e. one which changes in time). The following approach has therefore been used: the particle size distribution at the final time of crystallization is known, and it is generally (close to) log normal on a number basis.

In a typical case, the distribution has upper and lower limits at 140 and 840 micrometers (i.e. it is truncated). If it is assumed that during a certain time period of the process, nucleation is negligible and the number of particles in suspension is constant, then the distribution of particles at this time is also log normal with particle sizes from 840-q' to 140-q' microns (provided q' is not too large). If e.g. q' is 139, then the limits at the onset of the period of constant particle count would be 1 to 701 micrometer. Ten time intervals leading from this truncated distribution to the one limited by 140 and 840 are now calculated. A log normal distribution by number is first constructed for the distribution from 1 to 701 micrometer. Next another distribution is constructed from 1+14= 15 to 701+14 = 715 micrometer and so on, adding 14 micrometer to each limit for each succeeding step. The values of $\Sigma n(i)(r(i))^2$ and $\Sigma n(i)(r(i))^3$ are then calculated for each fraction of the eleven

distributions. A Basic program written for this purpose is included and is listed in Program C-1.

Fig. C-1 shows a plot of $\Sigma n(i)(r(i))^2$ versus $(\Sigma n(i)(r(i))^3)^{2/3}$. The plot is linear and follows an equation of the form

$$A = f_{sv} V^{2/3} \qquad \text{Eq. C-9}$$

where f_{sv} is the slope, found to be 10.00 $\pm$0.01. (The latter is the standard error of the mean). The intercept fails to differ from zero. This value is in agreement with the factor of 10.3 found by Carstensen and Patel (1975), used to correlate the area to the volume ($V^{2/3}$) by geometric consideratons of an oxalic acid dihydrate crystal.

The volume of the solid at time t is given by

$$V = (m(0)-m(t))/\rho \quad = (C(0)-C)\ Q/\rho \qquad \text{Eq. C-10}$$

The parameters of this equation have been measured for some solutions. Comparison of these with the area expressed as $\Sigma n(i)\ (r(i))^2$ for the final time of the crystallization process is shown in Table C-1. The average f_{sv} calculated from these data is 8.9 $\pm$1.4. This is in good agreement with the value of f_{sv} obtained from the regression equation (Eq. C-9).

The validity of the assumption that nucleation is negligible

after a certain time during the process can be shown in the following manner: considering an example of typical simulation for the process where nucleation and growth are both occurring, it is possible to calculate the number of crystals born at each interval. This is shown in Table C-2.

It is observed that 70% of the total number of crystals were born during the first 10% of the time, and by 40% of the final time 90% of the crystals had been born.

PROGRAM C1

```
80   DIM D(20)
90   FOR I = 0 TO 10 STEP 1
95   PRINT "I=";I
100   FOR J = 1 TO 11
110   READ D(J),N
120   DATA  66,5,140,5,158,10,186,
      20
121   DATA  220,20,259,20,300,10,3
      38,5
122   DATA  381,3,427,1,575,1
127   LET D(J) = D(J) + (I * 14)
131   LET Q = N * (D(J) ^ 2)
140   LET P = N * (D(J) ^ 3)
150   LET A = A + Q
160   LET B = B + P
180   NEXT J
200   PRINT "A=";A;"      ";"B=";B
210   LET H = A * 1000
211   LET V = (B / 350) * 1000
212   PRINT "A'=";H;"      ";"B'=";
      V
213   PRINT
214   PRINT "--------------------
      ---"
220   RESTORE
221  A = 0
222  B = 0
230   NEXT I
```

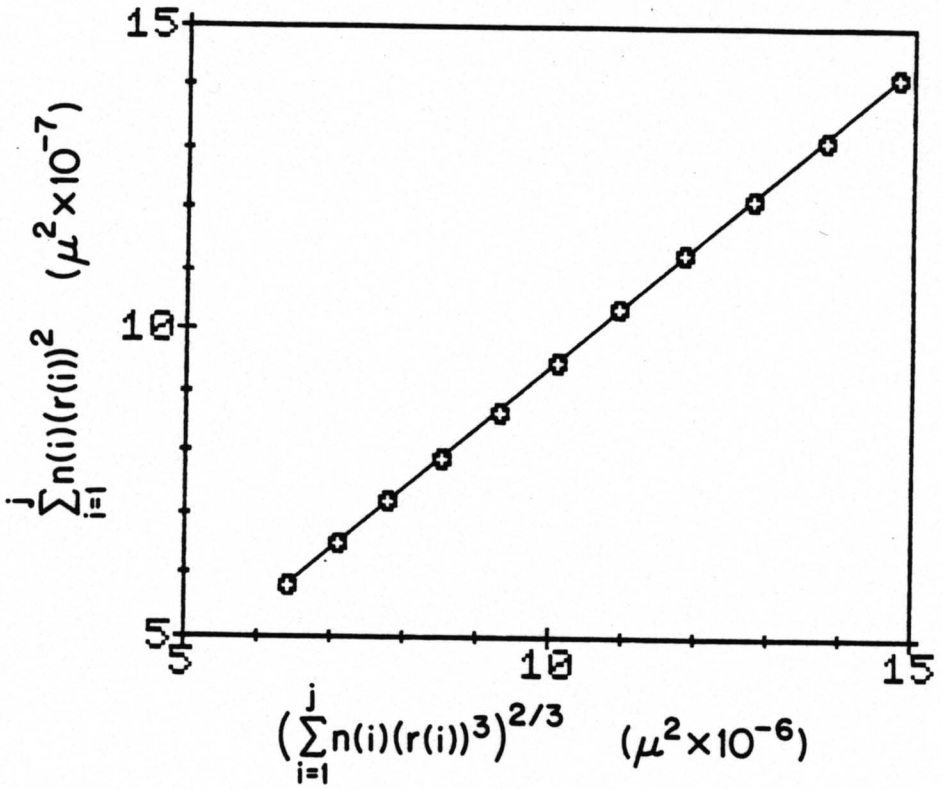

Figure C-1. Evaluation of the surface-volume shape factor during crystal growth.

Table C-1

Crystal Area: as a Function of the Volume of Oxalic Acid Precipitated during Non-isothermal Crystallization.

Experiment		$(M/\rho)^{2/3}$[a]	$\sum_{i=1}^{j} n(i)r(i)^{2b}$	
Solvent	T_S	cm^2	cm^2	f_{sv}[c]
glycerine 15%	30	0.087	0.786	11.1
glycerine 15%	40	0.205	1.875	9.2
acetone 50%	30	0.102	0.857	8.4
acetone 50%	40	0.216	2.03	9.4
water	30	0.084	0.661	7.9
water	40	0.192	1.355	7.1

[a] Calculated from the final $(C_0 - C)$ measured titrimetrically, expressed as gm oxalic acid dihydrate/gm of solvent.

[b] Measured from sieve analysis results; expressed as cm^2 for the number of crystals produced/gm of solvent.

[c] Factor that correlates the total area measured by sieve analysis with the total volume precipitated.

Table C-2

Birth of Nuclei during a Simulation of the Crystallization Process

($J^* = 7.6$, $G^* = 0.05$, $C_0^* = 108$, $S_F^* = 90$).

t^*	dN/dt^*[a]	N[b]
0.02	9.1	326
0.04	4.7	455
0.08	2.0	577
0.10	1.5	611
0.14	0.9	657
0.20	0.6	699
0.40	0.3	773
0.60	0.2	815
0.80	0.2	848
1.00	0.1	876

[a] Number of nuclei born during the (1/1000) interval dt^*, per gm of solvent.

[b] Sum of the number of nuclei born to t^*, per gm of solvent.

APPENDIX D

SIMULATION OF CRYSTALLIZATION

```
100  FOR C0 = 108 TO 116 STEP 4
120 C = C0
125 A3 = 100
130 A4 = 0
135 A5 = 900
138 V = 1
140 N = 0
150  FOR Z = 60 TO 90 STEP 15
160  FOR J = 1.0 TO 7.0 STEP 2.0
190  PRINT "S=";Z;"      ";"C=";C;
     "     ";"J=";J
191  PRINT
205  FOR I1 = 1 TO 4
206 C = C0
210  READ G
211  PRINT "G=";G
213  PRINT "A/W"; TAB( 8);"C";
214  PRINT  TAB( 13);"(C-S)";
215  PRINT  TAB( 21);"N"
230  DATA  .01,.025,.05,.1
240  REM  T IS TIME INTERVAL
250 H = 1
255 W = 1000
260  FOR T = 0 TO H STEP H / W
261 A = A + 1
262 S = 100 - ((100 - Z) * T / H)

263  IF (C - S) < 0 GOTO 540
264  REM  M IS NO OF NUCLEI FORME
     D IN TIME INTERVAL
265 M = J * ((C - S) ^ 4.0) * (H /
     W)
269  REM  N IS TOTAL NO OF NUCLEI

270 N = N + M
279  REM  Q IS TOTAL AMOUNT PRECI
     PITATED IN INTERVAL OF TIME
281 AREA = (M + (6 * (((C0 - C) *
     V) ^ (2 / 3))))
285 Q = G * AREA * (H / W) * ((C -
     S) ^ 2.4)
289  REM  X IS THE CONCENTRATION
     CORRESPONDING TO THE AMOUNT
     Q
290 X = Q / V
```

```
303  IF A = 1000 GOTO 465
305  IF (A < A4) OR (A > A5) GOTO
     375
314  IF A = A3 *  INT (A / A3) GOTO
     356
355  GOTO 375
356 C2 = (C - S)
357 C2 =  INT (C2 * 1000 + .5) /
     1000
358 M1 =  INT (M * 1000 + .5)
359 M1 = M1 / 1000
360 C5 =  INT (C * 100 + .5) / 10
     0
366  PRINT A / W; TAB( 5);C5;
368  PRINT  TAB( 13);C2;
369  PRINT  TAB( 20);M1
375 C = C - X
378  NEXT T
465  PRINT
466 N2 =  INT (N * 100 + .5) / 10
     0
467 C6 =  INT (C * 100 + .5) / 10
     0
468 S6 =  INT (S * 100 + .5) / 10
     0
470  PRINT "NUCLEI=",N2
475  PRINT "FINAL CONC=";C6;"  ";

480  PRINT "S=";S6
540 A = 0
543 C = C0
545 N = 0
550  PRINT "--------------------
     -----"
565  NEXT I1
570  RESTORE
575  PRINT "**********************
     *******"
580  PRINT
590  NEXT J
600  NEXT Z
610  NEXT C0
```

APPENDIX E

Growth Rate Constant Evaluation

Growth rates have been found to be proportional to the supersaturation to a power and to the surface area of the crystals. The amount of material, dM, precipitated in a time element dt, at time t, is given by:

$$dM/dt = G\ A\ (C-S)^g \qquad \text{Eq. E-1}$$

Three approaches based on this growth equation have been followed to evaluate the growth rate constant.

Case 1 - Growth During Simulation of the Crystallization Process

Considering the mass precipitated in one interval dt = t, Eq. E-1 becomes

$$M = G\ A\ (C-S)^g t \qquad \text{Eq. E-2}$$

where A is a function of the total mass available for crystallization, and is given by:

$$A = f_{sv}\ (M/\rho)^{2/3} \qquad \text{Eq. E-3}$$

The reduced variables used in this analysis are

$$C^* = 100\ C/S_0 \qquad \text{Eq. E-4}$$

$$S^* = 100\ S/S_0 \qquad \text{Eq. E-5}$$

$$t^* = (t-t')/(t''-t') \qquad \text{Eq. E-6}$$

where

S_0 = solubilty of oxalic acid dihydrate (g/g)

t' = the time at the onset of precipitation

t'' = the time at the end of precipitation

C^* = reduced concentration

S^* = reduced solubility

t^* = reduced time.

The total mass precipitated at a given time, t^*, can be expressed as a function of the concentration remaining in solution by

$$M = (100\ (C_0-C)\ Q/S_0)^{2/3} \qquad \text{Eq. E-7}$$

where C is the concentration of oxalic acid dihydrate (g/g of solvent) at time t^* and C_0 is the initial concentration before any crystallization has occurred. Q is the number of grams of solvent.

By substituting the reduced form of the variables into Eq. E-2 one obtains:

$$M = G^*\ A\ (C^*-S^*)^g\ t^* \qquad \text{Eq. E-8}$$

where

$$G^* = G\ S_0^{\ g}(t''-t')/100^g \qquad \text{Eq. E-9}$$

Case II Growth During Constant Supersaturation

The differential form of Eq. E-8 is

$$dM/dt^* = G^* A (C^*-S^*)^g \qquad \text{Eq. E-10}$$

By introducing Eq. E-3 into Eq. E-10 one obtains:

$$dM/dt^* = G^* (M/\rho)^{2/3} (C^*-S^*)^g \qquad \text{Eq. E-11}$$

Integration over the interval where (C^*-S^*) remains constant, $t^*_o < t^* < t^*_F$, yields

$$M^{1/3}-M_o^{1/3} = G' (C^*-S^*)^g (t^*-t_o^*) \qquad \text{Eq. E-12}$$

where $G' = G^* f_{sv} / 3 \rho^{2/3}$

Introducing the reduced variable for the mass m

$$M^* = 100 M/M_F \qquad \text{Eq. E-13}$$

gives

$$M^{*1/3} - M_0^{*1/3} = G^*_1 \, f_{sv} \, \rho^{-2/3} \, (C^* - S^*)^g (t^* - t_0^*) \qquad \text{Eq. E-14}$$

where $G^*_1 = G^* \, 100^{1/3} / 3 \, M_F^{1/3}$ Eq. E-15

Case III Growth Rate Constant From the Particle Size Distribution

Eq. E-20 is rewritten for the growth of one particle

$$dm/dt = G^* \, a \, (C^* - S^*)^g \qquad \text{Eq. E-16}$$

where the area is

$$a = f_a \, r^2 \qquad \text{Eq. E-17}$$

and the mass can be expressed by

$$m = \rho \, v = f_v \, \rho \, r^3 \qquad \text{Eq. E-18}$$

Substituting Eq. E-17 and E-18 into Eq. E-16 gives

$$dm/dt^* = G^* f_a \, r^2 \, (C^* - S^*)^g \qquad \text{Eq. E-19}$$

or $$dr/dt^* = G^* f_a (C^*-S^*)^g / (3 \rho f_v) \qquad \text{Eq. E-20}$$

By substituting the exponential form of the desupersaturation equation viz.:

$$(C^*-S^*) = E \exp(-q\, t^*) \qquad \text{Eq. E-21}$$

Eq. E-20 becomes

$$dr/dt^* = F\, q\, g \exp(-g\, q\, t^*) \qquad \text{Eq. E-22}$$

where F is defined as

$$F = G^* f_a E^g/(3 f_v g q \rho) \qquad \text{Eq. E-23}$$

G* can be expressed as

$$G^* = F g q 3 \rho f_v/(f_a E^g) \qquad \text{Eq. E-24}$$